Examining metabolic vulnerabilities for cancer therapy

by

Alba Luengo

B.S. Biomedical Engineering
Columbia University, 2012

Submitted to the Department of Biology
in Partial Fulfillment of the Requirements for the Degree of

DOCTOR OF PHILOSOPHY

at the

MASSACHUSETTS INSTITUTE OF TECHNOLOGY

June 2018

Signature of the Author .....
Department of Biology
May 25, 2018

Certified By .....
Matthew G. Vander Heiden
Professor of Biology
Thesis Supervisor

Accepted By .....
Amy E. Keating
Professor of Biology
Chair of the Graduate Committee

Examining metabolic vulnerabilities for cancer therapy

by

Alba Luengo

Submitted to the Department of Biology
in Partial Fulfillment of the Requirements for the Degree of
Doctor of Philosophy in Biology

Abstract

Metabolic reprogramming is essential for cancer cells to balance energetics, maintain redox homeostasis, and synthesize biosynthetic precursors. Many chemotherapeutics that target metabolism are essential components of standard cancer treatment regimens, arguing that there is a therapeutic window to target the metabolic dependencies of cancer cells. However, the use of these drugs as cancer therapies was determined empirically, and rational approaches to directly target the metabolism of cancer cells, especially reprogrammed glucose metabolism, have proved challenging, in part because it is not well understood which metabolic processes are most important for cancer cell proliferation and survival.

The goal of this dissertation is to explore metabolic pathways preferentially used by cancer cells in order to identify potential tumor dependencies that could be exploited for clinical benefit. We first determined that production of reactive byproducts is an indirect consequence of the altered glucose metabolism of cancer cells, which suggests that clinically targeting secondary effects of reprogrammed tumor metabolism could be an approach for designing novel cancer treatments. Next, we found that a molecular driver for the altered glucose metabolism of cancer cells is limited electron acceptor availability, suggesting that interventions that further restrict the oxidative capacity of tumors could also have anticancer efficacy. Finally, we interrogated the metabolic fluxes of breast cancers proliferating in different microenvironments and determined that tumors in the brain parenchyma display enhanced lipid biosynthesis, which could guide therapeutic strategies to treat cancer based on tumor site. Collectively, these studies contribute to an understanding of how the reprogrammed metabolism of cancer cells introduces targetable dependencies, with the aim of optimizing cancer therapies.

Thesis Supervisor: Matthew G. Vander Heiden
Title: Associate Professor of Biology

Biographical Note

Alba Luengo

EDUCATION

2012-2018	Massachusetts Institute of Technology Ph.D. Department of Biology
2008-2012	Columbia University B.S. Biomedical Engineering, Cell and Tissue Engineering

RESEARCH EXPERIENCE

2012-present	Massachusetts Institute of Technology, Ph.D. Candidate David H. Koch Institute for Integrative Cancer Research Laboratory of Dr. Matthew G. Vander Heiden Assess whether a toxic metabolite byproduct of glucose metabolism can serve as a targetable liability of tumors Examine the metabolic consequences of increasing glucose oxidation in cancer cells Investigate the metabolism of primary and metastatic breast cancer utilizing a novel method of delivering isotope-labeled substrates in vivo
2009-2012	Columbia University, Undergraduate Research Assistant Laboratory of Dr. Clark T. Hung Designed 3D chondrocyte scaffolds from cells of the annulus fibrosis region of the intervertebral disc to mimic mechanical and structural properties of native nucleus pulposus tissue
2011	Memorial Sloan Kettering Cancer Center, Undergraduate Research Assistant Laboratory of Dr. Neal Rosen Investigate negative feedback in the PI3K signaling pathway upon treatment of cancer cells with mTOR kinase inhibitors
2010	CNIC (National Cardiology Research Center), Undergraduate Research Assistant Laboratory of Dr. José Antonio Enríquez Examined the relationship between autophagy and mutations in mitochondrial DNA

HONORS AND AWARDS

2018	Keystone Symposia Future of Science Fund Scholarship
2017	Rising Stars in Biomedicine
2017	MIT IMPACT Program, Fellow
2016-2017	Ludwig Center for Graduate Research Fellowship
2013-2016	NSF Graduate Research Fellowship
2012	Robert E. and Claire S. Reiss Prize in Biomedical Engineering, Columbia University
2012	Tau Beta Pi National Engineering Honor Society, New York Alpha Chapter, Columbia University
2012	Magna Cum Laude, Columbia University
2008-2012	Dean's List, Columbia University

TEACHING EXPERIENCE

2016	Teaching Assistant, General Biochemistry (7.05), Massachusetts Institute of Technology
2013	Teaching Assistant, Experimental Biology & Communication (7.02), Massachusetts Institute of Technology
2012	Teaching Assistant, Introduction to Cellular and Molecular Biology II (C2006), Columbia University
2011	Teaching Assistant, Introduction to Cellular and Molecular Biology I (C2005), Columbia University
2011-2012	Private Tutor, Ivy League Tutors Network

PRESENTATIONS

2018	Keystone Symposia, Tumor Metabolism, poster
2017	Rising Stars in Biomedicine, oral
2017	Koch Institute Fall Retreat, oral
2017	Judith Ann Lippard Memorial Lectureship in Cancer Research, Flash Talk, oral
2017	Smith Family Scientific Meeting and Dinner, poster
2017	Keystone Symposia, Tumor Metabolism: Mechanisms and Targets, poster
2017	Keystone Symposia, New Frontiers in Understanding Tumor Metabolism, poster
2011	BMES Annual Meeting, poster

PUBLICATIONS

1. Sullivan LB, **Luengo A**, Danai LV, Bush LN, Diehl FF, Hosios AM, Lau AN, Lewis CA, Vander Heiden MG. Evidence for aspartate as an endogenous metabolic limitation for tumour growth. Nat. Cell. Biol. Manuscript Accepted
2. Alkan HF, Walter KE, **Luengo A**, Madreiter-Sokolowski CT, Stryeck S, Al-Zhoughbi W, Lewis CA, Thomas CJ, Hoefler G, Graier WF, Madl T, Vander Heiden MG, Bogner-Strauss JG. Cytosolic aspartate availability determines cell survival when glutamine is limiting. Manuscript under review.
3. **Luengo A***, Gui DY*, Vander Heiden MG. Targeting metabolism for cancer therapy. Cell Chem Biol. 2017 Sep 21;24(9):1161-1180.
4. Davidson SM*, Jonas O*, Keibler MA, Hou HW, **Luengo A**, Mayers JR, Wyckoff J, Del Rosario AM, Whitman M, Chin CR, Condon KJ, Lammers A, Kellersberger KA, Stall BK, Stephanopolous G, Bar-Sagi D, Han J, Rabinowitz JD, Cima MJ, Langer R, Vander Heiden MG. Direct evidence for cancer-cell-autonomous extracellular protein catabolism in pancreatic tumors. Nat Med. 2017 Feb; 23(2):235-241.
5. Gui DY*, Sullivan LB*, **Luengo A**, Hosios AM, Bush LN, Gitego N, Davidson SM, Freinkman E, Thomas, CJ, Vander Heiden, MG. Environment dictates dependence on mitocondrial complex I for NAD+ and aspartate production and determines cancer cell sensitivity to metformin. Cell Metab. 2016 Nov 8; 24(5):716-727.
6. Dayton TL, Gocheva V, Miller KM, Israelsen WJ, Bhutkar A, Clish CB, Davidson SM, **Luengo A**, Bronson RT, Jacks T, Vander Heiden MG. Germline loss of PKM2 promotes metabolic distress and hepatocellular carcinoma. Genes Dev. 2016 May 1; 30(9):1020-33.
7. Pacold ME, Brimacombe KR, Chan SH, Rohde JM, Lewis CA, Swier LJ, Possemato R, Chen WW, Sullivan LB, Fiske BP, Cho S, Freinkman E, Birsoy K, Abu-Remaileh M, Shaul YD, Liu CM, Zhou M, Koh MJ, Chung H, Davidson SM, **Luengo A**, Wang AQ, Xu X, Yasgar A, Liu L, Rai G, Westover KD, Vander Heiden MG, Shen M, Gray NS, Boxer MB, Sabatini DM. A PHGDH inhibitor reveals coordination of serine synthesis and one-carbon unit fate. Nat Chem Biol. 2016 Jun; 12(6):452-6.
8. Davidson SM, Papagiannakopoulos T, Olenchock BA, Heyman JE, Keibler MA, **Luengo A**, Bauer MR, Jha AK, O'Brien JP, Pierce KA, Gui DY, Wasylenko TM, Subarraj L, Chin CR, Stephanopolous G, Mott BT, Jacks TE, Clish CB, Vander Heiden MG. Oxidative glucose metabolism is essential for Ras-driven non-small cell lung cancer. Cell Metab. 2016 Mar 8; 23(3):517-28.
9. **Luengo A**, Sullivan LB, Vander Heiden MG. Understanding the complex-I-ty of metformin action: limiting mitochondrial respiration to improve cancer therapy. BMC Biol. 2014 Oct 24; 12:82.
10. Gunja NJ, Dujari D, Chen A, **Luengo A**, Fong JV, Hung CT. Migration responses of outer and inner meniscus cells to applied direct current electric fields. J Orthop Res. 2012 Jan;30(1):103-11.

Acknowledgements

This thesis would not have been possible without the many people that offered support, encouragement, and guidance over the course of my PhD. First, I would like to thank my advisor, Matthew Vander Heiden for his bottomless enthusiasm and constant support, insight, and patience. I am grateful for the opportunities he has given me to travel to conferences, give scientific talks and collaborate with external groups and clinicians. All of these experiences have enriched my graduate work and contributed to my scientific development. I feel lucky to have been a member of his lab.

I am grateful Professors Tyler Jacks and Michael Hemann, who have provided helpful advice during and outside of thesis committee meetings over the years. I would also like to thank Joan Brugge for her willingness to serve as an external faculty member for my thesis defense.

I like to acknowledge the fellow members of the Vander Heiden Lab for contributing to a collaborative and collegial atmosphere. In particular, I would like to thank Aaron Hosios, who has been an invaluable scientific resource and an even better friend. I am indebted to his support over the course of my PhD. I have very much enjoyed working with Zhaoqi Li and I am grateful to him for injecting some much-needed enthusiasm into the final year of my PhD. I have been fortunate to always be well accompanied in the "back bay," with Peggy Hsu and Dan Gui, both of which have made great coffee partners, workout buddies, and provided me some company during late nights in lab. Additionally, I thank Dan Gui and Lucas Sullivan for advice, mentorship, and friendship. I am also grateful to Shawn Davidson for being the first person to train me in the lab and introducing me to in vivo metabolism. I have enjoyed many conversations and interactions, scientific and not so scientific, with all current and former members of the Vander Heiden lab. I thank Mark Sullivan, Furkan Alkan, Chris Chin, Alex Muir, Evan Lien, Allison Lau, Nick Matheson, Brian Fiske, Will Israelsen, Katie Mattiani, Jared Mayers, Ben Olenchock, Laura Danai, Daniel Schmidt, Franny Diehl, Brooke Bevis, Anna Nguyen, Emily Dennstedt, Sharanya Sivanand, and Alicia Darnell for their camaraderie.

I have had the privilege of working with a number of excellent external collaborators. I would like to especially thank Gino Ferraro and Divya Bezwada for being wonderful colleagues and sharing fun times together at Keystone Conferences. I have enjoyed working with Caroline Lewis, and am especially glad she did not travel too far after leaving the Vander Heiden Lab. Isaac Harris has also been a source of support and helpful conversations.

I am grateful for the many friendships I've made during this time, and would like to especially acknowledge Sahin Naqvi, Lisa Cunden, Kristin Knouse, Lucas Manuelli, Daniel Miller, and Ian Campbell for being a source of fun, support and sometimes commiseration.

I am grateful to my friends Spencer Almen, Javier Rivera, Leandra Gerena, and Courtney Giannini for being a source of unwavering support and a helpful reminder that there is a life outside of grad school.

I would like to offer special thanks to Lukas Murmann, I am grateful to have you in my life.

Above all, I would like to thank my family – this thesis is dedicated to them. Thank you for your unconditional love, support, and always believing in me. I couldn't have done it without you. Os quiero muchísimo.

Table of Contents

Chapter 1: Targeting metabolism for cancer therapy

A version of this chapter has been published previously:
Luengo, A., Gui, D.Y., and Vander Heiden, M.G. (2017). Targeting Metabolism for Cancer Therapy. Cell Chem Biol 24, 1161-1180.

Summary

Metabolic reprogramming contributes to tumor development and introduces metabolic liabilities that can be exploited to treat cancer. Chemotherapies targeting metabolism have been effective cancer treatments for decades, and the success of these therapies demonstrates that a therapeutic window exists to target malignant metabolism. New insights into the differential metabolic dependencies of tumors have provided novel therapeutic strategies to exploit altered metabolism, some of which are being evaluated in pre-clinical models or clinical trials. In this chapter, we review our current understanding of cancer metabolism and discuss how this might guide treatments targeting the metabolic requirements of tumor cells.

Introduction

In 1947, Sidney Farber, one of the pioneers of modern chemotherapy, discovered that aminopterin could cause disease remission in children with acute lymphoblastic leukemia (Farber and Diamond, 1948). Aminopterin is the precursor of the currently used drugs methotrexate and pemetrexed, both of which are folate

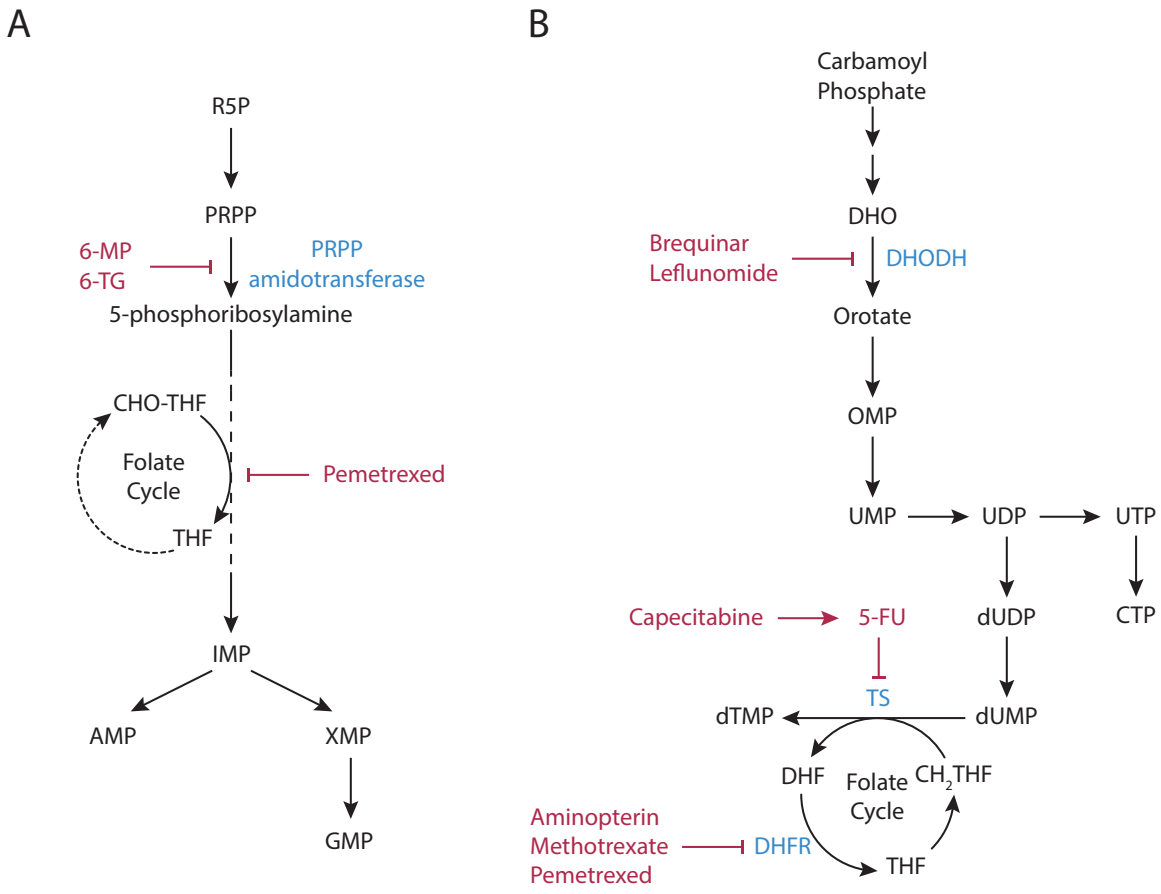
A
R5P
PRPP
6-MP
6-TG
PRPP
amidotransferase
5-phosphoribosylamine
CHO-THF
Folate
Cycle
THF
Pemetrexed
IMP
AMP
XMP
GMP
B
Carbamoyl
Phosphate
DHO
Brequinar
Leflunomide
DHODH
Orotate
OMP
UMP
UDP
UTP
dUDP
CTP
Capecitabine
5-FU
TS
dTMP
dUMP
DHF
Folate
Cycle
CH2THF
Aminopterin
Methotrexate
Pemetrexed
DHFR
THF

Figure 1. Nucleotide Biosynthesis

(A) Purine nucleotide synthesis. The first reaction in purine production generates 5-phosphoribosyl-1-pyrophosphatae (PRPP) from ribose 5-phosphate (R5P). The second step is catalyzed by PRPP amidotransferase, and commits PRPP to purine synthesis. This step can be inhibited by the antimetabolites, 6-mercaptopurine (6-MP) and 6-thioguanine (6-TG). Subsequent steps in the pathway assemble the purine ring and result in the formation of inosine monophosphate (IMP), which in turn can be converted to either adenosine monophosphate (AMP) or guanosine monophosphate (GMP) by distinct reactions. The synthesis of the purine ring requires N^{10}-formyl-tetrahydrofolate (CHO-THF) via a reaction that can be inhibited by pemetrexed.

(B) Pyrimidine nucleotide synthesis. Pyrimidine nucleotide synthesis begins with the conversion of carbamoyl phosphate to the pyrimidine base orotate. One of the steps in pathway is catalyzed by dihydroorotate dehydrogenase (DHODH), which can be inhibited by brequinar sodium and leflunomide. Next, orotate is combined with PRPP to generate orotate monophosphate (OMP), which is subsequently converted to uridine monophosphate (UMP). UMP can be phosphorylated to form UDP and UTP, and the latter can be further converted to cytidine triphosphate (CTP). Uridine nucleotides can also be used for de novo thymine nucleotide synthesis. UDP is converted to deoxy-UMP (dUMP), and the enzyme thymidylate synthase (TS) generates dTMP by catalyzing the methylation of dUMP using N^5,N^{10}-methylene-tetrahydrofolate (CH2-THF) as the methyl donor. TS activity is inhibited by the antipyrimidine 5-fluorouracil (5-FU) and the 5-FU pro-drug capecitabine. Thymidine synthesis can also be inhibited by the antifolates aminopterin, methotrexate, and pemetrexed, as these drugs inhibit the enzyme dihydrofolate reductase (DHFR), limiting the availability of CH_2-THF

analogues that inhibit one-carbon transfer reactions required for de novo nucleotide synthesis (**Figure 1, Figure 2A**) (Walling, 2006). The early clinical success of antifolates led to the development of an entire class of drugs known as 'antimetabolites.' Antimetabolites are small molecules that resemble nucleotide metabolites and inhibit the activity of enzymes involved in nucleotide base synthesis (**Table 1**). Notable examples include the purine analogues 6-mercaptopurine (6-MP) and 6-thioguanine (6-TG), which inhibit 5-phosphoribosyl-1-pyrophosphatase (PRPP) amidotransferase, the first enzyme in de novo purine biosynthesis (**Figure 1A, Figure 2B**). 6-MP and 6-TG have been successful in treating many cancers, including childhood leukemia (Elion, 1989). The pyrimidine analogue 5-fluorouracil (5-FU) is a synthetic analogue of uracil that inhibits thymidylate synthase, limiting the availability of thymidine nucleotides for DNA synthesis (**Figure 1B, Figure 2C**). 5-FU and the related 5-FU-prodrug capecitabine remain widely used chemotherapies today and are an important treatment for gastrointestinal cancers (Heidelberger et al., 1957; Wagner et al., 2006). Other antimetabolite nucleoside analogues, such as gemcitabine and cytarabine, are incorporated into DNA, resulting in inhibition of DNA polymerases, and are commonly used to treat select cancers (Parker, 2009).

The clinical success of antimetabolites for treating cancer is attributed to the increased metabolic demand of neoplastic cells for nucleotide biosynthesis and DNA replication. However, nucleotide metabolism is only one of many metabolic dependencies altered to support cancer cell proliferation. Proliferating cells have

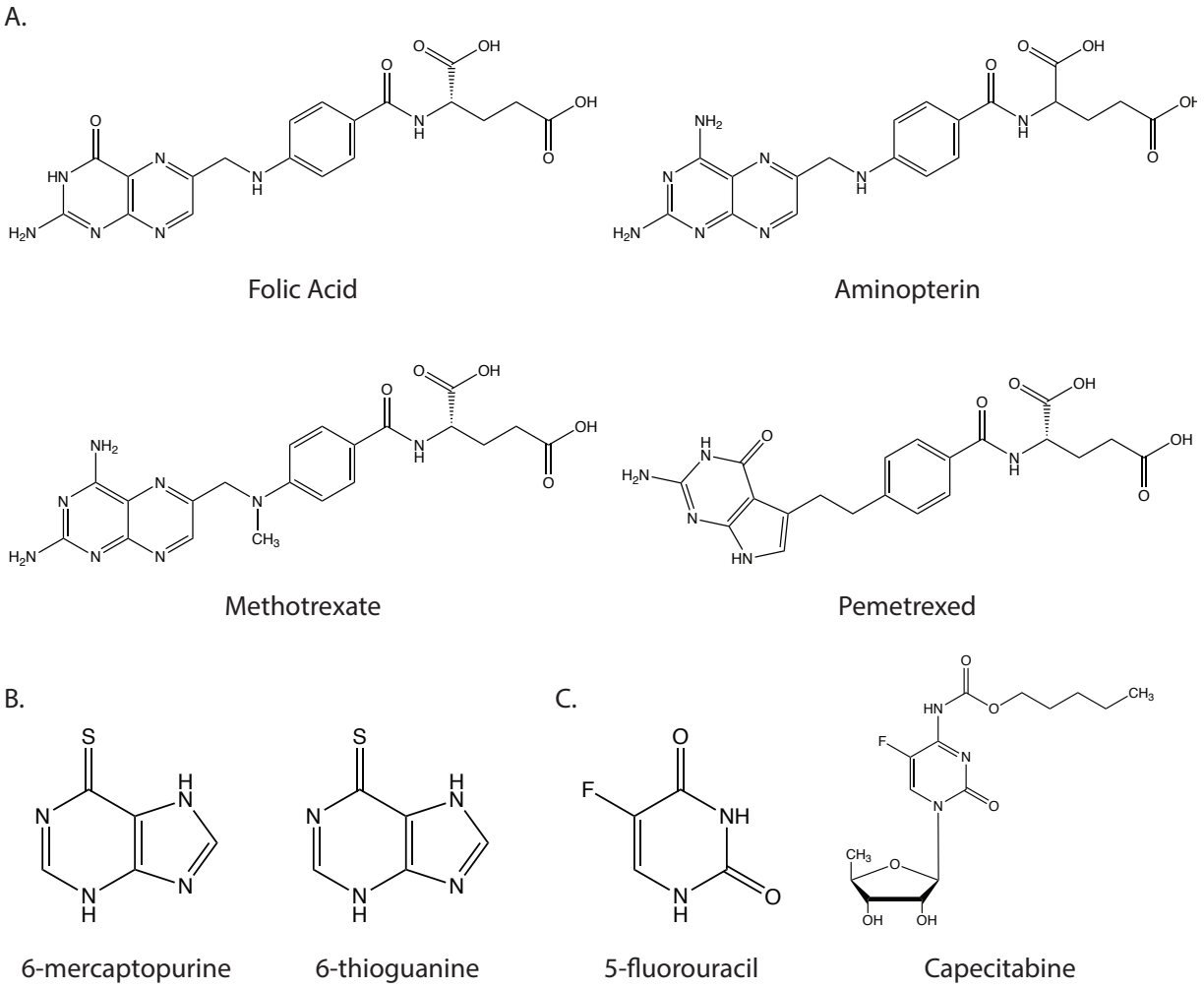

Figure 2. Antimetabolites

(A) Structures of folic acid and the antifolate compounds aminopterin, methotrexate and pemetrexed.

(B) Structures of the purine analogues 6-mercaptopurine and 6-thioguanine

(C) Structures of pyrimidine analogue 5-fluorouracil and the 5-fluorouracil prodrug capecitabine.

different metabolic requirements from non-proliferating cells (Hsu and Sabatini, 2008; Lunt and Vander Heiden, 2011; Pavlova and Thompson, 2016). While non-proliferating cells have primarily catabolic demands, proliferating cells must balance the divergent catabolic and anabolic requirements of sustaining cellular homeostasis while duplicating cell mass, and thus engage in a metabolic program distinct from that of the normal tissue from which they arise. From a therapeutic perspective, the aberrant metabolism of proliferating cancer cells presents potential opportunities, and there has been a growing interest in studying how best to target cancer metabolism (Bobrovnikova-Marjon and Hurov, 2014; Galluzzi et al., 2013; Martinez-Outschoorn et al., 2017; Vander Heiden, 2011).

Targeting general proliferative metabolism may not offer an adequate therapeutic window since many non-malignant cells, including those in bone marrow, intestinal crypts, and hair follicles, are rapidly proliferating. Furthermore, the proliferation rates of normal cells are often greater than those of cancer cells (Vander Heiden and DeBerardinis, 2017), and prominent side effects of antimetabolite chemotherapy are caused by the destruction of non-cancerous rapidly proliferating cells. Myeloid suppression or gastrointestinal toxicity are often dose-limiting toxicities for these drugs.

In spite of toxicity, antimetabolites are standard in many modern chemotherapy regimens that increase patient survival and, in some cases, help cure disease. Factors other than proliferation rate may account for the efficacy of these drugs. Inducing DNA damage with the use of genotoxic chemotherapies can

sensitize cells to inhibitors of nucleotide biosynthesis (Brown et al., 2017; Peters et al., 2000), suggesting that oncogenic mutations that reduce the DNA damage response is one explanation for why a therapeutic window exists for antimetabolite compounds. However, antimetabolite drugs are only effective against a subset of cancer types. Many resistant cancers have the same mutational spectrum as sensitive cancers, and defining genetic predictors of chemotherapy response for most malignancies has been difficult. Nevertheless, the fact that antimetabolite chemotherapies are clinically effective suggests that a metabolic therapeutic window exists beyond proliferation rate and response to DNA damage. While the precise mechanisms underlying the differential efficacies of existing antimetabolite therapies are unknown, a better understanding of these and other metabolic therapeutic windows may lead to the development of more effective and selective cancer treatments. In this chapter, we discuss recent advances in cancer metabolism research that have identified metabolic targets and highlight features that might be exploited for improved cancer therapy.

Altered glucose metabolism

More than thirty years preceding Farber's work on antifolates, Otto Warburg reported that cancer cells consume tremendous amounts of glucose and metabolize the majority of the glucose into lactate, even in the presence of oxygen (Warburg, 1924). This phenomenon is now referred to as aerobic glycolysis, or the Warburg effect, and represents a striking metabolic difference between cancer and most

normal tissues. Substantial work has sought to clinically target increased glycolysis including efforts to inhibit lactate production and excretion (Doherty and Cleveland, 2013; Hamanaka and Chandel, 2012; Hay, 2016; Pelicano et al., 2006; Zhao et al., 2013). One compound known to block glucose metabolism is 2-deoxyglucose (2-DG) (Wick et al., 1957). 2-DG is phosphorylated by hexokinase to produce 2-deoxyglucose-6-phosphate, which cannot be further metabolized by cells. It therefore accumulates intracellularly and competitively inhibits hexokinase to slow glucose uptake (**Figure 3**). Numerous preclinical studies have demonstrated anti-proliferative effects of 2-DG (Zhang et al., 2014a). Although early clinical testing yielded responses in some patients, the use of this drug was limited by toxicity associated with hypoglycemia symptoms (Landau et al., 1958). Recent clinical trials have revisited use of 2-DG at lower doses, but these doses are insufficient to inhibit disease progression (Raez et al., 2013; Stein et al., 2010). The relative lack of 2-DG clinical efficacy at tolerable doses has been echoed by most other attempts to directly target aerobic glycolysis. Though efforts to target glucose uptake or lactate production have found some success in preclinical models (Fantin et al., 2006; Hay, 2016; Shim et al., 1997; Xie et al., 2014), clinical success has been limited (Vander Heiden and DeBerardinis, 2017).

Regulation of pyruvate kinase activity can influence aerobic glycolysis (Dayton et al., 2016). Paradoxically, decreased pyruvate kinase activity is associated with increased aerobic glycolysis, suggesting the activation of pyruvate kinase

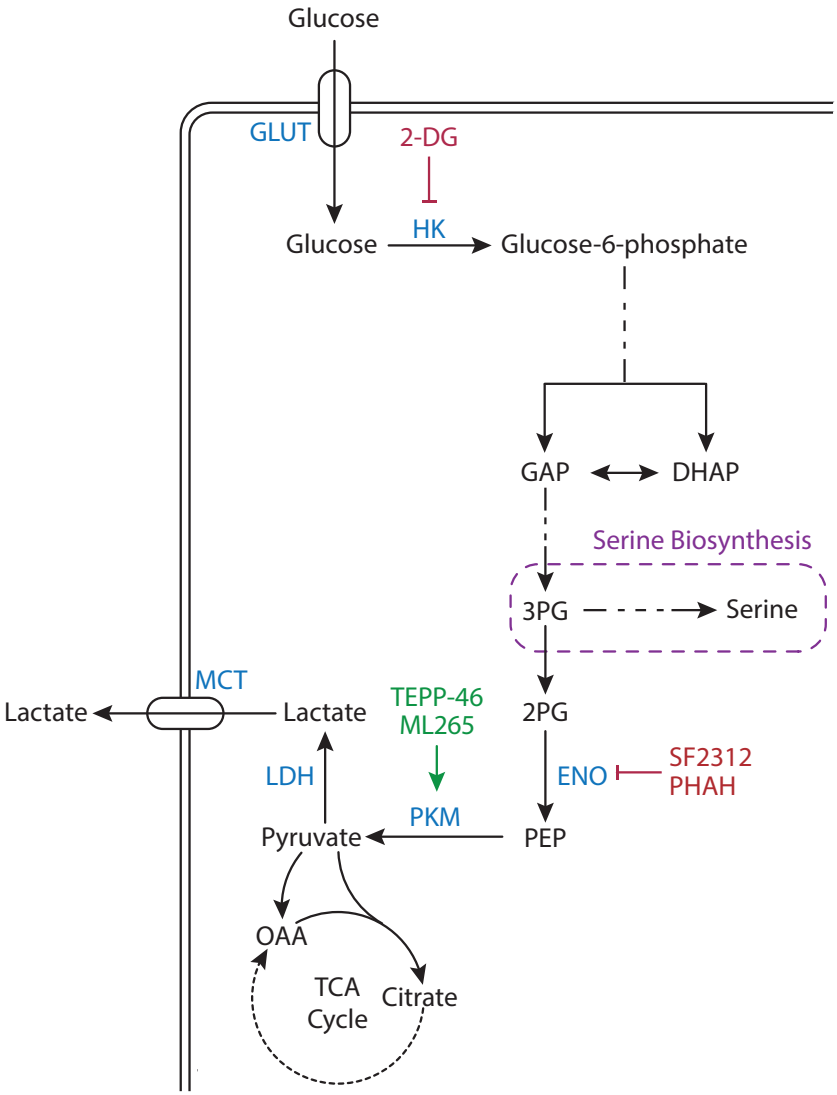

Figure 3. Glycolysis

Glucose is imported in cells by one of several glucose transporters (GLUT). Glucose is phosphorylated by hexokinase (HK), a step that can be competitively inhibited by the compound 2-deoxyglucose (2-DG). In a later step of glycolysis, glucose carbon is cleaved into two interconvertible three-carbon units, dihydroxyacetone phosphate (DHAP) and glyceraldehyde 3-phosphate (GAP). Downstream of GAP, 3-phosphoglycerate (3-PG) is converted to 2-phosphoglycerate (2-PG), and the enzyme enolase (ENO) generates phosphoenolpyruvate (PEP) from 2-PG. ENO activity can be inhibited by the compounds phosphonoacetohydroxamate (PHAH) and SF-2312. PEP is converted to pyruvate by pyruvate kinase (PKM), which can be activated by the drugs TEPP-46 and AG-348. Pyruvate can be oxidized in the TCA cycle, or it can produce lactate via lactate dehydrogenase (LDH), with lactate excreted by monocarboxylate transporters (MCT). MCT isoform 1 can be inhibited by the compound AZD3965.

activity might be a way to target cancer (Christofk et al., 2008). Indeed, activation of pyruvate kinase can inhibit cancer cell proliferation and tumor growth in some settings (Anastasiou et al., 2012; Kung et al., 2012; Walsh et al., 2010), but because pyruvate kinase expression is dispensable for the growth of some tumors (Cortes-Cros et al., 2013; Israelsen et al., 2013; Lau et al., 2017), whether pyruvate kinase activation will lead to durable responses remains an area of active study (Israelsen et al., 2013; Israelsen and Vander Heiden, 2015).

Despite challenges associated with targeting glucose metabolism directly, glucose uptake by cancer cells has been successfully exploited in patients through the use of the fluoro-deoxy-glucose positron-emission-tomography (FDG-PET) imaging to stage cancers and assess response to therapy (d'Amico, 2015; Farwell et al., 2014; Zhu et al., 2011). Notably, many non-cancerous tissues, including the brain, are FDG-PET avid (Berti et al., 2014; Cohade, 2010), illustrating that high glucose uptake is not a unique feature of tumors and offering a potential explanation for the relative lack of success in directly targeting glucose metabolism for cancer treatment. Doses of 2-DG that inhibit glycolysis enough to limit cancer growth may not be tolerated due to similar effects in normal tissues that also rely on glucose metabolism.

Altered Metabolic Enzyme Expression

The expression of metabolic genes is frequently altered in cancer. Some changes in metabolic enzyme expression result from gene amplification or deletion,

while others are downstream of growth signaling pathways or are consequences of epigenetic changes. The activity of metabolic enzymes can also be affected by mutations in the genes encoding these enzymes. Regardless of the underlying mechanism, alterations in basal enzymatic activity of a given reaction present potential vulnerabilities that might be targeted for cancer therapy.

Oncogenic isocitrate dehydrogenase mutations

Recurrent somatic point mutations in the genes coding for isocitrate dehydrogenase 1 and 2 (*IDH1*, *IDH2*) are found in a wide variety of cancers, including glioblastoma multiforme (GBM) (Yan et al., 2009) and acute myeloid leukemia (AML) (Dang et al., 2016; Mardis et al., 2009). Cancers expressing mutant IDH represent a unique case in which a metabolic enzyme can act as an oncogene and contribute to tumor development. Wild-type IDH1 and IDH2 catalyze the reversible oxidative decarboxylation of isocitrate to alpha-ketoglutarate (αKG) and CO_2 (**Figure 4A**). Cancer associated mutations in *IDH1* and *IDH2* eliminate this function and confer a neomorphic activity to the enzyme, generating D-2-hydroxyglutarate (D-2HG) via the reduction of αKG (**Figure 4B**) (Dang et al., 2009; Ward et al., 2010). Though it is found at low levels in normal cells, D-2HG can accumulate to millimolar levels in cancer cells expressing mutant IDH. At these high concentrations, D-2HG can inhibit αKG-dependent dioxygenases, including enzymes involved in histone and DNA demethylation (Chowdhury et al., 2011; Janke et al., 2017; Koivunen et al., 2012; Xu et al., 2011). As a result, D-2HG

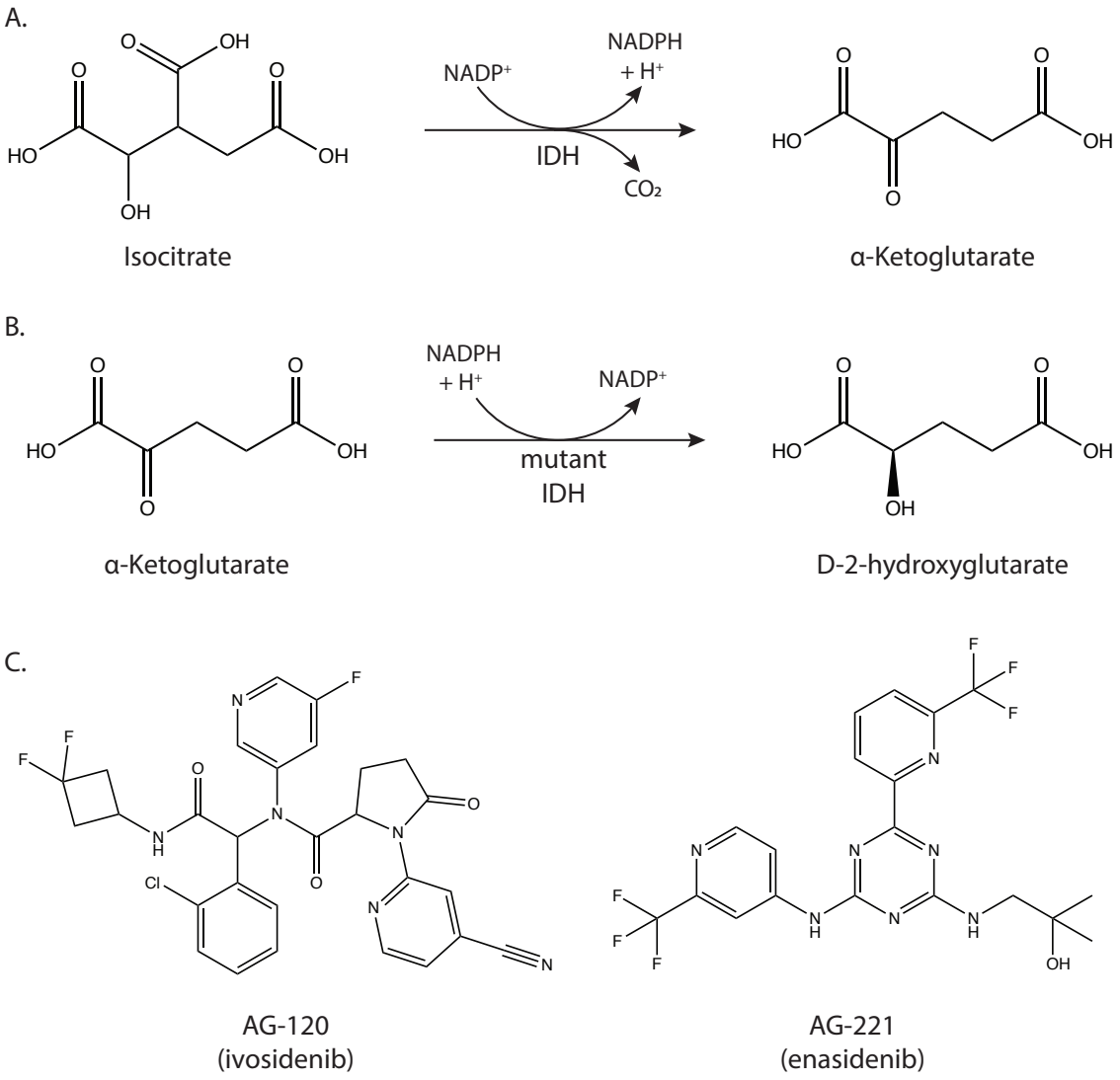

Figure 4. Mutant IDH

(A) The reaction catalyzed by wild-type IDH is the decarboxylation of isocitrate to α-ketoglutarate.

(B) The reaction catalyzed by mutant IDH1 and IDH2 is the reduction of α-ketoglutarate to D-2-hydroxyglutarate.

(C) Structures of AG-120 (ivosidenib) and AG-221 (enasidenib), which inhibit mutant IDH1 and IDH2 respectively.

accumulation in cancer cells expressing mutant IDH results in hypermethylation of histones and CpG islands in DNA (Figueroa et al., 2010; Lu et al., 2012; Turcan et al., 2012). These epigenetic changes caused by D-2HG contribute to cancer phenotypes (Losman et al., 2013; Rohle et al., 2013; Saha et al., 2014; Wang et al., 2013), and have been proposed to promote oncogenesis by preventing normal cellular differentiation (Losman and Kaelin, 2013).

Pharmacological agents that inhibit mutant IDH1 and IDH2 enzyme activity are being developed and assessed for antitumor efficacy **(Figure 4C)** (Dang et al., 2016). One of the first compounds reported was AGI-5198, which targets mutant IDH1. AGI-5198 reduces intratumoral D-2HG levels, induces expression of genes involved in glial cell differentiation, and suppresses growth of IDH1-mutant human glioma cells in a xenograft model (Rohle et al., 2013). A specific inhibitor of mutant IDH2, AG-221 (enasidenib) confers survival benefit in a mouse model of *IDH2*-mutant AML (Quivoron et al., 2014; Yen et al., 2017) and became the first compound targeting mutant IDH to enter clinical trials in 2014. Early results in *IDH2*-mutant AML patients have suggested enasidenib can provide clinical benefit (DiNardo et al., 2015; Stein et al., 2014), and this drug is also being evaluated in solid tumors. Mutant IDH1 inhibitors including AG-120 (ivosidenib) and IDH305, as well as the pan-mutant IDH inhibitor AG-881 (Table 1), are also in clinical trials to treat both hematologic malignancies and solid tumors, and will further inform whether targeting mutant IDH can control disease where IDH mutations are prevalent.

Despite success in some preclinical models and patients with AML, mutant IDH inhibitors may not be effective in all IDH-mutant cancers. For example, these drugs are unable to reverse epigenetic changes or inhibit tumor proliferation in many models of IDH-mutant glioma, despite a robust ability to lower 2-HG in cells and tumors (Tateishi et al., 2015; Turcan et al., 2013). *IDH1* mutations are early events in the development of glial cancer (Watanabe et al., 2009), raising the possibility that IDH mutations are important for tumor initiation, but accumulation of additional oncogenic mutations renders GBM tumors less dependent on constitutive expression of mutant IDH for tumor proliferation and progression (Johnson et al., 2014; Wakimoto et al., 2014). Nevertheless, the presence of a mutation in *IDH1* or *IDH2* and high levels of 2-HG might still drive dependencies on some pathways and introduce therapeutic vulnerability. For example, tumors harboring an IDH mutation have increased sensitivity to hypomethylating agents (Turcan et al., 2013), electron transport chain inhibitors (Grassian et al., 2014), depletion of the coenzyme NAD+ (Tateishi et al., 2015) and chemoradiotherapy (Cairncross et al., 2014). However, some evidence suggests that inhibiting mutant IDH could confer resistance to some therapies, as inhibitors targeting mutant IDH1 can antagonize the effects of radiation therapy in glioma (Molenaar et al., 2015). Thus, testing whether combination therapies are synergistic or antagonistic with inhibition of mutant enzyme function is needed to guide treatment.

Drug	Target Enzyme
Methotrexate	dihydrofolate reductase (DHFR)
Pemetrexed	DHFR thymidylate synthase (TS) glycinamide ribonucleotide formyltransferase (GARFT)
6-Mercaptopurine **6-Thioguanine**	PRPP amidotransferase
Capecitabine **5-Fluorouracil**	thymidylate synthase (TS)
Gemcitabine **Cytarabine**	DNA polymerase/ribonucleotide reductase(RnR)
Leflunomide	dihydroorotate dehydrogenase (DHODH)
CB-839	glutaminase (GLS)
PEG-BCT-100 (ADI-PEG20) **AEB-1102**	depletion of circulating arginine
L-Asparaginase	depletion of circulating asparagine
TVB-2640	fatty-acid synthase (FASN)
AG-120 (Ivosidenib) **IDH305** **BAY1436032** **FT-2102** **AG-221 (Enasidenib)** **AG-881**	mutant IDH1 mutant IDH2 mutant IDH1/2
AZD3965	monocarboxylate transporter 1 (MCT1)
CPI-613	pyruvate dehydrogenase (PDH) α-ketoglutarate dehydrogenase
Metformin	mitochondrial complex I

Table 1.
Select agents targeting metabolism that are approved, or are in trials, for the treatment of cancer, focusing on targets discussed in this dissertation chapter.

Upregulated glutaminolysis

Glutamine is a non-essential amino acid, and yet cancer cells proliferating in vitro consume glutamine far in excess of any other amino acid and are often dependent on extracellular glutamine for survival (DeBerardinis and Cheng, 2010; Eagle, 1955; Jain et al., 2012). Glutamine is an important nitrogen donor for amino acids and nucleotides (Hosios et al., 2016), but glutamine uptake can exceed the nitrogen requirement of some cancer cells (DeBerardinis et al., 2007). Glutamine carbon has been found to contribute to aspartate, glutamate and tricarboxylic acid (TCA) cycle metabolites via glutaminolysis (**Figure 5**) (Altman et al., 2016). High rates of glutaminolysis has been proposed to support rapid proliferation by supplying precursors to low-flux biosynthetic pathways (Newsholme et al., 1985). Providing cells with αKG, oxaloacetate, or pyruvate is sufficient to rescue cancer cell proliferation in conditions of glutamine starvation, confirming that glutamine supports proliferation by replenishing depleted TCA cycle intermediates, a process termed anaplerosis (Altman et al., 2016; Weinberg et al., 2010; Yuneva et al., 2007).

Glutamine metabolism is upregulated by various oncogenic signaling pathways (Altman et al., 2016). In certain contexts, MYC-transformed cancers become glutamine dependent and undergo apoptosis in the absence of glutamine (Yuneva et al., 2007). MYC has been found to increase mRNA and protein levels of glutamine transporters as well as expression of the enzyme glutaminase, which catalyzes the first step in glutaminolysis (Gao et al., 2009; Wise et al., 2008; Yuneva et al., 2012). Importantly, inhibiting glutamine entry into the TCA cycle can blunt

tumor progression in a MYC-driven model of liver cancer (Xiang et al., 2015; Yuneva et al., 2012) and a MYC-inducible Burkitt lymphoma model (Le et al., 2012; Xiang et al., 2015).

The dependence of cancer cells on glutamine has made glutaminolysis an attractive cancer therapy target (Altman et al., 2016; Daye and Wellen, 2012; DeBerardinis and Cheng, 2010; Vander Heiden, 2011). Clinical trials using glutamine analogues to treat cancers were initiated decades ago, but these trials were abandoned due to lack of efficacy and/or severe patient toxicity (Livingston et al., 1970; O'Dwyer et al., 1984). The absence of a therapeutic window for these studies can likely be attributed to fact that these drugs were relatively non-specific and a panoply of glutamine utilizing enzymes were likely affected.

Current attempts to target glutaminolysis clinically have largely focused on inhibiting glutaminase. Mammals have two glutaminase genes, *GLS* and *GLS2*, and targeting the enzymes encoded by these genes with chemical inhibitors has been found to decrease cancer cell proliferation in both in vitro and in vivo models (Gross et al., 2014; Jacque et al., 2015; Le et al., 2012; Xiang et al., 2015; Yuneva et al., 2012). One potent glutaminase inhibitor, CB-839, is currently being evaluated in cancer trials in patients (**Table 1**), although the exact disease context where glutaminase inhibition will be most effective remains an area of active investigation. There is also data that GLS2 activity can be tumor suppressive (Hu et al., 2010), underscoring the importance of defining the patient population likely to benefit from glutaminase inhibition.

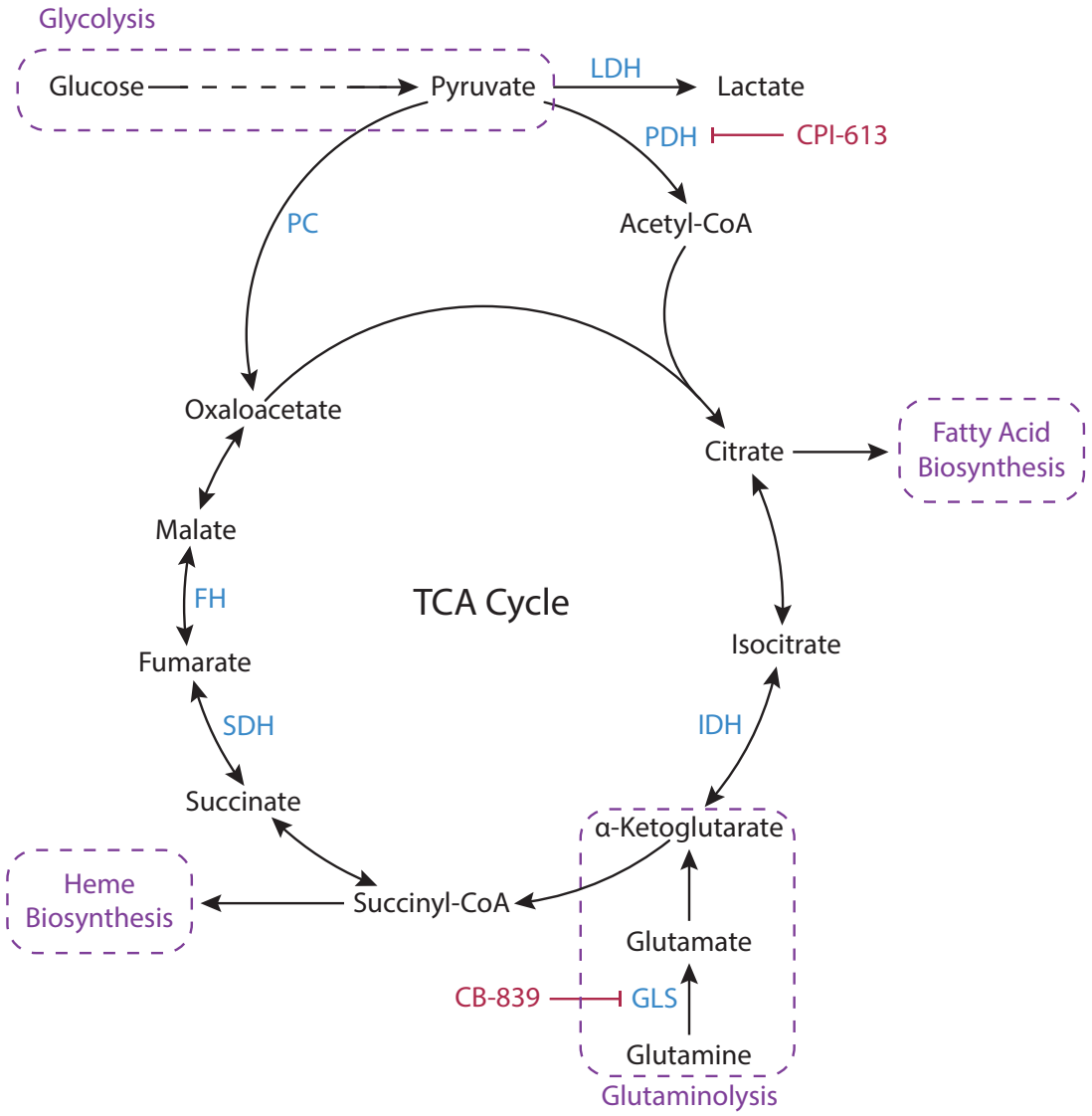

Figure 5. TCA Cycle

Pyruvate produced by glycolysis can be metabolized by the TCA cycle. Pyruvate is oxidized via pyruvate dehydrogenase (PDH) to the two-carbon unit acetyl-CoA, and subsequently combined with the four-carbon oxaloacetate to generate citrate. The cycle regenerates oxaloacetate while generating precursors that are important for biosynthetic processes including heme and fatty acid synthesis. When molecules are removed from the TCA cycle to feed these pathways, TCA intermediates must be replenished in a process termed anaplerosis. Pyruvate can serve as an anaplerotic substrate when converted to oxaloacetate by the enzyme pyruvate carboxylase (PC). Glutaminolysis, the conversion of glutamine to glutamate via glutaminase (GLS), can also support anaplerosis via production of -ketoglutarate. PDH activity is inhibited by the lipoic acid derivative CPI-613 and GLS activity is inhibited by CB-839.

Increased dependence on serine

Increased activity of de novo serine synthesis enzymes in cancer has been observed for more than 30 years (Snell, 1984; Snell et al., 1988). More recently, it was found that expression of the serine synthesis enzyme phosphoglycerate dehydrogenase (*PHGDH*) is increased in some cancers due to copy number gain of a region on chromosome 1p (Beroukhim et al., 2010; Locasale et al., 2011; Possemato et al., 2011) or as a consequence of oncogenic signaling, including NRF2 and ATF4 signaling (DeNicola et al., 2015), or hypoxia responses (Samanta et al., 2016). The PHGDH gene encodes the enzyme that catalyzes conversion of the glycolytic intermediate 3-phosphoglycerate into 3-phosphohydroxypyruvate, and 3-phosphohydroxypyruvate is converted to serine via two subsequent reactions (**Figure 6**). Increased *PHGDH* gene expression leads to greater production of serine from glucose and is associated with specific subsets of breast cancer, lung adenocarcinoma, and melanoma (Locasale et al., 2011; Possemato et al., 2011; Zhang et al., 2017). Serine is present in plasma and can be taken up by cells via amino acid transporters, yet *PHGDH* expression and increased serine biosynthesis have been shown to be important for supporting cancer cell proliferation and survival in both in vitro and in vivo settings (Locasale et al., 2011; Possemato et al., 2011). However, PHGDH activity may not be a requirement for proliferation for all PHGDH-amplified cancers, as expression has been shown to be dispensable in a breast cancer xenograft model (Chen et al., 2013).

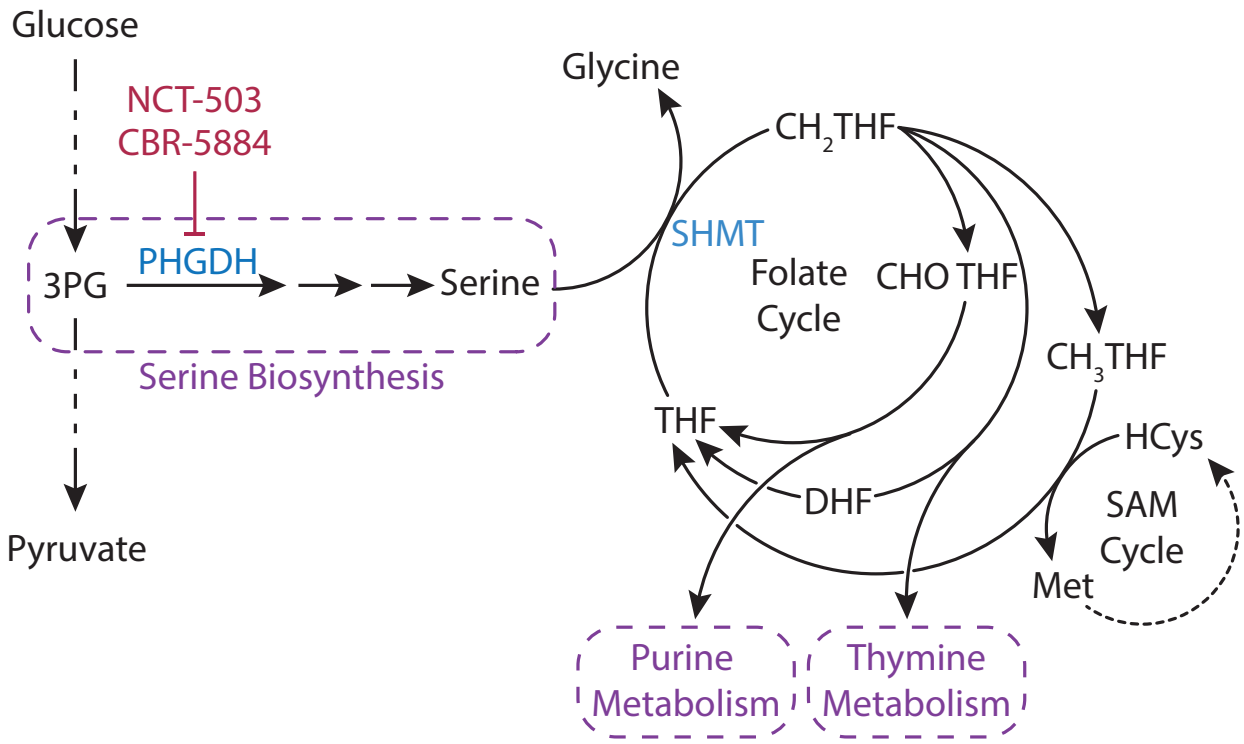

Figure 6. Serine Biosynthesis and Folate Cycle

The glycolytic intermediate 3-phophoglycerate (3-PG) is metabolized to serine in a three-step pathway where the first step is catalyzed by the enzyme phosphoglycerate dehydrogenase (PHGDH), which can be inhibited by NCT-503 and CBR-5884. Serine metabolism to glycine by serine hydroxymethyltransferase (SHMT) transfers a one carbon unit to tetrahydrofolate (THF) to form N^5,N^{10}-methylene-tetrahydrofolate (CH_2-THF). CH_2-THF is the methyl donor for thymidine nucleotides, or it can be converted to N^{10}-formyl-tetrahydrofolate (CHO-THF) for purine biosynthesis or to N^5-methyl-THF (CH_3-THF) to support methionine production and numerous methylation reactions via the S-adenosyl methionine (SAM) cycle.

Why some cancers are dependent on increased serine production is unknown, but increased flux through this pathway may serve to maintain adequate intracellular serine levels. Serine is an amino acid, and thus is required for protein synthesis, but serine can also support many other important critical metabolic processes including synthesis of glycine, glutathione, and phospholipids. With respect to proliferating cells such as cancer, serine is the primary carbon donor to the tetrahydrofolate (THF) cycle, which is required for both purine and pyrimidine nucleotide biosynthesis (**Figure 6**) (Snell et al., 1987). Serine can also contribute to NADPH production via the folate cycle, which serves to maintain redox homeostasis and support anabolic reactions (Fan et al., 2014; Lewis et al., 2014; Ye et al., 2014). Emerging work suggests that increased serine synthesis may be particularly important for maintaining redox homeostasis during metastasis (Piskounova et al., 2015).

Given the cancer cell requirement for serine, de novo serine synthesis is a potential target for cancer therapy. Functional PHGDH loss is toxic to tumor cells with *PHGDH* amplification or high serine biosynthetic flux (Locasale et al., 2011; Mattaini et al., 2015; Possemato et al., 2011; Zhang et al., 2017), and small-molecule inhibitors targeting PHGDH have been shown to inhibit serine synthesis and tumor proliferation in vitro and in xenograft cancer models (Mullarky et al., 2016; Pacold et al., 2016; Wang et al., 2017). However, inhibitors of PHGDH might have a limited therapeutic index, as de novo serine synthesis has an important physiological role in the central nervous system (Furuya, 2008) and *Phgdh*-deficient

mice exhibit severe brain morphogenesis defects (Yoshida et al., 2004). Compounds with decreased distribution in the brain may be more effective for cancer therapy.

Certain tumors are dependent on uptake of environmental serine (Jain et al., 2012; Maddocks et al., 2013; Maddocks et al., 2017), and limiting plasma serine availability can be beneficial for patients with these cancers. Removing serine from culture media limits incorporation of one-carbon units into nucleotides and impairs proliferation (Labuschagne et al., 2014). Additionally, serine deprivation by dietary restriction is sufficient to slow growth of both xenograft (Gravel et al., 2014; Maddocks et al., 2013) and autochthonous cancer models, although efficacy of serine deprivation appears to be influenced by both the oncogenic driver mutation and tissue context (Maddocks et al., 2017). Combining serine restriction with other drugs may also potentiate antitumor responses (Gravel et al., 2014; Maddocks et al., 2013; Maddocks et al., 2017). Further understanding the roles of de novo serine synthesis and serine uptake in different tumor contexts can yield important insights into how to target serine metabolism.

FH and SDH loss in heritable cancer syndromes

In addition to genetic events that increase metabolic enzyme expression, some cancers select for deletion of metabolic enzymes. Familial cancer syndromes caused by fumarate hydratase (*FH*) or succinate dehydrogenase (*SDH*) deletion suggest that these TCA enzymes can behave as classical tumor suppressors. Affected families inherit one defective copy of either *FH* or *SDH*, and develop an

aggressive form of cancer upon loss of heterozygosity (Baysal et al., 2000; Tomlinson et al., 2002). Loss of FH activity or SDH activity results in disruption of the TCA cycle and accumulation of fumarate or succinate, respectively. Like D-2HG, fumarate and succinate accumulation can inhibit some αKG-dependent dioxygenases, resulting in hypermethylation of DNA and histones in tumors exhibiting loss of *FH* or *SDH* (Hoekstra et al., 2015; Letouze et al., 2013; Xiao et al., 2012). Additionally, succinate and fumarate inhibit the prolyl hydroxylase domain-containing (PHD) enzymes that regulate stability of hypoxia-inducible factors (HIFs), such that *FH* and *SDH*-deficient cancers activate the hypoxic gene expression program even under normoxic conditions (Hewitson et al., 2007; Pollard et al., 2005; Selak et al., 2005). Both epigenetic changes and aberrant HIF activation can contribute to tumor initiation and progression in these cancers.

Loss of *FH* or *SDH* introduces vulnerabilities that may be amenable to therapeutic targeting. In silico modeling of metabolic networks suggests that FH-null cells can upregulate heme metabolism to enable their survival (Frezza et al., 2011). The heme biosynthesis pathway uses succinyl-CoA to generate heme (**Figure 5**), which can be degraded to bilirubin and excreted from cells, allowing cells to dispose of excess TCA cycle carbon. Thus, *FH*-null cells may increase flux through this pathway as a means to allow partial TCA cycle activity. Consequently, *FH* deletion renders mouse and human cells more sensitive to genetic and pharmacological inhibition of heme oxygenase 1 (HMOX1), an enzyme involved in heme degradation.

Another potentially targetable metabolic liability of renal cell cancers that have lost *FH* expression is a dependence on exogenous arginine. The high levels of fumarate resulting from *FH* deficiency drives argininosuccinate lyase (ASL) and argininosuccinate synthase (ASS1) in a direction that consumes arginine (**Figure 7**). Depletion of intracellular arginine causes these cells to become arginine auxotrophs (Adam et al., 2013; Zheng et al., 2013), and therapies that deplete exogenous arginine (**Table 1**) may be effective in treating malignancies where *FH* is lost (Phillips et al., 2013).

Loss of *SDH* also results in TCA cycle dysfunction, leading to the accumulation of succinate and depletion of aspartate, fumarate, citrate, and malate. In this context, aspartate cannot be synthesized from glutamine or other sources of αKG, and aspartate production is dependent on pyruvate carboxylase (PC) activity. PC catalyzes carboxylation of pyruvate to oxaloacetate (**Figure 5**), which can then undergo transamination to form aspartate (**Figure 7**). To cope with TCA cycle truncation and still produce aspartate, *SDH* defective cells upregulate PC protein expression in culture and in tumors to synthesize aspartate from glucose (Cardaci et al., 2015; Lussey-Lepoutre et al., 2015). *PC* ablation impairs *SDH*-deficient cell proliferation and tumor formation, and thus targeting PC might be exploited to treat these types of cancers.

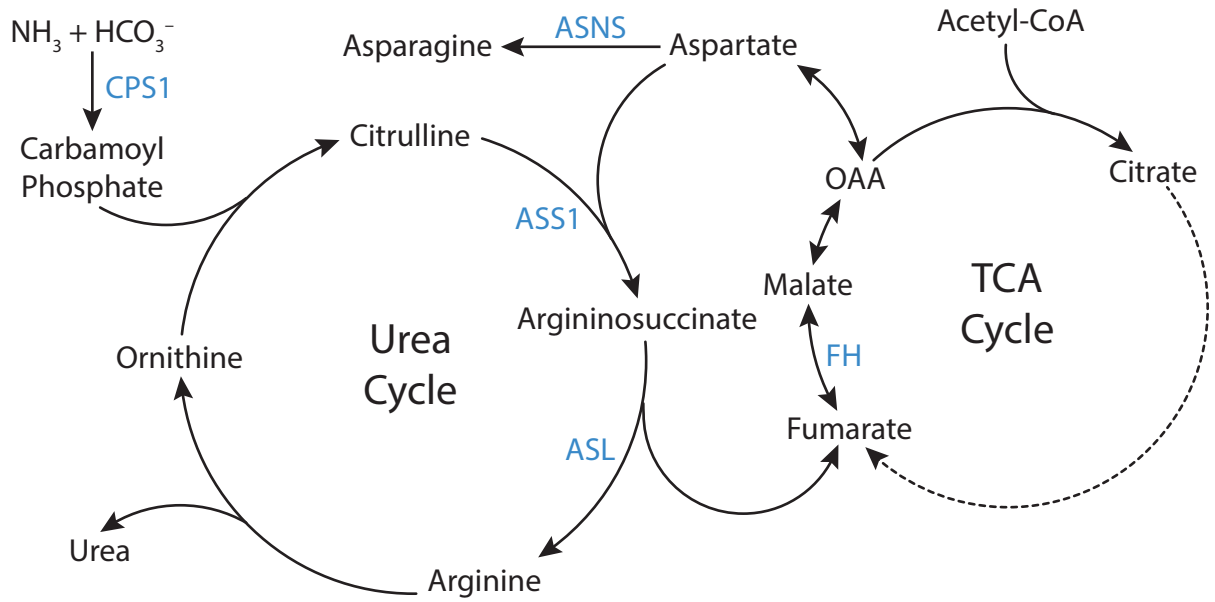

Figure 7. Urea Cycle

The urea cycle permits excretion of excess nitrogen as urea. Carbamoyl phosphate is synthesized from ammonia and bicarbonate by the enzyme carbamoyl phosphate synthetase 1 (CPS1), and subsequently carbamoyl phosphate and ornithine are used to produce citrulline. The enzyme argininosuccinate synthase (ASS1) condenses citrulline with aspartate to form argininosuccinate, which is then cleaved to arginine and fumarate by argininosuccinate lyase (ASL). Arginine is then hydrolyzed to produce urea and regenerate ornithine, completing the cycle. Fumarate produced by the urea cycle can regenerate aspartate via enzymes involved in the tricarboxylic acid (TCA) cycle as shown. Asparagine synthetase (ASNS) catalyzes production of asparagine from aspartate.

Loss of argininosuccinate synthase 1 expression

Somatic loss of metabolic enzyme expression may be selected for in other tumor types. For example, some melanoma, lymphoma, glioma, and prostate cancers reduce or lose the expression of the urea cycle enzyme argininosuccinate synthase 1 (*ASS1*) (Delage et al., 2010). As noted above, ASS1 is involved in arginine synthesis, catalyzing the conversion of citrulline and aspartate to the arginine precursor argininosuccinate (**Figure 7**). Genetic or epigenetic silencing of *ASS1* provides an advantage to tumor cells by allowing them to preserve cellular aspartate (Rabinovich et al., 2015), a poorly transported nutrient that can be a critical output of the TCA cycle to support de novo nucleotide synthesis and cell proliferation (Birsoy et al., 2015; Sullivan et al., 2015).

A potential liability of *ASS1*-deficient cancers is that, like *FH*-null cancers, they are unable to synthesize arginine de novo. As functional arginine auxotrophs, these cells are reliant on exogenous arginine for proliferation and survival and may be sensitive to therapies that lower arginine availability (**Table 1**). Arginine deiminase (ADI) is a microbial enzyme that catabolizes arginine and can be used to deplete extracellular arginine levels. Recombinant pegylated arginine deiminase (ADI-PEG20) has been tested in clinical trials to treat melanoma and hepatocellular carcinoma with some therapeutic benefit (Ascierto et al., 2005; Izzo et al., 2004; Ott et al., 2013; Szlosarek et al., 2013; Yang et al., 2010). However, the use of arginine-catabolizing enzymes may not be an effective therapeutic strategy for all *ASS1*-deficient cancers, as some ADI-treated tumors have been found to re-express *ASS1*

(Feun et al., 2012; Long et al., 2013; Shen et al., 2003). Whether some tumors require loss of *ASS1* expression to proliferate is an area of active investigation, as these may be more responsive to arginine depleting drugs. The combination of arginine depletion with other therapies might also limit resistance, and the identification of synthetic lethal targets with *ASS1*-loss is another approach being evaluated to increase the clinical efficacy of therapies that deplete circulating arginine (Bean et al., 2016; Kremer et al., 2017; Locke et al., 2016).

Metabolic collateral lethality

Loss of metabolic enzyme expression can also occur as a passenger event. For example, genomic deletions leading to loss of tumor suppressor genes can also lead to loss of adjacent non-essential metabolic genes. Because cells often exhibit redundancy in essential pathways, this phenomenon can introduce a therapeutic opportunity to target cancer cells that has been termed collateral lethality (Muller et al., 2015). Pancreatic ductal adenocarcinoma (PDAC) cells exhibiting homozygous deletion of the tumor suppressor *SMAD4* often lose malic enzyme 2 (*ME2*) expression due to the chromosomal proximity of the two genes. Targeting the malic enzyme 3 (ME3) isoform was found to impair tumor proliferation of PDAC xenografts lacking *ME2* expression, but had no effect on tumors with intact *ME2* (Dey et al., 2017). Similarly, the gene encoding enolase 1 (*ENO1*) is on the tumor-suppressor locus 1p36, and undergoes homozygous deletion in 1-5% of GBM cancers. Knockdown of enolase 2 (*ENO2*) in *ENO1*-null GBM cells resulted in significant

inhibition of proliferation and intracranial tumorigenesis, whereas *ENO1* expressing cancer cells were insensitive to *ENO2* ablation. Furthermore, *ENO1* loss results in extreme sensitivity to the pan-enolase inhibitor phosphonoacetohydroxamate (PHAH) and SF2312 (Leonard et al., 2016; Muller et al., 2012). In both examples, decreased metabolic enzyme redundancy rendered the cells dependent on a specific isoform of an enzyme that could be selectively targeted. It also decreases total cellular levels of enzymatic activity for a given reaction, thereby lowering the threshold for toxicity for targeting the corresponding enzyme.

Passenger deletion of metabolic genes can introduce vulnerabilities involving other pathways as well. Deletion of the tumor suppressor *CDKN2A* results in concomitant deletion of the gene encoding the methionine salvage pathway enzyme methylthioadenosine phosphorylase (*MTAP*) in many cancers, including 53% of glioblastomas and 26% of pancreatic cancers (Mavrakis et al., 2016). MTAP cleaves methylthioadenosine (MTA), a product of polyamine biosynthesis, into 5-methylthioribose-1-phosphate (MTR) and adenine, which are further metabolized to methionine and adenosine monophosphate (AMP), respectively (**Figure 8**). *MTAP*-deficient cells require de novo purine synthesis to generate AMP, since they are unable to cleave MTA to salvage adenine, and thus *MTAP* loss makes cells more susceptible to inhibitors of purine biosynthesis as well as to methionine depletion (Hori et al., 1996). Co-administration of MTA with toxic adenosine analogues has been shown to be selectively lethal to *MTAP*-null cancer cells, since normal tissues expressing MTAP are able to convert MTA to adenine to competitively inhibit the

effects of the analogues (Lubin and Lubin, 2009). L-alanosine inhibits conversion of inosine monophosphate (IMP) to AMP, and shows selective toxicity towards *MTAP*-null cancer cells (Batova et al., 1999; Efferth et al., 2003; Harasawa et al., 2002), but was found to be clinically ineffective in patients with advanced *MTAP*-deficient tumors in a Phase II trial (Kindler et al., 2009). Pharmacokinetic analyses confirming successful purine biosynthesis inhibition by doses of L-alanosine used in the study were not reported, so further exploration of why this approach failed may yield insight into how best to exploit *MTAP* deficiency.

Loss of *MTAP* expression can introduce another vulnerability to cancers because MTA that accumulates following *MTAP* loss can act as a potent inhibitor of the enzyme arginine methyltransferase 5 (PRMT5). *MTA*P loss results in reduced PRMT5 activity and renders *MTAP*-null cancer cell more sensitive to PRMT5 depletion than isogenic counterparts that express MTAP (Kryukov et al., 2016; Marjon et al., 2016; Mavrakis et al., 2016). Additionally, ablation of methionine adenosyltransferase II alpha (MAT2A), the enzyme that produces the canonical and high-affinity PRMT5 substrate, S-adenosylmethionine (SAM), also reduces PRMT5-dependent methylation and proliferation in *MTAP*-deleted cancer cells (Marjon et al., 2016). However, PRMT5 inhibitors in current clinical trials may not be effective in *MTAP*-null cancers, in part because the high levels of MTA in these cells compete for binding with inhibitors to the enzyme. Future studies will better define whether reducing PRMT5 activity using drugs that act via a different mechanism could be used as effective treatments in tumors where *MTAP* is co-deleted with *CDKN2A*.

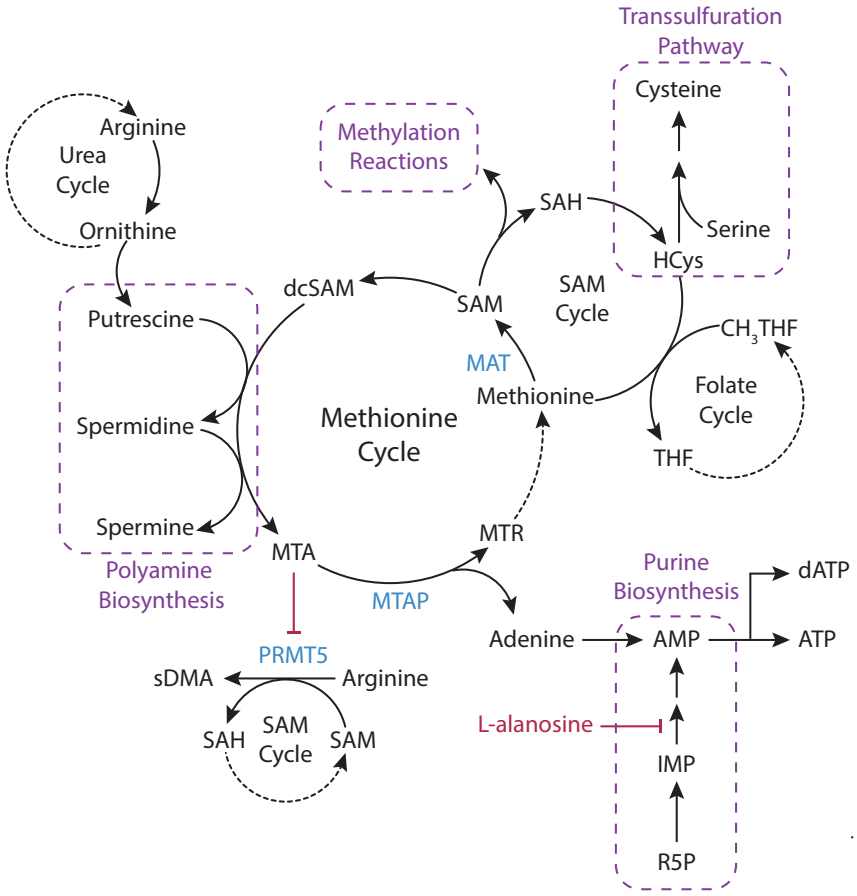

Figure 8. Methionine Cycle

Methionine is an essential amino acid used for methylation reactions, cysteine synthesis, and polyamine generation. Methionine adenosyltransferase (MAT) converts methionine to S-adenosylmethionine (SAM). Methyl transferases use SAM as the methyl donor for methylation reactions. Demethylation of SAM generates S-adenosylhomocysteine (SAH), which is hydrolyzed to homocysteine (HCys) and adenosine. Methionine is regenerated from HCys by transfer of the methyl group from N^5-methyl-THF (CH_3-THF). HCys is also an intermediate of cysteine synthesis, where serine and HCys condense to form cysteine by the transsulfuration pathway. SAM can also support polyamine synthesis when SAM is converted to decarboxylated SAM(dcSAM). Together with the urea cycle metabolite ornithine, this compound generates putrescine and subsequently spermine and spermidine. In these reactions, dcSAM is converted to 5'-methylthioadenosine (MTA). MTA accumulation inhibits the enzyme protein arginine N-methyltrasferase 5 (PRMT5), which uses SAM as a methyl donor to synthesize symmetrical dimethylarginine (sDMA) from arginine. MTA is cleaved to 5-methylthioribose-1-phosphate (MTR) and adenine in the methionine cycle by the enzyme methylthioadenosine phosphorylase (MTAP). Adenine can be converted to AMP, and the adenosine analogue L-alanosine can limit AMP production via the purine synthesis pathway. MTR can be converted to methionine, completing the methionine cycle.

Emerging Metabolic Targets

Numerous metabolic differences between cancer cells and normal cells have been described. Some recent examples to illustrate how these differences might be exploited for therapy are highlighted, but many other targets have been proposed and are discussed in detail elsewhere (Bobrovnikova-Marjon and Hurov, 2014; Galluzzi et al., 2013; Martinez-Outschoorn et al., 2017).

Targeting de novo lipid synthesis

Several lines of evidence suggest that targeting de novo fatty acid synthesis might be effective in the treatment of some cancers. Fatty acids are a key component of cell membranes and can also act as signaling molecules or store energy. It was first discovered in the 1950s that tumors are able to synthesize lipids, and a subsequent study determined that the large majority of lipids in tumor cells are synthesized de novo, rather than being obtained from exogenous sources (Medes et al., 1953; Ookhtens et al., 1984). Since then, numerous studies have identified de novo fatty acid biosynthesis as a key metabolic requirement for some cancers, and it has been dubbed by some as a distinct metabolic "hallmark of the transformed phenotype" (Kuhajda et al., 1994; Menendez and Lupu, 2006; Röhrig and Schulze, 2016). With the exception of liver, adipose tissue, and lactating breast, adult tissues do not synthesize fatty acids de novo under normal physiological conditions (Menendez and Lupu, 2006), so inhibition of de novo fatty acid synthesis might have an adequate therapeutic window.

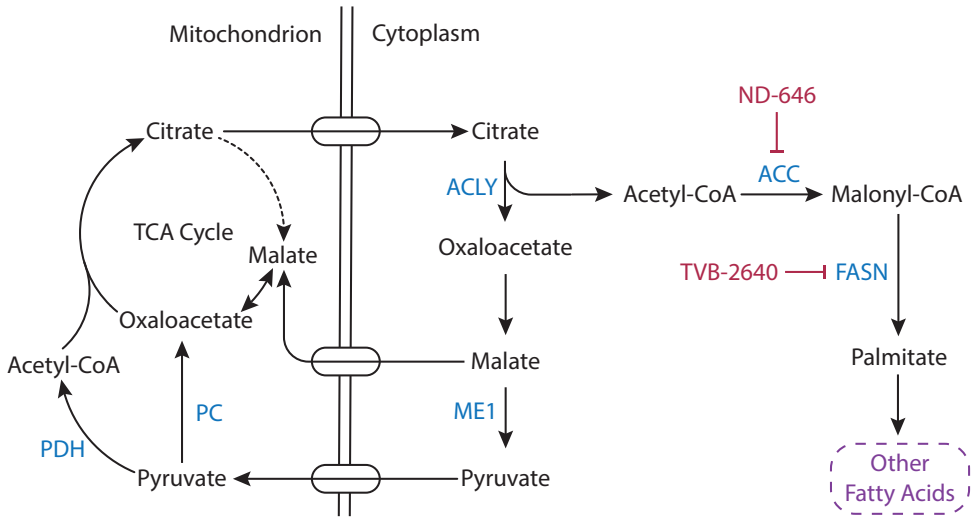

Figure 9. Fatty Acid Synthesis

Citrate is a carrier of acetyl groups from the mitochondria to the cytoplasm to support fatty acid synthesis. Mitochondrial citrate is transported into the cytosol where ATP citrate lyase (ACLY) cleaves citrate to acetyl-CoA and oxaloacetate. Oxaloacetate is converted to malate, and malate can be transported back into the mitochondrial matrix or can be converted into pyruvate in the cytoplasm by malic enzyme 1 (ME1). Cytosolic acetyl-CoA contributes to fatty acid synthesis. First, the enzyme acetyl-CoA carboxylase (ACC) catalyzes carboxylation of acetyl CoA to malonyl CoA. Fatty acid synthase (FASN) then uses malonyl-CoA to sequentially add two carbon units to a growing acyl chain and synthesize the saturated 16-carbon fatty acid palmitate, which serves as a precursor to other fatty acids. The compound ND-464 and TVB-2640 are inhibitors of ACC and FASN, respectively.

Fatty acid synthesis is a multi-step process that primarily occurs in the cytosol of cells. First, acetyl-CoA groups are converted to malonyl-CoA via the enzyme acetyl-CoA carboxylase (ACC). Next, the multidomain enzyme fatty acid synthase (FASN) assembles the fatty acid chain palmitate from malonyl-CoA. Although fatty acid synthesis occurs in the cytosol, cytosolic acetyl-CoA is produced from mitochondrial citrate, which is exported from mitochondria and cleaved by cytosolic ATP-citrate lyase (ACLY) (**Figure 9**). Cancer cells are also able to generate acetyl-CoA from cytosolic acetate (Comerford et al., 2014; Gao et al., 2016; Kamphorst et al., 2014; Mashimo et al., 2014). However, acetate is not always abundant in blood and is not the predominate source of acetyl-CoA used for fatty acid synthesis in some cells (Hosios and Vander Heiden, 2014). Certain cancers are nevertheless dependent on expression of acetyl-CoA synthetase 2 (ACSS2), the cytosolic enzyme that allows cells to synthesize acetyl-CoA from acetate, making this a potential therapeutic target (Comerford et al., 2014; Schug et al., 2015).

Numerous inhibitors have been developed to target fatty acid synthesis, with attempts to limit cytosolic acetyl-CoA availability via ACLY inhibition as well as direct targeting of the enzymes ACC and FASN (**Figure 9**). ACLY activity is elevated in cancers (Migita et al., 2008), and targeting ACLY genetically or chemically prevents xenograft tumor formation and proliferation (Adam et al., 2013; Bauer et al., 2005; Hatzivassiliou et al., 2005; Migita et al., 2008). Genetic knockdown of ACC induces apoptosis in cancer cell lines (Brusselmans et al., 2005; Chajes et al., 2006), and an allosteric inhibitor of ACC, ND-646, has shown

antitumor efficacy in autochthonous mouse lung tumor models (Svensson et al., 2016). Targeting FASN has been found to reduce palmitoylation of tubulin and disrupt microtubule organization, inhibiting tumor cell growth (Heuer et al., 2017). The compound TVB-2640 is the first compound targeting FASN to enter clinical trials (**Table 1**), and when combined with paclitaxel, can cause partial responses or prolonged stable disease (Brenner et al., 2017).

Differential requirements for NAD+/NADH homeostasis

Warburg's observation that cancer cells have dramatically increased glucose consumption and lactate production, even in the presence of oxygen, led to the hypothesis that cancer cells have diminished mitochondrial function (Warburg, 1956). However, subsequent work determined that despite engaging in aerobic glycolysis, cancer cells consume oxygen at levels comparable to normal tissue (Weinhouse, 1956; Zu and Guppy, 2004). Moreover, inhibitors of cellular respiration block proliferation, suggesting that most cancer cells require respiration in order to proliferate (Harris, 1980; Howell and Sager, 1979; Kroll et al., 1983; Loffer and Schneider, 1982; Zhang et al., 2014b). Respiration is also needed for tumor initiation, as tumor cells with impaired oxidative phosphorylation due to depletion of mitochondrial DNA (mtDNA) exhibit increased tumor latency upon subcutaneous transplantation. In fact, cells derived from these tumors acquire host mtDNA to regain the ability carry out respiration, providing compelling evidence that

mitochondrial respiration is required and selected for in tumorigenesis (Tan et al., 2015a).

Most cells in the body generate ATP via respiration, so targeting this process might be expected to be toxic with a limited therapeutic window. However, metformin, one of the commonly prescribed drugs for treating type II diabetes, is safe despite acting as a mitochondrial complex I inhibitor that impairs respiration (Bridges et al., 2014; El-Mir et al., 2000; Owen et al., 2000; Wheaton et al., 2014). Furthermore, retrospective clinical studies have found that metformin use is associated with improved cancer outcomes, reductions in cancer incidence, and decreased cancer mortality (Evans et al., 2005; Franciosi et al., 2013; Gandini et al., 2014; Lee et al., 2012; Noto et al., 2012). Metformin has also been found to cooperate with neo-adjuvant chemotherapy to result in complete tumor regression in some breast cancer patients (Jiralerspong et al., 2009).

The anti-tumorigenic properties of metformin and other biguanides have been modeled in various mouse cancer models (Buzzai et al., 2007; Huang et al., 2008; Shackelford et al., 2013; Wheaton et al., 2014). Although the precise mechanism of metformin action remains controversial (Luengo et al., 2014), recent work has shown that the anti-tumorigenic effect of metformin can at least be partially accounted for by direct mitochondrial complex I inhibition in tumors (Gui et al., 2016; Wheaton et al., 2014). Consistent with this notion, other complex I inhibitors have shown efficacy as anti-tumor agents (Appleyard et al., 2012; Schockel et al., 2015) and may show selective toxicity against oncogene-ablation

resistant cells (Viale et al., 2014) and cancer stem cells (Sancho et al., 2015). Additional complex I inhibitors are under development (Bastian et al., 2017), and other inhibitors of respiration or mitochondrial metabolism, including the lipoic acid derivative CPI-613 (Table 1), are currently being assessed in clinical trials (Lycan et al., 2016; Pardee et al., 2014).

Recent work has shed some light on the potential therapeutic window for treating tumors with respiration inhibitors. Mitochondria are viewed as the powerhouse of the cell, with respiration considered primarily as an ATP-producing catabolic process. However, mitochondrial ATP production appears dispensable for many proliferating cells (Birsoy et al., 2015; Sullivan et al., 2015; Titov et al., 2016). Instead, respiration serves an alternative anabolic role for proliferating cells by regenerating the oxidized form of nicotinamide adenine dinucleotide (NAD+) from the reduced form (NADH) (Birsoy et al., 2015; Sullivan et al., 2015; Titov et al., 2016). Maintenance of intracellular NAD+ is required for many cellular processes, including protein deacetylation, ADP-ribosylation and calcium signaling (Chiarugi et al., 2012). Additionally, NAD+ serves as a critical redox cofactor required to generate oxidized molecules, such as amino acids and nucleotides necessary for biomass accumulation (Birsoy et al., 2015; Sullivan et al., 2015; Titov et al., 2016). Proliferating cells often require a high NAD+/NADH ratio to support anabolic reactions and in some contexts the NAD+/NADH ratio directly correlates with proliferation rate (Gui et al., 2016). Higher NAD+/NADH ratios appear important for proliferation while lower ratios favor mitochondrial ATP production. Thus, one

possible explanation for the potential therapeutic window of respiration inhibitors is that the regime in which NAD+/NADH required for proliferation of tumor cells is distinct from that which is required to maintain ATP production in normal cells.

Targeting NAD+ synthesis could be another mechanism to limit NAD+ pools and target proliferative metabolism. NAD+ is produced via multiple synthesis and salvage pathways, but a major source of NAD+ in proliferating cells is salvage from nicotinamide. The rate-limiting enzyme in this pathway is nicotinamide phosphoribosyltransferase (NAMPT), which is highly expressed in tumors arising from diverse tissues. Small-molecules targeting NAMPT can be effective anti-tumor agents in vitro and in xenograft cancer models (Nahimana et al., 2009; Tan et al., 2015b; Watson et al., 2009). In clinical trials, use of these inhibitors as single agents has not caused tumor remission (von Heideman et al., 2010), but additional studies may uncover how best to safely use these drugs for patient benefit. For example, NAMPT inhibitors may be more effective in contexts of *MYC*-amplified glioblastoma (Tateishi et al., 2016) or when used in combination with other drugs known to deplete NAD+ pools (Bajrami et al., 2012; Chan et al., 2014).

Targeting nucleotide acquisition and synthesis

Acquiring nucleotides is critical for cell proliferation. Nucleic acids can be synthesized de novo or scavenged from the environment. Though nucleotide salvage pathways can support tumor cell proliferation in certain contexts (Tabata et al., 2017), concentrations of circulating nucleotides are likely too low for many tumors

to satisfy their nucleotides demand via salvage alone (Traut, 1994). Nevertheless, the ability of some tumor cells to scavenge nucleotides is exploited for cancer therapy. While most cells are able to scavenge the epigenetically modified cytosine bases 5-hydroxymethyl-2'deoxycytidine (5hmdC) and 5-formy-2'deoxycytidine (5fdC) and incorporate these bases into the DNA without compromising genome integrity, cancer cell lines overexpressing cytidine deaminase (CDA) convert these bases to the corresponding modified uracil analogues, which induce cytotoxicity when incorporated into DNA (Zauri et al., 2015). Thus, administering 5hmdC and 5fdC may selectively target tumors overexpressing CDA.

The clinical success of some antimetabolites argues select tumors are reliant on de novo nucleotide synthesis. Nucleotide biosynthesis interfaces with other metabolic pathways; ribose is synthesized from glucose via the pentose phosphate pathway and nucleotide bases require carbon atoms from amino acids and the one-carbon pool as well as nitrogen atoms from aspartate and glutamine. Consequently, targeting amino acid and folate metabolism can affect nucleotide production. For example, eliminating environmental serine, limiting aspartate synthesis via mitochondrial inhibition, and ablating the mitochondrial folate pathway impairs purine biosynthesis (Ducker et al., 2016; Labuschagne et al., 2014; Sullivan et al., 2015). This raises the possibility that these interventions can widen the therapeutic window of established antimetabolites, and future studies will determine whether targeting these pathways is synergistic with existing antimetabolite therapies in certain contexts.

Nucleotide production is downstream of some oncogenic signaling pathways. Activation of mTOR can increase ribose synthesis via the oxidative pentose phosphate pathway (Duvel et al., 2010) and enhance flux through the pyrimidine and purine synthesis pathways (Ben-Sahra et al., 2013; Ben-Sahra et al., 2016; Robitaille et al., 2013), suggesting that targeting nucleotide metabolism in tumors exhibiting mTOR hyperactivation may be more effective. *PTEN*-deficient cells, which have active mTOR signaling, are more sensitive to inhibition of DHODH by brequinar and leflunomide (Mathur et al., 2017). Conversely, inhibiting oncogenic signaling using PI3K inhibitors has been found to deplete DNA nucleotides, decrease DNA synthesis, and cause DNA damage (Juvekar et al., 2016). Lung cancer cells with oncogenic *KRAS* plus *LKB1* loss are more reliant on the urea cycle enzyme carbamoyl phosphate synthetase-1 (CPS1) for pyrimidine biosynthesis, although this dependency is independent of mTOR signaling (Kim et al., 2017).

Increased requirement for detoxification of reactive metabolites

Cancer cells generally have increased levels of reactive metabolites (DeBerardinis and Chandel, 2016; Sullivan et al., 2016). These metabolites can be formed as error products of metabolic enzymes or can be formed non-enzymatically due to the intrinsic reactivity of certain metabolic intermediates. Some of these byproducts, including reactive oxygen species (ROS) and methylglyoxal, are themselves chemically unstable and, thus, can covalently modify amino acids and nucleic acids. While elevation of reactive metabolites can support oncogenesis in

some contexts (Arnold et al., 2001; Irani et al., 1997; Suh et al., 1999; Weinberg et al., 2010), at high levels reactive metabolites become toxic and kill cells due to the resulting damage to the proteome and genome (Karisch et al., 2011; Rabbani and Thornalley, 2014). Cancer cells rely on several pathways to prevent reactive metabolite accumulation. For example, the transcription factor NRF2, which mediates an antioxidant response program to detoxify ROS, is downstream of several oncogenic drivers, and loss of NRF2 in this context can impair tumor proliferation (Chio et al., 2016; DeNicola et al., 2011). Disruption of this and other detoxification pathways is predicted to have a more deleterious effect on cancer cells than normal cells, and thus serves as a potential targetable metabolic liability.

An alternative strategy for exploiting the increased production of reactive metabolites observed in cancer cells is to target the synthesis or utilization of antioxidants such as glutathione. Glutathione is a cysteine-containing tripeptide that plays a crucial role in many detoxification pathways. It is one of the most abundant metabolites in the cell and serves to reduce the levels of reactive metabolites by serving as a substrate for electrophilic attack. Several screens for small-molecules that selectively kill transformed cells have identified compounds that reduce glutathione levels (Dolma et al., 2003; Raj et al., 2011; Trachootham et al., 2006), and genetic or pharmacological inhibition of glutathione synthesis results in ROS accumulation and impedes cancer initiation and cell proliferation (Harris et al., 2015; Lien et al., 2016). Therapeutic interventions that decrease intracellular glutathione levels, such as administration of the oxidized form of vitamin C,

dehydroascorbate (DHA), can result in cancer cell death and impaired tumor progression (Yun et al., 2015)

Another way to deplete intracellular glutathione is by limiting availability of the amino acid cysteine, the key reactive residue of glutathione that is required for its synthesis. Many cancer cells are auxotrophic for this amino acid, and lowering whole body cysteine levels with bacterial cysteineases is a potential cancer treatment being evaluated in clinical trials (Graczyk-Jarzynka et al., 2017). Targeting the cystine and glutamate transporter xCT (SLC7A11) is another approach to limit intracellular cysteine availability and prevent cysteine-dependent glutathione synthesis. Inhibitors of this transporter have been found to deplete intracellular glutathione in cancer cells, resulting in iron-dependent accumulation of ROS and a form of cell death termed ferroptosis (Dixon et al., 2012; Dixon et al., 2014; Yang et al., 2014).

Lineage and Environment Specific Vulnerabilities:

Analysis of gene expression across different cancer types has determined that metabolic enzyme expression is heterogeneous across tumors, and there is no universal metabolic transformation common to all cancers. In fact, tumors retain many features that correspond to their parental normal tissue (Gaude and Frezza, 2016; Hu et al., 2013). It is not known whether this effect results from rigid lineage-specific metabolic expression programs or from the similar local microenvironment experienced by the tumor and normal tissue. However, these analyses suggest that

metabolic vulnerabilities may not be universal across all cancers and highlight the possibility that some metabolic dependencies of cancer may be modulated by environment or defined by tumor lineage.

Differential utilization of amino acids

Acquisition of amino acids is an important biosynthetic requirement for cancer cells to support proliferation (Hosios et al., 2016). How cells acquire amino acids can vary according to cell type and environment, and therefore targeting amino acid metabolism could offer a therapeutic window for cancer treatment (Yuneva et al., 2012). Recently, it has been determined that mouse lung and pancreatic tumors exhibit differences in amino acid metabolism, even when harboring the same genetic lesion. Lung tumors support their nitrogen requirement by catabolizing free branched chain amino acids (BCAA), whereas pancreatic tumors expressing the same driver mutation do not. Targeting BCAA transaminases inhibits lung tumor formation better than pancreatic tumor formation, suggesting that dependence on branched chain amino acid catabolism is determined by cell lineage rather than by tumor site (Mayers et al., 2016). Tumors of other lineages are also dependent on BCAA transaminases, including some glioblastomas and blast crisis chronic myeloid leukemia (Hattori et al., 2017; Tonjes et al., 2013). Together, these observations suggest that tissue-of-origin can influence metabolic requirements and vulnerabilities.

Asparagine auxotrophy in acute lymphoblastic leukemia

The non-essential amino acid asparagine is abundant in plasma and can also be synthesized by many cell types, so asparagine is dispensable for most cells. Acute lymphoblastic leukemia (ALL) and related lymphomas, however, are auxotrophic for asparagine (Neuman and McCoy, 1956). Bacterial L-asparaginase deamidates asparagine to aspartic acid, thereby limiting the availability of asparagine for cancer cells. L-asparaginase has been found to be effective in the treatment of ALL and is included in standard chemotherapy regimens for this disease (**Table 1**) (Egler et al., 2016). Though the mechanism of asparagine auxotrophy in ALL cells was assumed to be genetically defined, studies have shown that clinical response to L-asparaginase treatment is independent of asparagine synthase (ASNS) expression, the enzyme that converts aspartate to asparagine (**Figure 7**) (Appel et al., 2006; Stams et al., 2003). In fact, genome-wide analysis has shown that there is no consistent gene expression pattern that dictates sensitivity to L-asparaginase (Fine et al., 2005). The absence of a genetic driver for asparagine auxotrophy, combined with the fact that L-asparaginase has little known clinical utility outside of the context of ALL, suggests that this metabolic vulnerability may be lineage dependent.

Inducing differentiation in myeloid cells

A common feature of acute myeloid leukemia (AML) is that leukemic myeloblasts arrest at an immature stage of differentiation. This differentiation

blockade is a hallmark of AML even though there are multiple driver mutations for this disease. Inhibitors of mutant IDH1 or IDH2 have been shown to induce differentiation in AML cells harboring mutant *IDH* (Okoye-Okafor et al., 2015; Wang et al., 2013). The transcription factor HOXA9 is overexpressed in 70% of AML cases, and overexpression of this transcription factor alone is sufficient to immortalize murine bone marrow derived myeloid cells (Ayton and Cleary, 2003; Golub et al., 1999; Kroon et al., 1998). Recently, a myeloid cell screen involving HOXA9-enforced differentiation arrest found that inhibition of dihydroorotate dehydrogenase (DHODH), an enzyme in the pyrimidine biosynthesis pathway (**Figure 1B**), can induce differentiation (Sykes et al., 2016). Targeting DHODH depletes uridine and downstream metabolites, and providing uridine is sufficient to maintain myeloid arrest, even in the presence of compounds targeting DHODH. Treatment with brequinar sodium (BRQ), an inhibitor of DHODH that is approved to treat autoimmune disease, is able to overcome myeloid differentiation blockade and reduces leukemic cell burden in patient-derived xenografts and syngeneic mouse AML models of diverse genetic subtypes. BRQ was previously evaluated to treat advanced solid tumors but was not shown to be effective in clinical trials (Arteaga et al., 1989; Noe et al., 1990; Peters et al., 1990). However, the effect of BRQ on patients with hematologic malignancies has not yet been evaluated. Future trials will determine whether targeting DHODH could exploit a cell lineage-dependent liability in hematological malignancies.

Non-tumor cells can influence tumor cell metabolism

Metabolic symbiosis likely exists between tumor cells and the surrounding stroma, and this interaction could also contribute to tumor growth and proliferation. Typically, lactate is excreted at high rates by tumor cells, but lactate has also been described as an oxidative substrate for some cancers. It has been reported that lactate produced by cancer-associated fibroblasts can enter the TCA cycle of cancer cells (Bonuccelli et al., 2014; Witkiewicz et al., 2012), and lactate produced in hypoxic regions of a tumor can fuel respiration in well-oxygenated tumor cells (Kennedy et al., 2013; Sonveaux et al., 2008). Intraoperative isotopically-labeled glucose infusions performed on non-small cell lung cancer patients revealed higher contribution of glucose carbon to TCA intermediates than glycolytic intermediates in tumors, leading the authors to conclude that lactate could serve as an anaplerotic substrate in this context as well (Hensley et al., 2016; Faubert et al. 2017). Lactate utilization by tumors is dependent on monocarboxylate transporters (MCTs) (**Figure 3**), which are highly expressed in a variety of tumors (Pinheiro et al., 2012). Compounds targeting MCT1 are currently being evaluated for antitumor efficacy (**Table 1**) (Marchiq and Pouyssegur, 2016).

Alanine is rarely limiting for proliferation, as cancer cells typically excrete, rather than consume, alanine (DeBerardinis et al., 2007; Hosios et al., 2016; Jain et al., 2012). However, in some contexts cells may not synthesize alanine in excess of their biosynthetic requirements. Pancreatic ductal adenocarcinoma cells can consume alanine produced by pancreatic stellate cells in vitro, and the secreted

alanine appears to help promote tumor cell proliferation and survival under nutrient-limited conditions (Sousa et al., 2016). An improved understanding of the interaction between PDAC tumors and stroma can help determine the metabolic limitations of pancreatic tumor growth, and guide target selection to exploit this symbiotic relationship for therapy.

Metabolic dependencies can be modulated by environment

Differences in nutrient availability may contribute to sensitivity or resistance of cancer cells to some drugs. For example, most cells in culture rely on glutamine metabolism, but targeting glutaminase is not an effective cancer therapy in all contexts. Glutamine tracing studies have demonstrated that in some tumor tissues, glutamine contributes minimally to TCA cycle intermediates, and those cancers can be resistant to glutaminase inhibition (Davidson et al., 2016; Hensley et al., 2016; Marin-Valencia et al., 2012; Sellers et al., 2015; Tardito et al., 2015). Importantly, cell lines derived from resistant lung tumors become sensitive to glutaminase inhibition in vitro, highlighting that environment can be a contributor to glutaminase sensitivity (Davidson et al., 2016). What factors determine the differential use of glutamine in different environments remains an active question, although environmental cystine can influence glutamine anaplerosis via xCT (Muir et al., 2017). Targeting redox is another example where environment can influence drug efficacy, as altering culture media conditions is sufficient to change cancer cell sensitivity to metformin (Gui et al., 2016). Metabolite levels can also influence the

amount of nucleotide synthesis (Cantor et al., 2017), highlighting the importance of environment in modulating metabolic dependencies.

What Dictates Metabolic Dependencies?

One of the biggest hurdles for cancer drug development is identifying the patients most likely to respond to a given therapy. With the recent success of some targeted cancer therapies, patient selection for drugs is often predicated on expression of an oncogene or the increased activity of a downstream signaling pathway. However, this same approach may not identify responders for all metabolic cancer therapies and response to chemotherapies that target metabolism has not been well predicted by this approach. The protein targets of methotrexate and 5-FU are present in almost all cancers, but the efficacy of these drugs varies dramatically across malignancies. Many of the emerging metabolic targets discussed in this thesis chapter are also expressed widely in cancer, but dependency on these metabolic pathways is not always universal. For example, while targeting ACC to limit fatty synthesis can suppress lung tumor progression in some models (Svensson et al., 2016), loss of ACC activity can accelerate tumor growth in other cancer models (Jeon et al., 2012). Similarly, many *PHGDH*-amplified tumors and cell lines are sensitive to genetic or pharmacological inhibition of the enzyme (Locasale et al., 2011; Mullarky et al., 2016; Pacold et al., 2016; Possemato et al., 2011; Wang et al., 2017; Zhang et al., 2017), but for some tumor models PHGDH expression can be dispensable for growth (Chen et al., 2013). Even among cancers

where mutant *IDH* is an oncogenic driver, sensitivity to mutant IDH inhibitors appears to differ between leukemia and solid tumor models (Tateishi et al., 2015; Turcan et al., 2013).

There is growing evidence that metabolic dependencies in cancer are influenced by tissue environment, cancer lineage, as well as genetic events. Cancer tissue-of-origin has served as a successful way to select patients for chemotherapies targeting metabolism for decades. Environment can also influence the efficacy of drugs targeting DHODH, mitochondrial complex I, and glutaminase, and using more physiological culture conditions can better define how nutrient levels influence cancer cell metabolism (Cantor et al., 2017; Davidson et al., 2016; Gui et al., 2016; Marin-Valencia et al., 2012; Muir et al., 2017; Sellers et al., 2015; Sykes et al., 2016; Tardito et al., 2015). Unraveling the complexity for how lineage, environment and genetics interact to create metabolic dependencies will be challenging, but may provide a path to exploit metabolism in a way that could be transformative for patients. Additionally, immunotherapies are playing an increasing role in cancer therapy, and immune cell fate can also be influenced by metabolism. Determining how immune cell metabolism interacts with tumor metabolism, and how this is modulated by drugs targeting metabolic enzymes, might aid in the design of more effective immunotherapies (Buck et al., 2017; Mockler et al., 2014).

Many drugs targeting metabolism are among the most effective clinical drugs for particular diseases, and many newer metabolic therapies are limited more by toxicities than by their ability to kill cancer cells. A better understanding of the

metabolic dependencies in specific tumor tissues holds the key for defining the aspects of metabolism most limiting for tumor growth and finding a therapeutic window to exploit those vulnerabilities for better cancer treatment.

References

Adam, J., Yang, M., Bauerschmidt, C., Kitagawa, M., O'Flaherty, L., Maheswaran, P., Ozkan, G., Sahgal, N., Baban, D., Kato, K., et al. (2013). A role for cytosolic fumarate hydratase in urea cycle metabolism and renal neoplasia. Cell Rep 3, 1440-1448.

Altman, B.J., Stine, Z.E., and Dang, C.V. (2016). From Krebs to clinic: glutamine metabolism to cancer therapy. Nat Rev Cancer 16, 619-634.

Anastasiou, D., Yu, Y., Israelsen, W.J., Jiang, J.K., Boxer, M.B., Hong, B.S., Tempel, W., Dimov, S., Shen, M., Jha, A., et al. (2012). Pyruvate kinase M2 activators promote tetramer formation and suppress tumorigenesis. Nat Chem Biol 8, 839-847.

Appel, I.M., den Boer, M.L., Meijerink, J.P., Veerman, A.J., Reniers, N.C., and Pieters, R. (2006). Up-regulation of asparagine synthetase expression is not linked to the clinical response L-asparaginase in pediatric acute lymphoblastic leukemia. Blood 107, 4244-4249.

Appleyard, M.V., Murray, K.E., Coates, P.J., Wullschleger, S., Bray, S.E., Kernohan, N.M., Fleming, S., Alessi, D.R., and Thompson, A.M. (2012). Phenformin as prophylaxis and therapy in breast cancer xenografts. Br J Cancer 106, 1117-1122.

Arnold, R.S., Shi, J., Murad, E., Whalen, A.M., Sun, C.Q., Polavarapu, R., Parthasarathy, S., Petros, J.A., and Lambeth, J.D. (2001). Hydrogen peroxide mediates the cell growth and transformation caused by the mitogenic oxidase Nox1. Proc Natl Acad Sci U S A 98, 5550-5555.

Arteaga, C.L., Brown, T.D., Kuhn, J.G., Shen, H.S., O'Rourke, T.J., Beougher, K., Brentzel, H.J., Von Hoff, D.D., and Weiss, G.R. (1989). Phase I clinical and pharmacokinetic trial of Brequinar sodium (DuP 785; NSC 368390). Cancer Res 49, 4648-4653.

Ascierto, P.A., Scala, S., Castello, G., Daponte, A., Simeone, E., Ottaiano, A., Beneduce, G., De Rosa, V., Izzo, F., Melucci, M.T., et al. (2005). Pegylated arginine deiminase treatment of patients with metastatic melanoma: results from phase I and II studies. J Clin Oncol 23, 7660-7668.

Ayton, P.M., and Cleary, M.L. (2003). Transformation of myeloid progenitors by MLL oncoproteins is dependent on Hoxa7 and Hoxa9. Genes Dev 17, 2298-2307.

Bajrami, I., Kigozi, A., Van Weverwijk, A., Brough, R., Frankum, J., Lord, C.J., and Ashworth, A. (2012). Synthetic lethality of PARP and NAMPT inhibition in triple-negative breast cancer cells. EMBO Mol Med 4, 1087-1096.

Bastian, A., Matsuzaki, S., Humphries, K.M., Pharaoh, G.A., Doshi, A., Zaware, N., Gangjee, A., and Ihnat, M.A. (2017). AG311, a small molecule inhibitor of complex I and hypoxia-induced HIF-1alpha stabilization. Cancer Lett 388, 149-157.

Batova, A., Diccianni, M.B., Omura-Minamisawa, M., Yu, J., Carrera, C.J., Bridgeman, L.J., Kung, F.H., Pullen, J., Amylon, M.D., and Yu, A.L. (1999). Use of alanosine as a methylthioadenosine phosphorylase-selective therapy for T-cell acute lymphoblastic leukemia in vitro. Cancer Res 59, 1492-1497.

Bauer, D.E., Hatzivassiliou, G., Zhao, F., Andreadis, C., and Thompson, C.B. (2005). ATP citrate lyase is an important component of cell growth and transformation. Oncogene 24, 6314-6322.

Baysal, B.E., Ferrell, R.E., Willett-Brozick, J.E., Lawrence, E.C., Myssiorek, D., Bosch, A., van der Mey, A., Taschner, P.E., Rubinstein, W.S., Myers, E.N., et al. (2000). Mutations in SDHD, a mitochondrial complex II gene, in hereditary paraganglioma. Science 287, 848-851.

Bean, G.R., Kremer, J.C., Prudner, B.C., Schenone, A.D., Yao, J.C., Schultze, M.B., Chen, D.Y., Tanas, M.R., Adkins, D.R., Bomalaski, J., et al. (2016). A metabolic synthetic lethal strategy with arginine deprivation and chloroquine leads to cell death in ASS1-deficient sarcomas. Cell Death Dis 7, e2406.

Ben-Sahra, I., Howell, J.J., Asara, J.M., and Manning, B.D. (2013). Stimulation of de novo pyrimidine synthesis by growth signaling through mTOR and S6K1. Science 339, 1323-1328.

Ben-Sahra, I., Hoxhaj, G., Ricoult, S.J.H., Asara, J.M., and Manning, B.D. (2016). mTORC1 induces purine synthesis through control of the mitochondrial tetrahydrofolate cycle. Science 351, 728-733.

Beroukhim, R., Mermel, C.H., Porter, D., Wei, G., Raychaudhuri, S., Donovan, J., Barretina, J., Boehm, J.S., Dobson, J., Urashima, M., et al. (2010). The landscape of somatic copy-number alteration across human cancers. Nature 463, 899-905.

Berti, V., Mosconi, L., and Pupi, A. (2014). Brain: normal variations and benign findings in fluorodeoxyglucose-PET/computed tomography imaging. PET Clin 9, 129-140.

Birsoy, K., Wang, T., Chen, W.W., Freinkman, E., Abu-Remaileh, M., and Sabatini, D.M. (2015). An Essential Role of the Mitochondrial Electron Transport Chain in Cell Proliferation Is to Enable Aspartate Synthesis. Cell 162, 540-551.

Bobrovnikova-Marjon, E., and Hurov, J.B. (2014). Targeting metabolic changes in cancer: novel therapeutic approaches. Annu Rev Med 65, 157-170.

Bonuccelli, G., Avnet, S., Grisendi, G., Salerno, M., Granchi, D., Dominici, M., Kusuzaki, K., and Baldini, N. (2014). Role of mesenchymal stem cells in osteosarcoma and metabolic reprogramming of tumor cells. Oncotarget 5, 7575-7588.

Brenner, A., Falchook, G., Patel, M., Infante, J., Arkenau, H.-T., Dean, E., Borazanci, E., Lopez, J., Moore, K., Schmid, P., et al. (2017). Abstract P6-11-09: Heavily pre-treated breast cancer patients show promising responses in the first in human study of the first-In-class fatty acid synthase (FASN) inhibitor, TVB-2640 in combination with paclitaxel. Cancer Research 77, P6-11-09-P16-11-09.

Bridges, H.R., Jones, A.J., Pollak, M.N., and Hirst, J. (2014). Effects of metformin and other biguanides on oxidative phosphorylation in mitochondria. Biochem J 462, 475-487.

Brown, K.K., Spinelli, J.B., Asara, J.M., and Toker, A. (2017). Adaptive Reprogramming of De Novo Pyrimidine Synthesis Is a Metabolic Vulnerability in Triple-Negative Breast Cancer. Cancer Discov 7, 391-399.

Brusselmans, K., De Schrijver, E., Verhoeven, G., and Swinnen, J.V. (2005). RNA interference-mediated silencing of the acetyl-CoA-carboxylase-alpha gene induces growth inhibition and apoptosis of prostate cancer cells. Cancer Res 65, 6719-6725.

Buck, M.D., Sowell, R.T., Kaech, S.M., and Pearce, E.L. (2017). Metabolic Instruction of Immunity. Cell 169, 570-586.

Buzzai, M., Jones, R.G., Amaravadi, R.K., Lum, J.J., DeBerardinis, R.J., Zhao, F., Viollet, B., and Thompson, C.B. (2007). Systemic treatment with the antidiabetic drug metformin selectively impairs p53-deficient tumor cell growth. Cancer Res 67, 6745-6752.

Cairncross, J.G., Wang, M., Jenkins, R.B., Shaw, E.G., Giannini, C., Brachman, D.G., Buckner, J.C., Fink, K.L., Souhami, L., Laperriere, N.J., et al. (2014). Benefit from procarbazine, lomustine, and vincristine in oligodendroglial tumors is associated with mutation of IDH. J Clin Oncol 32, 783-790.

Cantor, J.R., Abu-Remaileh, M., Kanarek, N., Freinkman, E., Gao, X., Louissaint, A., Jr., Lewis, C.A., and Sabatini, D.M. (2017). Physiologic Medium Rewires Cellular Metabolism and Reveals Uric Acid as an Endogenous Inhibitor of UMP Synthase. Cell 169, 258-272 e217.

Cardaci, S., Zheng, L., MacKay, G., van den Broek, N.J., MacKenzie, E.D., Nixon, C., Stevenson, D., Tumanov, S., Bulusu, V., Kamphorst, J.J., et al. (2015). Pyruvate carboxylation enables growth of SDH-deficient cells by supporting aspartate biosynthesis. Nat Cell Biol 17, 1317-1326.

Chajes, V., Cambot, M., Moreau, K., Lenoir, G.M., and Joulin, V. (2006). Acetyl-CoA carboxylase alpha is essential to breast cancer cell survival. Cancer Res 66, 5287-5294.

Chan, M., Gravel, M., Bramoulle, A., Bridon, G., Avizonis, D., Shore, G.C., and Roulston, A. (2014). Synergy between the NAMPT inhibitor GMX1777(8) and pemetrexed in non-small cell lung cancer cells is mediated by PARP activation and enhanced NAD consumption. Cancer Res 74, 5948-5954.

Chen, J., Chung, F., Yang, G., Pu, M., Gao, H., Jiang, W., Yin, H., Capka, V., Kasibhatla, S., Laffitte, B., et al. (2013). Phosphoglycerate dehydrogenase is dispensable for breast tumor maintenance and growth. Oncotarget 4, 2502-2511.

Chiarugi, A., Dolle, C., Felici, R., and Ziegler, M. (2012). The NAD metabolome--a key determinant of cancer cell biology. Nat Rev Cancer 12, 741-752.

Chio, II, Jafarnejad, S.M., Ponz-Sarvise, M., Park, Y., Rivera, K., Palm, W., Wilson, J., Sangar, V., Hao, Y., Ohlund, D., et al. (2016). NRF2 Promotes Tumor Maintenance by Modulating mRNA Translation in Pancreatic Cancer. Cell 166, 963-976.

Chowdhury, R., Yeoh, K.K., Tian, Y.M., Hillringhaus, L., Bagg, E.A., Rose, N.R., Leung, I.K., Li, X.S., Woon, E.C., Yang, M., et al. (2011). The oncometabolite 2-hydroxyglutarate inhibits histone lysine demethylases. EMBO Rep 12, 463-469.

Christofk, H.R., Vander Heiden, M.G., Harris, M.H., Ramanathan, A., Gerszten, R.E., Wei, R., Fleming, M.D., Schreiber, S.L., and Cantley, L.C. (2008). The M2 splice isoform of pyruvate kinase is important for cancer metabolism and tumour growth. Nature 452, 230-233.

Cohade, C. (2010). Altered biodistribution on FDG-PET with emphasis on brown fat and insulin effect. Semin Nucl Med 40, 283-293.

Comerford, S.A., Huang, Z., Du, X., Wang, Y., Cai, L., Witkiewicz, A.K., Walters, H., Tantawy, M.N., Fu, A., Manning, H.C., et al. (2014). Acetate dependence of tumors. Cell 159, 1591-1602.

Cortes-Cros, M., Hemmerlin, C., Ferretti, S., Zhang, J., Gounarides, J.S., Yin, H., Muller, A., Haberkorn, A., Chene, P., Sellers, W.R., et al. (2013). M2 isoform of pyruvate kinase is dispensable for tumor maintenance and growth. Proc Natl Acad Sci U S A 110, 489-494.

d'Amico, A. (2015). Review of clinical practice utility of positron emission tomography with 18F-fluorodeoxyglucose in assessing tumour response to therapy. Radiol Med 120, 345-351.

Dang, L., White, D.W., Gross, S., Bennett, B.D., Bittinger, M.A., Driggers, E.M., Fantin, V.R., Jang, H.G., Jin, S., Keenan, M.C., et al. (2009). Cancer-associated IDH1 mutations produce 2-hydroxyglutarate. Nature 462, 739-744.

Dang, L., Yen, K., and Attar, E.C. (2016). IDH mutations in cancer and progress toward development of targeted therapeutics. Ann Oncol 27, 599-608.

Davidson, S.M., Papagiannakopoulos, T., Olenchock, B.A., Heyman, J.E., Keibler, M.A., Luengo, A., Bauer, M.R., Jha, A.K., O'Brien, J.P., Pierce, K.A., et al. (2016). Environment Impacts the Metabolic Dependencies of Ras-Driven Non-Small Cell Lung Cancer. Cell Metab 23, 517-528.

Daye, D., and Wellen, K.E. (2012). Metabolic reprogramming in cancer: unraveling the role of glutamine in tumorigenesis. Semin Cell Dev Biol 23, 362-369.

Dayton, T.L., Jacks, T., and Vander Heiden, M.G. (2016). PKM2, cancer metabolism, and the road ahead. EMBO Rep 17, 1721-1730.

DeBerardinis, R.J., and Chandel, N.S. (2016). Fundamentals of cancer metabolism. Sci Adv 2, e1600200.

DeBerardinis, R.J., and Cheng, T. (2010). Q's next: the diverse functions of glutamine in metabolism, cell biology and cancer. Oncogene 29, 313-324.

DeBerardinis, R.J., Mancuso, A., Daikhin, E., Nissim, I., Yudkoff, M., Wehrli, S., and Thompson, C.B. (2007). Beyond aerobic glycolysis: transformed cells can engage in glutamine metabolism that exceeds the requirement for protein and nucleotide synthesis. Proc Natl Acad Sci U S A 104, 19345-19350.

Delage, B., Fennell, D.A., Nicholson, L., McNeish, I., Lemoine, N.R., Crook, T., and Szlosarek, P.W. (2010). Arginine deprivation and argininosuccinate synthetase expression in the treatment of cancer. Int J Cancer 126, 2762-2772.

DeNicola, G.M., Chen, P.H., Mullarky, E., Sudderth, J.A., Hu, Z., Wu, D., Tang, H., Xie, Y., Asara, J.M., Huffman, K.E., et al. (2015). NRF2 regulates serine biosynthesis in non-small cell lung cancer. Nat Genet 47, 1475-1481.

DeNicola, G.M., Karreth, F.A., Humpton, T.J., Gopinathan, A., Wei, C., Frese, K., Mangal, D., Yu, K.H., Yeo, C.J., Calhoun, E.S., et al. (2011). Oncogene-induced Nrf2 transcription promotes ROS detoxification and tumorigenesis. Nature 475, 106-109.

Dey, P., Baddour, J., Muller, F., Wu, C.C., Wang, H., Liao, W.T., Lan, Z., Chen, A., Gutschner, T., Kang, Y., et al. (2017). Genomic deletion of malic enzyme 2 confers collateral lethality in pancreatic cancer. Nature 542, 119-123.

DiNardo, C.D., Ravandi, F., Agresta, S., Konopleva, M., Takahashi, K., Kadia, T., Routbort, M., Patel, K.P., Mark, B., Pierce, S., et al. (2015). Characteristics, clinical outcome, and prognostic significance of IDH mutations in AML. Am J Hematol 90, 732-736.

Dixon, S.J., Lemberg, K.M., Lamprecht, M.R., Skouta, R., Zaitsev, E.M., Gleason, C.E., Patel, D.N., Bauer, A.J., Cantley, A.M., Yang, W.S., et al. (2012). Ferroptosis: an iron-dependent form of nonapoptotic cell death. Cell 149, 1060-1072.

Dixon, S.J., Patel, D.N., Welsch, M., Skouta, R., Lee, E.D., Hayano, M., Thomas, A.G., Gleason, C.E., Tatonetti, N.P., Slusher, B.S., et al. (2014). Pharmacological inhibition of cystine-glutamate exchange induces endoplasmic reticulum stress and ferroptosis. Elife 3, e02523.

Doherty, J.R., and Cleveland, J.L. (2013). Targeting lactate metabolism for cancer therapeutics. J Clin Invest 123, 3685-3692.

Dolma, S., Lessnick, S.L., Hahn, W.C., and Stockwell, B.R. (2003). Identification of genotype-selective antitumor agents using synthetic lethal chemical screening in engineered human tumor cells. Cancer Cell 3, 285-296.

Ducker, G.S., Chen, L., Morscher, R.J., Ghergurovich, J.M., Esposito, M., Teng, X., Kang, Y., and Rabinowitz, J.D. (2016). Reversal of Cytosolic One-Carbon Flux Compensates for Loss of the Mitochondrial Folate Pathway. Cell Metab 23, 1140-1153.

Duvel, K., Yecies, J.L., Menon, S., Raman, P., Lipovsky, A.I., Souza, A.L., Triantafellow, E., Ma, Q., Gorski, R., Cleaver, S., et al. (2010). Activation of a metabolic gene regulatory network downstream of mTOR complex 1. Mol Cell 39, 171-183.

Eagle, H. (1955). The specific amino acid requirements of a human carcinoma cell (Stain HeLa) in tissue culture. J Exp Med 102, 37-48.

Efferth, T., Gebhart, E., Ross, D.D., and Sauerbrey, A. (2003). Identification of gene expression profiles predicting tumor cell response to L-alanosine. Biochem Pharmacol 66, 613-621.

Egler, R.A., Ahuja, S.P., and Matloub, Y. (2016). L-asparaginase in the treatment of patients with acute lymphoblastic leukemia. J Pharmacol Pharmacother 7, 62-71.

El-Mir, M.Y., Nogueira, V., Fontaine, E., Averet, N., Rigoulet, M., and Leverve, X. (2000). Dimethylbiguanide inhibits cell respiration via an indirect effect targeted on the respiratory chain complex I. J Biol Chem 275, 223-228.

Elion, G.B. (1989). The purine path to chemotherapy. Science 244, 41-47.

Evans, J.M., Donnelly, L.A., Emslie-Smith, A.M., Alessi, D.R., and Morris, A.D. (2005). Metformin and reduced risk of cancer in diabetic patients. BMJ 330, 1304-1305.

Fan, J., Ye, J., Kamphorst, J.J., Shlomi, T., Thompson, C.B., and Rabinowitz, J.D. (2014). Quantitative flux analysis reveals folate-dependent NADPH production. Nature 510, 298-302.

Fantin, V.R., St-Pierre, J., and Leder, P. (2006). Attenuation of LDH-A expression uncovers a link between glycolysis, mitochondrial physiology, and tumor maintenance. Cancer Cell 9, 425-434.

Farber, S., and Diamond, L.K. (1948). Temporary remissions in acute leukemia in children produced by folic acid antagonist, 4-aminopteroyl-glutamic acid. N Engl J Med 238, 787-793.

Farwell, M.D., Pryma, D.A., and Mankoff, D.A. (2014). PET/CT imaging in cancer: current applications and future directions. Cancer 120, 3433-3445.

Faubert, B., Li, K.Y., Cai, L., Hensley, C.T., Kim, J., Zacharias, L.G., Yang, C., Do, Q.N., Doucette, S., Burguete, D., et al. (2017). Lactate Metabolism in Human Lung Tumors. Cell 171, 358-371 e359.

Feun, L.G., Marini, A., Walker, G., Elgart, G., Moffat, F., Rodgers, S.E., Wu, C.J., You, M., Wangpaichitr, M., Kuo, M.T., et al. (2012). Negative argininosuccinate synthetase expression in melanoma tumours may predict clinical benefit from arginine-depleting therapy with pegylated arginine deiminase. Br J Cancer 106, 1481-1485.

Figueroa, M.E., Abdel-Wahab, O., Lu, C., Ward, P.S., Patel, J., Shih, A., Li, Y., Bhagwat, N., Vasanthakumar, A., Fernandez, H.F., et al. (2010). Leukemic IDH1 and IDH2 mutations result in a hypermethylation phenotype, disrupt TET2 function, and impair hematopoietic differentiation. Cancer Cell 18, 553-567.

Fine, B.M., Kaspers, G.J., Ho, M., Loonen, A.H., and Boxer, L.M. (2005). A genome-wide view of the in vitro response to l-asparaginase in acute lymphoblastic leukemia. Cancer Res 65, 291-299.

Franciosi, M., Lucisano, G., Lapice, E., Strippoli, G.F., Pellegrini, F., and Nicolucci, A. (2013). Metformin therapy and risk of cancer in patients with type 2 diabetes: systematic review. PLoS One 8, e71583.

Frezza, C., Zheng, L., Folger, O., Rajagopalan, K.N., MacKenzie, E.D., Jerby, L., Micaroni, M., Chaneton, B., Adam, J., Hedley, A., et al. (2011). Haem oxygenase is synthetically lethal with the tumour suppressor fumarate hydratase. Nature 477, 225-228.

Furuya, S. (2008). An essential role for de novo biosynthesis of L-serine in CNS development. Asia Pac J Clin Nutr 17 Suppl 1, 312-315.

Galluzzi, L., Kepp, O., Vander Heiden, M.G., and Kroemer, G. (2013). Metabolic targets for cancer therapy. Nat Rev Drug Discov 12, 829-846.

Gandini, S., Puntoni, M., Heckman-Stoddard, B.M., Dunn, B.K., Ford, L., DeCensi, A., and Szabo, E. (2014). Metformin and cancer risk and mortality: a systematic review and meta-analysis taking into account biases and confounders. Cancer Prev Res (Phila) 7, 867-885.

Gao, M., Tashiro, Y., Wang, Q., Sakai, K., and Sonomoto, K. (2016). High acetone-butanol-ethanol production in pH-stat co-feeding of acetate and glucose. J Biosci Bioeng 122, 176-182.

Gao, P., Tchernyshyov, I., Chang, T.C., Lee, Y.S., Kita, K., Ochi, T., Zeller, K.I., De Marzo, A.M., Van Eyk, J.E., Mendell, J.T., et al. (2009). c-Myc suppression of miR-23a/b enhances mitochondrial glutaminase expression and glutamine metabolism. Nature 458, 762-765.

Gaude, E., and Frezza, C. (2016). Tissue-specific and convergent metabolic transformation of cancer correlates with metastatic potential and patient survival. Nat Commun 7, 13041.

Golub, T.R., Slonim, D.K., Tamayo, P., Huard, C., Gaasenbeek, M., Mesirov, J.P., Coller, H., Loh, M.L., Downing, J.R., Caligiuri, M.A., et al. (1999). Molecular classification of cancer: class discovery and class prediction by gene expression monitoring. Science 286, 531-537.

Graczyk-Jarzynka, A., Zagozdzon, R., Muchowicz, A., Siernicka, M., Firczuk, M., and Juszczynski, P. (2017). New insights into redox homeostasis as a therapeutic target in B-cell malignancies. Curr Opin Hematol.

Grassian, A.R., Parker, S.J., Davidson, S.M., Divakaruni, A.S., Green, C.R., Zhang, X., Slocum, K.L., Pu, M., Lin, F., Vickers, C., et al. (2014). IDH1 mutations alter citric acid cycle metabolism and increase dependence on oxidative mitochondrial metabolism. Cancer Res 74, 3317-3331.

Gravel, S.P., Hulea, L., Toban, N., Birman, E., Blouin, M.J., Zakikhani, M., Zhao, Y., Topisirovic, I., St-Pierre, J., and Pollak, M. (2014). Serine deprivation enhances antineoplastic activity of biguanides. Cancer Res 74, 7521-7533.

Gross, M.I., Demo, S.D., Dennison, J.B., Chen, L., Chernov-Rogan, T., Goyal, B., Janes, J.R., Laidig, G.J., Lewis, E.R., Li, J., et al. (2014). Antitumor activity of the glutaminase inhibitor CB-839 in triple-negative breast cancer. Mol Cancer Ther 13, 890-901.

Gui, D.Y., Sullivan, L.B., Luengo, A., Hosios, A.M., Bush, L.N., Gitego, N., Davidson, S.M., Freinkman, E., Thomas, C.J., and Vander Heiden, M.G. (2016). Environment Dictates Dependence on Mitochondrial Complex I for NAD+ and Aspartate Production and Determines Cancer Cell Sensitivity to Metformin. Cell Metab 24, 716-727.

Hamanaka, R.B., and Chandel, N.S. (2012). Targeting glucose metabolism for cancer therapy. J Exp Med 209, 211-215.

Harasawa, H., Yamada, Y., Kudoh, M., Sugahara, K., Soda, H., Hirakata, Y., Sasaki, H., Ikeda, S., Matsuo, T., Tomonaga, M., et al. (2002). Chemotherapy targeting methylthioadenosine phosphorylase (MTAP) deficiency in adult T cell leukemia (ATL). Leukemia 16, 1799-1807.

Harris, I.S., Treloar, A.E., Inoue, S., Sasaki, M., Gorrini, C., Lee, K.C., Yung, K.Y., Brenner, D., Knobbe-Thomsen, C.B., Cox, M.A., et al. (2015). Glutathione and thioredoxin antioxidant pathways synergize to drive cancer initiation and progression. Cancer Cell 27, 211-222.

Harris, M. (1980). Pyruvate blocks expression of sensitivity to antimycin A and chloramphenicol. Somatic Cell Genet 6, 699-708.

Hattori, A., Tsunoda, M., Konuma, T., Kobayashi, M., Nagy, T., Glushka, J., Tayyari, F., McSkimming, D., Kannan, N., Tojo, A., et al. (2017). Cancer progression by reprogrammed BCAA metabolism in myeloid leukaemia. Nature 545, 500-504.

Hatzivassiliou, G., Zhao, F., Bauer, D.E., Andreadis, C., Shaw, A.N., Dhanak, D., Hingorani, S.R., Tuveson, D.A., and Thompson, C.B. (2005). ATP citrate lyase inhibition can suppress tumor cell growth. Cancer Cell 8, 311-321.

Hay, N. (2016). Reprogramming glucose metabolism in cancer: can it be exploited for cancer therapy? Nat Rev Cancer 16, 635-649.

Heidelberger, C., Chaudhuri, N.K., Danneberg, P., Mooren, D., Griesbach, L., Duschinsky, R., Schnitzer, R.J., Pleven, E., and Scheiner, J. (1957). Fluorinated pyrimidines, a new class of tumour-inhibitory compounds. Nature 179, 663-666.

Hensley, C.T., Faubert, B., Yuan, Q., Lev-Cohain, N., Jin, E., Kim, J., Jiang, L., Ko, B., Skelton, R., Loudat, L., et al. (2016). Metabolic Heterogeneity in Human Lung Tumors. Cell 164, 681-694.

Heuer, T.S., Ventura, R., Mordec, K., Lai, J., Fridlib, M., Buckley, D., and Kemble, G. (2017). FASN Inhibition and Taxane Treatment Combine to Enhance Anti-tumor Efficacy in Diverse Xenograft Tumor Models through Disruption of Tubulin Palmitoylation and Microtubule Organization and FASN Inhibition-Mediated Effects on Oncogenic Signaling and Gene Expression. EBioMedicine 16, 51-62.

Hewitson, K.S., Lienard, B.M., McDonough, M.A., Clifton, I.J., Butler, D., Soares, A.S., Oldham, N.J., McNeill, L.A., and Schofield, C.J. (2007). Structural and mechanistic studies on the inhibition of the hypoxia-inducible transcription factor hydroxylases by tricarboxylic acid cycle intermediates. J Biol Chem 282, 3293-3301.

Hoekstra, A.S., de Graaff, M.A., Briaire-de Bruijn, I.H., Ras, C., Seifar, R.M., van Minderhout, I., Cornelisse, C.J., Hogendoorn, P.C., Breuning, M.H., Suijker, J., et al. (2015). Inactivation of SDH and FH cause loss of 5hmC and increased H3K9me3 in paraganglioma/pheochromocytoma and smooth muscle tumors. Oncotarget 6, 38777-38788.

Hori, H., Tran, P., Carrera, C.J., Hori, Y., Rosenbach, M.D., Carson, D.A., and Nobori, T. (1996). Methylthioadenosine phosphorylase cDNA transfection alters sensitivity to depletion of purine and methionine in A549 lung cancer cells. Cancer Res 56, 5653-5658.

Hosios, A.M., Hecht, V.C., Danai, L.V., Johnson, M.O., Rathmell, J.C., Steinhauser, M.L., Manalis, S.R., and Vander Heiden, M.G. (2016). Amino Acids Rather than Glucose Account for the Majority of Cell Mass in Proliferating Mammalian Cells. Dev Cell 36, 540-549.

Hosios, A.M., and Vander Heiden, M.G. (2014). Acetate metabolism in cancer cells. Cancer Metab 2, 27.

Howell, N., and Sager, R. (1979). Cytoplasmic genetics of mammalian cells: conditional sensitivity to mitochondrial inhibitors and isolation of new mutant phenotypes. Somatic Cell Genet 5, 833-845.

Hsu, P.P., and Sabatini, D.M. (2008). Cancer cell metabolism: Warburg and beyond. Cell 134, 703-707.

Hu, J., Locasale, J.W., Bielas, J.H., O'Sullivan, J., Sheahan, K., Cantley, L.C., Vander Heiden, M.G., and Vitkup, D. (2013). Heterogeneity of tumor-induced gene expression changes in the human metabolic network. Nat Biotechnol 31, 522-529.

Hu, W., Zhang, C., Wu, R., Sun, Y., Levine, A., and Feng, Z. (2010). Glutaminase 2, a novel p53 target gene regulating energy metabolism and antioxidant function. Proc Natl Acad Sci U S A 107, 7455-7460.

Huang, X., Wullschleger, S., Shpiro, N., McGuire, V.A., Sakamoto, K., Woods, Y.L., McBurnie, W., Fleming, S., and Alessi, D.R. (2008). Important role of the LKB1-AMPK pathway in suppressing tumorigenesis in PTEN-deficient mice. Biochem J 412, 211-221.

Irani, K., Xia, Y., Zweier, J.L., Sollott, S.J., Der, C.J., Fearon, E.R., Sundaresan, M., Finkel, T., and Goldschmidt-Clermont, P.J. (1997). Mitogenic signaling mediated by oxidants in Ras-transformed fibroblasts. Science 275, 1649-1652.

Israelsen, W.J., Dayton, T.L., Davidson, S.M., Fiske, B.P., Hosios, A.M., Bellinger, G., Li, J., Yu, Y., Sasaki, M., Horner, J.W., et al. (2013). PKM2 isoform-specific deletion reveals a differential requirement for pyruvate kinase in tumor cells. Cell 155, 397-409.

Israelsen, W.J., and Vander Heiden, M.G. (2015). Pyruvate kinase: Function, regulation and role in cancer. Semin Cell Dev Biol 43, 43-51.

Izzo, F., Marra, P., Beneduce, G., Castello, G., Vallone, P., De Rosa, V., Cremona, F., Ensor, C.M., Holtsberg, F.W., Bomalaski, J.S., et al. (2004). Pegylated arginine deiminase treatment of patients with unresectable hepatocellular carcinoma: results from phase I/II studies. J Clin Oncol 22, 1815-1822.

Jacque, N., Ronchetti, A.M., Larrue, C., Meunier, G., Birsen, R., Willems, L., Saland, E., Decroocq, J., Maciel, T.T., Lambert, M., et al. (2015). Targeting glutaminolysis has antileukemic activity in acute myeloid leukemia and synergizes with BCL-2 inhibition. Blood 126, 1346-1356.

Jain, M., Nilsson, R., Sharma, S., Madhusudhan, N., Kitami, T., Souza, A.L., Kafri, R., Kirschner, M.W., Clish, C.B., and Mootha, V.K. (2012). Metabolite profiling identifies a key role for glycine in rapid cancer cell proliferation. Science 336, 1040-1044.

Janke, R., Iavarone, A.T., and Rine, J. (2017). Oncometabolite D-2-Hydroxyglutarate enhances gene silencing through inhibition of specific H3K36 histone demethylases. Elife 6.

Jeon, S.M., Chandel, N.S., and Hay, N. (2012). AMPK regulates NADPH homeostasis to promote tumour cell survival during energy stress. Nature 485, 661-665.

Jiralerspong, S., Palla, S.L., Giordano, S.H., Meric-Bernstam, F., Liedtke, C., Barnett, C.M., Hsu, L., Hung, M.C., Hortobagyi, G.N., and Gonzalez-Angulo, A.M. (2009). Metformin and pathologic complete responses to neoadjuvant chemotherapy in diabetic patients with breast cancer. J Clin Oncol 27, 3297-3302.

Johnson, B.E., Mazor, T., Hong, C., Barnes, M., Aihara, K., McLean, C.Y., Fouse, S.D., Yamamoto, S., Ueda, H., Tatsuno, K., et al. (2014). Mutational analysis reveals the origin and therapy-driven evolution of recurrent glioma. Science 343, 189-193.

Juvekar, A., Hu, H., Yadegarynia, S., Lyssiotis, C.A., Ullas, S., Lien, E.C., Bellinger, G., Son, J., Hok, R.C., Seth, P., et al. (2016). Phosphoinositide 3-kinase inhibitors induce DNA damage through nucleoside depletion. Proc Natl Acad Sci U S A 113, E4338-4347.

Kamphorst, J.J., Chung, M.K., Fan, J., and Rabinowitz, J.D. (2014). Quantitative analysis of acetyl-CoA production in hypoxic cancer cells reveals substantial contribution from acetate. Cancer Metab 2, 23.

Karisch, R., Fernandez, M., Taylor, P., Virtanen, C., St-Germain, J.R., Jin, L.L., Harris, I.S., Mori, J., Mak, T.W., Senis, Y.A., et al. (2011). Global proteomic assessment of the classical protein-tyrosine phosphatome and "Redoxome". Cell 146, 826-840.

Kennedy, K.M., Scarbrough, P.M., Ribeiro, A., Richardson, R., Yuan, H., Sonveaux, P., Landon, C.D., Chi, J.T., Pizzo, S., Schroeder, T., et al. (2013). Catabolism of exogenous lactate reveals it as a legitimate metabolic substrate in breast cancer. PLoS One 8, e75154.

Kim, J., Hu, Z., Cai, L., Li, K., Choi, E., Faubert, B., Bezwada, D., Rodriguez-Canales, J., Villalobos, P., Lin, Y.F., et al. (2017). CPS1 maintains pyrimidine pools and DNA synthesis in KRAS/LKB1-mutant lung cancer cells. Nature 546, 168-172.

Kindler, H.L., Burris, H.A., 3rd, Sandler, A.B., and Oliff, I.A. (2009). A phase II multicenter study of L-alanosine, a potent inhibitor of adenine biosynthesis, in patients with MTAP-deficient cancer. Invest New Drugs 27, 75-81.

Koivunen, P., Lee, S., Duncan, C.G., Lopez, G., Lu, G., Ramkissoon, S., Losman, J.A., Joensuu, P., Bergmann, U., Gross, S., et al. (2012). Transformation by the (R)-enantiomer of 2-hydroxyglutarate linked to EGLN activation. Nature 483, 484-488.

Kremer, J.C., Prudner, B.C., Lange, S.E., Bean, G.R., Schultze, M.B., Brashears, C.B., Radyk, M.D., Redlich, N., Tzeng, S.C., Kami, K., et al. (2017). Arginine Deprivation Inhibits the Warburg Effect and Upregulates Glutamine Anaplerosis and Serine Biosynthesis in ASS1-Deficient Cancers. Cell Rep 18, 991-1004.

Kroll, W., Loffler, M., and Schneider, F. (1983). Energy parameters, macromolecular synthesis and cell cycle progression of in vitro grown Ehrlich ascites tumor cells after inhibition of oxidative ATP synthesis by oligomycin. Z Naturforsch C 38, 604-612.

Kroon, E., Krosl, J., Thorsteinsdottir, U., Baban, S., Buchberg, A.M., and Sauvageau, G. (1998). Hoxa9 transforms primary bone marrow cells through specific collaboration with Meis1a but not Pbx1b. EMBO J 17, 3714-3725.

Kryukov, G.V., Wilson, F.H., Ruth, J.R., Paulk, J., Tsherniak, A., Marlow, S.E., Vazquez, F., Weir, B.A., Fitzgerald, M.E., Tanaka, M., et al. (2016). MTAP deletion confers enhanced dependency on the PRMT5 arginine methyltransferase in cancer cells. Science 351, 1214-1218.

Kuhajda, F.P., Jenner, K., Wood, F.D., Hennigar, R.A., Jacobs, L.B., Dick, J.D., and Pasternack, G.R. (1994). Fatty acid synthesis: a potential selective target for antineoplastic therapy. Proc Natl Acad Sci U S A 91, 6379-6383.

Kung, C., Hixon, J., Choe, S., Marks, K., Gross, S., Murphy, E., DeLaBarre, B., Cianchetta, G., Sethumadhavan, S., Wang, X., et al. (2012). Small molecule activation of PKM2 in cancer cells induces serine auxotrophy. Chem Biol 19, 1187-1198.

Labuschagne, C.F., van den Broek, N.J., Mackay, G.M., Vousden, K.H., and Maddocks, O.D. (2014). Serine, but not glycine, supports one-carbon metabolism and proliferation of cancer cells. Cell Rep 7, 1248-1258.

Landau, B.R., Laszlo, J., Stengle, J., and Burk, D. (1958). Certain metabolic and pharmacologic effects in cancer patients given infusions of 2-deoxy-D-glucose. J Natl Cancer Inst 21, 485-494.

Lau, A.N., Israelsen, W.J., Roper, J., Sinnamon, M.J., Georgeon, L., Dayton, T.L., Hillis, A.L., Yilmaz, O.H., Di Vizio, D., Hung, K.E., et al. (2017). PKM2 is not required for colon cancer initiated by APC loss. Cancer Metab 5, 10.

Le, A., Lane, A.N., Hamaker, M., Bose, S., Gouw, A., Barbi, J., Tsukamoto, T., Rojas, C.J., Slusher, B.S., Zhang, H., et al. (2012). Glucose-independent glutamine metabolism via TCA cycling for proliferation and survival in B cells. Cell Metab 15, 110-121.

Lee, J.H., Kim, T.I., Jeon, S.M., Hong, S.P., Cheon, J.H., and Kim, W.H. (2012). The effects of metformin on the survival of colorectal cancer patients with diabetes mellitus. Int J Cancer 131, 752-759.

Leonard, P.G., Satani, N., Maxwell, D., Lin, Y.H., Hammoudi, N., Peng, Z., Pisaneschi, F., Link, T.M., Lee, G.R.t., Sun, D., et al. (2016). SF2312 is a natural phosphonate inhibitor of enolase. Nat Chem Biol 12, 1053-1058.

Letouze, E., Martinelli, C., Loriot, C., Burnichon, N., Abermil, N., Ottolenghi, C., Janin, M., Menara, M., Nguyen, A.T., Benit, P., et al. (2013). SDH mutations establish a hypermethylator phenotype in paraganglioma. Cancer Cell 23, 739-752.

Lewis, C.A., Parker, S.J., Fiske, B.P., McCloskey, D., Gui, D.Y., Green, C.R., Vokes, N.I., Feist, A.M., Vander Heiden, M.G., and Metallo, C.M. (2014). Tracing compartmentalized NADPH metabolism in the cytosol and mitochondria of mammalian cells. Mol Cell 55, 253-263.

Lien, E.C., Lyssiotis, C.A., Juvekar, A., Hu, H., Asara, J.M., Cantley, L.C., and Toker, A. (2016). Glutathione biosynthesis is a metabolic vulnerability in PI(3)K/Akt-driven breast cancer. Nat Cell Biol 18, 572-578.

Livingston, R.B., Venditti, J.M., Cooney, D.A., and Carter, S.K. (1970). Glutamine antagonists in chemotherapy. Adv Pharmacol Chemother 8, 57-120.

Locasale, J.W., Grassian, A.R., Melman, T., Lyssiotis, C.A., Mattaini, K.R., Bass, A.J., Heffron, G., Metallo, C.M., Muranen, T., Sharfi, H., et al. (2011). Phosphoglycerate dehydrogenase diverts glycolytic flux and contributes to oncogenesis. Nat Genet 43, 869-874.

Locke, M., Ghazaly, E., Freitas, M.O., Mitsinga, M., Lattanzio, L., Lo Nigro, C., Nagano, A., Wang, J., Chelala, C., Szlosarek, P., et al. (2016). Inhibition of the Polyamine Synthesis Pathway Is Synthetically Lethal with Loss of Argininosuccinate Synthase 1. Cell Rep 16, 1604-1613.

Loffer, M., and Schneider, F. (1982). Further characterization of the growth inhibitory effect of rotenone on in vitro cultured Ehrlich ascites tumour cells. Mol Cell Biochem 48, 77-90.

Long, Y., Tsai, W.B., Wangpaichitr, M., Tsukamoto, T., Savaraj, N., Feun, L.G., and Kuo, M.T. (2013). Arginine deiminase resistance in melanoma cells is associated with metabolic reprogramming, glucose dependence, and glutamine addiction. Mol Cancer Ther 12, 2581-2590.

Losman, J.A., and Kaelin, W.G., Jr. (2013). What a difference a hydroxyl makes: mutant IDH, (R)-2-hydroxyglutarate, and cancer. Genes Dev 27, 836-852.

Losman, J.A., Looper, R.E., Koivunen, P., Lee, S., Schneider, R.K., McMahon, C., Cowley, G.S., Root, D.E., Ebert, B.L., and Kaelin, W.G., Jr. (2013). (R)-2-hydroxyglutarate is sufficient to promote leukemogenesis and its effects are reversible. Science 339, 1621-1625.

Lu, C., Ward, P.S., Kapoor, G.S., Rohle, D., Turcan, S., Abdel-Wahab, O., Edwards, C.R., Khanin, R., Figueroa, M.E., Melnick, A., et al. (2012). IDH mutation impairs histone demethylation and results in a block to cell differentiation. Nature 483, 474-478.

Lubin, M., and Lubin, A. (2009). Selective killing of tumors deficient in methylthioadenosine phosphorylase: a novel strategy. PLoS One 4, e5735.

Luengo, A., Sullivan, L.B., and Heiden, M.G. (2014). Understanding the complex-I-ty of metformin action: limiting mitochondrial respiration to improve cancer therapy. BMC Biol 12, 82.

Lunt, S.Y., and Vander Heiden, M.G. (2011). Aerobic glycolysis: meeting the metabolic requirements of cell proliferation. Annu Rev Cell Dev Biol 27, 441-464.

Lussey-Lepoutre, C., Hollinshead, K.E., Ludwig, C., Menara, M., Morin, A., Castro-Vega, L.J., Parker, S.J., Janin, M., Martinelli, C., Ottolenghi, C., et al. (2015). Loss of succinate dehydrogenase activity results in dependency on pyruvate carboxylation for cellular anabolism. Nat Commun 6, 8784.

Lycan, T.W., Pardee, T.S., Petty, W.J., Bonomi, M., Alistar, A., Lamar, Z.S., Isom, S., Chan, M.D., Miller, A.A., and Ruiz, J. (2016). A Phase II Clinical Trial of CPI-613 in Patients with Relapsed or Refractory Small Cell Lung Carcinoma. PLoS One 11, e0164244.

Maddocks, O.D., Berkers, C.R., Mason, S.M., Zheng, L., Blyth, K., Gottlieb, E., and Vousden, K.H. (2013). Serine starvation induces stress and p53-dependent metabolic remodelling in cancer cells. Nature 493, 542-546.

Maddocks, O.D.K., Athineos, D., Cheung, E.C., Lee, P., Zhang, T., van den Broek, N.J.F., Mackay, G.M., Labuschagne, C.F., Gay, D., Kruiswijk, F., et al. (2017). Modulating the therapeutic response of tumours to dietary serine and glycine starvation. Nature 544, 372-376.

Marchiq, I., and Pouyssegur, J. (2016). Hypoxia, cancer metabolism and the therapeutic benefit of targeting lactate/H(+) symporters. J Mol Med (Berl) 94, 155-171.

Mardis, E.R., Ding, L., Dooling, D.J., Larson, D.E., McLellan, M.D., Chen, K., Koboldt, D.C., Fulton, R.S., Delehaunty, K.D., McGrath, S.D., et al. (2009). Recurring mutations found by sequencing an acute myeloid leukemia genome. N Engl J Med 361, 1058-1066.

Marin-Valencia, I., Yang, C., Mashimo, T., Cho, S., Baek, H., Yang, X.L., Rajagopalan, K.N., Maddie, M., Vemireddy, V., Zhao, Z., et al. (2012). Analysis of tumor metabolism reveals mitochondrial glucose oxidation in genetically diverse human glioblastomas in the mouse brain in vivo. Cell Metab 15, 827-837.

Marjon, K., Cameron, M.J., Quang, P., Clasquin, M.F., Mandley, E., Kunii, K., McVay, M., Choe, S., Kernytsky, A., Gross, S., et al. (2016). MTAP Deletions in Cancer Create Vulnerability to Targeting of the MAT2A/PRMT5/RIOK1 Axis. Cell Rep 15, 574-587.

Martinez-Outschoorn, U.E., Peiris-Pages, M., Pestell, R.G., Sotgia, F., and Lisanti, M.P. (2017). Cancer metabolism: a therapeutic perspective. Nat Rev Clin Oncol 14, 11-31.

Mashimo, T., Pichumani, K., Vemireddy, V., Hatanpaa, K.J., Singh, D.K., Sirasanagandla, S., Nannepaga, S., Piccirillo, S.G., Kovacs, Z., Foong, C., et al. (2014). Acetate is a bioenergetic substrate for human glioblastoma and brain metastases. Cell 159, 1603-1614.

Mathur, D., Stratikopoulos, E., Ozturk, S., Steinbach, N., Pegno, S., Schoenfeld, S., Yong, R., Murty, V.V., Asara, J.M., Cantley, L.C., et al. (2017). PTEN Regulates Glutamine Flux to Pyrimidine Synthesis and Sensitivity to Dihydroorotate Dehydrogenase Inhibition. Cancer Discov 7, 380-390.

Mattaini, K.R., Brignole, E.J., Kini, M., Davidson, S.M., Fiske, B.P., Drennan, C.L., and Vander Heiden, M.G. (2015). An epitope tag alters phosphoglycerate dehydrogenase structure and impairs ability to support cell proliferation. Cancer Metab 3, 5.

Mavrakis, K.J., McDonald, E.R., 3rd, Schlabach, M.R., Billy, E., Hoffman, G.R., deWeck, A., Ruddy, D.A., Venkatesan, K., Yu, J., McAllister, G., et al. (2016). Disordered methionine metabolism in MTAP/CDKN2A-deleted cancers leads to dependence on PRMT5. Science 351, 1208-1213.

Mayers, J.R., Torrence, M.E., Danai, L.V., Papagiannakopoulos, T., Davidson, S.M., Bauer, M.R., Lau, A.N., Ji, B.W., Dixit, P.D., Hosios, A.M., et al. (2016). Tissue of origin dictates branched-chain amino acid metabolism in mutant Kras-driven cancers. Science 353, 1161-1165.

Medes, G., Thomas, A., and Weinhouse, S. (1953). Metabolism of neoplastic tissue. IV. A study of lipid synthesis in neoplastic tissue slices in vitro. Cancer Res 13, 27-29.

Menendez, J.A., and Lupu, R. (2006). Oncogenic properties of the endogenous fatty acid metabolism: molecular pathology of fatty acid synthase in cancer cells. Curr Opin Clin Nutr Metab Care 9, 346-357.

Migita, T., Narita, T., Nomura, K., Miyagi, E., Inazuka, F., Matsuura, M., Ushijima, M., Mashima, T., Seimiya, H., Satoh, Y., et al. (2008). ATP citrate lyase: activation and therapeutic implications in non-small cell lung cancer. Cancer Res 68, 8547-8554.

Mockler, M.B., Conroy, M.J., and Lysaght, J. (2014). Targeting T cell immunometabolism for cancer immunotherapy; understanding the impact of the tumor microenvironment. Front Oncol 4, 107.

Molenaar, R.J., Botman, D., Smits, M.A., Hira, V.V., van Lith, S.A., Stap, J., Henneman, P., Khurshed, M., Lenting, K., Mul, A.N., et al. (2015). Radioprotection of IDH1-Mutated Cancer Cells by the IDH1-Mutant Inhibitor AGI-5198. Cancer Res 75, 4790-4802.

Muir, A., Danai, L.V., Gui, D.Y., Waingarten, C.Y., Lewis, C.A., and Vander Heiden, M.G. (2017). Environmental cystine drives glutamine anaplerosis and sensitizes cancer cells to glutaminase inhibition. Elife 6.

Mullarky, E., Lucki, N.C., Beheshti Zavareh, R., Anglin, J.L., Gomes, A.P., Nicolay, B.N., Wong, J.C., Christen, S., Takahashi, H., Singh, P.K., et al. (2016). Identification of a small molecule inhibitor of 3-phosphoglycerate dehydrogenase to target serine biosynthesis in cancers. Proc Natl Acad Sci U S A 113, 1778-1783.

Muller, F.L., Aquilanti, E.A., and DePinho, R.A. (2015). Collateral Lethality: A new therapeutic strategy in oncology. Trends Cancer 1, 161-173.

Muller, F.L., Colla, S., Aquilanti, E., Manzo, V.E., Genovese, G., Lee, J., Eisenson, D., Narurkar, R., Deng, P., Nezi, L., et al. (2012). Passenger deletions generate therapeutic vulnerabilities in cancer. Nature 488, 337-342.

Nahimana, A., Attinger, A., Aubry, D., Greaney, P., Ireson, C., Thougaard, A.V., Tjornelund, J., Dawson, K.M., Dupuis, M., and Duchosal, M.A. (2009). The NAD biosynthesis inhibitor APO866 has potent antitumor activity against hematologic malignancies. Blood 113, 3276-3286.

Neuman, R.E., and McCoy, T.A. (1956). Dual requirement of Walker carcinosarcoma 256 in vitro for asparagine and glutamine. Science 124, 124-125.

Newsholme, E.A., Crabtree, B., and Ardawi, M.S. (1985). The role of high rates of glycolysis and glutamine utilization in rapidly dividing cells. Biosci Rep 5, 393-400.

Noe, D.A., Rowinsky, E.K., Shen, H.S., Clarke, B.V., Grochow, L.B., McGuire, W.B., Hantel, A., Adams, D.B., Abeloff, M.D., Ettinger, D.S., et al. (1990). Phase I and pharmacokinetic study of brequinar sodium (NSC 368390). Cancer Res 50, 4595-4599.

Noto, H., Goto, A., Tsujimoto, T., and Noda, M. (2012). Cancer risk in diabetic patients treated with metformin: a systematic review and meta-analysis. PLoS One 7, e33411.

O'Dwyer, P.J., Alonso, M.T., and Leyland-Jones, B. (1984). Acivicin: a new glutamine antagonist in clinical trials. J Clin Oncol 2, 1064-1071.

Okoye-Okafor, U.C., Bartholdy, B., Cartier, J., Gao, E.N., Pietrak, B., Rendina, A.R., Rominger, C., Quinn, C., Smallwood, A., Wiggall, K.J., et al. (2015). New IDH1 mutant inhibitors for treatment of acute myeloid leukemia. Nat Chem Biol 11, 878-886.

Ookhtens, M., Kannan, R., Lyon, I., and Baker, N. (1984). Liver and adipose tissue contributions to newly formed fatty acids in an ascites tumor. Am J Physiol 247, R146-153.

Ott, P.A., Carvajal, R.D., Pandit-Taskar, N., Jungbluth, A.A., Hoffman, E.W., Wu, B.W., Bomalaski, J.S., Venhaus, R., Pan, L., Old, L.J., et al. (2013). Phase I/II study of pegylated arginine deiminase (ADI-PEG 20) in patients with advanced melanoma. Invest New Drugs 31, 425-434.

Owen, M.R., Doran, E., and Halestrap, A.P. (2000). Evidence that metformin exerts its anti-diabetic effects through inhibition of complex 1 of the mitochondrial respiratory chain. Biochem J 348 Pt 3, 607-614.

Pacold, M.E., Brimacombe, K.R., Chan, S.H., Rohde, J.M., Lewis, C.A., Swier, L.J., Possemato, R., Chen, W.W., Sullivan, L.B., Fiske, B.P., et al. (2016). A PHGDH inhibitor reveals coordination of serine synthesis and one-carbon unit fate. Nat Chem Biol 12, 452-458.

Pardee, T.S., Lee, K., Luddy, J., Maturo, C., Rodriguez, R., Isom, S., Miller, L.D., Stadelman, K.M., Levitan, D., Hurd, D., et al. (2014). A phase I study of the first-in-class antimitochondrial metabolism agent, CPI-613, in patients with advanced hematologic malignancies. Clin Cancer Res 20, 5255-5264.

Parker, W.B. (2009). Enzymology of purine and pyrimidine antimetabolites used in the treatment of cancer. Chem Rev 109, 2880-2893.

Pavlova, N.N., and Thompson, C.B. (2016). The Emerging Hallmarks of Cancer Metabolism. Cell Metab 23, 27-47.

Pelicano, H., Martin, D.S., Xu, R.H., and Huang, P. (2006). Glycolysis inhibition for anticancer treatment. Oncogene 25, 4633-4646.

Peters, G.J., Nadal, J.C., Laurensse, E.J., de Kant, E., and Pinedo, H.M. (1990). Retention of in vivo antipyrimidine effects of Brequinar sodium (DUP-785; NSC 368390) in murine liver, bone marrow and colon cancer. Biochem Pharmacol 39, 135-144.

Peters, G.J., van der Wilt, C.L., van Moorsel, C.J., Kroep, J.R., Bergman, A.M., and Ackland, S.P. (2000). Basis for effective combination cancer chemotherapy with antimetabolites. Pharmacol Ther 87, 227-253.

Phillips, M.M., Sheaff, M.T., and Szlosarek, P.W. (2013). Targeting arginine-dependent cancers with arginine-degrading enzymes: opportunities and challenges. Cancer Res Treat 45, 251-262.

Pinheiro, C., Longatto-Filho, A., Azevedo-Silva, J., Casal, M., Schmitt, F.C., and Baltazar, F. (2012). Role of monocarboxylate transporters in human cancers: state of the art. J Bioenerg Biomembr 44, 127-139.

Piskounova, E., Agathocleous, M., Murphy, M.M., Hu, Z., Huddlestun, S.E., Zhao, Z., Leitch, A.M., Johnson, T.M., DeBerardinis, R.J., and Morrison, S.J. (2015). Oxidative stress inhibits distant metastasis by human melanoma cells. Nature 527, 186-191.

Pollard, P.J., Briere, J.J., Alam, N.A., Barwell, J., Barclay, E., Wortham, N.C., Hunt, T., Mitchell, M., Olpin, S., Moat, S.J., et al. (2005). Accumulation of Krebs cycle intermediates and over-expression of HIF1alpha in tumours which result from germline FH and SDH mutations. Hum Mol Genet 14, 2231-2239.

Possemato, R., Marks, K.M., Shaul, Y.D., Pacold, M.E., Kim, D., Birsoy, K., Sethumadhavan, S., Woo, H.K., Jang, H.G., Jha, A.K., et al. (2011). Functional genomics reveal that the serine synthesis pathway is essential in breast cancer. Nature 476, 346-350.

Quivoron, C., David, M., Straley, K., Travins, J., Kim, H., Chen, Y., Zhu, D., Saada, V., Bawa, O., Opolon, P., et al. (2014). AG-221, an Oral, Selective, First-in-Class, Potent IDH2-R140Q Mutant Inhibitor, Induces Differentiation in a Xenotransplant Model. Blood 124, 3735-3735.

Rabbani, N., and Thornalley, P.J. (2014). Dicarbonyl proteome and genome damage in metabolic and vascular disease. Biochem Soc Trans 42, 425-432.

Rabinovich, S., Adler, L., Yizhak, K., Sarver, A., Silberman, A., Agron, S., Stettner, N., Sun, Q., Brandis, A., Helbling, D., et al. (2015). Diversion of aspartate in ASS1-deficient tumours fosters de novo pyrimidine synthesis. Nature 527, 379-383.

Raez, L.E., Papadopoulos, K., Ricart, A.D., Chiorean, E.G., Dipaola, R.S., Stein, M.N., Rocha Lima, C.M., Schlesselman, J.J., Tolba, K., Langmuir, V.K., et al. (2013). A phase I dose-escalation trial of 2-deoxy-D-glucose alone or combined with docetaxel in patients with advanced solid tumors. Cancer Chemother Pharmacol 71, 523-530.

Raj, L., Ide, T., Gurkar, A.U., Foley, M., Schenone, M., Li, X., Tolliday, N.J., Golub, T.R., Carr, S.A., Shamji, A.F., et al. (2011). Selective killing of cancer cells by a small molecule targeting the stress response to ROS. Nature 475, 231-234.

Robitaille, A.M., Christen, S., Shimobayashi, M., Cornu, M., Fava, L.L., Moes, S., Prescianotto-Baschong, C., Sauer, U., Jenoe, P., and Hall, M.N. (2013). Quantitative phosphoproteomics reveal mTORC1 activates de novo pyrimidine synthesis. Science 339, 1320-1323.

Rohle, D., Popovici-Muller, J., Palaskas, N., Turcan, S., Grommes, C., Campos, C., Tsoi, J., Clark, O., Oldrini, B., Komisopoulou, E., et al. (2013). An inhibitor of mutant IDH1 delays growth and promotes differentiation of glioma cells. Science 340, 626-630.

Röhrig, F., and Schulze, A. (2016). The multifaceted roles of fatty acid synthesis in cancer. Nat Rev Cancer 16, 732-749.

Saha, S.K., Parachoniak, C.A., Ghanta, K.S., Fitamant, J., Ross, K.N., Najem, M.S., Gurumurthy, S., Akbay, E.A., Sia, D., Cornella, H., et al. (2014). Mutant IDH inhibits HNF-4alpha to block hepatocyte differentiation and promote biliary cancer. Nature 513, 110-114.

Samanta, D., Park, Y., Andrabi, S.A., Shelton, L.M., Gilkes, D.M., and Semenza, G.L. (2016). PHGDH Expression Is Required for Mitochondrial Redox Homeostasis, Breast Cancer Stem Cell Maintenance, and Lung Metastasis. Cancer Res 76, 4430-4442.

Sancho, P., Burgos-Ramos, E., Tavera, A., Bou Kheir, T., Jagust, P., Schoenhals, M., Barneda, D., Sellers, K., Campos-Olivas, R., Grana, O., et al. (2015). MYC/PGC-1alpha Balance Determines the Metabolic Phenotype and Plasticity of Pancreatic Cancer Stem Cells. Cell Metab 22, 590-605.

Schockel, L., Glasauer, A., Basit, F., Bitschar, K., Truong, H., Erdmann, G., Algire, C., Hagebarth, A., Willems, P.H., Kopitz, C., et al. (2015). Targeting mitochondrial complex I using BAY 87-2243 reduces melanoma tumor growth. Cancer Metab 3, 11.

Schug, Z.T., Peck, B., Jones, D.T., Zhang, Q., Grosskurth, S., Alam, I.S., Goodwin, L.M., Smethurst, E., Mason, S., Blyth, K., et al. (2015). Acetyl-CoA synthetase 2 promotes acetate utilization and maintains cancer cell growth under metabolic stress. Cancer Cell 27, 57-71.

Selak, M.A., Armour, S.M., MacKenzie, E.D., Boulahbel, H., Watson, D.G., Mansfield, K.D., Pan, Y., Simon, M.C., Thompson, C.B., and Gottlieb, E. (2005). Succinate links TCA cycle dysfunction to oncogenesis by inhibiting HIF-alpha prolyl hydroxylase. Cancer Cell 7, 77-85.

Sellers, K., Fox, M.P., Bousamra, M., 2nd, Slone, S.P., Higashi, R.M., Miller, D.M., Wang, Y., Yan, J., Yuneva, M.O., Deshpande, R., et al. (2015). Pyruvate carboxylase is critical for non-small-cell lung cancer proliferation. J Clin Invest 125, 687-698.

Shackelford, D.B., Abt, E., Gerken, L., Vasquez, D.S., Seki, A., Leblanc, M., Wei, L., Fishbein, M.C., Czernin, J., Mischel, P.S., et al. (2013). LKB1 inactivation dictates therapeutic response of non-small cell lung cancer to the metabolism drug phenformin. Cancer Cell 23, 143-158.

Shen, L.J., Lin, W.C., Beloussow, K., and Shen, W.C. (2003). Resistance to the anti-proliferative activity of recombinant arginine deiminase in cell culture correlates with the endogenous enzyme, argininosuccinate synthetase. Cancer Lett 191, 165-170.

Shim, H., Dolde, C., Lewis, B.C., Wu, C.S., Dang, G., Jungmann, R.A., Dalla-Favera, R., and Dang, C.V. (1997). c-Myc transactivation of LDH-A: implications for tumor metabolism and growth. Proc Natl Acad Sci U S A 94, 6658-6663.

Snell, K. (1984). Enzymes of serine metabolism in normal, developing and neoplastic rat tissues. Adv Enzyme Regul 22, 325-400.

Snell, K., Natsumeda, Y., Eble, J.N., Glover, J.L., and Weber, G. (1988). Enzymic imbalance in serine metabolism in human colon carcinoma and rat sarcoma. Br J Cancer 57, 87-90.

Snell, K., Natsumeda, Y., and Weber, G. (1987). The modulation of serine metabolism in hepatoma 3924A during different phases of cellular proliferation in culture. Biochem J 245, 609-612.

Sonveaux, P., Vegran, F., Schroeder, T., Wergin, M.C., Verrax, J., Rabbani, Z.N., De Saedeleer, C.J., Kennedy, K.M., Diepart, C., Jordan, B.F., et al. (2008). Targeting lactate-fueled respiration selectively kills hypoxic tumor cells in mice. J Clin Invest 118, 3930-3942.

Sousa, C.M., Biancur, D.E., Wang, X., Halbrook, C.J., Sherman, M.H., Zhang, L., Kremer, D., Hwang, R.F., Witkiewicz, A.K., Ying, H., et al. (2016). Pancreatic stellate cells support tumour metabolism through autophagic alanine secretion. Nature 536, 479-483.

Stams, W.A., den Boer, M.L., Beverloo, H.B., Meijerink, J.P., Stigter, R.L., van Wering, E.R., Janka-Schaub, G.E., Slater, R., and Pieters, R. (2003). Sensitivity to L-asparaginase is not associated with expression levels of asparagine synthetase in t(12;21)+ pediatric ALL. Blood 101, 2743-2747.

Stein, E.M., Altman, J.K., Collins, R., DeAngelo, D.J., Fathi, A.T., Flinn, I., Frankel, A., Levine, R.L., Medeiros, B.C., Patel, M., et al. (2014). AG-221, an Oral, Selective, First-in-Class, Potent Inhibitor of the IDH2 Mutant Metabolic Enzyme, Induces Durable Remissions in a Phase I Study in Patients with IDH2 Mutation Positive Advanced Hematologic Malignancies. Blood 124, 115-115.

Stein, M., Lin, H., Jeyamohan, C., Dvorzhinski, D., Gounder, M., Bray, K., Eddy, S., Goodin, S., White, E., and Dipaola, R.S. (2010). Targeting tumor metabolism with 2-deoxyglucose in patients with castrate-resistant prostate cancer and advanced malignancies. Prostate 70, 1388-1394.

Suh, Y.A., Arnold, R.S., Lassegue, B., Shi, J., Xu, X., Sorescu, D., Chung, A.B., Griendling, K.K., and Lambeth, J.D. (1999). Cell transformation by the superoxide-generating oxidase Mox1. Nature 401, 79-82.

Sullivan, L.B., Gui, D.Y., Hosios, A.M., Bush, L.N., Freinkman, E., and Vander Heiden, M.G. (2015). Supporting Aspartate Biosynthesis Is an Essential Function of Respiration in Proliferating Cells. Cell 162, 552-563.

Sullivan, L.B., Gui, D.Y., and Vander Heiden, M.G. (2016). Altered metabolite levels in cancer: implications for tumour biology and cancer therapy. Nat Rev Cancer 16, 680-693.

Svensson, R.U., Parker, S.J., Eichner, L.J., Kolar, M.J., Wallace, M., Brun, S.N., Lombardo, P.S., Van Nostrand, J.L., Hutchins, A., Vera, L., et al. (2016). Inhibition of acetyl-CoA carboxylase suppresses fatty acid synthesis and tumor growth of non-small-cell lung cancer in preclinical models. Nat Med 22, 1108-1119.

Sykes, D.B., Kfoury, Y.S., Mercier, F.E., Wawer, M.J., Law, J.M., Haynes, M.K., Lewis, T.A., Schajnovitz, A., Jain, E., Lee, D., et al. (2016). Inhibition of Dihydroorotate Dehydrogenase Overcomes Differentiation Blockade in Acute Myeloid Leukemia. Cell 167, 171-186 e115.

Szlosarek, P.W., Luong, P., Phillips, M.M., Baccarini, M., Stephen, E., Szyszko, T., Sheaff, M.T., and Avril, N. (2013). Metabolic response to pegylated arginine deiminase in mesothelioma with promoter methylation of argininosuccinate synthetase. J Clin Oncol 31, e111-113.

Tabata, S., Yamamoto, M., Goto, H., Hirayama, A., Ohishi, M., Kuramoto, T., Mitsuhashi, A., Ikeda, R., Haraguchi, M., Kawahara, K., et al. (2017). Thymidine Catabolism as a Metabolic Strategy for Cancer Survival. Cell Rep 19, 1313-1321.

Tan, A.S., Baty, J.W., Dong, L.F., Bezawork-Geleta, A., Endaya, B., Goodwin, J., Bajzikova, M., Kovarova, J., Peterka, M., Yan, B., et al. (2015a). Mitochondrial genome acquisition restores respiratory function and tumorigenic potential of cancer cells without mitochondrial DNA. Cell Metab 21, 81-94.

Tan, B., Dong, S., Shepard, R.L., Kays, L., Roth, K.D., Geeganage, S., Kuo, M.S., and Zhao, G. (2015b). Inhibition of Nicotinamide Phosphoribosyltransferase (NAMPT), an Enzyme Essential for NAD+ Biosynthesis, Leads to Altered Carbohydrate Metabolism in Cancer Cells. J Biol Chem 290, 15812-15824.

Tardito, S., Oudin, A., Ahmed, S.U., Fack, F., Keunen, O., Zheng, L., Miletic, H., Sakariassen, P.O., Weinstock, A., Wagner, A., et al. (2015). Glutamine synthetase activity fuels nucleotide biosynthesis and supports growth of glutamine-restricted glioblastoma. Nat Cell Biol 17, 1556-1568.

Tateishi, K., Iafrate, A.J., Ho, Q., Curry, W.T., Batchelor, T.T., Flaherty, K.T., Onozato, M.L., Lelic, N., Sundaram, S., Cahill, D.P., et al. (2016). Myc-Driven Glycolysis Is a Therapeutic Target in Glioblastoma. Clin Cancer Res 22, 4452-4465.

Tateishi, K., Wakimoto, H., Iafrate, A.J., Tanaka, S., Loebel, F., Lelic, N., Wiederschain, D., Bedel, O., Deng, G., Zhang, B., et al. (2015). Extreme Vulnerability of IDH1 Mutant Cancers to NAD+ Depletion. Cancer Cell 28, 773-784.

Titov, D.V., Cracan, V., Goodman, R.P., Peng, J., Grabarek, Z., and Mootha, V.K. (2016). Complementation of mitochondrial electron transport chain by manipulation of the NAD+/NADH ratio. Science 352, 231-235.

Tomlinson, I.P., Alam, N.A., Rowan, A.J., Barclay, E., Jaeger, E.E., Kelsell, D., Leigh, I., Gorman, P., Lamlum, H., Rahman, S., et al. (2002). Germline mutations in FH predispose to dominantly inherited uterine fibroids, skin leiomyomata and papillary renal cell cancer. Nat Genet 30, 406-410.

Tonjes, M., Barbus, S., Park, Y.J., Wang, W., Schlotter, M., Lindroth, A.M., Pleier, S.V., Bai, A.H.C., Karra, D., Piro, R.M., et al. (2013). BCAT1 promotes cell proliferation through amino acid catabolism in gliomas carrying wild-type IDH1. Nat Med 19, 901-908.

Trachootham, D., Zhou, Y., Zhang, H., Demizu, Y., Chen, Z., Pelicano, H., Chiao, P.J., Achanta, G., Arlinghaus, R.B., Liu, J., et al. (2006). Selective killing of oncogenically transformed cells through a ROS-mediated mechanism by beta-phenylethyl isothiocyanate. Cancer Cell 10, 241-252.

Traut, T.W. (1994). Physiological concentrations of purines and pyrimidines. Mol Cell Biochem 140, 1-22.

Turcan, S., Fabius, A.W., Borodovsky, A., Pedraza, A., Brennan, C., Huse, J., Viale, A., Riggins, G.J., and Chan, T.A. (2013). Efficient induction of differentiation and growth inhibition in IDH1 mutant glioma cells by the DNMT Inhibitor Decitabine. Oncotarget 4, 1729-1736.

Turcan, S., Rohle, D., Goenka, A., Walsh, L.A., Fang, F., Yilmaz, E., Campos, C., Fabius, A.W., Lu, C., Ward, P.S., et al. (2012). IDH1 mutation is sufficient to establish the glioma hypermethylator phenotype. Nature 483, 479-483.

Vander Heiden, M.G. (2011). Targeting cancer metabolism: a therapeutic window opens. Nat Rev Drug Discov 10, 671-684.

Vander Heiden, M.G., and DeBerardinis, R.J. (2017). Understanding the Intersections between Metabolism and Cancer Biology. Cell 168, 657-669.

Viale, A., Pettazzoni, P., Lyssiotis, C.A., Ying, H., Sanchez, N., Marchesini, M., Carugo, A., Green, T., Seth, S., Giuliani, V., et al. (2014). Oncogene ablation-resistant pancreatic cancer cells depend on mitochondrial function. Nature 514, 628-632.

von Heideman, A., Berglund, A., Larsson, R., and Nygren, P. (2010). Safety and efficacy of NAD depleting cancer drugs: results of a phase I clinical trial of CHS 828 and overview of published data. Cancer Chemother Pharmacol 65, 1165-1172.

Wagner, A.D., Grothe, W., Haerting, J., Kleber, G., Grothey, A., and Fleig, W.E. (2006). Chemotherapy in advanced gastric cancer: a systematic review and meta-analysis based on aggregate data. J Clin Oncol 24, 2903-2909.

Wakimoto, H., Tanaka, S., Curry, W.T., Loebel, F., Zhao, D., Tateishi, K., Chen, J., Klofas, L.K., Lelic, N., Kim, J.C., et al. (2014). Targetable signaling pathway mutations are associated with malignant phenotype in IDH-mutant gliomas. Clin Cancer Res 20, 2898-2909.

Walling, J. (2006). From methotrexate to pemetrexed and beyond. A review of the pharmacodynamic and clinical properties of antifolates. Invest New Drugs 24, 37-77.

Walsh, M.J., Brimacombe, K.R., Anastasiou, D., Yu, Y., Israelsen, W.J., Hong, B.S., Tempel, W., Dimov, S., Veith, H., Yang, H., et al. (2010). ML265: A potent PKM2 activator induces tetramerization and reduces tumor formation and size in a mouse xenograft model. In Probe Reports from the NIH Molecular Libraries Program (Bethesda (MD)).

Wang, F., Travins, J., DeLaBarre, B., Penard-Lacronique, V., Schalm, S., Hansen, E., Straley, K., Kernytsky, A., Liu, W., Gliser, C., et al. (2013). Targeted inhibition of mutant IDH2 in leukemia cells induces cellular differentiation. Science 340, 622-626.

Wang, Q., Liberti, M.V., Liu, P., Deng, X., Liu, Y., Locasale, J.W., and Lai, L. (2017). Rational Design of Selective Allosteric Inhibitors of PHGDH and Serine Synthesis with Anti-tumor Activity. Cell Chem Biol 24, 55-65.

Warburg, O. (1924). Über den Stoffwechsel der Carcinomzelle. Naturwissenschaften 12, 1131-1137.

Warburg, O. (1956). On the origin of cancer cells. Science 123, 309-314.

Ward, P.S., Patel, J., Wise, D.R., Abdel-Wahab, O., Bennett, B.D., Coller, H.A., Cross, J.R., Fantin, V.R., Hedvat, C.V., Perl, A.E., et al. (2010). The common feature of leukemia-associated IDH1 and IDH2 mutations is a neomorphic enzyme activity converting alpha-ketoglutarate to 2-hydroxyglutarate. Cancer Cell 17, 225-234.

Watanabe, T., Nobusawa, S., Kleihues, P., and Ohgaki, H. (2009). IDH1 mutations are early events in the development of astrocytomas and oligodendrogliomas. Am J Pathol 174, 1149-1153.

Watson, M., Roulston, A., Belec, L., Billot, X., Marcellus, R., Bedard, D., Bernier, C., Branchaud, S., Chan, H., Dairi, K., et al. (2009). The small molecule GMX1778 is a potent inhibitor of NAD+ biosynthesis: strategy for enhanced therapy in nicotinic acid phosphoribosyltransferase 1-deficient tumors. Mol Cell Biol 29, 5872-5888.

Weinberg, F., Hamanaka, R., Wheaton, W.W., Weinberg, S., Joseph, J., Lopez, M., Kalyanaraman, B., Mutlu, G.M., Budinger, G.R., and Chandel, N.S. (2010). Mitochondrial metabolism and ROS generation are essential for Kras-mediated tumorigenicity. Proc Natl Acad Sci U S A 107, 8788-8793.

Weinhouse, S. (1956). On respiratory impairment in cancer cells. Science 124, 267-269.

Wheaton, W.W., Weinberg, S.E., Hamanaka, R.B., Soberanes, S., Sullivan, L.B., Anso, E., Glasauer, A., Dufour, E., Mutlu, G.M., Budigner, G.S., et al. (2014). Metformin inhibits mitochondrial complex I of cancer cells to reduce tumorigenesis. Elife 3, e02242.

Wick, A.N., Drury, D.R., Nakada, H.I., and Wolfe, J.B. (1957). Localization of the primary metabolic block produced by 2-deoxyglucose. J Biol Chem 224, 963-969.

Wise, D.R., DeBerardinis, R.J., Mancuso, A., Sayed, N., Zhang, X.Y., Pfeiffer, H.K., Nissim, I., Daikhin, E., Yudkoff, M., McMahon, S.B., et al. (2008). Myc regulates a transcriptional program that stimulates mitochondrial glutaminolysis and leads to glutamine addiction. Proc Natl Acad Sci U S A 105, 18782-18787.

Witkiewicz, A.K., Whitaker-Menezes, D., Dasgupta, A., Philp, N.J., Lin, Z., Gandara, R., Sneddon, S., Martinez-Outschoorn, U.E., Sotgia, F., and Lisanti, M.P. (2012). Using the "reverse Warburg effect" to identify high-risk breast cancer patients: stromal MCT4 predicts poor clinical outcome in triple-negative breast cancers. Cell Cycle 11, 1108-1117.

Xiang, Y., Stine, Z.E., Xia, J., Lu, Y., O'Connor, R.S., Altman, B.J., Hsieh, A.L., Gouw, A.M., Thomas, A.G., Gao, P., et al. (2015). Targeted inhibition of tumor-specific glutaminase diminishes cell-autonomous tumorigenesis. J Clin Invest 125, 2293-2306.

Xiao, M., Yang, H., Xu, W., Ma, S., Lin, H., Zhu, H., Liu, L., Liu, Y., Yang, C., Xu, Y., et al. (2012). Inhibition of alpha-KG-dependent histone and DNA demethylases by fumarate and succinate that are accumulated in mutations of FH and SDH tumor suppressors. Genes Dev 26, 1326-1338.

Xie, H., Hanai, J., Ren, J.G., Kats, L., Burgess, K., Bhargava, P., Signoretti, S., Billiard, J., Duffy, K.J., Grant, A., et al. (2014). Targeting lactate dehydrogenase--a inhibits tumorigenesis and tumor progression in mouse models of lung cancer and impacts tumor-initiating cells. Cell Metab 19, 795-809.

Xu, W., Yang, H., Liu, Y., Yang, Y., Wang, P., Kim, S.H., Ito, S., Yang, C., Wang, P., Xiao, M.T., et al. (2011). Oncometabolite 2-hydroxyglutarate is a competitive inhibitor of alpha-ketoglutarate-dependent dioxygenases. Cancer Cell 19, 17-30.

Yan, H., Parsons, D.W., Jin, G., McLendon, R., Rasheed, B.A., Yuan, W., Kos, I., Batinic-Haberle, I., Jones, S., Riggins, G.J., et al. (2009). IDH1 and IDH2 mutations in gliomas. N Engl J Med 360, 765-773.

Yang, T.S., Lu, S.N., Chao, Y., Sheen, I.S., Lin, C.C., Wang, T.E., Chen, S.C., Wang, J.H., Liao, L.Y., Thomson, J.A., et al. (2010). A randomised phase II study of pegylated arginine deiminase (ADI-PEG 20) in Asian advanced hepatocellular carcinoma patients. Br J Cancer 103, 954-960.

Yang, W.S., SriRamaratnam, R., Welsch, M.E., Shimada, K., Skouta, R., Viswanathan, V.S., Cheah, J.H., Clemons, P.A., Shamji, A.F., Clish, C.B., et al. (2014). Regulation of ferroptotic cancer cell death by GPX4. Cell 156, 317-331.

Ye, J., Fan, J., Venneti, S., Wan, Y.W., Pawel, B.R., Zhang, J., Finley, L.W., Lu, C., Lindsten, T., Cross, J.R., et al. (2014). Serine catabolism regulates mitochondrial redox control during hypoxia. Cancer Discov 4, 1406-1417.

Yen, K., Travins, J., Wang, F., David, M.D., Artin, E., Straley, K., Padyana, A., Gross, S., DeLaBarre, B., Tobin, E., et al. (2017). AG-221, a First-in-Class Therapy Targeting Acute Myeloid Leukemia Harboring Oncogenic IDH2 Mutations. Cancer Discov.

Yoshida, K., Furuya, S., Osuka, S., Mitoma, J., Shinoda, Y., Watanabe, M., Azuma, N., Tanaka, H., Hashikawa, T., Itohara, S., et al. (2004). Targeted disruption of the mouse 3-phosphoglycerate dehydrogenase gene causes severe neurodevelopmental defects and results in embryonic lethality. J Biol Chem 279, 3573-3577.

Yun, J., Mullarky, E., Lu, C., Bosch, K.N., Kavalier, A., Rivera, K., Roper, J., Chio, II, Giannopoulou, E.G., Rago, C., et al. (2015). Vitamin C selectively kills KRAS and BRAF mutant colorectal cancer cells by targeting GAPDH. Science 350, 1391-1396.

Yuneva, M., Zamboni, N., Oefner, P., Sachidanandam, R., and Lazebnik, Y. (2007). Deficiency in glutamine but not glucose induces MYC-dependent apoptosis in human cells. J Cell Biol 178, 93-105.

Yuneva, M.O., Fan, T.W., Allen, T.D., Higashi, R.M., Ferraris, D.V., Tsukamoto, T., Mates, J.M., Alonso, F.J., Wang, C., Seo, Y., et al. (2012). The metabolic profile of tumors depends on both the responsible genetic lesion and tissue type. Cell Metab 15, 157-170.

Zauri, M., Berridge, G., Thezenas, M.L., Pugh, K.M., Goldin, R., Kessler, B.M., and Kriaucionis, S. (2015). CDA directs metabolism of epigenetic nucleosides revealing a therapeutic window in cancer. Nature 524, 114-118.

Zhang, B., Zheng, A., Hydbring, P., Ambroise, G., Ouchida, A.T., Goiny, M., Vakifahmetoglu-Norberg, H., and Norberg, E. (2017). PHGDH Defines a Metabolic Subtype in Lung Adenocarcinomas with Poor Prognosis. Cell Rep 19, 2289-2303.

Zhang, D., Li, J., Wang, F., Hu, J., Wang, S., and Sun, Y. (2014a). 2-Deoxy-D-glucose targeting of glucose metabolism in cancer cells as a potential therapy. Cancer Lett 355, 176-183.

Zhang, X., Fryknas, M., Hernlund, E., Fayad, W., De Milito, A., Olofsson, M.H., Gogvadze, V., Dang, L., Pahlman, S., Schughart, L.A., et al. (2014b). Induction of mitochondrial dysfunction as a strategy for targeting tumour cells in metabolically compromised microenvironments. Nat Commun 5, 3295.

Zhao, Y., Butler, E.B., and Tan, M. (2013). Targeting cellular metabolism to improve cancer therapeutics. Cell Death Dis 4, e532.

Zheng, L., Mackenzie, E.D., Karim, S.A., Hedley, A., Blyth, K., Kalna, G., Watson, D.G., Szlosarek, P., Frezza, C., and Gottlieb, E. (2013). Reversed argininosuccinate lyase activity in fumarate hydratase-deficient cancer cells. Cancer Metab 1, 12.

Zhu, A., Lee, D., and Shim, H. (2011). Metabolic positron emission tomography imaging in cancer detection and therapy response. Semin Oncol 38, 55-69.

Zu, X.L., and Guppy, M. (2004). Cancer metabolism: facts, fantasy, and fiction. Biochem Biophys Res Commun 313, 459-465.

Chapter 2: Methylglyoxal production is a targetable liability of glycolytic metabolism in lung cancer

Authors: Alba Luengo[1,2], Shawn M. Davidson[1,2,3], Sahin Naqvi[2,4], Aaron M. Hosios[1,2], Caroline A. Lewis[4], Elizaveta Freinkman[4], Brandon Faubert[5], Ralph J. Deberardinis[5,6,7], Clary B. Clish[3], Robert J. Downey[8], Matthew G. Vander Heiden[1,2,9]

Author Affiliations:
[1] Koch Institute for Integrative Cancer Research, Massachusetts Institute of Technology, Cambridge, MA 02139, USA
[2] Department of Biology, Massachusetts Institute of Technology, Cambridge, MA 02139, USA
[3] Broad Institute of MIT and Harvard University, Cambridge, MA 02142, USA
[4] Whitehead Institute for Biomedical Research, Massachusetts Institute of Technology, Cambridge, MA 02142, USA
[5] Children's Medical Center Research Institute, University of Texas Southwestern Medical Center, Dallas, TX, USA
[6] Department of Pediatrics, University of Texas Southwestern Medical Center, Dallas, TX, USA
[7] Eugene McDermott Center for Human Growth and Development, University of Texas Southwestern Medical Center, Dallas, TX, USA
[8] Thoracic Service, Department of Surgery, Memorial Sloan Kettering Cancer Center, New York, NY United States of America
[9] Dana-Farber Cancer Institute, Boston, MA 02115, USA

This chapter is unpublished as of May 2018

Abstract

Increased glycolytic metabolism is a prominent phenotype of most cancers, but how best to exploit this metabolic alteration for cancer therapy is unknown. Efforts to clinically target increased glucose uptake directly have been challenging, suggesting that alternative strategies are needed. Here, we find that the reactive metabolite methylglyoxal, a byproduct of glycolysis, accumulates at high levels in both human and murine non-small cell lung cancers (NSCLC). Methylglyoxal reacts non-enzymatically with basic amino acids and guanyl nucleotides to damage macromolecules, reducing cellular fitness. Detoxification of methylglyoxal requires both reduced glutathione and the methylglyoxal detoxification enzyme glyoxalase 1 (Glo1). Ablation of *Glo1* potentiates sensitivity to methylglyoxal and reduces tumor growth in mice, arguing that targeting pathways involved in the detoxification of reactive metabolites is an alternative approach to therapeutically target consequences of increased glucose metabolism in cancer.

Introduction

Cancer cells engage in altered metabolism to support the biosynthetic demands of malignant proliferation (Pavlova and Thompson, 2016; Vander Heiden and DeBerardinis, 2017). The reprogrammed metabolism of cancer cells distinguishes tumors from the tissues from which they arise, raising the possibility that tumor metabolism could be targeted for cancer therapy. For example, elevated

glucose uptake and flux through glycolysis is a salient feature of cancer metabolism (Liberti and Locasale, 2016; Lunt and Vander Heiden, 2011), and compounds that target this phenotype have been developed and tested for clinical efficacy. However, efforts to target glucose metabolism, including inhibitors of glucose uptake, glycolysis, and lactate excretion, have had limited clinical success, likely because all cells require glucose and glycolytic enzymes for survival (Hay, 2016; Luengo et al., 2017). Targeting secondary effects of increased glucose metabolism may be an alternative therapeutic approach, and synthetic lethality approaches involving metabolism have been proposed as a more tractable strategy to clinically target features of cancer metabolism. For example, passenger deletion of one isoform of the glycolytic enzyme enolase can result in increased dependence on the remaining isoform (Leonard et al., 2016; Muller et al., 2012). Additionally, cancers with loss of the mitochondrial enzyme fumarate hydratase (*FH*) accumulate fumarate, which introduces metabolic vulnerabilities including arginine auxotrophy and dependency on heme metabolism (Adam et al., 2013; Frezza et al., 2011; Zheng et al., 2013). While these examples are based on the presence of specific mutations, other indirect consequences of increased glucose metabolism can cause different metabolic dependencies in cancer cells relative to normal cells, and these dependencies may be applicable to broader subsets of patients. Here, we show that increased production of the reactive metabolite methylglyoxal is a consequence of the reprogrammed glucose metabolism of lung tumors and determine that blocking detoxification of this metabolite impairs cancer growth and introduces targetable vulnerabilities.

Results

Untargeted metabolomics reveals increased antioxidant capacity in lung cancers

Increased glucose metabolism in cancer results in different steady-state concentrations of metabolites in tumors relative to normal tissues, which can have implications for cell signaling, bioenergetics, and the availability of substrates that support biosynthesis and cell proliferation (DeBerardinis and Chandel, 2016; Sullivan et al., 2016). To identify metabolites that accumulate in lung cancers with high glucose metabolism, we performed untargeted liquid chromatography mass-spectrometry (LCMS)-based metabolomics on normal lung tissue and lung tumor tissue derived from two autochthonous mouse models of $Kras^{G12D}$-driven non-small cell lung cancers (NSCLC) that have been shown to avidly consume glucose (Chen et al., 2012; Davidson et al., 2016; Shackelford et al., 2013). These two models, the latent model (LA2), which is initiated by mutant $Kras^{G12D}$ expression (Johnson et al., 2001), and a second model, which involves Cre-mediated activation of $Kras^{G12D}$ expression and deletion of *Trp53* (KP), form lung tumors of different grades and invasiveness (Tuveson et al., 2004). From this analysis, we determined that elevations in the tripeptide glutathione was the metabolite change that was most significantly different between tumors and normal lung tissue (**Figure 1A**).

Reduced glutathione (GSH) is a critical cofactor for cells required to detoxify reactive oxygen species (ROS), which include a number of oxygen-containing reactive chemical species produced as byproducts of mitochondrial metabolism and

other cellular processes (Cairns et al., 2011). Increased ROS generation is associated with malignancy, and increased GSH levels in tumors has been proposed to benefit cancer cells by enabling increased ROS detoxification (DeNicola et al., 2011; Harris et al., 2015; Piskounova et al., 2015). Accumulation of intracellular ROS can damage DNA, proteins, and lipids, and thus cells neutralize ROS via the action of various enzyme complexes, some of which ultimately result in the oxidation of reduced GSH to GSSH, the oxidized form of glutathione (Gorrini et al., 2013). Thus, we reasoned that if elevated glutathione levels in lung cancer were a response to enhanced oxidative stress, the increase in GSH should be accompanied by an increase in GSSG, indicating a more oxidized GSH/GSSG ratio. However, even though GSH was significantly elevated in lung tumors, levels of GSSG were increased only in tumors arising in the LA2 model, and not in the more aggressive KP model which displayed higher levels of GSH (**Figure 1B**). Furthermore, the increase in GSH was greater in both models than any change in GSSG, consistent with a more reduced GSH/GSSG ratio and indicating increased antioxidant capacity in lung tumors relative to normal lung. This argues against oxidative stress as the only explanation for GSH elevation, and suggests that the increase in GSH levels may serve an additional function beyond ROS detoxification in lung cancers.

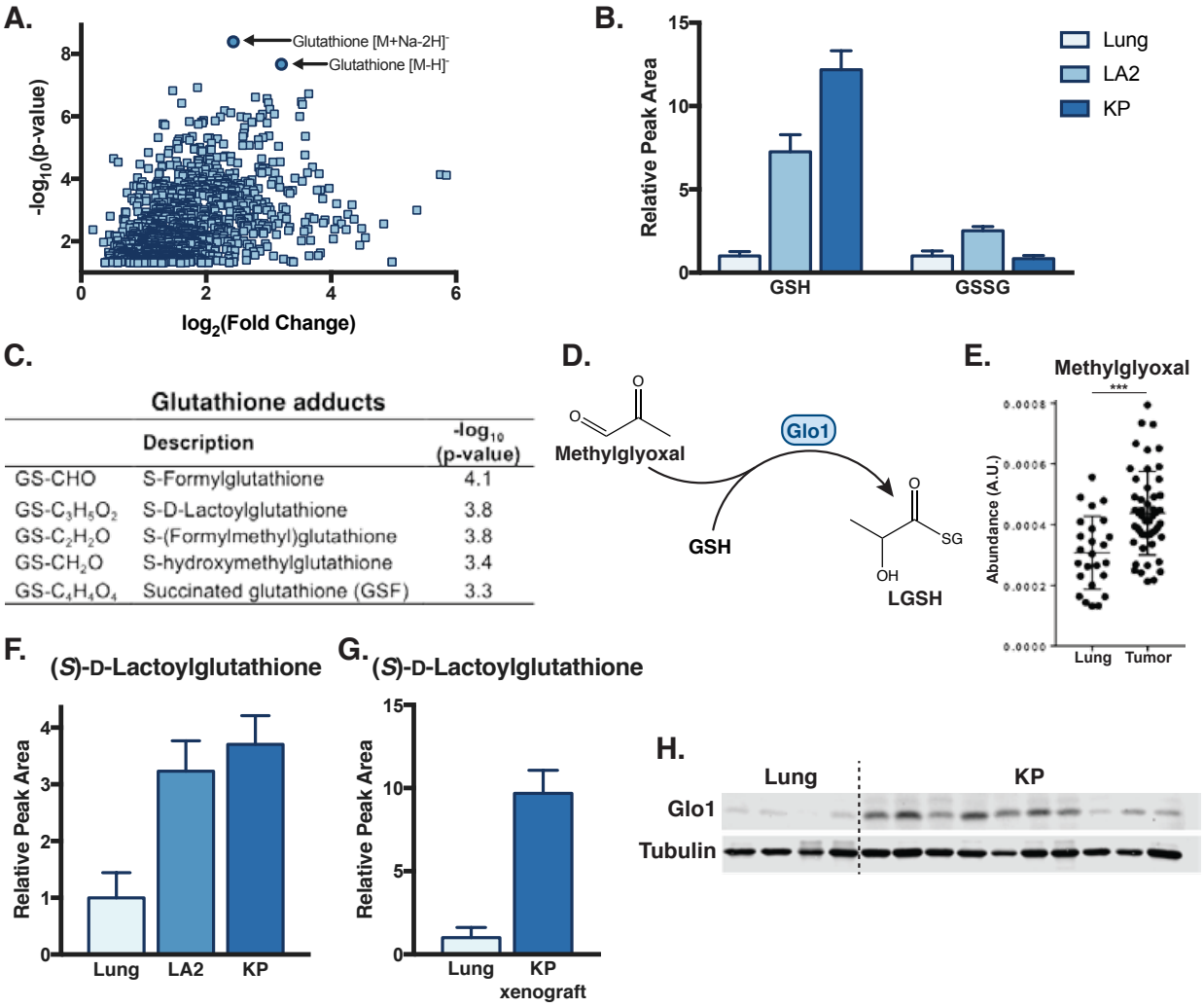
A.
Glutathione [M+Na-2H]-
Glutathione [M-H]-
-log10(p-value)
log2(Fold Change)
B.
Relative Peak Area
Lung
LA2
KP
GSH
GSSG
C.
Glutathione adducts
Description
-log10 (p-value)
GS-CHO
S-Formylglutathione
4.1
GS-C3H5O2
S-D-Lactoylglutathione
3.8
GS-C2H2O
S-(Formylmethyl)glutathione
3.8
GS-CH2O
S-hydroxymethylglutathione
3.4
GS-C4H4O4
Succinated glutathione (GSF)
3.3
D.
Methylglyoxal
Glo1
GSH
LGSH
E.
Methylglyoxal
***
Abundance (A.U.)
Lung
Tumor
F.
(S)-D-Lactoylglutathione
Relative Peak Area
Lung
LA2
KP
G.
(S)-D-Lactoylglutathione
Relative Peak Area
Lung
KP
xenograft
H.
Lung
KP
Glo1
Tubulin

Figure 1. Methylglyoxal and reduced glutathione accumulate in NSCLC tumors compared to normal lung.

(A) Volcano plot indicating metabolites significantly elevated ($p>0.05$) in mouse lung tumors relative to normal lung tissue as determined by untargeted LCMS analysis. Lung lesions were generated from the LA2 and the KP *Kras*^{G12D}-driven NSCLC mouse models. Two negative ionizations of glutathione ($[M+Na-2H]^-$ and $[M-H]^-$) are indicated with arrows. Peaks with fewer than 1×10^5 ion counts were excluded from the analysis.

(B) Relative levels of reduced glutathione (GSH) and oxidized glutathione (GSSG) in extracts from normal mouse lung tissue (Lung), and NSCLC tumors arising in from the LA2 and KP mouse model as measured by targeted LCMS.
(Lung, n = 9; LA2, n = 6; KP, n = 11).

(C) Glutathione adducts found to be significantly higher in lung tumors compared to normal lung are shown, with statistical significance determined by Welch's t-test. Predicted glutathione-electrophile conjugates were identified by untargeted LCMS analysis of mouse lung tissues and NSCLC generated from the LA2 and KP models.

(D) Schematic depicting the reaction catalyzed by glyoxalase 1 (Glo1) to conjugate methylglyoxal with reduced glutathione (GSH) to produce (*S*)-D-lactoylglutathione (LGSH).

(E) Relative methylglyoxal metabolite levels detected in lung cancer and normal lung tissue resected from 25 patients with lung cancer as determined by LCMS. Each dot represents the average value of three biological replicates from a single tissue region. Data are displayed as average and SD. The increase in methylglyoxal in tumors compared to normal lung is statistically significant ($p<0.001$).

(F) Relative levels of (*S*)-D-lactoylglutathione in normal mouse lung tissue, LA2 tumors, and KP tumors as assessed by LCMS. Data is normalized to tissue weight and peak area. (Lung, n = 9; K, n = 6; KP, n = 11).

(G) Quantification of (*S*)-D-lactoylglutathione in normal lung tissue and in KP allografts by LCMS. The allografts were generated from the LG lung cancer cell line, which had derived from a KP mouse lesion as previously described. The lungs were collected from the same animals.

(H) Western blot analysis to assess Glo1 expression in normal mouse lung tissue and in KP lung tumors. Tubulin expression was also assessed as a loading control.

Values shown denote the mean ± SEM for panels B, F, and G.

Evidence for increased methylglyoxal production in lung tumors

Reduced glutathione has a nucleophilic cysteine sulfhydryl group that permits glutathione to react with electrophiles and form GSH-conjugates. The formation of GSH-conjugates promotes electrophile detoxification because it prevents these reactive metabolites from reacting with and damaging other macromolecules in the cell (Blair, 2010). Furthermore, higher levels of glutathione might be expected to more effectively prevent non-specific reaction of reactive metabolites with macromolecules to cause damage. To explore this possibility, we queried whether known glutathione-electrophile conjugates could be identified in the untargeted metabolomics data from normal lung and lung tumors. Consistent with a role for GSH in detoxifying electrophiles in tumors, we identified a number of glutathione-electrophile conjugates that were increased in tumors relative to normal lung (**Figure 1C**). Among these was (*S*)-D-lactoylglutathione (LGSH), which is the conjugation of methylglyoxal with reduced glutathione (**Figure 1D**).

LGSH accumulation is of interest because methylglyoxal is known to be a byproduct of increased glucose metabolism associated with hyperglycemia and diabetes (Han et al., 2009) and can contribute to vascular damage and other complications secondary to increased glucose levels that are observed in this disease (Bierhaus et al., 2012; Dobler et al., 2006; Moraru et al., 2018). This raises the possibility that methylglyoxal also accumulates in tumors secondary to increased glucose metabolism. Consistent with this idea, methylglyoxal levels are elevated in human lung tumors relative to normal lung (**Figure 1E**), which additionally

suggests that this finding could have translational applications for the treatment of human lung cancer.

At high levels, methylglyoxal induces cytotoxicity because it potently and irreversibly reacts with proteins and nucleic acids to form stable adducts referred to as advanced glycation end-products (AGEs) (Rabbani and Thornalley, 2015). Glycation by methylglyoxal interrupts normal electrostatic interactions, thereby altering the structure and function of biomolecules and, by extension, the proliferative capacity and viability of cells. In order to prevent AGE formation, the enzyme glyoxalase 1 (Glo1, EC 4.4.1.5) is broadly expressed (Sousa Silva et al., 2013), and catalyzes the covalent conjugation of methylglyoxal with GSH to form LGSH (**Figure 1D**). Methylglyoxal reacts non-enzymatically with GSH to form a hemithioacetal intermediate. However, this process is reversible, and Glo1 catalyzes the isomerization of the hemithioacetal intermediate to produce LGSH, which is more stable. In this way, Glo1 acts to irreversibly sequester reactive methylglyoxal and prevent the non-specific reaction of this electrophile with macromolecules to damage cells (Sousa Silva et al., 2013).

To assess whether Glo1-mediated detoxification of methylglyoxal is important in lung cancer, we used targeted LCMS to assess levels of LGSH in mouse lung tumors. We found that relative to normal lung, levels of LGSH were higher in metabolite extracts collected from tumors arising in both LA2 and KP mice (**Figure 1F**) and from allografts generated from KP lung tumors cells (**Figure 1G**). We next assessed Glo1 expression in these lung tumors and found that protein

levels of Glo1 were increased in KP lung tumors relative to normal lung tissues (**Figure 1H**). Together, these data support the hypothesis that Glo1 expression in tumor tissues catalyzes the production of LGSH to detoxify increased production of methylglyoxal in lung tumors.

Methylglyoxal is a byproduct of glycolysis

Methylglyoxal can be produced from glucose, as is the case in hyperglycemia (Han et al., 2009). One mechanism of methylglyoxal production is non-enzymatic formation from the degradation of triose-phosphate intermediates in glycolysis (Rabbani and Thornalley, 2015). However, methylglyoxal can also be generated as a byproduct of threonine and glycine interconversion (Elliott, 1960; Ravichandran et al., 2018; Sartori et al., 2008), and methylglyoxal production from glycine has been reported in some cancer contexts (Kim et al., 2015). To distinguish between these possibilities in lung tumors, we performed stable-isotope tracing experiments to assess the source of methylglyoxal production in lung cancer. We cultured lung cancer cells derived from KP lung tumors in media containing [U-$^{13}C_2$]glycine or [U-$^{13}C_6$]glucose and measured label incorporation into methylglyoxal using LCMS. Conversion of [U-$^{13}C_2$]glycine to methylglyoxal generates methylglyoxal with one labeled carbon (m+1) (**Figure 2A**), and conversion of [U-$^{13}C_6$]glucose to methylglyoxal results in fully labeled (m+3) methylglyoxal (**Figure 2B**). We found that in the conditions tested only ~5% of the methylglyoxal is m+1 labeled from [U-$^{13}C_2$]glycine, suggesting that glycine is not a major contributor to methylglyoxal

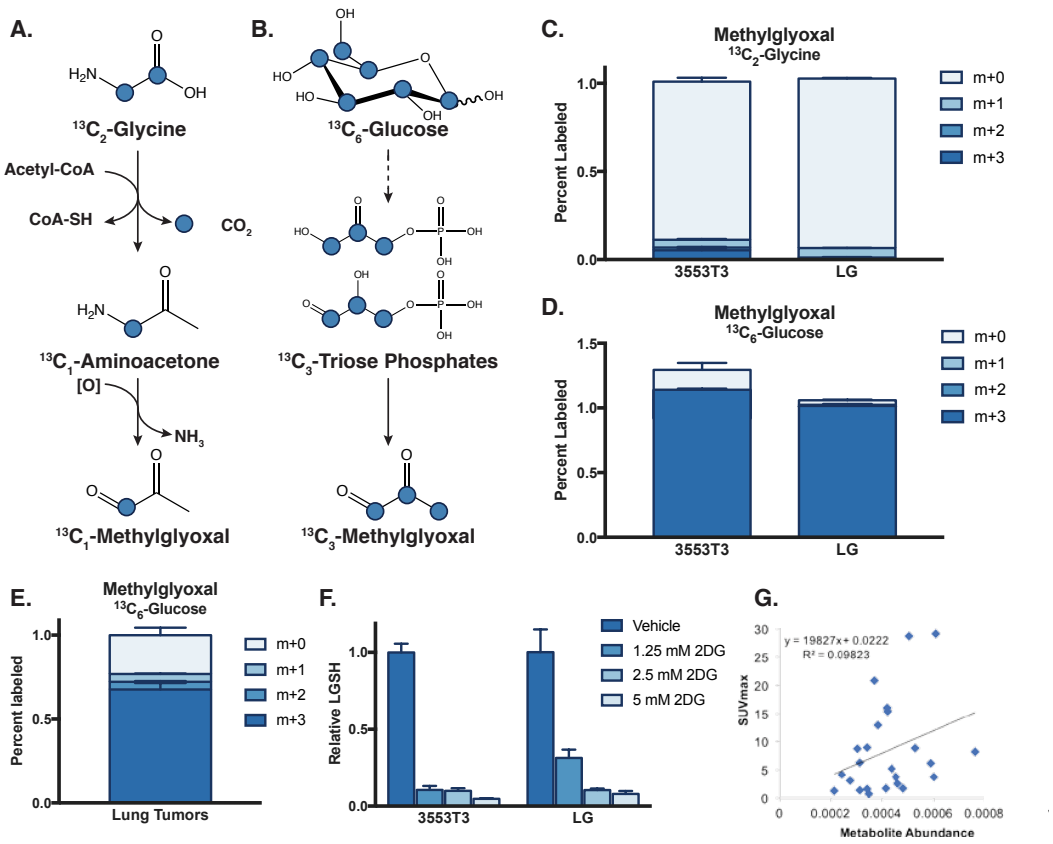

Figure 2. Methylglyoxal is produced as a byproduct of glycolysis in NSCLC

(A and B) Schematic detailing how carbon from (A) [U-$^{13}C_2$]glycine or (B) [U-$^{13}C_6$]glucose would be incorporated into methylglyoxal based on known pathways. ^{13}C labeled carbons are denoted by blue circles.

(C and D) Isotopomer distribution of methylglyoxal in lung cancer cell lines independently derived from KP mice that were cultured for 24 hours in the presence of (C) [U-$^{13}C_2$]glycine or (D) [U-$^{13}C_6$]glucose.

(E) Isotopomer distribution of methylglyoxal in autochthonous lung tumors arising in LA2 mice following a 6 hour infusion of 30mg/kg/min [U-$^{13}C_6$]glucose. Values were normalized to plasma enrichment of glucose.

(F) Relative (*S*)-D-lactoylglutathione (LGSH) levels in two lung cancer cell lines derived from KP mice as detected by LCMS. Levels are shown for cells cultured in the indicated doses of 2-deoxyglucose (2DG) for 24 hours. Values shown are the peak area of LGSH normalized to peak area of reduced glutathione (n=3).

(G) Correlation analysis of SUVmax and methylglyoxal abundance in human lung tumors. Each dot represents the average value of all tumor region fractions for each patient (n=24).

Values in panels C,D,E and F denote mean ± SEM.

formation in these cells (**Figure 2C**). Conversely, when lung cancer cells were cultured with [U-$^{13}C_6$]glucose, virtually all of the methylglyoxal was m+3 labeled, matching the labeling pattern expected when methylglyoxal is produced from glycolytic intermediates (**Figure 2D**). These results indicate that for lung cancer cells in culture, the majority of methylglyoxal is produced from glucose, likely as a byproduct of increased glycolysis. To determine whether methylglyoxal is also derived from glucose in lung tumors, we assessed the contribution of [U-$^{13}C_6$]glucose to methylglyoxal in NSCLC in vivo (Davidson et al., 2016). We infused [U-$^{13}C_6$]glucose into mice bearing LA2 tumors for six hours and analyzed metabolite labeling in tumor tissue by LCMS. Consistent with results obtained from cell lines, the majority of methylglyoxal in lung tumors was found to be generated from glucose (**Figure 2E**).

Glyoxalase 1 is required for methylglyoxal detoxification and to prevent accumulation of protein adducts

The increased production of methylglyoxal as a reactive byproduct of glucose metabolism, along with the accumulation of GSH, raises the possibility that detoxification of this reactive metabolite is important for lung tumor growth. To test this hypothesis, we first examined whether manipulating levels of intracellular glutathione could affect sensitivity to exogenous methylglyoxal. Because glutathione is a required substrate of Glo1, we expected depletion of glutathione to impair methylglyoxal detoxification and thus increase sensitivity to this metabolite.

Indeed, treatment of lung cancer cells with buthionine sulfoximine (BSO), a compound that inhibits glutathione synthesis (Griffith, 1982), renders cells exquisitely sensitive to exogenous methylglyoxal (**Figure 3A**).

To inhibit detoxification of methylglyoxal genetically, we utilized CRISPR/Cas9-based genome editing to delete *Glo1* from lung cancer cells (**Figure 3B**). Consistent with functional deletion of *Glo1*, levels of intracellular LGSH were dramatically lower in *Glo1*-deficient cells (**Figure 3C**). Loss of *Glo1* also resulted in a modest growth defect (**Figure 3D**) and greatly increased sensitivity to exogenous methylglyoxal (**Figure 3E**). To confirm that *Glo1* deletion and reduced LGSH production leads to increased reaction of methylglyoxal with macromolecules, we measured methylglyoxal glycation adducts in cells with and without *Glo1* expression. Methylglyoxal can react with free arginine or arginine residues in proteins to form stable covalent adducts, including hydroimidazolone (MG-H1) (**Figure 3F**). Concentrations of free MG-H1 as measured by LCMS were increased in cells that did not express *Glo1* (**Figure 3G**). Levels of MG-H1 were further elevated in Glo1-null cells that had been incubated with exogenous methylglyoxal (**Figure 3H**) and proteins containing MG-H1 adducts were also detected by Western blot in this context (**Figure 3I**). Together, these data suggest that inhibition of the glyoxalase system in lung cancer cells can lead to accumulation of methylglyoxal-derived adducts on protein. Furthermore, loss of *Glo1* can impair cell viability if methylglyoxal is present at high levels.

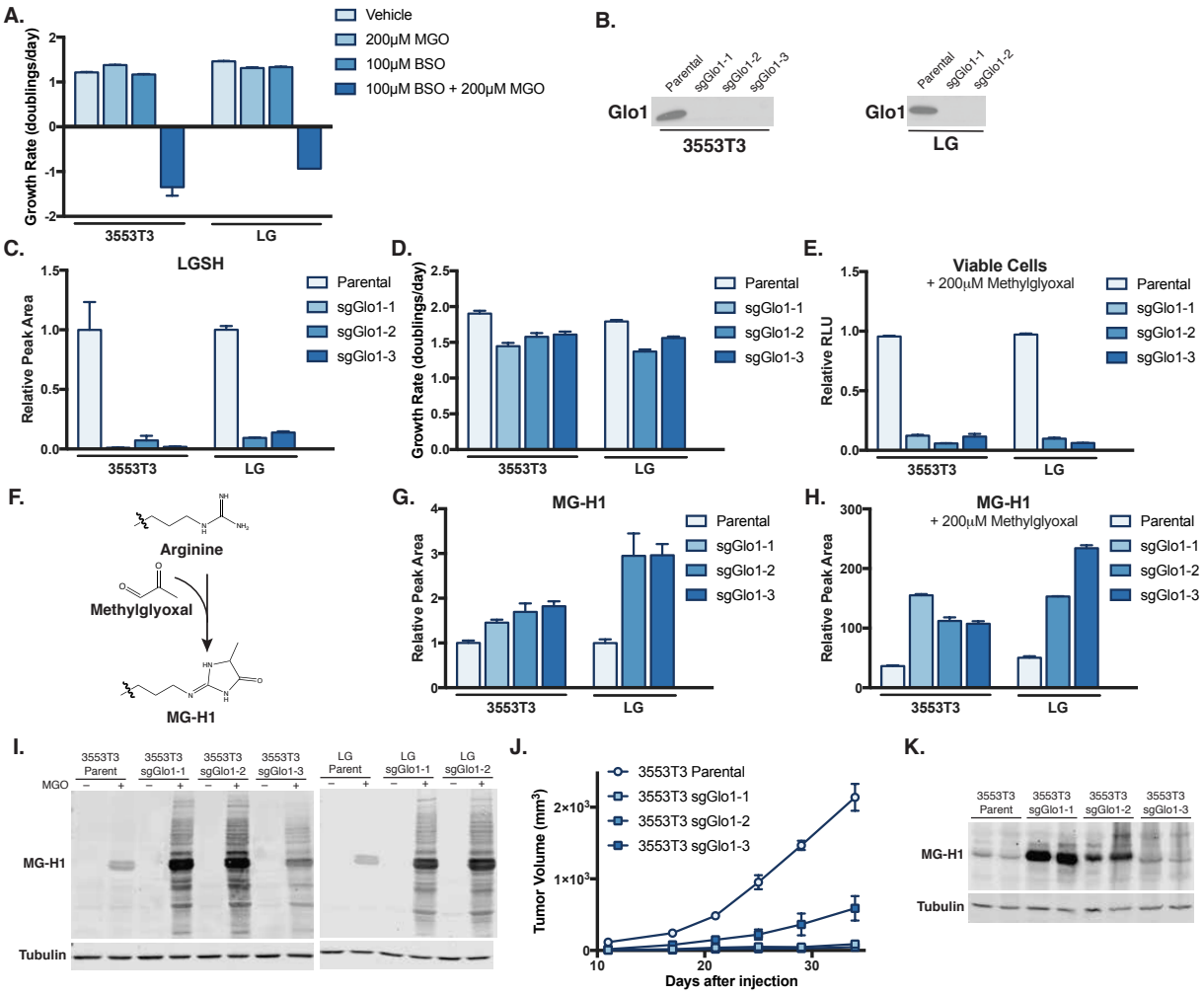
A.
Vehicle
200μM MGO
100μM BSO
100μM BSO + 200μM MGO
Growth Rate (doublings/day)
3553T3
LG
B.
Parental
sgGlo1-1
sgGlo1-2
sgGlo1-3
Glo1
3553T3
LG
C.
LGSH
Relative Peak Area
D.
Growth Rate (doublings/day)
E.
Viable Cells
+ 200μM Methylglyoxal
Relative RLU
F.
Arginine
Methylglyoxal
MG-H1
G.
MG-H1
Relative Peak Area
H.
MG-H1
+ 200μM Methylglyoxal
I.
MGO
MG-H1
Tubulin
J.
3553T3 Parental
3553T3 sgGlo1-1
3553T3 sgGlo1-2
3553T3 sgGlo1-3
Tumor Volume (mm3)
Days after injection
K.
MG-H1
Tubulin

Figure 3. Glyoxalase 1 is required for methylglyoxal detoxification and NSCLC tumor growth

(A) Proliferation rates of two NSCLC cell lines independently derived from KP mice cultured in standard media or in media containing the indicated doses of methylglyoxal (MGO) or buthionine sulfoximine (BSO), an inhibitor of glutathione synthesis. Cells treated with BSO had been pre-treated with BSO for 48 hours prior to the initiation of the experiment.

(B) Western blot analysis of glyoxalase 1 (Glo1) expression in parental 3553T3 and LG lung cancer cells and in independent clones where *Glo1* was deleted using CRISPR/Cas9 (sg*Glo1*) as shown.

(C) Relative levels of (*S*)-D-lactoylglutathione (LGSH) in 3553T3 and LG parental NSCLC cells or the clones shown in (B) where *Glo1* was deleted was detected using LCMS. Values are peak area of LGSH normalized to peak area of GSH (n=3).

(D) Proliferation rates of 3553T3 and LG parental cells and sg*Glo1* clones (n=3).

(E) Relative number of viable 3553T3 and LG lung cancer cells and in clones in which *Glo1* was deleted as determined by CellTiter-Glo Luminescence Assay following a 48 hour incubation with 200μM methylglyoxal (n=3).

(F) Schematic detailing how methylglyoxal can react non-enzymatically with arginine to form hydroimidazolone (MG-H1).

(G) LCMS quantification of relative free MG-H1 abundance in 3553T3 and LG parental lung cancer cells and *Glo1*-deleted clones. Values are peak area of MG-H1 normalized to peak area of arginine (n=3).

(H) LCMS quantification of free MG-H1 abundance in 3553T3 parental lung cancer cell lines or in *Glo1*-null clones following incubation with 200μM methylglyoxal for 16 hours. Values are normalized to MG-H1 peak area in parental lung cancer cell lines incubated without methylglyoxal treatment (n=3).

(G) Western blot analysis of proteins containing MG-H1 epitopes in lysates of lung cancer parent cell lines and sg*Glo1* cell lines that had been treated 200μM of methylglyoxal (MGO) for 12 hours or untreated.

(H) Tumor growth over time of allografts generated from parental 3553T3 lung cancer cells and clones in which *Glo1* has been deleted (n=6).

(I) Western blot analysis of proteins containing MG-H1 epitopes in lysates of allografts generated from parental 3553T3 lines and *Glo1*-null clones.

(J) Tumor growth over time of allografts generated from parental 3553T3 lung cancer cells and clones in which Glo1 has been deleted (n=6).

(K) Western blot analysis of proteins containing MG-H1 epitopes in lysates of allografts generated from parental 3553T3 lines and Glo1-null clones.

Values in panels A, C, D, E, G, H, and J indicate mean ± SEM

Deletion of glyoxalase 1 *impairs tumor proliferation*

A major difference between cells in culture and in tumors is that in vivo, tumors must acquire nutrients and excrete waste via the vasculature. Tumors are known to be poorly vascularized, potentially reducing their ability to dispose of waste and toxic metabolites. Thus, lung cancer cells in vivo might be more sensitive to methylglyoxal accumulation under basal conditions than cells in culture. To determine whether Glo1 expression is important for lung tumor growth, we implanted parental lung cancer cells and *Glo1*-deficient cells subcutaneously as mouse allografts. The ability to proliferate in vivo was severely impaired in cells that did not express *Glo1* compared to parental NSCLC cancer lines (**Figure 3J**). Tumors from *Glo1*-deleted cells also had increased MG-H1 protein adducts, suggesting that accumulation of glycated proteins might contribute to reduced tumor growth in vivo (**Figure 3K**). Taken together, these data argue that lung cancer cells are dependent on the glyoxalase system to detoxify methylglyoxal produced as a byproduct of increased glucose metabolism.

Methylglyoxal accumulation induces formation of DNA-protein crosslinks

To better characterize the molecular repercussions of Glo1 deletion and exogenous methylglyoxal treatment in lung cancer cell lines, we utilized RNA sequencing to probe the global gene expression profiles of a lung cancer parental cell line and one *Glo1*-null that had been cultured in the presence or absence of exogenous methylglyoxal. We performed hierarchical clustering of all samples based

on pairwise Euclidean distances of normalized gene counts and found that samples clustered first by *Glo1* status, and second by methylglyoxal treatment (**Figure 4A**). Interestingly, the distance between vehicle and methylglyoxal treatment in the parental cell line was small, suggesting that in cell culture conditions, the glyoxalase system is robust and can efficiently detoxify exogenous methylglyoxal without significant repercussions for cell homeostasis.

Next, we wanted to determine which biological processes were perturbed by methylglyoxal administration or caused by *Glo1* loss. We found that transcripts of genes involved in cell cycle, DNA replication, and DNA repair were significantly enriched upon methylglyoxal treatment (**Figure 4B**). Performing the same analysis using genes that were differentially expressed upon deletion of *Glo1*, we found that the transcriptional response was similar to that induced by exogenous methylglyoxal, as transcripts involved in DNA replication and response to DNA damage were found to be enriched (**Figure 4C**). This data set provides insight into changes to cellular homeostasis that arise upon addition of exogenous methylglyoxal or ablation of *Glo1*, and can suggest possible molecular targets that would be selectively lethal in contexts in which lung cancer cells accumulate macromolecules damaged by methylglyoxal.

As our differential expression analysis revealed that transcripts relating to DNA replication and DNA repair were stimulated by exogenous methylglyoxal and *Glo1* loss, we wondered whether accumulation of methylglyoxal could affect DNA stability. Methylglyoxal can react with guanyl bases, forming nucleotide adducts

A.

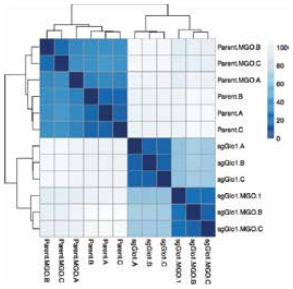

B.

Vehicle vs. Methylglyoxal Treatment

Term ID	Description	log_{10} p-value
GO:0007049	Cell cycle	-26.6517
GO:0006260	DNA replication	-7.0516
GO:0051302	Regulation of cell division	-8.6180
GO:0007059	Chromosome segregation	-9.3468
GO:0006281	DNA repair	-3.5638

C.

Parental vs. sgGlo1

Term ID	Description	log_{10} p-value
GO:0006260	DNA replication	-11.1337
GO:0006974	Cellular response to DNA damage stimulus	-4.2668
GO:0006457	Protein folding	-3.1838
GO:0007049	Cell cycle	-5.9281
GO:0006334	Nucleosome assemply	-5.8996

D.

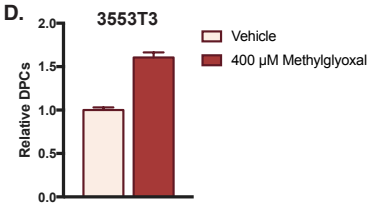

F.

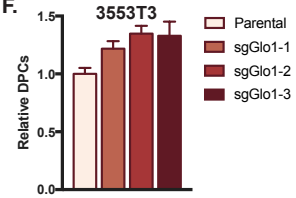

H.

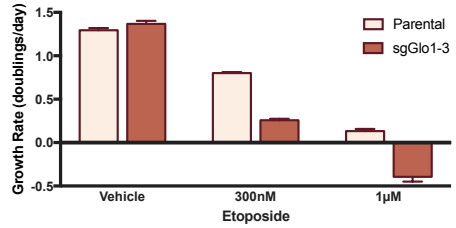

E.

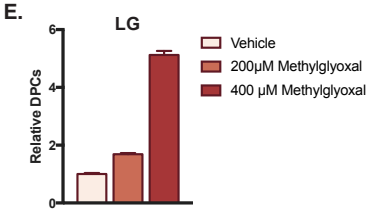

G.

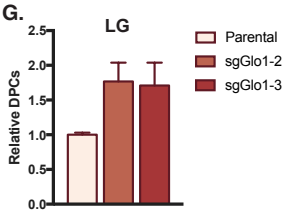

I.

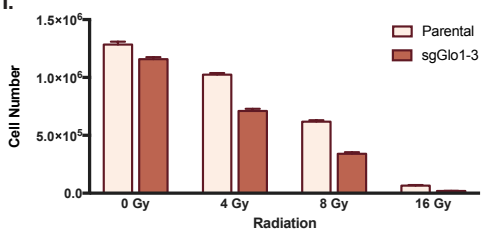

Figure 4. Methylglyoxal accumulation results in DNA damage and formation of DNA-protein crosslinks

(A) RNA sequencing was performed on three biological replicates of the 3553T3 parental and 3553T3 sg*Glo1*-3 lung cancer cell line that had been cultured in the presence or absence 200μM methylglyoxal (MGO) for 12 hours. The heat map is a representation of the Euclidean distance matrix with dark blue indicating zero distance and light blue indicating large distance. The dendogram represents hierarchical clustering across the samples.

(B) List of biological process gene ontology (GO) terms associated with genes that were more highly expressed when 200μM methylglyoxal was administered to 3553T3 parental cells and 3553T3 sg*Glo1*-3 cells relative to untreated cells.

(C) List of GO terms that were associated with transcripts enriched in 3553T3 sg*Glo1*-3 cells relative to 3553T3 parental cell lines.

(D and E) Quantification of DNA-protein crosslink (DPC) isolates was performed by the SDS/KCl precipitation method in (D) 3553T3 and (E) LG parental lung cancer cell lines that were cultured in the indicated dose of methylglyoxal. DPC levels were normalized to the untreated condition (n=6).

(F and G) Quantification of DPC isolates was performed by the SDS/KCl precipitation method in (F) 3553T3 and (G) LG parental lung cancer cell lines and clones in which *Glo1* was deleted. DPC levels were normalized to those of parental cell lines (n=6).

(H) Proliferation rates of 3553T3 parental and 3553T3 sg*Glo1*-3 cell lines cultured at the indicated concentration of etoposide (n=6).

(I) Cell number of 3553T3 parental and 3553T3 sg*Glo1*-3 cell lines 48 hours after treatment with the indicated dose of ionizing radiation in grays (Gy) (n=6).

Values shown denote the mean ± SEM.

and causing mutagenesis and DNA damage when levels of this metabolite are elevated (Rabbani and Thornalley, 2014; Thornalley et al., 2010). Furthermore, it has been reported that methylglyoxal accumulation can result in formation of covalent DNA-protein crosslinks (DPCs) (Brambilla et al., 1985; Vaz et al., 2016). These are cytotoxic DNA lesions that can be caused by exogenous agents, such as ionizing radiation, and by endogenously produced reactive aldehyde-containing metabolites, including formaldehyde and methylglyoxal (Stingele and Jentsch, 2015). We isolated and quantified DPCs using a KCl/SDS precipitation assay (Zhitkovich and Costa, 1992) and determined that DPCs accumulate upon methylglyoxal administration (**Figure 4D,E**). Furthermore, DPCs were found to be elevated in lung cancer cell lines in which *Glo1* was deleted (**Figure 4F,G**). Together with the finding that MG-H1 levels increase upon *Glo1* loss (**Figure 3G,K**), this result argues that inhibiting detoxification of methylglyoxal can cause this metabolite to accumulate and react with macromolecules in the cell.

To test whether increased reaction of methylglyoxal with DNA could be a liability for cells that accumulate this metabolite, we assessed whether Glo1 loss could sensitize lung cancer cells to agents that induce DNA damage. We found that relative to the parental lung cancer cell line, a *Glo1*-deficient clone was more sensitive to etoposide, a chemotherapy that induces DNA strand breaks by inhibition of topoisomerase II (**Figure 4D**) and ionizing radiation (**Figure 4E**) revealing a potential vulnerability of cells with impaired ability to detoxify methylglyoxal.

Exogenous methylglyoxal treatment and glyoxalase 1 ablation sensitizes cells to proteasome inhibition

It has been shown that in contexts of hyperglycemia, methylglyoxal accumulation increases dependency on proteolytic degradation (Queisser et al., 2010; Rabbani and Thornalley, 2012). Additionally, we determined that expression of transcripts involved in protein folding were increased by *Glo1* deletion (**Figure 4C**), suggesting that inhibiting this detoxification pathway can result in accumulation of damaged, misfolded proteins modified by methylglyoxal. To determine whether exogenous methylglyoxal could render lung cancer cells more reliant on protein degradation, we assessed whether culturing lung cancer cell lines in the presence of methylglyoxal could increase dependency on proteasome inhibition. Indeed, we determined that exogenous methylglyoxal increased the sensitivity of lung cancer cells to MG-132, a potent proteasome inhibitor (**Figure 5A,B**). Cells with deleted *Glo1* were also found to be more susceptible to proteasome inhibition than parental lung cell lines, displaying reduced cell number (**Figure 5C**) and impaired viability (**Figure 5D**) upon treatment with MG-132. Together, this data suggest that the proteasome is important for degradation of proteins damaged by methylglyoxal, and inhibition of the proteasome results in impaired viability in contexts where methylglyoxal accumulates.

We next wanted to determine whether we could further decrease in vivo proliferation of lung cancer cells with *Glo1* loss by targeting the proteasome. We generated allografts from the *Glo1*-deleted lung cancer cell line that exhibited the

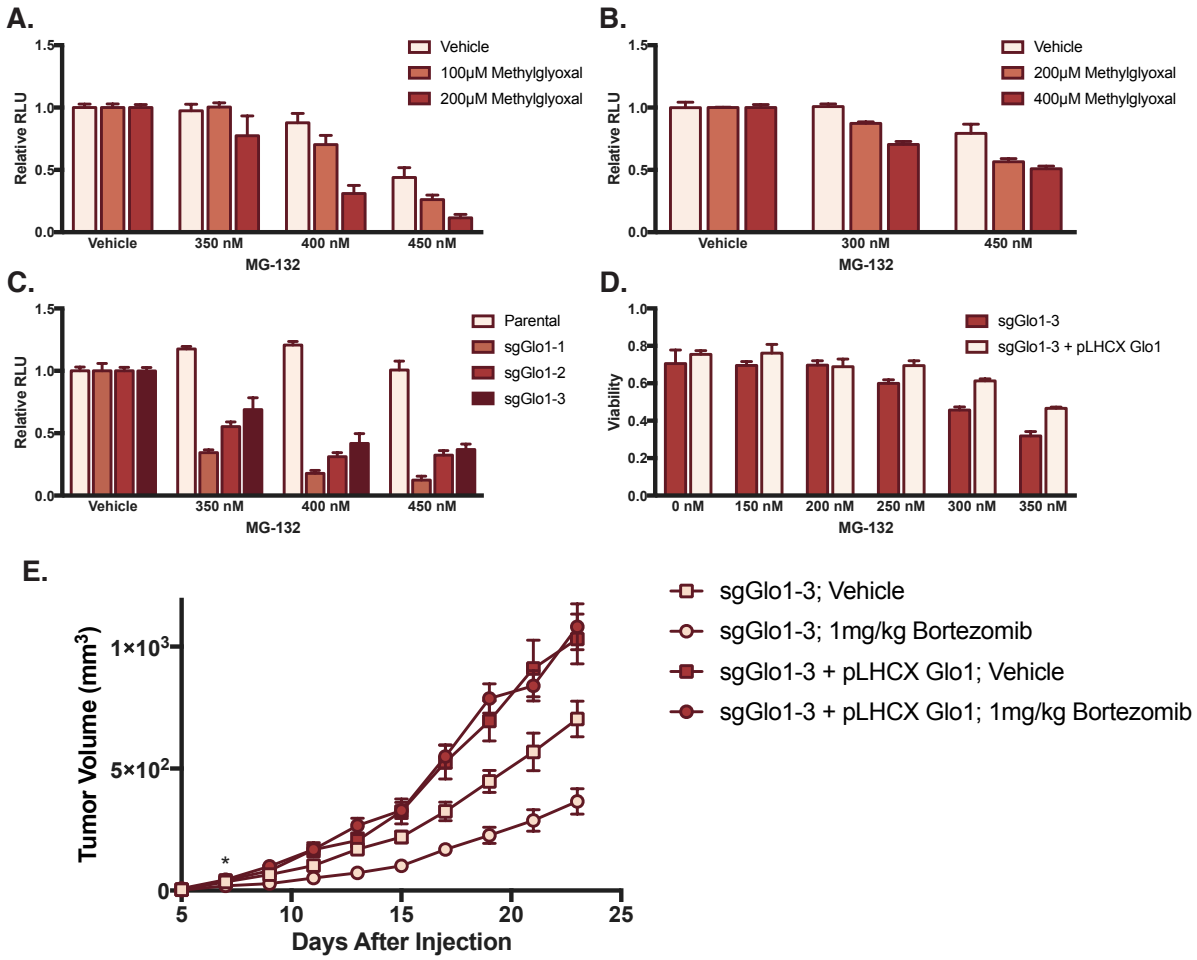

Figure 5. Methylglyoxal accumulation and *glyoxalase 1* loss sensitizes lung cancer cells to proteasome inhibition in vitro and in tumors

(A and B) Relative number of viable (A) 3553T3 and (B) LG lung cancer cells as determined by CellTiter-Glo Luminescence Assay following a 48 hr incubation with the indicated doses of methylglyoxal and the proteasome inhibitor MG-132 (n=4).

(C) Relative number of viable 3553T3 parental and 3553T3 *Glo1*-null cells was determined by CellTiter-Glo Luminescence Assay following a 48 hr incubation with the indicated doses of the proteasome inhibitor MG-132 (n=3).

(D) Percent viability was assessed by flow cytometry in 3553T3 sg*Glo1*-3 cells and the same clone in which *Glo1* had been re-expressesd (3553T3 sg*Glo1*-3 pLHCX Glo1) following a 24 hr incubation with the indicated concentration of MG-132.

(E) Assessment of tumor volume over time of allograft tumors generated from 3553T3 sg*Glo1*-3 pLHCX Glo1 and 3553T3 sg*Glo1*-3 cancer cells in mice that had been dosed with vehicle or the 1mg/kg bortezomib. Treatment with bortezomib was initiated one week after allograft injection, as indicated by the asterisk (n=15).

Values shown denote the mean ± SEM.

best in vivo proliferation (**Figure 3H**) and the same cell line in which Glo1 had been re-expressed as a control. One week after the tumor cells were injected, mice were randomized into two groups and were dosed daily with 1mg/kg bortezomib, a proteasome inhibitor with better pharmacokinetics than MG-132. While the Glo1 overexpressing clone was insensitive to bortezomib treatment, this regimen decreased proliferation of tumors lacking *Glo1* (**Figure 5E**). This data suggests that cancer cells that accumulate methylglyoxal are more reliant on the proteasome, and that a potential liability of reactive metabolite production is inducing accumulation of damaged macromolecules.

Discussion

Changes in metabolite levels in cancer tissues can have important implications for cell physiology and homeostasis, and can also inform how fluxes through the metabolic network change in tumor contexts. In this study, we performed untargeted metabolomics on lung tumors and determined that glutathione, which has been shown to be required for malignant transformation (Harris et al., 2015), is the metabolite that most significantly accumulates in NSCLC lesions relative to normal lung. Interestingly, levels of the oxidized form of glutathione were not elevated to the same extent in these tumors, indicating that the ratio of GSH to GSSG is increased and that NSCLC have higher antioxidant capacity than normal lung. This finding is consistent with emerging data that suggests that tumors are in a more reduced state than normal tissues (Gamcsik et

al., 2012; Hung et al., 2011; Hung and Yellen, 2014; Zhao et al., 2016), and this state can be limiting for tumor growth (Sullivan et al. 2018).

We also determined that NSCLC tumors accumulate GSH-electrophile conjugates, and that the reactive electrophile methylglyoxal is produced at greater levels in tumors than normal lung in both mouse and humans. Since we determine that methylglyoxal is formed as a byproduct of glycolysis in NSCLC, we propose that the increased production of methylglyoxal observed in this context is likely due to the elevated glucose consumption of tumors. Though direct attempts to target glycolysis for cancer therapy have been challenging, consequences of reprogrammed glucose metabolism, such as increased production of methylglyoxal, could serve as an alternative therapeutic strategy to exploit increased glucose metabolism. We determine that inhibiting detoxification of methylglyoxal by deletion of Glo1 results in accumulation of DNA and proteins damaged by this metabolite, and sensitizes lung cancer cells to agents that induce DNA damage or inhibit proteasome activity. This suggests that interventions that promote methylglyoxal accumulation in tumors could be one strategy to enhance the efficacy of existent cancer treatments.

Taken more broadly, the findings presented in this study suggest that production of reactive metabolites as a secondary consequence of reprogrammed cancer metabolism could lead to other targetable vulnerability of tumor cells. Glutathione appears to be critical for the detoxification of many reactive electrophiles, including fumarate, which accumulates in FH-null cancers (Sullivan et al., 2013; Zheng et al., 2015) and ROS (Garama et al., 2015; Harris et al., 2015).

Limiting glutathione availability or targeting detoxification pathways of reactive metabolites could be a mechanism to selectively target cancer cells that produce reactive metabolites at higher levels than normal tissues. A greater understanding of which detoxification pathways are amenable to clinical targeting could reveal novel therapeutic strategies for the treatment of cancer.

Materials and Methods

Mouse Models: For experiments involving the LA2 model (Johnson et al., 2001) 4 to 6-month old mice of a mixed 129/Sv and C57Bl6 genetic background were used. For experiments involving KP animals, 2 to 6-month old mice of a mixed 129/Sv and C57Bl6 genetic background were used. Lesions in the KP model were initiated by 2×10^7 PFU of adenovirus with Cre-recombinase (Gene Transfer Vector Core, University of Iowa) delivered intratracheally.

For allograft experiments, 1×10^5 cancer cells were suspended in 100μL PBS and injected into the flanks of 4 to 6-week old male nu/nu Nude mice (Charles River Laboratories, 088). Tumor volume was measured by caliper in two dimensions, and volumes were calculated using the equation $V = (\pi/6)LW^2$, where L is the longer of the two measured dimension. Mice were sacrificed after the first tumor was measured to be greater than $1cm^3$ or if recommended by the veterinary staff. Bortezomib was diluted in sterile PBS and administered intraperitoneally at 1mg/kg. All animal work was approved by the Massachusetts Institute of Technology's Committee on Animal Care.

Venous Infusions: Catheters were surgically implanted into the jugular veins of tumor bearing animals three days prior to the infusion experiment. The day of the experiment, animals were fasted for six hours and subsequently [U-$^{13}C_6$]glucose (Cambridge Isotope Laboratories, CLM-1396-PK) was infused for six hours at a rate of 30mg/kg/min into conscious, free-moving animals. Animals were terminally anesthetized with 120mg/kg sodium pentobarbital and tumors were rapidly excised and frozen utilizing a BioSqueezer (Bio Spec Products Inc.) that had been pre-cooled in liquid nitrogen. Tumors were stored at -80°C for subsequent analysis.

Tumor Metabolite Extraction: A tissue fragment weighing 10-40 mg was homogenized cryogenically (CryoMill, Retsch). Metabolites were extracted using ice-cold HPLC grade methanol, water, and chloroform in a 600:400:300 ratio. Samples were vortexed at 4°C for 10 minutes, and then centrifuged at 4°C degrees for 10 minutes to separate the aqueous and organic layers. The top aqueous layer was collected and dried under nitrogen gas for subsequent analysis by mass-spectrometry.

Untargeted Metabolomics: For untargeted metabolomics analysis, data were acquired using a liquid chromatography mass-spectrometry (LCMS) system comprised of a Nexera X2 U-HPLC (Shimadzu, Marlborough, MA) coupled to a Q-Exactive hybrid quadrupole orbitrap mass spectrometer (Thermo Fisher Scientific; Waltham, MA). Negative ion mode analyses of polar metabolites were achieved

using a HILIC method under basic conditions. Briefly, 30µl of tissue homogenate was homogenate extracted using 120µL of 80% methanol containing [^{15}N]inosine, thymine-d4, and glycocholate-d4 as internal standards (Cambridge Isotope Laboratories; Andover, MA). The samples were centrifuged (10 min, 9000×g, 4°C) and the supernatants were injected directly onto a 150 × 2.0 mm Luna NH2 column (Phenomenex; Torrance, CA). Samples were eluted at a flow rate of 400µl/min with initial conditions of 10% mobile phase A (20mM ammonium acetate and 20mM ammonium hydroxide in water) and 90% mobile phase B (10mM ammonium hydroxide in 75:25 vol/vol acetonitrile/methanol) followed by a 10 minute linear gradient to 100% mobile phase A. MS full scan data were acquired over m/z 70–750. The ionization source voltage is −3.0 kV and the source temperature is 325°C. Spectra were processed utilizing XCMS Online to identify metabolites that differentially accumulate in lung and tumors. (Tautenhahn et al., 2012). To identify GSH-electrophile conjugates that were elevated in NSCLC tumors relative to normal lung, the human metabolome database (Wishart et al., 2018) was used to identify peaks in the untargeted metabolomics data set with masses corresponding to annotated conjugates.

Cell culture experiments: Cell lines were generated from tumors arising from the KP lung cancer model as previously described (Davidson et al., 2016). Briefly, KP lung lesions were digested in collagenase IV/dispase/trypsin for 30 minutes at 37°C. All cell lines were cultured in DMEM (Corning 10-013-CV) supplemented with 10%

fetal bovine serum. For all experiments, media was changed to DMEM without pyruvate (Corning 10-017-CV) supplemented with 10% dialyzed fetal bovine serum, treatment condition as indicated. The reagents used in this study include methylglyoxal (Sigma, M0252), 2-deoxy-D-glucose (2DG, Sigma, D6134), L-buthionine-sulfoximine (BSO, Sigma, B2515), etoposide (Sigma, E1383), MG-132 (Selleck Chemicals, S2619), bortezomib (Selleck Chemicals, S1013).

For LCMS experiments, 1×10^6 cells were seeded in 10cm tissue culture dishes. After 24 hours, cells were washed three times with PBS and media was changed to 5mL of the appropriate treatment condition. For isotope labeling experiments, the media contained either 25mM [U-$^{13}C_6$]glucose (Cambridge Isotope Laboratories, CLM-1396-PK) or 400μM [U-$^{13}C_2$]glycine (Cambridge Isotope Laboratories, CLM-1017-PK). After 12 hours, cells were washed rapidly with ice-cold blood bank saline and lysed on the dish with 1mL of ice-cold 80% HPLC grade methanol in HPLC grade water. Next, samples were vortexed at 4°C for 10 minutes, and then centrifuged at 4°C degrees for 10 minutes to precipitate the protein. The supernatant was collected, dried under nitrogen gas, and resuspended in 100μL of 80% HPLC grade methanol in HPLC grade water for subsequent analysis by mass-spectrometry.

For proliferation experiments, 2×10^4 cells were seeded replicate six-well dishes. To deplete intracellular glutathione prior to the initiation of the experiment, half the wells were seeded in media containing 200μM buthionine sulfoximine. After 24 hours, one dish was counted to determine the starting cell number prior to

treatment. All remaining dishes were washed three times in phosphate buffered saline (PBS), and 4mL of media containing the indicated treatment was added to cells. Three days following the treatment, cell counts were determined utilizing a Cellometer Auto T4 Plus Cell Counter (Nexcelom Bioscience).

For experiments in which number of viable cells were measured, cells were plated in 96-well dishes at a seeding density of 5,000 cells per well. Cells were permitted to settle overnight, and subsequently were washed three times PBS and cultured in the indicated treatment condition for 48 hours. Number of viable cells was assessed utilizing the CellTiter-Glo Luminescent Cell Viability Assay (Promega G7572) to count number of viable cells.

Targeted Metabolomics: Metabolite profiling was conducted on a QExactive bench top orbitrap mass spectrometer equipped with an Ion Max source and a HESI II probe, which was coupled to a Dionex UltiMate 3000 HPLC system (Thermo Fisher Scientific, San Jose, CA). External mass calibration was performed using the standard calibration mixture every 7 days. For each sample 4μL were injected onto a SeQuant® ZIC®-pHILIC 150 × 2.1mm analytical column equipped with a 2.1 × 20mm guard column (both 5mm particle size; EMD Millipore). Buffer A was 20mM ammonium carbonate, 0.1% ammonium hydroxide; Buffer B was acetonitrile. The column oven and autosampler tray were held at 25°C and 4°C, respectively. The chromatographic gradient was run at a flow rate of 0.150mL/min as follows: 0-20 min: linear gradient from 80-20% B; 20-20.5 min: linear gradient form 20-80% B;

20.5-28 min: hold at 80% B. The mass spectrometer was operated in full-scan, polarity-switching mode, with the spray voltage set to 3.0 kV, the heated capillary held at 275°C, and the HESI probe held at 350°C. The sheath gas flow was set to 40 units, the auxiliary gas flow was set to 15 units, and the sweep gas flow was set to 1 unit. MS data acquisition was performed in a range of m/z = 70–1000, with the resolution set at 70,000, the AGC target at 1×10^6, and the maximum injection time (Max IT) at 20 msec. For detection of metabolites associated with methylglyoxal, targeted selected ion monitoring (tSIM) scans in positive mode were included. The isolation window was set at 1.0 m/z and tSIM scans were centered at m/z = 229.1295 (Positive Mode) for hydroimidazolone (MG-H1) and m/z = 380.1122 (Positive Mode) and 378.0966 (Negative Mode) for (*S*)-D-lactoylglutathione. For all tSIM scans, the resolution was set at 70,000, the AGC target was 1×10^5, and the max IT was 250 msec.

Cell Line Generation: E-CRISP (e-crisp.org) was used to design sgRNA targeting Glo1 (F 5' CACCGCTGTCACCCACCTTGGTGCTGTTT 3'; R 5' 5' AAACAGCACCAAGGTGGGTGACAGCGGTG 3'). The sgRNA was cloned into lentiCRISPR v2 (Addgene, 52961). Isogenic clones were selected for comparison of CRISPR cell lines. To generate Glo1 overexpressing cells, mouse-tagged ORF clone of Glo1 (OriGene Technologies, MR201690) was cloned into pLHCX overexpression retroviral vector.

Calculation of Methylglyoxal Isotopomer distribution: The isotopomer distribution of methylglyoxal was calculated using the matrix equation as described below.

$$Ax = B$$
$$[GSH][MGO] = [LGSH]$$
$$[GSH]^T[GSH][MGO] = [GSH]^T[LGSH]$$
$$[MGO] = ([GSH]^T[GSH])^{-1}\,[GSH]^T[LGSH]$$

Where

$$[MGO] = \begin{bmatrix} m+0 \\ m+1 \\ m+2 \\ m+3 \end{bmatrix}$$

$$[GSH] = \begin{bmatrix} m+0 & 0 & 0 & 0 \\ m+1 & m+0 & 0 & 0 \\ m+2 & m+1 & m+0 & 0 \\ m+3 & m+2 & m+1 & m+0 \\ \vdots & \vdots & \vdots & \vdots \\ m+10 & m+9 & m+8 & m+7 \\ 0 & m+10 & m+9 & m+8 \\ 0 & 0 & m+10 & m+9 \\ 0 & 0 & 0 & m+10 \end{bmatrix}$$

$$[LGSH] = \begin{bmatrix} m+0 \\ m+1 \\ \vdots \\ m+13 \end{bmatrix}$$

RNA-seq Analysis: RNA was extracted from 3553T3 Parental cell lines and the 3553T3 sgGlo1-3 following a 12 hour incubation in the presence or the absence of 500μM methylglyoxal using a RNA isolation kit according to the manufacturer's

instructions (QIAGEN, RNeasy Mini Kit, 74104). RNA sequencing reads were mapped to the mouse genome (mm10) using bwa v0.7.12 (Li and Durbin, 2009), and gene counts were obtained using featureCounts v1.6 with Ensembl 84 mouse transcript annotations. Genes with fewer than 5 reads in at least 3 samples were filtered out as not expressed. Count normalization was performed using the rlog function in the DESeq2 v1.18.1 R package (Love et al., 2014), and clustering was performed with the pheatmap function based on pairwise Euclidean distances calculated using the dist function. Briefly, the Euclidean distance between two samples p and q with N genes each was calculated with the following equation:

$$d(p,q) = \sqrt{\sum_{i=1}^{N} (q_i - p_i)^2}$$

Both *Glo1* genotype (knockout or wild-type) and treatment (methylglyoxal or vehicle), were included as covariates in the DESeq2 model, as well as an interaction term between the two covariates. For each covariate (*Glo1* genotype or methylglyoxal treatment), the Wald test was used to estimate the significance and direction of effect. We performed differential expression analysis (Love et al., 2014), and utilized gene ontology (GO) enrichment analysis to discover terms overrepresented among the list of genes upregulated upon exogenous methylglyoxal treatment (Eden et al., 2007; Eden et al., 2009) and summarized the results by eliminating functionally redundant GO terms (Supek et al., 2011).

Immunoblot: Cells were washed with cold PBS and lysed with cold RIPA buffer containing cOmplete Mini protease inhibitor (Roche, 11836170001). Protein concentration was quantified by BCA Protein Assay (Pierce, 23225) with BSA as a standard. Lysates were resolved by SDS-PAGE using standard techniques. Proteins were transferred onto nitrocellulose membranes using the iBlot2 Dry Blotting System (Thermo Fisher, IB21001, IB23001) and protein was detected with the following primary antibodies: anti-Methylglyoxal (Cell Biolabs, STA-011), anti-Glyoxalase 1 (Novus Biologicals, 19015), anti-Vinculin (Sigma, V9131), anti-Tubulin (Abcam, ab4074). The secondary antibodies used were IR680LT dye conjugated anti-rabbit IgG (Licor Biosciences, 925-68021) and IRDye 800CW conjugated anti-mouse IgG (Licor Biosciences, s 925-32210).

DNA-Protein Crosslinks Quantification: DPCs were quantified using a KCl/SDS precipitation assay (Zhitkovich and Costa, 1992). 2×10^6 cells were lysed in 500µL of lysis buffer (2% SDS in 20mM Tris-HCl, pH=7.5) and snap-frozen in liquid nitrogen. Next, cells were thawed at 55ºC for 5 minutes and sonicated in a 4ºC water bath for 5 cycle at 20 seconds each. To precipitate the protein and DPCs, 500µL of assay buffer (200mM KCl in 20mM Tris, pH 7.5) was added to each sample. The samples were kept on ice for 5 minutes, and then centrifuged at 15,000×g at 4ºC for 5 minutes. The supernatant was kept to quantify the soluble DNA by Quant-iT PicoGreen dsDNA Assay (ThermoFisher Scientific, P11496)

The pellet was resuspended in 500µL of assay buffer, incubated shaking at 55ºC for 5 minutes, cooled on ice for 5 minutes, and centrifuged at 15,000×g at 4ºC for 5 minutes. This wash procedure was repeated three additional times prior to final resuspension in 500µL of assay buffer. Protein was digested with 0.2 mg/mL proteinase K (New England BioLabs, P8107S) and held at 55ºC for 3 hours shaking. Next, 10µL of 50mg/mL of BSA (UltraPure, Invitrogen, AM2616) was added to each sample to precipitate the SDS. Samples were cooled on ice for 5 minutes and centrifuged 15,000×g at 4ºC for 5 minutes. The DNA that had been crosslinked is in the supernatant and can be quantified by Quant-iT PicoGreen dsDNA Assay (ThermoFisher Scientific, P11496). DPCs were calculated as the ratio between DNA precipitated by SDS/KCl and the total DNA (soluble DNA + DNA precipitated by SDS/KCl).

Irradiation of cells: Cells were cultured in standard plastic tissue culture plates at 37 degrees Celsius, 5% CO^2. Immediately prior to irradiation they were removed from the incubator and were irradiated at room temperature in ambient air with a single dose of gamma radiation in a dual 137Cs source low dose-rate irradiator (Gammacell 40 Exactor, Best Theratronics). The total dose delivered was 0 (control), 4, 8, or 16 Gy. During radiation, there was minimum 3 mm media above the cells and 5 mm water-equivalent bolus material below the plate to ensure that irradiated cells were not within the dose buildup region. The dose was verified using a thermoluminescent dosimeter.

References

Adam, J., Yang, M., Bauerschmidt, C., Kitagawa, M., O'Flaherty, L., Maheswaran, P., Ozkan, G., Sahgal, N., Baban, D., Kato, K., et al. (2013). A role for cytosolic fumarate hydratase in urea cycle metabolism and renal neoplasia. Cell Rep 3, 1440-1448.

Bierhaus, A., Fleming, T., Stoyanov, S., Leffler, A., Babes, A., Neacsu, C., Sauer, S.K., Eberhardt, M., Schnolzer, M., Lasitschka, F., et al. (2012). Methylglyoxal modification of Nav1.8 facilitates nociceptive neuron firing and causes hyperalgesia in diabetic neuropathy. Nat Med 18, 926-933.

Blair, I.A. (2010). Analysis of endogenous glutathione-adducts and their metabolites. Biomed Chromatogr 24, 29-38.

Brambilla, G., Sciaba, L., Faggin, P., Finollo, R., Bassi, A.M., Ferro, M., and Marinari, U.M. (1985). Methylglyoxal-induced DNA-protein cross-links and cytotoxicity in Chinese hamster ovary cells. Carcinogenesis 6, 683-686.

Cairns, R.A., Harris, I.S., and Mak, T.W. (2011). Regulation of cancer cell metabolism. Nat Rev Cancer 11, 85-95.

Chen, Z., Cheng, K., Walton, Z., Wang, Y., Ebi, H., Shimamura, T., Liu, Y., Tupper, T., Ouyang, J., Li, J., et al. (2012). A murine lung cancer co-clinical trial identifies genetic modifiers of therapeutic response. Nature 483, 613-617.

Davidson, S.M., Papagiannakopoulos, T., Olenchock, B.A., Heyman, J.E., Keibler, M.A., Luengo, A., Bauer, M.R., Jha, A.K., O'Brien, J.P., Pierce, K.A., et al. (2016). Environment Impacts the Metabolic Dependencies of Ras-Driven Non-Small Cell Lung Cancer. Cell Metab 23, 517-528.

DeBerardinis, R.J., and Chandel, N.S. (2016). Fundamentals of cancer metabolism. Sci Adv 2, e1600200.

DeNicola, G.M., Karreth, F.A., Humpton, T.J., Gopinathan, A., Wei, C., Frese, K., Mangal, D., Yu, K.H., Yeo, C.J., Calhoun, E.S., et al. (2011). Oncogene-induced Nrf2 transcription promotes ROS detoxification and tumorigenesis. Nature 475, 106-109.

Dobler, D., Ahmed, N., Song, L., Eboigbodin, K.E., and Thornalley, P.J. (2006). Increased dicarbonyl metabolism in endothelial cells in hyperglycemia induces anoikis and impairs angiogenesis by RGD and GFOGER motif modification. Diabetes 55, 1961-1969.

Eden, E., Lipson, D., Yogev, S., and Yakhini, Z. (2007). Discovering motifs in ranked lists of DNA sequences. PLoS Comput Biol 3, e39.

Eden, E., Navon, R., Steinfeld, I., Lipson, D., and Yakhini, Z. (2009). GOrilla: a tool for discovery and visualization of enriched GO terms in ranked gene lists. BMC Bioinformatics 10, 48.

Elliott, W.H. (1960). Methylglyoxal formation from aminoacetone by ox plasma. Nature 185, 467-468.

Frezza, C., Zheng, L., Folger, O., Rajagopalan, K.N., MacKenzie, E.D., Jerby, L., Micaroni, M., Chaneton, B., Adam, J., Hedley, A., et al. (2011). Haem oxygenase is synthetically lethal with the tumour suppressor fumarate hydratase. Nature 477, 225-228.

Gamcsik, M.P., Kasibhatla, M.S., Teeter, S.D., and Colvin, O.M. (2012). Glutathione levels in human tumors. Biomarkers 17, 671-691.

Gorrini, C., Harris, I.S., and Mak, T.W. (2013). Modulation of oxidative stress as an anticancer strategy. Nat Rev Drug Discov 12, 931-947.

Griffith, O.W. (1982). Mechanism of action, metabolism, and toxicity of buthionine sulfoximine and its higher homologs, potent inhibitors of glutathione synthesis. J Biol Chem 257, 13704-13712.

Han, Y., Randell, E., Vasdev, S., Gill, V., Curran, M., Newhook, L.A., Grant, M., Hagerty, D., and Schneider, C. (2009). Plasma advanced glycation endproduct, methylglyoxal-derived hydroimidazolone is elevated in young, complication-free patients with Type 1 diabetes. Clin Biochem 42, 562-569.

Harris, I.S., Treloar, A.E., Inoue, S., Sasaki, M., Gorrini, C., Lee, K.C., Yung, K.Y., Brenner, D., Knobbe-Thomsen, C.B., Cox, M.A., et al. (2015). Glutathione and thioredoxin antioxidant pathways synergize to drive cancer initiation and progression. Cancer Cell 27, 211-222.

Hay, N. (2016). Reprogramming glucose metabolism in cancer: can it be exploited for cancer therapy? Nat Rev Cancer 16, 635-649.

Hung, Y.P., Albeck, J.G., Tantama, M., and Yellen, G. (2011). Imaging cytosolic NADH-NAD(+) redox state with a genetically encoded fluorescent biosensor. Cell Metab 14, 545-554.

Hung, Y.P., and Yellen, G. (2014). Live-cell imaging of cytosolic NADH-NAD+ redox state using a genetically encoded fluorescent biosensor. Methods Mol Biol 1071, 83-95.

Johnson, L., Mercer, K., Greenbaum, D., Bronson, R.T., Crowley, D., Tuveson, D.A., and Jacks, T. (2001). Somatic activation of the K-ras oncogene causes early onset lung cancer in mice. Nature 410, 1111-1116.

Kim, D., Fiske, B.P., Birsoy, K., Freinkman, E., Kami, K., Possemato, R.L., Chudnovsky, Y., Pacold, M.E., Chen, W.W., Cantor, J.R., et al. (2015). SHMT2 drives glioma cell survival in ischaemia but imposes a dependence on glycine clearance. Nature 520, 363-367.

Leonard, P.G., Satani, N., Maxwell, D., Lin, Y.H., Hammoudi, N., Peng, Z., Pisaneschi, F., Link, T.M., Lee, G.R.t., Sun, D., et al. (2016). SF2312 is a natural phosphonate inhibitor of enolase. Nat Chem Biol 12, 1053-1058.

Li, H., and Durbin, R. (2009). Fast and accurate short read alignment with Burrows-Wheeler transform. Bioinformatics 25, 1754-1760.

Liberti, M.V., and Locasale, J.W. (2016). The Warburg Effect: How Does it Benefit Cancer Cells? Trends Biochem Sci 41, 211-218.

Love, M.I., Huber, W., and Anders, S. (2014). Moderated estimation of fold change and dispersion for RNA-seq data with DESeq2. Genome Biol 15, 550.

Luengo, A., Gui, D.Y., and Vander Heiden, M.G. (2017). Targeting Metabolism for Cancer Therapy. Cell Chem Biol 24, 1161-1180.

Lunt, S.Y., and Vander Heiden, M.G. (2011). Aerobic glycolysis: meeting the metabolic requirements of cell proliferation. Annu Rev Cell Dev Biol 27, 441-464.

Moraru, A., Wiederstein, J., Pfaff, D., Fleming, T., Miller, A.K., Nawroth, P., and Teleman, A.A. (2018). Elevated Levels of the Reactive Metabolite Methylglyoxal Recapitulate Progression of Type 2 Diabetes. Cell Metab 27, 926-934 e928.

Muller, F.L., Colla, S., Aquilanti, E., Manzo, V.E., Genovese, G., Lee, J., Eisenson, D., Narurkar, R., Deng, P., Nezi, L., et al. (2012). Passenger deletions generate therapeutic vulnerabilities in cancer. Nature 488, 337-342.

Pavlova, N.N., and Thompson, C.B. (2016). The Emerging Hallmarks of Cancer Metabolism. Cell Metab 23, 27-47.

Piskounova, E., Agathocleous, M., Murphy, M.M., Hu, Z., Huddlestun, S.E., Zhao, Z., Leitch, A.M., Johnson, T.M., DeBerardinis, R.J., and Morrison, S.J. (2015). Oxidative stress inhibits distant metastasis by human melanoma cells. Nature 527, 186-191.

Queisser, M.A., Yao, D., Geisler, S., Hammes, H.P., Lochnit, G., Schleicher, E.D., Brownlee, M., and Preissner, K.T. (2010). Hyperglycemia impairs proteasome function by methylglyoxal. Diabetes 59, 670-678.

Rabbani, N., and Thornalley, P.J. (2012). Methylglyoxal, glyoxalase 1 and the dicarbonyl proteome. Amino Acids 42, 1133-1142.

Rabbani, N., and Thornalley, P.J. (2014). Dicarbonyl proteome and genome damage in metabolic and vascular disease. Biochem Soc Trans 42, 425-432.

Rabbani, N., and Thornalley, P.J. (2015). Dicarbonyl stress in cell and tissue dysfunction contributing to ageing and disease. Biochem Biophys Res Commun 458, 221-226.

Ravichandran, M., Priebe, S., Grigolon, G., Rozanov, L., Groth, M., Laube, B., Guthke, R., Platzer, M., Zarse, K., and Ristow, M. (2018). Impairing L-Threonine Catabolism Promotes Healthspan through Methylglyoxal-Mediated Proteohormesis. Cell Metab 27, 914-925 e915.

Riester, M., Xu, Q., Moreira, A., Zheng, J., Michor, F., and Downey, R.J. (2018). The Warburg effect: persistence of stem-cell metabolism in cancers as a failure of differentiation. Ann Oncol 29, 264-270.

Sartori, A., Garay-Malpartida, H.M., Forni, M.F., Schumacher, R.I., Dutra, F., Sogayar, M.C., and Bechara, E.J. (2008). Aminoacetone, a putative endogenous source of methylglyoxal, causes oxidative stress and death to insulin-producing RINm5f cells. Chem Res Toxicol 21, 1841-1850.

Shackelford, D.B., Abt, E., Gerken, L., Vasquez, D.S., Seki, A., Leblanc, M., Wei, L., Fishbein, M.C., Czernin, J., Mischel, P.S., et al. (2013). LKB1 inactivation dictates therapeutic response of non-small cell lung cancer to the metabolism drug phenformin. Cancer Cell 23, 143-158.

Sousa Silva, M., Gomes, R.A., Ferreira, A.E., Ponces Freire, A., and Cordeiro, C. (2013). The glyoxalase pathway: the first hundred years... and beyond. Biochem J 453, 1-15.

Stingele, J., and Jentsch, S. (2015). DNA-protein crosslink repair. Nat Rev Mol Cell Biol 16, 455-460.

Sullivan, L.B., Gui, D.Y., and Vander Heiden, M.G. (2016). Altered metabolite levels in cancer: implications for tumour biology and cancer therapy. Nat Rev Cancer 16, 680-693.

Sullivan, L.B., Martinez-Garcia, E., Nguyen, H., Mullen, A.R., Dufour, E., Sudarshan, S., Licht, J.D., Deberardinis, R.J., and Chandel, N.S. (2013). The proto-oncometabolite fumarate binds glutathione to amplify ROS-dependent signaling. Mol Cell 51, 236-248.

Sullivan, L.B., Luengo, A., Danai L.V., Bush L.N., Diehl F.F., Hosios A.M., Lau A.N., Elmiligy S., Malstrom S., Lewis C.A., Vander Heiden M.G. (2018). Evidence for Aspartate as an Endogenous Metabolic Limitation for Tumour Growth. Nat Cell Bio. Manuscript Accepted

Supek, F., Bosnjak, M., Skunca, N., and Smuc, T. (2011). REVIGO summarizes and visualizes long lists of gene ontology terms. PLoS One 6, e21800.

Tautenhahn, R., Patti, G.J., Rinehart, D., and Siuzdak, G. (2012). XCMS Online: a web-based platform to process untargeted metabolomic data. Anal Chem 84, 5035-5039.

Thornalley, P.J., Waris, S., Fleming, T., Santarius, T., Larkin, S.J., Winklhofer-Roob, B.M., Stratton, M.R., and Rabbani, N. (2010). Imidazopurinones are markers of physiological genomic damage linked to DNA instability and glyoxalase 1-associated tumour multidrug resistance. Nucleic Acids Res 38, 5432-5442.

Tuveson, D.A., Shaw, A.T., Willis, N.A., Silver, D.P., Jackson, E.L., Chang, S., Mercer, K.L., Grochow, R., Hock, H., Crowley, D., et al. (2004). Endogenous oncogenic K-ras(G12D) stimulates proliferation and widespread neoplastic and developmental defects. Cancer Cell 5, 375-387.

Vander Heiden, M.G., and DeBerardinis, R.J. (2017). Understanding the Intersections between Metabolism and Cancer Biology. Cell 168, 657-669.

Vaz, B., Popovic, M., Newman, J.A., Fielden, J., Aitkenhead, H., Halder, S., Singh, A.N., Vendrell, I., Fischer, R., Torrecilla, I., et al. (2016). Metalloprotease SPRTN/DVC1 Orchestrates Replication-Coupled DNA-Protein Crosslink Repair. Mol Cell 64, 704-719.

Wishart, D.S., Feunang, Y.D., Marcu, A., Guo, A.C., Liang, K., Vazquez-Fresno, R., Sajed, T., Johnson, D., Li, C., Karu, N., et al. (2018). HMDB 4.0: the human metabolome database for 2018. Nucleic Acids Res 46, D608-D617.

Zhao, Y., Wang, A., Zou, Y., Su, N., Loscalzo, J., and Yang, Y. (2016). In vivo monitoring of cellular energy metabolism using SoNar, a highly responsive sensor for NAD(+)/NADH redox state. Nat Protoc 11, 1345-1359.

Zheng, L., Cardaci, S., Jerby, L., MacKenzie, E.D., Sciacovelli, M., Johnson, T.I., Gaude, E., King, A., Leach, J.D., Edrada-Ebel, R., et al. (2015). Fumarate induces redox-dependent senescence by modifying glutathione metabolism. Nat Commun 6, 6001.

Zheng, L., Mackenzie, E.D., Karim, S.A., Hedley, A., Blyth, K., Kalna, G., Watson, D.G., Szlosarek, P., Frezza, C., and Gottlieb, E. (2013). Reversed argininosuccinate lyase activity in fumarate hydratase-deficient cancer cells. Cancer Metab 1, 12.

Zhitkovich, A., and Costa, M. (1992). A simple, sensitive assay to detect DNA-protein crosslinks in intact cells and in vivo. Carcinogenesis 13, 1485-1489.

Chapter 3: Mitochondrial membrane hyperpolarization limits NAD+ regeneration in cancer cells

Authors: Alba Luengo[1,2,6], Zhaoqi Li[1,2,6], Dan Y. Gui[1,2], Lucas B. Sullivan[1,2], , Caroline A. Lewis[3], Maria Zagorulya[2], Craig J. Thomas[4], Matthew G. Vander Heiden[1,2,5]

Author Affiliations:
[1] Koch Institute for Integrative Cancer Research, Massachusetts Institute of Technology, Cambridge, MA 02139, USA
[2] Department of Biology, Massachusetts Institute of Technology, Cambridge, MA 02139, USA
[3] Whitehead Institute for Biomedical Research, Massachusetts Institute of Technology, Cambridge, MA 02142, USA
[4] NIH Chemical Genomics Center, National Center for Advancing Translational Sciences, NIH, Bethesda, MD 20892, USA
[5] Dana-Farber Cancer Institute, Boston MA 02115, USA
[6] Co-first author

This chapter is unpublished as of May 2018

Abstract

The propensity of cancer cells to consume large quantities of glucose and metabolize this glucose primarily to lactate, regardless of oxygen availability, is known as aerobic glycolysis or the Warburg effect and is one of the most prominent features of cancer cell metabolism. The pyruvate dehydrogenase complex (PDH) catalyzes the oxidation of pyruvate in the mitochondria as an alternative to lactate production, and regulation of PDH activity can influence pyruvate fate in cells. Here, we utilize the compound AZD7545 to activate PDH by inhibiting its negative regulator, pyruvate dehydrogenase kinase (PDK). PDK inhibition increases pyruvate oxidation and mitochondrial respiration, suppresses the Warburg effect, and reduces cancer cell proliferation. We show that PDK inhibition slows proliferation by perturbing NAD+/NADH homeostasis, as increasing the capacity of cancer cells to generate NAD+ by orthogonal pathways decreases sensitivity to AZD7545. We also establish that electron acceptor insufficiency observed upon PDK inhibition is caused by mitochondrial hyperpolarization, which in turn limits the capacity of the mitochondrial electron transport chain (ETC) to regenerate NAD+. Surprisingly, increasing ETC by uncoupling mitochondrial respiration from ATP synthesis or by increasing ATP consumption suppresses the proliferation defect caused by PDK inhibition. This suggests electron acceptor generation, rather than mitochondrial ATP production, is a limiting function of mitochondrial respiration when PDK is inhibited. Finally, targeting the ETC with the complex I inhibitor metformin can further disrupt NAD+/NADH balance and potentiate the anti-

proliferative effect of AZD7545 in vitro and in vivo. These findings suggest that cancer cells have limited capacity to regenerate NAD+ by mitochondrial respiration, arguing that the production of lactate from glucose is a consequence of redox requirements and providing an explanation for the Warburg effect in cancer cells.

Introduction

Cancer cells reprogram metabolism to support the biochemical demands of increased proliferation (Locasale and Cantley, 2011; Lunt and Vander Heiden, 2011; Ward and Thompson, 2012). A universal feature of the altered metabolism of cancer cells is increased glucose uptake and the propensity to secrete glucose as lactate rather than oxidizing glucose carbons via pathways that require mitochondrial respiration, regardless of oxygen availability. This phenomenon, known as the "Warburg effect" or aerobic glycolysis, is common among cancers and has been shown to be a requirement for tumor proliferation in some contexts (Fantin et al., 2006; Le et al., 2010; Shim et al., 1998; Xie et al., 2014)

Why aerobic glycolysis is a prominent feature of cancer metabolism remains controversial. Proliferating cells have increased demand for ATP to support biomass synthesis, yet aerobic glycolysis is less efficient for ATP production than oxidative metabolism. This discrepancy caused Otto Warburg, who first observed this phenotype, to conclude that tumors must have defects in mitochondrial respiration (Warburg, 1956). However, it has since been shown that tumors not only have functional mitochondria (Koppenol et al., 2011), but that tumors require

mitochondria and respiration for growth, progression, and metastasis (LeBleu et al., 2014; Tan et al., 2015; Viale et al., 2014; Weinberg et al., 2010). Thus, an explanation for high glycolytic flux and lactate production in cancer must also account for the fact that mitochondrial respiration is also needed for cancer cell proliferation.

One proposed benefit of the Warburg effect is that the increased glucose consumption observed in cancer cells can shunt important biosynthetic precursors into anabolic reactions that branch from glycolysis, including pathways that contribute to production of nucleosides, lipids and proteins (Boroughs and DeBerardinis, 2015; Cairns et al., 2011; Levine and Puzio-Kuter, 2010). Though the idea that inefficient ATP production is a tradeoff for supporting anabolic reactions is an attractive one, glycolytic intermediates are not necessarily elevated in proliferating cells (Lunt et al., 2015; Williamson et al., 1970) and many cancer cells excrete the majority of glucose carbons as lactate, which questions the extent to which glucose can fuel the biosynthetic reactions that contribute to cell mass (DeBerardinis et al., 2007; Lunt and Vander Heiden, 2011). Indeed, it has been shown that amino acids, rather than glucose, account for the majority of new biomass in proliferating cells (Hosios et al., 2016). Another proposed function of the Warburg effect is to increase the rate of ATP generation, as many have argued that ATP can be produced faster by aerobic glycolysis than by oxidative phosphorylation (Pfeiffer et al., 2001). Yet another explanation is that lactate production facilitates generation of electron carriers, which are required as cofactors for redox reactions in

cells. Increased glucose uptake permits higher production of the reducing equivalent NADPH via the oxidative branch of the pentose phosphate pathway and production of the oxidizing equivalent NAD+ via the action of lactate dehydrogenase (LDH) (Vander Heiden et al., 2009). However, it remains unclear whether either of these cofactors could be limiting for cancer cell proliferation (Vander Heiden and DeBerardinis, 2017). A definitive explanation for how the Warburg effect promotes cancer cell growth remains an area of active investigation (Liberti and Locasale, 2016).

Critical to the phenotype of aerobic glycolysis is the metabolic fate of glucose-derived pyruvate. Pyruvate is the end-product of glycolysis and lies at the intersection of glycolysis in the cytosol and the tricarboxylic acid cycle (TCA) in the mitochondria. Pyruvate oxidation requires the activity of the pyruvate dehydrogenase complex (PDH), which catalyzes the conversion of pyruvate to acetyl-CoA, thereby supplying carbon for the TCA cycle. The oxidation of pyruvate to acetyl-CoA is irreversible under physiological conditions, and thus PDH is a critical regulatory point for energy metabolism in cells. PDH activity can be tuned by pyruvate dehydrogenase kinases (PDK), which inactivate PDH by phosphorylation (Korotchkina and Patel, 2001). The PDK enzymes are transcriptionally upregulated by a number of signaling pathways that are dysregulated in cancer, including aberrant HIF1α activation (Kim et al., 2006; Papandreou et al., 2006), constitutive Wnt signaling (Pate et al., 2014) and p53 loss (Contractor and Harris, 2012). Thus, oncogenic signaling pathways could be an

important contributor to metabolic reprogramming in cancer cells, since these pathways can suppress pyruvate oxidation by activating PDK to suppress PDH.

To understand the contribution of PDH inhibition to the Warburg effect, we increased PDH activity in cancer cells with the small molecule PDK inhibitor AZD7545. We found that PDK inhibition results in a proliferation defect that can be rescued with interventions that increase NAD+ regeneration, suggesting that high PDH activity limits the ability of cells to regenerate electron acceptors. Surprisingly, we find that the NAD+/NADH imbalance caused by AZD7545 is due to insufficient mitochondrial electron transport, which in this context is constrained by the mitochondrial proton gradient. Increasing electron transport chain activity with FCCP, which uncouples mitochondrial respiration from ATP production, or with gramicidin D, which increases ATPase activity, confers resistance to PDK inhibition, suggesting that a requirement for NAD+ regeneration can supersede that of mitochondrial ATP synthesis to support proliferation. Further limiting the capacity for NAD+ regeneration by inhibiting electron transport with the biguanide metformin, which blocks complex I activity, sensitizes cells to AZD7545 in culture and reduces tumor growth in vivo. These data indicate that the ability of mitochondrial respiration to regenerate electron acceptors may be inadequate to support maximal cancer cell proliferation, providing an explanation for why cancer cells increase flux from glucose to lactate.

Results

The PDK inhibitor AZD7545 activates PDH and increases glucose oxidation

To study the metabolic consequences of PDH enzyme regulation in cancer cells, we wanted to stimulate pyruvate oxidation by increasing PDH complex activity. The activity of PDH depends on its phosphorylation state, which in turn is determined by its negative regulator, PDK. Active PDK results in accumulation of inactive, phosphorylated PDH. To determine whether we could promote pyruvate oxidation in mitochondria by repressing PDK (**Figure 1A**), we utilized AZD7545, a potent and selective inhibitor of this enzyme (Kato et al., 2007; Morrell et al., 2003). To validate that this compound functionally inhibits PDK, we first assessed phosphorylation of the PDH complex in cells that had been treated with AZD7545. As expected, AZD7545 treatment resulted in decreased phosphorylation of the E1α subunit of the PDH complex (**Figure 1B**). We further confirmed that the decrease in PDH phosphorylation corresponded to an increase in PDH activity by a dynamic stable-isotope labeling experiment. We found that AZD7545 increased the rate of citrate labeling from [U-$^{13}C_6$]glucose, consistent with increased PDH flux (**Figure 1C**).

Glutamine is the primary substrate for TCA cycle metabolism for cells in culture (Altman et al., 2016; DeBerardinis and Cheng, 2010). A longer, steady-state, labeling experiment confirmed that while glucose incorporation into citrate was increased by AZD7545 treatment (**Figure 1D**), glutamine entry to the TCA cycle was decreased by PDK inhibition (**Figure 1E**), suggesting that PDK inhibition

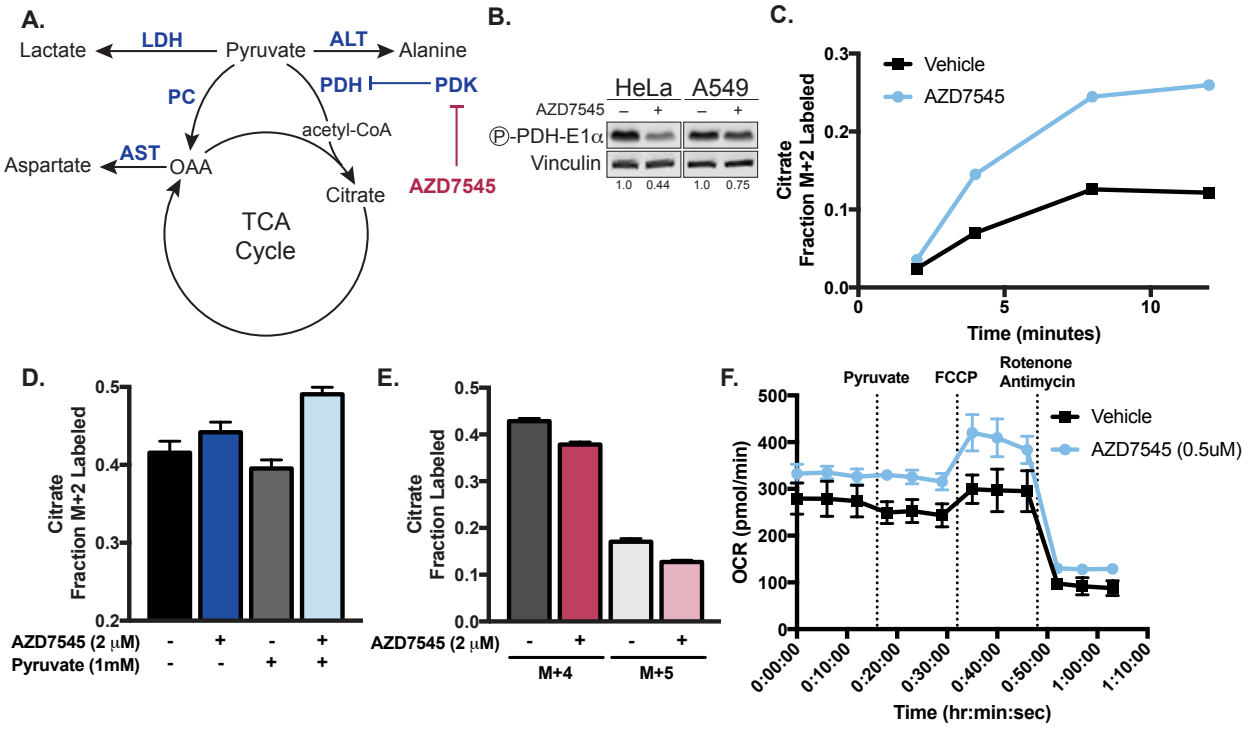
A.
Lactate
LDH
Pyruvate
ALT
Alanine
PC
PDH
PDK
acetyl-CoA
Aspartate
AST
OAA
Citrate
TCA
Cycle
AZD7545
B.
HeLa
A549
AZD7545
Ⓟ-PDH-E1α
Vinculin
1.0 0.44 1.0 0.75
C.
Vehicle
AZD7545
Citrate
Fraction M+2 Labeled
Time (minutes)
D.
Citrate
Fraction M+2 Labeled
AZD7545 (2 μM)
Pyruvate (1mM)
E.
Citrate
Fraction Labeled
AZD7545 (2 μM)
M+4
M+5
F.
Pyruvate
FCCP
Rotenone
Antimycin
Vehicle
AZD7545 (0.5uM)
OCR (pmol/min)
Time (hr:min:sec)

Figure 1. Stimulating PDH activity increases glucose oxidation and oxygen consumption

(A) Schematic illustrating the relationship between pyruvate dehydrogenase kinase (PDK) activity and pyruvate fate. The primary metabolic fates of pyruvate include: (1) metabolism to lactate by lactate dehydrogenase (LDH), (2) entry into the TCA cycle via the enzyme pyruvate carboxylase (PC), which converts pyruvate to oxaloacetate (OAA), (3) entry into the TCA cycle via oxidation by pyruvate dehydrogenase (PDH) to acetyl-CoA, (4) conversion to alanine by alanine transaminase (ALT). PDH is under negative regulation of pyruvate dehydrogenase kinase (PDK) enzymes, which can be inhibited by the compound AZD7545. OAA can be converted to aspartate via aspartate transaminase (AST).

(B) Western blot analysis to assess phosphorylation of the S293 site of the pyruvate dehydrogenase E1-alpha (PDH-E1α) enzyme subunit in cell lines treated with vehicle or 1μM AZD7545 for 2 hours. Vinculin expression was assessed as a loading control. Signal intensity of phosphorylated PDH normalized to vinculin expression is indicated below each lane.

(C) Kinetic labeling of citrate from labeled glucose to assess PDH flux with and without PDK inhibition. The fraction of m+2 citrate was measured after addition of[U-$^{13}C_6$]glucose to HeLa cells for the indicated amount of time. Cells were incubated for 5 hours in media containing 5mM unlabeled glucose with vehicle or 1μM AZD7545, after which 20mM [U-$^{13}C_6$]glucose was added to all conditions. Metabolites were rapidly extracted at the indicated time points and citrate labeling was determined by LCMS (n=3 per time point).

(D) Fraction of citrate that is m+2 labeled from [U-$^{13}C_6$]glucose, measured by GCMS, after culturing HeLa cells in vehicle or 2μM AZD7545 and for 5 hours (n=3).

(E) Fraction of citrate that was m+4 or m+5 labeled from [U-$^{13}C_5$]glutamine, assessed by GCMS, after culturing HeLa cells in vehicle or 2μM AZD7545 for 5 hours (n=3).

(F) Oxygen consumption measured in HeLa cells that that had been treated with vehicle or 0.5μM AZD7545 for five hours. How oxygen consumption changes following the addition of pyruvate, the mitochondrial uncoupler FCCP, and the combination of the complex I inhibitor rotenone and the complex III inhibitor antimycin (n=12).

Values shown denote the mean ± SD.

results in higher levels of glucose oxidation, but not necessarily increased TCA cycle flux. Relevant to this question, mitochondrial oxygen consumption rate (OCR) was increased by AZD7545 (**Figure 1F**), arguing that mitochondrial oxidation reactions are increased in this context. Taken together, we can conclude that PDK inhibition increases oxidative glucose metabolism and suppresses aerobic glycolysis in cancer cells.

Pyruvate, but not lactate, can restore proliferation to PDK inhibited cells

We found that treatment with AZD7545 decreased the proliferation rate of cancer cells in a dose-dependent manner (**Figure 2A-C**). This result is consistent with numerous findings in the literature that argue that repressing the Warburg effect in cancer cells can suppress cell proliferation and tumor growth (Fantin et al., 2006; Le et al., 2010; Xie et al., 2014). Thus, PDK inhibition provides an opportunity to study the molecular consequences of increased glucose oxidation and could reveal the benefit conferred by the glycolytic metabolism observed in cancer cells. Since pyruvate is the substrate of the PDH reaction, we wanted to first determine whether adding exogenous pyruvate could alter sensitivity to PDK inhibition. We found that supplementing media with 1mM pyruvate greatly decreased sensitivity to AZD7545 (**Figure 2D-F**).

One potential explanation for why pyruvate rescues PDK inhibition is that because the PDH reaction consumes pyruvate, higher PDH flux caused by PDK

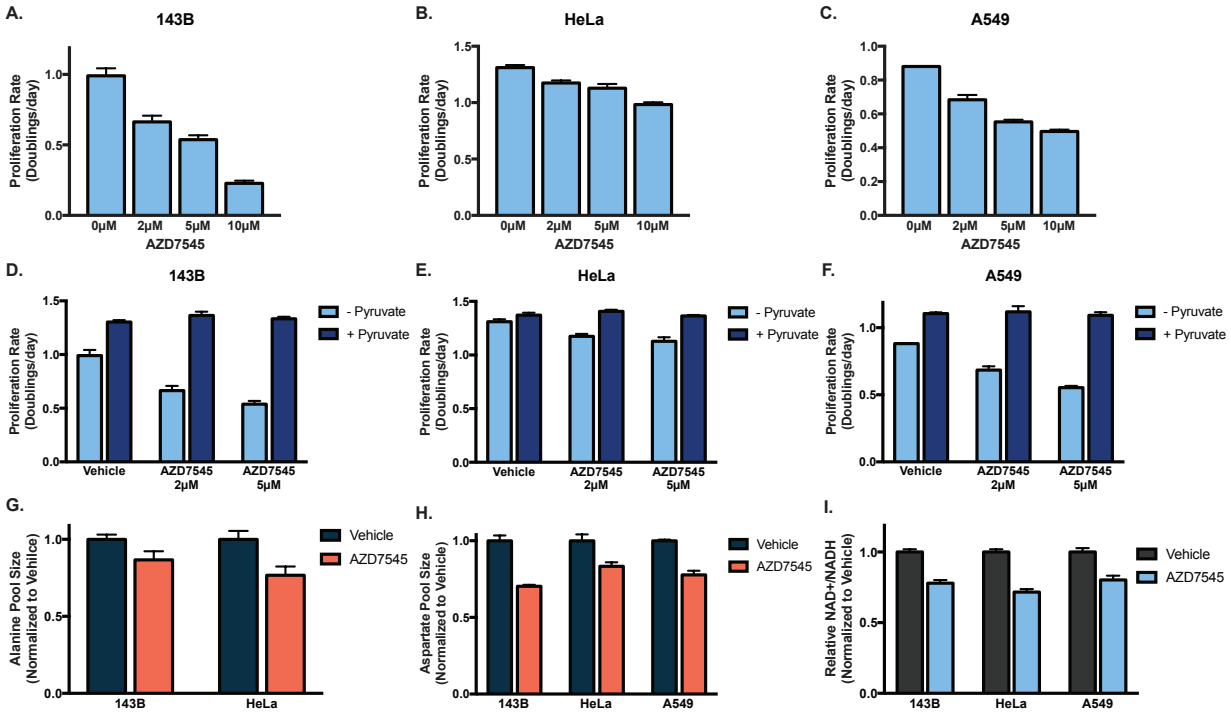

Figure 2. PDK inhibition slows proliferation, and this effect is suppressed by exogenous pyruvate

(A, B, and C) Proliferation rate of (A) 143B (B) HeLa and (C) A549 cells incubated with the indicated doses of AZD7545 (n=3).

(D, E, and F) Proliferation rate of (D) 143B (E) HeLa and (F) A549 cells as measured after treatment with the indicated doses of AZD7545 in the presence or absence of 1mM pyruvate (n=3).

(G) Intracellular alanine levels were measured by LCMS in 143B and HeLa cells following treatment with 1μM AZD7545 for five hours (n=4).

(H) Aspartate levels were measured by LCMS in 143B, A549 and HeLa cells following a five-hour incubation with 1μM AZD7545 (n=4).

(I) Relative change of ratio of NAD+ to NADH was measured by LCMS in 143B, HeLa, and A549 cells that had been incubated in media containing vehicle or 1μM AZD7545 for five hours (n=3).

Values shown denote the mean ± SEM.

inhibition may limit the availability of pyruvate for anabolic pathways, resulting in a proliferation defect that is rescued by providing additional pyruvate. Pyruvate carbon has many metabolic fates, including transamination to alanine and conversion to oxaloacetate via pyruvate carboxylase (Corbet and Feron, 2017) (**Figure 1A**). PDK inhibition was found to deplete levels of intracellular alanine (**Figure 2E**) and aspartate (**Figure 2F**), which is generated by transamination of oxaloacetate. The decreased levels of these substrates in cells caused by PDK inhibition suggest that active PDH could prevent pyruvate carbons from fueling anabolic reactions important for cell proliferation.

An alternative hypothesis is that pyruvate could rescue cells with inhibited PDK by acting as an electron acceptor (Birsoy et al., 2015; Gui et al., 2016; Sullivan et al., 2015). The reaction catalyzed by PDH requires NAD+ as a cofactor, and thus inhibition of PDK would be expected to increase NAD+ consumption. Furthermore, PDH competes with LDH for pyruvate that would otherwise produce an NAD+ in the conversion to lactate, further decreasing the NAD+/NADH ratio in cells. We confirm that the high PDH activity induced by AZD7545 treatment depletes NAD+, treatment with the PDK inhibitor lowers the relative NAD+/NADH ratio in cancer cells (**Figure 2D**).

To determine whether pyruvate suppressed the effects of PDK inhibition by providing carbons required for anabolism or by acting as an exogenous electron acceptor, we utilized lactate to distinguish these two possibilities. It has been reported that lactate can act as a fuel and contribute to central carbon metabolism

(Faubert et al., 2017; Hui et al., 2017; Kennedy et al., 2013) and thus could fulfill some of the anabolic requirements of pyruvate carbon. Indeed, we determine that the addition of exogenous lactate to PDK-inhibited cells was sufficient to increase intracellular pool sizes of alanine and aspartate (**Figure 3A,B**). However, from a redox perspective, lactate is reduced relative to pyruvate, and thus acts as an electron donor rather than an electron acceptor. As expected, exogenous lactate further decreased the NAD+/NADH ratio of cells treated with AZD7545 further (**Figure 3C**).

Since lactate can fulfill some of the of the anabolic functions of pyruvate, but further decreases NAD+ generation, we could use lactate to assess which of these two roles of pyruvate is more important to suppress the anti-proliferative effects of PDK inhibition. We found that adding lactate to the culture media not only failed to rescue AZD7545 treatment, but instead increased the sensitivity of cancer cells to PDK inhibition (**Figure 3D-F**). This suggests that response to AZD7545 can be influenced by the NAD+/NADH ratio in cells. Furthermore, the finding that pyruvate, which can act as an electron acceptor, decreases sensitivity to PDK inhibition, while lactate, which acts as an electron donor, potentiates the effects of AZD7545, argues that the proliferation defects caused active PDH result from insufficient NAD+ regeneration.

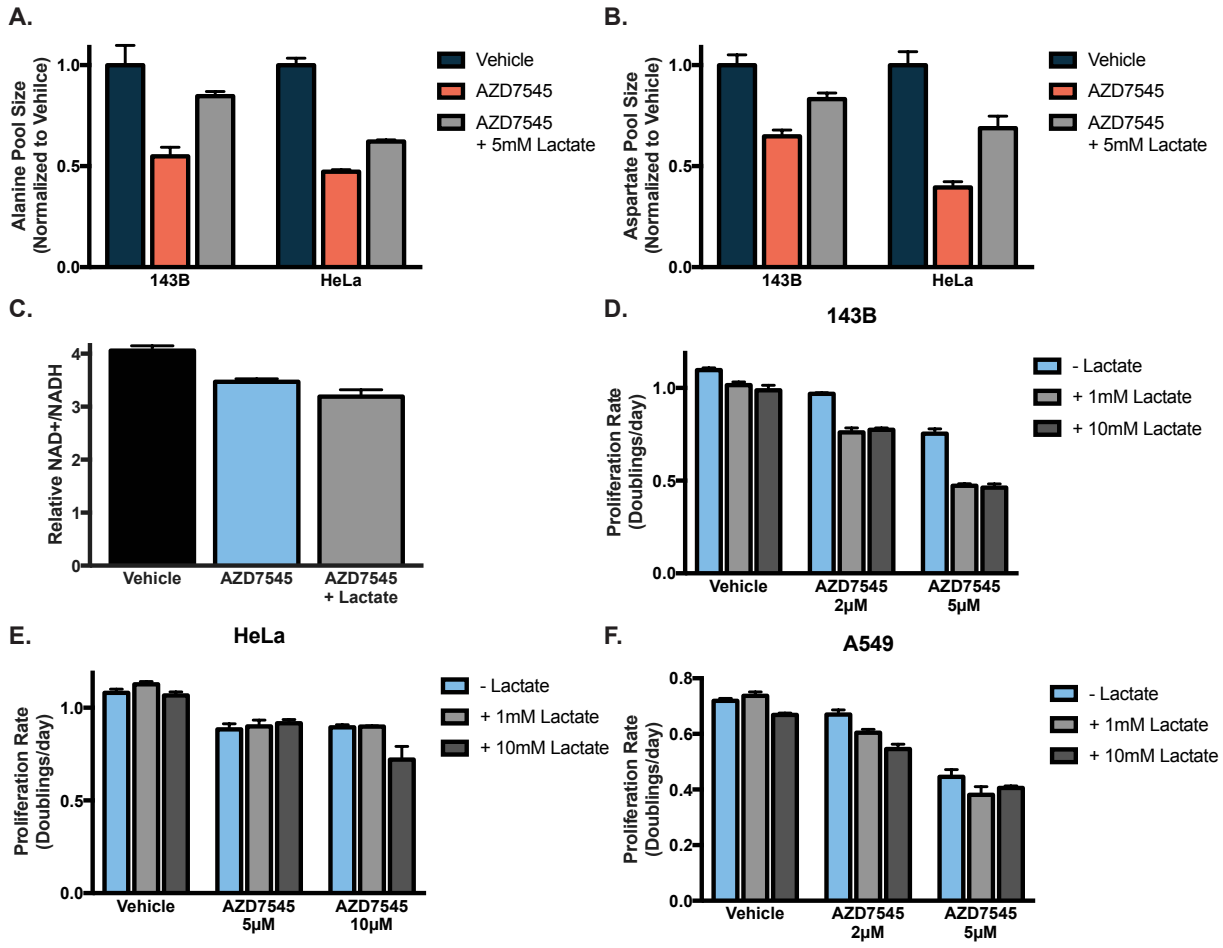

Figure 3. Lactate increases sensitivity of cancer cells to PDK inhibition

(A) Alanine levels were measured by GCMS in 143B and HeLa cells treated with vehicle, 1μM AZD7545, and 5mM lactate as indicated (n=3).

(B) Intracellular aspartate levels were measured by GCMS in 143B and HeLa cells that had been incubated with vehicle, 1μM AZD7545, and 5mM lactate as indicated (n=3).

(C) Relative change in NAD+/NADH as measured by LCMS in HeLa cells that had been incubated in media containing vehicle or 1μM AZD7545 in the presence or absence of 10mM lactate (n=3).

(D,E, and F) Proliferation rate of (D) 143B (E) HeLa and (F) A549 cells incubated with the indicated doses of AZD7545 and 1mM lactate, 10mM lactate, or untreated vehicle) (n=3).

Values shown denote the mean ± SEM.

Alternative pathways for NAD+ regeneration can render cells refractory to PDK inhibition

To further test the hypothesis that pyruvate rescues PDK inhibition by acting as an electron acceptor, we questioned whether orthogonal pathways that regenerate NAD+ could also reduce responsiveness to AZD7545. One method to alter the intracellular NAD+/NADH is to utilize redox reaction pairs that utilize NAD+ and NADH as cofactors. For example, duroquinone permits NAD+ regeneration via the quinone reductase NQO1 (Merker et al., 2006) (**Figure 4A**) and providing cells with duroquinone can rescue proliferation in conditions where NAD+ is limiting (Gui et al., 2016). We treated cells with AZD7545 in the absence or presence of duroquinone and found that duroquinone decreases AZD7545 sensitivity (**Figure 4B,C**). This finding is consistent with our prediction that the proliferation defect caused by PDK inhibition is due to NAD+/NADH imbalance. Another method for increasing the intracellular NAD+/NADH is by expression of NADH oxidase from *Lactobacillus brevis* (*Lb*NOX) (Titov et al., 2016) (**Figure 4D**). We generated cell lines expressing either *Lb*NOX or empty vector (E.V.) under a doxycycline-inducible promoter, allowing us to increase the capacity for NAD+ production of these cells (**Figure 4E**). We performed a titration of AZD7545 on E.V. or *Lb*NOX cancer cells in media containing doxycycline and assessed proliferation. We found that *Lb*NOX conferred resistance to PDK inhibition (**Figure 4F,G**), further arguing that restoring NAD+ regeneration and increasing the NAD+/NADH reduction potential can decrease sensitivity to PDK inhibition.

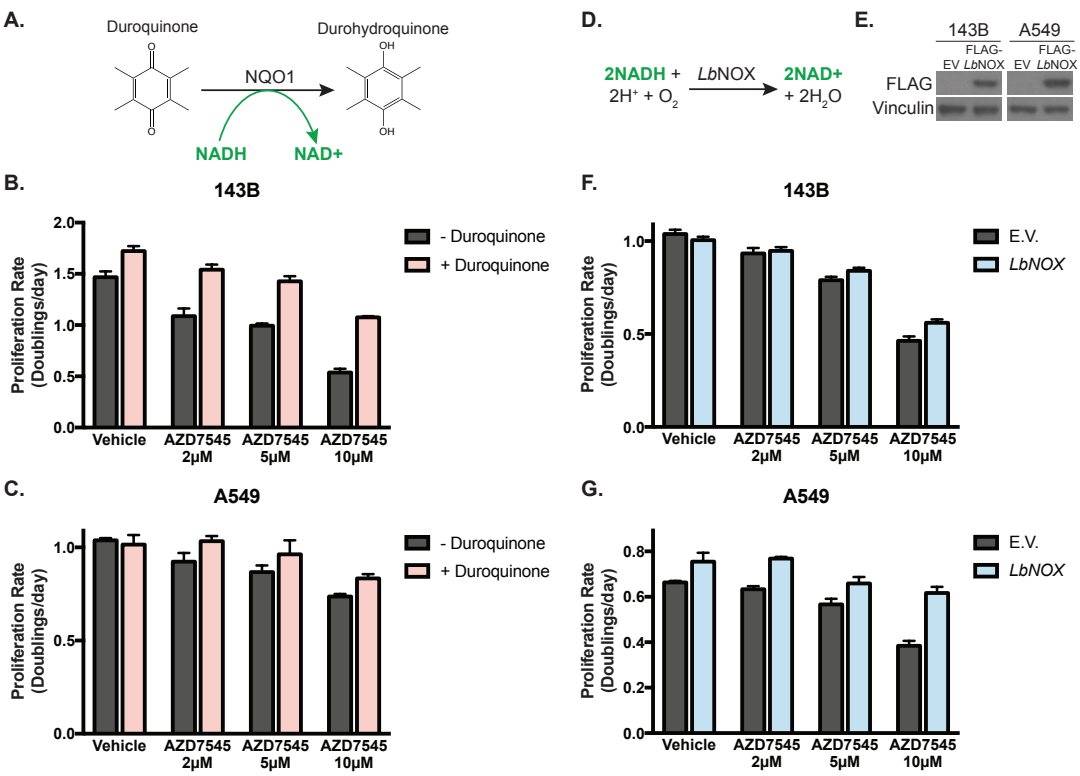

Figure 4. Antiproliferative effect of PDK inhibition is suppressed by increasing intracellular NAD+

(A) Schematic illustrating how duroquinone supplementation can increase NAD+. The enzyme NAD(P)H dehydrogenase, quinone 1 (NQO1) reduces duroquinone to durohydroquinone using NADH as a cofactor.

(B and C) Proliferation rate of (B) 143B and (C) A549 cells incubated with the indicated doses of AZD7545 and 5mM duroquinone as indicated (n=3).

(D) Schematic indicating the reaction catalyzed by the NADH oxidase from *Lactobacillus brevis* (*Lb*NOX).

(E) Western blot analysis using an anti-FLAG antibody to examine expression of *Lb*NOX in 143B and A549 cells that had been infected with pInducer20-E.V. or pInducer20-*Lb*NOX-FLAG and incubated with 500ng/mL doxycycline. Vinculin expression was also assessed as a loading control.

(G and F) Effect of *Lb*NOX expression on sensitivity to AZD7545. Proliferation rate of A549 and 143B cells incubated with the indicated doses of AZD7545 and doxycycline (500ng/mL) to induce *Lb*NOX expression. E.V. denotes cells with empty vector where *Lb*NOX is not expressed in response to doxycycline (n=3).

Values shown denote the mean ± SEM.

Increasing aspartate availability can rescue the proliferation defect caused by PDK inhibition

Maintaining NAD+/NADH balance can support de novo aspartate synthesis under conditions of electron transport chain inhibition (Birsoy et al., 2015; Sullivan et al., 2015). Aspartate is essential product of metabolism that is needed to make proteins as well as for purine and pyrimidine biosynthesis, and thus aspartate can be a limitation for cancer cell growth (Birsoy et al., 2015; Gui et al., 2016; Sullivan et al., 2015) Sullivan et al. 2018). Since we had found that PDK inhibition could constrain NAD+ regeneration and deplete intracellular aspartate, we wanted to assess whether exogenous aspartate could replace the requirement for electron acceptors in cells with active PDH. We found that supplementing culture media with aspartate could confer resistance to PDK inhibition, as assessed by proliferation rate (**Figure 5A-C**). Interestingly, we found that exogenous aspartate can increase the NAD+/NADH ratio in both basal conditions and upon treatment with AZD7545 (**Figure 5D**). Therefore, though AZD7545 limits aspartate production and results in aspartate deficiency (**Figure 2H**) it is difficult to distinguish whether the proliferation defect caused by this compound is caused by the biosynthetic demand of aspartate or electron acceptor limitation. It is likely that both parameters are related and contribute the responsiveness of cancer cells to AZD7545, particularly since lactate addition is sufficient to increase aspartate levels without rescuing proliferation.

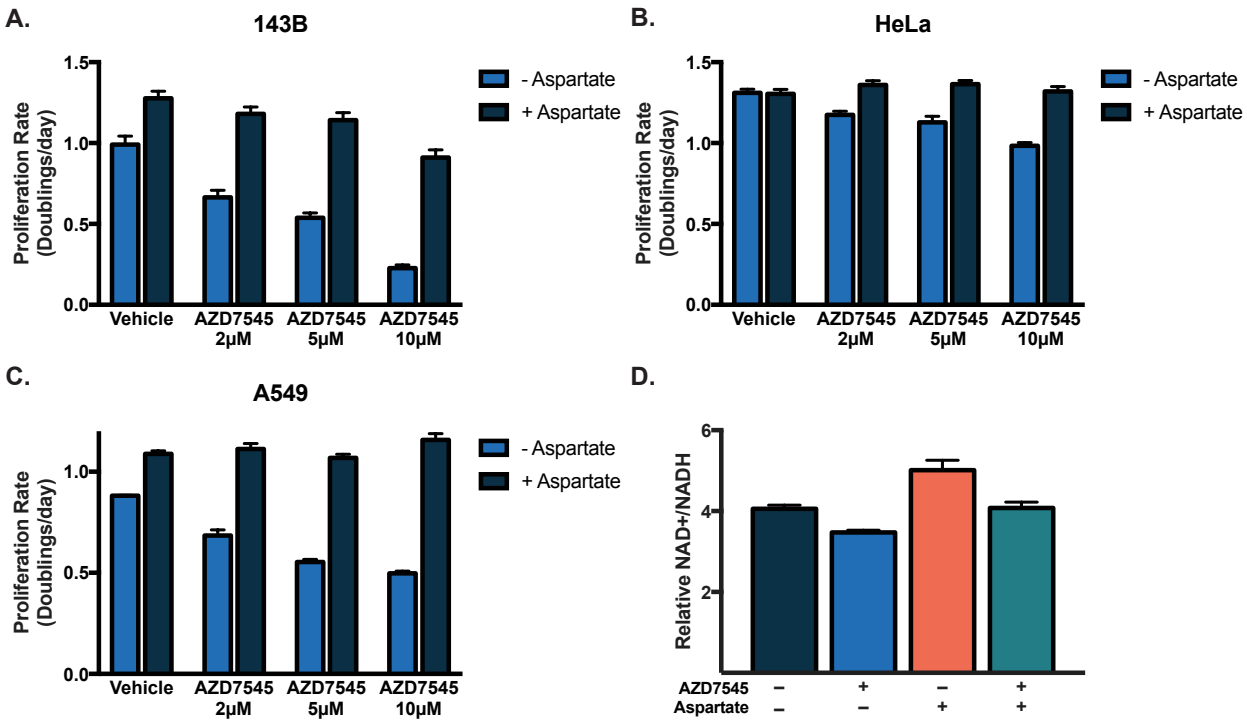

Figure 5. Proliferation of PDK-inhibited cells is restored by exogenous aspartate

(A, B, and C) Proliferation rate was measured in (A) 143B, (B) HeLa and (C) A549 cells that had been incubated with the indicated doses of AZD7545 and treated without or with 20mM of exogenous aspartate as indicated (n=3).

(D) Relative change in ratio of NAD+ to NADH was measured by LCMS in HeLa cells that had been incubated with vehicle or 1μM AZD7545 with or without 20mM aspartate as indicated (n=3).

Values shown denote the mean ± SEM.

FCCP treatment can relieve mitochondrial membrane hyperpolarization and the NAD+/NADH imbalance caused by PDK inhibition

Our data suggests that PDK inhibition reduces the availability of electron acceptors and perturbs NAD+/NADH balance. NAD+ is necessary to support the activities of many metabolic pathways, including oxidative catabolic reactions (Hosios and Vander Heiden, 2018). There are two primary mechanisms by which cells can regenerate NAD+ consumed by both glycolysis and anabolic pathways. In the cytosol, LDH can produce NAD+ by the reduction of pyruvate to lactate (Wuntch et al., 1970). NAD+ can also be regenerated by the mitochondrial electron transport chain (ETC), in which the electrons of NADH are transferred to oxygen to generate water. PDK inhibition decreases NAD+ regeneration by LDH, as this leads to increased PDH activity and competes with LDH for the same substrate. However, it is unclear why cells treated with AZD7545 should not be able to regenerate NAD+ via ETC, as these cells have functional mitochondrial electron transport, and in fact display increased rates of basal oxygen consumption (OCR) (**Figure 6A**). Nevertheless, cells display NAD+/NADH imbalance upon PDK inhibition, suggesting that despite increasing mitochondrial ETC, these cells remain deficient for electron acceptors. We therefore wondered what factor was limiting NAD+ regeneration by mitochondrial respiration in cells with PDK inhibition.

As the terminal substrate of ETC, oxygen can be limiting for electron transport, but we found this possibility unlikely because the mitochondrial respiration has been shown to function at oxygen levels as low as 0.5% (Rumsey et

al., 1990), and these cells were cultured at atmospheric 21% oxygen. Furthermore, the expression of *Lb*NOX, which requires oxygen as a substrate, suppressed the anti-proliferative effect of AZD7545, arguing against oxygen being limiting in PDK-inhibited cells. The oxidation-reduction reactions of the electron transport chain are coupled to proton pumping into the inter-membrane space of the mitochondria, forming an electrochemical gradient that drives ATP production via the F_oF_1 ATP synthase (Mitchell 1961). To test whether we could restore NAD+/NADH balance in cells with inhibited PDK by decoupling mitochondrial electron transport from ATP synthesis, we utilized the ionophore carbonyl cyanide-4-(trifluoromethoxy)phenylhydrazone (FCCP). FCCP is an uncoupling agent that dissipates the electrochemical gradient across the inner mitochondrial membrane, thereby permitting a higher rate of mitochondrial respiration that is dependent on the availability of substrates of ETC, including NADH. Treatment with FCCP increased oxygen consumption to a greater extent in cells treated with AZD7545 (**Figure 6B**), validating that cells with PDK inhibition have increased mitochondrial NADH generation (**Figure 2I**). Furthermore, uncoupling mitochondrial respiration from ATP production increases the capacity of cells to regenerate NAD+, as FCCP treatment was found to restore the NAD+/NADH ratio (**Figure 6C**) and intracellular aspartate pool sizes (**Figure 6D**) in cells with inhibited PDK.

If increasing the capacity for the ETC to regenerate NAD+ were sufficient to rescue the effects of PDK inhibition, then FCCP should restore the proliferation of

cells treated with AZD7545. We measured the growth rate of PDK-inhibited cells in the absence or presence of a low concentration of FCCP and determined that FCCP increased proliferation of cells treated with AZD7545 (**Figure 6E-G**). Thus, the regeneration of electron acceptors appears to be more important for cancer cell proliferation than mitochondrial ATP synthesis when PDK is inhibited. Furthermore, uncoupling the mitochondria was found to rescue the proliferation defects and NAD+/NADH imbalance caused by PDK treatment, suggesting that in the absence of FCCP, mitochondrial electron transport is limited by ATP consumption. In other words, a constraint for respiration in these cells could be the rate of ATP synthesis because the action of the F_oF_1 ATP synthase is insufficient to relieve the proton gradient generated by the ETC, leading to increased mitochondrial membrane polarization and limiting NAD+ regeneration via the ETC. To test this hypothesis, we utilized the electrochemical sensitive positive dye, tetramethylrhodamine ethyl ester (TMRE), which labels mitochondria with high membrane potentials. We assessed TMRE staining by flow cytometry and found that AZD7545 treatment increases the electrochemical gradient of mitochondria, and that FCCP reverses this effect (**Figure 6H**). This data suggests that though cells increase mitochondrial respiration upon PDK inhibition, ETC is not increased at sufficient levels to solve the NAD+/NADH imbalance caused by AZD7545. Our data also suggests that mitochondrial membrane potential, rather than availability of the terminal electron acceptor oxygen, constrains the respiration of PDK-inhibited cells.

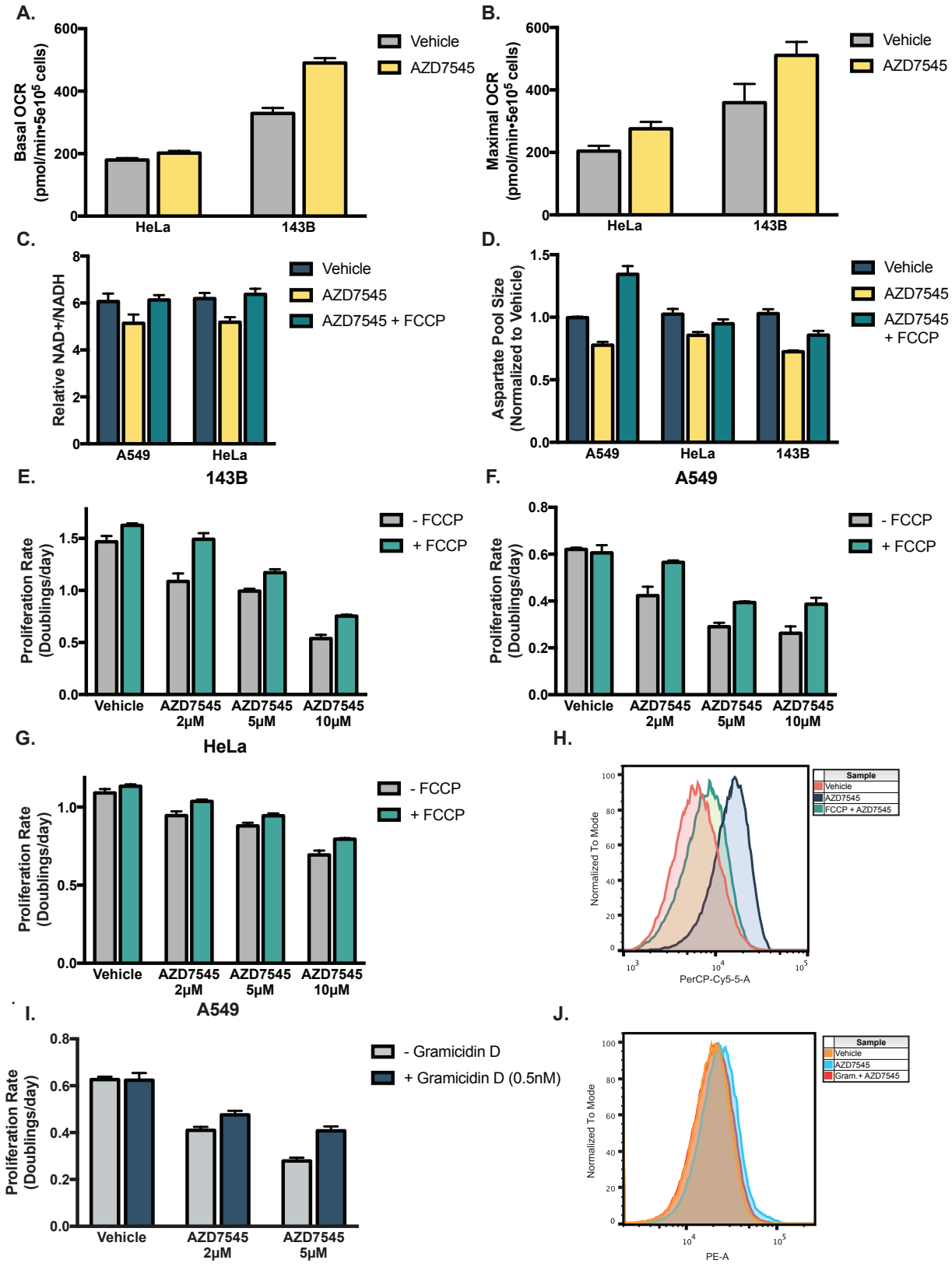
A.
Basal OCR (pmol/min•5e10^5 cells)
600
400
200
0
HeLa
143B
Vehicle
AZD7545
B.
Maximal OCR (pmol/min•5e10^5 cells)
600
400
200
0
HeLa
143B
Vehicle
AZD7545
C.
Relative NAD+/NADH
8
6
4
2
0
A549
HeLa
143B
Vehicle
AZD7545
AZD7545 + FCCP
D.
Aspartate Pool Size (Normalized to Vehicle)
1.5
1.0
0.5
0.0
A549
HeLa
143B
Vehicle
AZD7545
AZD7545 + FCCP
E.
Proliferation Rate (Doublings/day)
1.5
1.0
0.5
0.0
Vehicle
AZD7545 2μM
AZD7545 5μM
AZD7545 10μM
- FCCP
+ FCCP
HeLa
F.
Proliferation Rate (Doublings/day)
0.8
0.6
0.4
0.2
0.0
Vehicle
AZD7545 2μM
AZD7545 5μM
AZD7545 10μM
- FCCP
+ FCCP
A549
G.
Proliferation Rate (Doublings/day)
1.0
0.5
0.0
Vehicle
AZD7545 2μM
AZD7545 5μM
AZD7545 10μM
- FCCP
+ FCCP
A549
H.
Normalized To Mode
100
80
60
40
20
0
10^3
10^4
10^5
PerCP-Cy5-5-A
Sample
Vehicle
AZD7545
FCCP + AZD7545
I.
Proliferation Rate (Doublings/day)
0.8
0.6
0.4
0.2
0.0
Vehicle
AZD7545 2μM
AZD7545 5μM
- Gramicidin D
+ Gramicidin D (0.5nM)
J.
Normalized To Mode
100
80
60
40
20
0
10^4
10^5
PE-A
Sample
Vehicle
AZD7545
Gram.+ AZD7545

Figure 6. Uncoupling electron transport from ATP synthesis, and increasing ATP consumption, suppresses the antiproliferative effect of AZD7545.

(A) The basal oxygen consumption rate (OCR) of HeLa and 143B cells cultured with vehicle or 0.5μM AZD7545 is shown (n=4).

(B) The oxygen consumption rate was assessed upon administration of FCCP to HeLa and 143B cells that had been treated with vehicle or 0.5μM AZD7545 (n=4).

(C) The relative change in the ratio of NAD+ to NADH was measured by LCMS after treating A549 and HeLa cells with vehicle, 2μM AZD7545, or 2μM AZD7545 and 250nM FCCP for five hours (n=4).

(D) Intracellular aspartate levels were measured by LCMS in cells that had been treated with vehicle, 2μM AZD7545, or 2μM AZD7545 and 250nM FCCP for five hours (n=4).

(E, F, and G) Proliferation rate was assessed in (E) 143B, (F) A549 and (G) HeLa cells that had been incubated with the indicated doses of AZD7545 and in the presence or the absence of 500nM FCCP.

(H) Mitochondrial membrane potential was assessed in 143B cells that had been incubated with vehicle or 1μM AZD7545 and with or without 500nM of FCCP as indicated. Mitochondrial membrane potential was assessed by TMRE (tetramethylrhodamine, ethyl ester) dye uptake, and quantified by flow cytometry.

(I) Proliferation rate in A549 cells was measured after treating cells with vehicle, 5μM AZD7545, and/or 0.5nM gramicidin as indicated.

(J) Mitochondrial membrane potential was assessed in A549 cells that had been incubated with vehicle or 1μM AZD7545 and with or without 1nM of gramicidin as indicated. Mitochondrial membrane potential was assessed by TMRE (tetramethylrhodamine, ethyl ester) dye uptake, and quantified by flow cytometry.

Values in all panels denote the mean ± SEM.

ATP hydrolysis can suppress the proliferation defect caused by AZD7545

We next wanted to assess whether we could stimulate mitochondrial electron transport in PDK-inhibited cancer cells by increasing the activity of the F_oF_1 ATP synthase. Increasing mitochondrial ATP synthesis is predicted to relieve the hyperpolarized proton gradient across the inner mitochondrial membrane, increasing the capacity of cells to regenerate NAD+. One way to stimulate mitochondrial ATP synthesis, and consequently respiration, is to increase ATP consumption such that increased levels of ADP can stimulate ATP synthase activity (Brown, 1992). Thus, we sought to increase ADP availability in PDK-inhibited cells by pharmacologically increasing ATP hydrolysis by the plasma membrane Na+/K+ ATPase. Na+/K+ ATPase activity can be enhanced by low doses of gramicidin D, a sodium ionophore that forms channels in the plasma membrane and increases the permeability of Na+ and K+ ions (Nobes et al., 1989). Gramicidin D treatment has been shown to increase the rate of oxidative phosphorylation in cells (Vander Heiden et al., 1999), suggesting that this compound can increase mitochondrial ETC activity. We determined that cancer cells were more resistant to AZD7545 treatment when grown in the presence of gramicidin D (**Figure 6I**) and that this compound can relieve mitochondrial membrane hyperpolarization (**Figure 6J**), suggesting that stimulating ATP consumption in cells with inactive PDK can enhance mitochondrial respiration and restore NAD+/NADH homeostasis. More broadly these data indicate that ETC activity in intact cells may be limited by ADP

availability in some contexts and arguing limited ATP consumption, rather than a demand for increased ATP production, contribute to the Warburg effect in cancer.

PDH activation increases dependency on complex I for NAD+ regeneration and sensitizes cells to metformin treatment in vitro and in vivo

Cells treated with PDK inhibition have limited capacity to regenerate NAD+ via mitochondrial respiration, despite increased OCR. Therefore, interventions that inhibit the ETC could limit electron acceptor availability more severely and potentiate the anti-proliferative effects of AZD7545. To test this hypothesis, we assessed sensitivity of cancer cells to the biguanide metformin, which limits NAD+ regeneration via complex I (Wheaton et al., 2014). We found that the combination of metformin and AZD7545 reduced the proliferation of cancer cells in a synergistic manner (**Figure 7A-C**). Furthermore, low dose AZD7545 treatment is sufficient to decrease the IC_{50} of metformin by more than 30% in both HeLa and A549 cells (**Figure 7D,E**), confirming that PDK inhibition increases dependency on complex I for NAD+ regeneration. The anti-proliferative effect of the combination of AZD7545 and metformin was ablated by media supplementation with pyruvate, suggesting that as predicted, this effect is mediated by synergistic loss of NAD+/NADH homeostasis.

We next assessed whether we could recapitulate the synergistic effects of metformin and PDK inhibition to limit tumor growth. Availability of electron acceptors has been shown to be limiting for tumor growth in some contexts (Gui et

al., 2016; Schockel et al., 2015; Wheaton et al., 2014) and thus we hypothesized that further limiting NAD+ regeneration with the combination of AZD7545 and metformin could have a larger effect on tumor growth than either drug alone. We implanted A549 cells into the flanks of nude mice and when the tumors reached a size of 50mm^3, the mice were randomized into four groups. Mice were treated once per day by oral gavage of either vehicle, 500 mg/kg metformin, 45 mg/kg AZD7545, or a combination of the two treatments. Metformin was found to inhibit tumor growth as previously reported (Gui et al., 2016; Wheaton et al., 2014). AZD7545 had no effect on xenograft growth alone, but increased the effect of metformin (**Figure 7F**).

The finding that AZD7545 treatment did not decrease tumor growth as a single agent might be expected from the pharmacokinetics of this compound. Three hours after AZD7545 dosing, we find that levels of the compound in tumors and in serum correspond to concentrations that conferred a proliferation defect to cells in culture (**Figure 7G,H**). However, twenty-four hours after treatment, the compound could no longer be detected by LCMS in plasma (**Figure 7G**). This argues that more frequent dosing scheme of AZD7545 may be more effective for inhibiting growth in tumors alone, and enhancing the effects of metformin treatment. Nevertheless, once a day dosing of AZD7545 was sufficient potentiate the anti-tumor effects of metformin, suggesting that drug combinations that synergistically limit electron acceptor availability could be a mechanism to inhibit tumor growth.

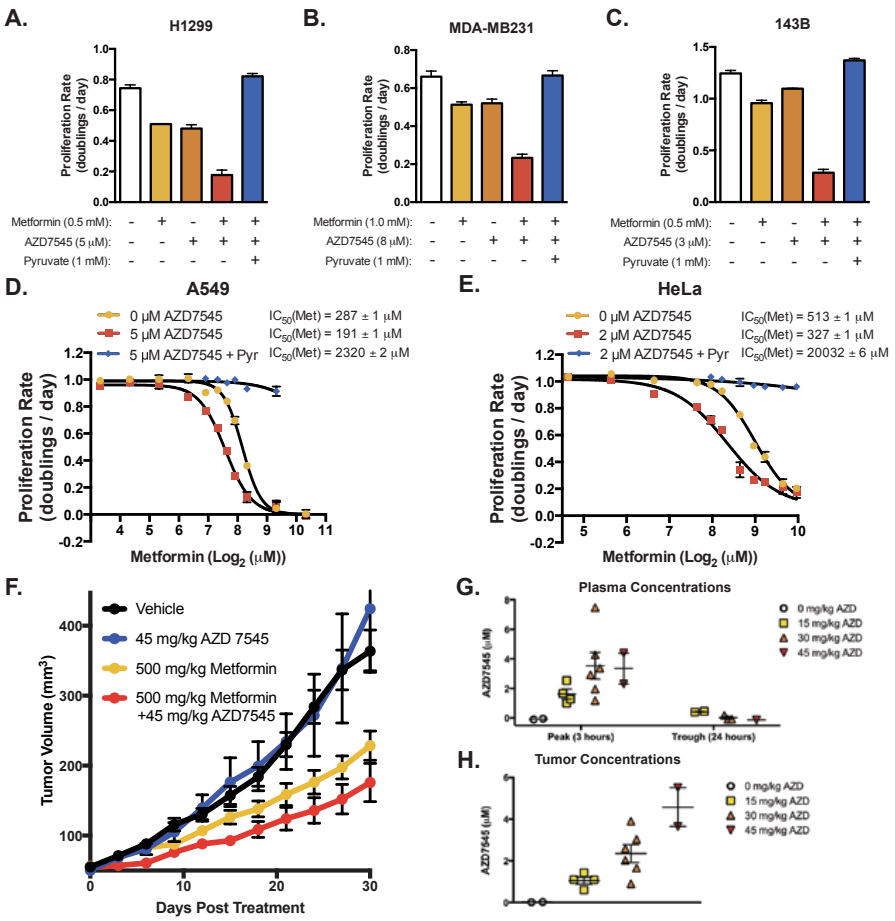

Figure 7. PDK inhibition synergizes with metformin to suppress cell proliferation and slow tumor growth.

(A, B, and C) Proliferation rates of (A) H1299, (B) MDA-MB231, and (C) 143B cells with the indicated doses of metformin and AZD7535 with and without pyruvate.

(D and E) Proliferation rates at different doses of metformin were measured in (D) A549 and (E) HeLa cells cultured in the presence or absence of AZD7545.

(F) Assessment of tumor volume over time of xenograft tumors generated from A549 cells. Mice were treated with either vehicle (water) or 500mg/kg metformin and with either vehicle (0.5% (w/w) methocel/0.1% polysorbate 80) or 45mg/kg AZD745 administered by daily oral gavage. Treatment was initiated in mice with size-matched tumors upon reaching a volume of 50mm^3.

(G) AZD7545 concentration in mouse plasma was measured by LCMS following administering the indicated doses of AZD7545 by oral gavage. Mouse serum was collected three hours (Peak) and 24 hours (Trough) after dosing.

(H) AZD7545 concentration in mouse tumors was measured by LCMS following treatment of mice with the indicated doses of AZD7545 by oral gavage.

Values denote mean ± SEM

Discussion

We find that suppressing the Warburg effect in cancer cells by targeting PDK perturbs NAD+/NADH homeostasis and decreases proliferation. Because PDH lies at the intersection between glycolysis and glucose oxidation, this enzyme represents critical regulator of aerobic glycolysis in cancer cells. For this reason, there has long been interest to increase PDH flux for cancer therapy (Stacpoole, 2017). Like AZD7545, the compound dichloroacetate (DCA) can inhibit PDK, and this compound has demonstrated antitumor activity in some contexts (Bonnet et al., 2007; Michelakis et al., 2010). However, DCA has generally shown limited capacity to decrease tumor growth as a single agent (Cairns et al., 2007; Garon et al., 2014; Shahrzad et al., 2010; Sun et al., 2010), with some studies requiring DCA concentrations as high as 50mM to inhibit cancer cell growth (Allen et al., 2015; Lin et al., 2014; Madhok et al., 2010). Our data suggests that compounds that inhibit PDK activity could be more effective when combined with other drugs that limit capacity for NAD+ regeneration, such as electron transport chain inhibitors like metformin. Efforts to clinically target features of Warburg effect, including glucose uptake and lactate excretion, have been challenging (Hay, 2016; Luengo et al., 2017), but interventions that restrict the oxidative capacity of cells could be one strategy to exploit the enhanced glycolytic flux observed in cancer cells.

Our data shows that electron acceptor availability can restrict cancer cell proliferation, supporting studies reporting that the NAD+/NADH ratio can correlate with tumor proliferation (Gui et al., 2016). Though the reactions that regenerate

NAD+ do not directly provide biomass to cancer cells, this cofactor is needed to catabolize reduced nutrients, including sugars and lipids, and to synthesize oxidized macromolecules, such as nucleotides and amino acids (Hosios and Vander Heiden, 2018; Lunt and Vander Heiden, 2011). Furthermore, cancer cells require NAD+ for many important cellular processes, including the histone deacetylation by sirtuins, maintenance of calcium homeostasis, and poly(ADP-ribose) polymerase activity (Ying, 2008). Proliferating cells have been described as having high NAD+/NADH ratios to support growth (Schwartz et al., 1974), but recently tumor cells have been shown to be more reduced than what was previously assumed (Hung et al., 2011; Zhao et al., 2016), supporting the hypothesis that electron acceptor availability can be limited in tumors.

Entry of glucose carbons into the mitochondria limits NAD+ regeneration by LDH and consequently increases dependency on mitochondrial electron transport for access to oxygen as an electron acceptor. Though cancer cells with inactive PDK have functional mitochondria, and in fact display elevated rates of mitochondrial respiration, we find that in this context the oxidative capacity of ETC is constrained by a high ATP/ADP ratio, and this can slow proliferation. Interestingly, human cancer cell lines have been described as having an increased mitochondrial proton gradient relative to non-cancerous tissues (Bonnet et al., 2007; Chen, 1988), and membrane hyperpolarization has been associated with tumor progression and invasion (Heerdt et al., 2005). This could indicate that the constrained oxidative capacity of mitochondrial respiration is a general feature of cancer cells in many

contexts, and suggests that one possible explanation for the Warburg effect phenotype is that the mitochondrial membrane potential constrains electron acceptor regeneration by ETC, and the resulting high NADH/NAD+ ratio promotes flux through LDH to regenerate NAD+ consumed in glycolysis.

While recent findings have confirmed that electron acceptors can be limiting under conditions of mitochondrial inhibition (Birsoy et al., 2015; Gui et al., 2016; Sullivan et al., 2016; Titov et al., 2016), the data presented in this study suggest that electron acceptor availability can be endogenously limited by mitochondrial membrane potential and intracellular ATP when glucose oxidation is enhanced. Why mitochondrial activity is regulated to limit pyruvate oxidation to not exceed the ATP production needs of a cell is not well understood, but this may restrict generation of reactive oxygen species and limit cell damage. It also suggests that regulation to uncouple ATP production from respiration might be beneficial in some contexts to allow oxidation reactions at rates that exceed the demand for ATP production, a state already known to be the case for heat generation in endothermic organs (Nicholls and Locke, 1984).

Aerobic glycolysis is an inefficient means of generating ATP when considering the yield per glucose molecule. However, our data provide further evidence that ATP is not necessarily limiting for cancer cell proliferation. Uncoupling the mitochondria with FCCP decreased the sensitivity of cells to AZD7545, suggesting that that requirement for electron acceptors supersedes that of ATP in this context. Furthermore, the finding that enhancing the rate of ATP

hydrolysis with gramicidin D restores growth of PDK-inhibited cells serves as further evidence that ATP consumption, rather than ATP itself, can be limiting for proliferation. It has been shown previously that ATP hydrolysis is important for prostate cancer cell growth, and that inhibiting ATPase activity and increasing the ATP/AMP ratio resulted in tumor regression (Fang et al., 2010). While the mechanism by which ATP consumption promotes cancer in this context was unexplained, it is possible that in these settings increasing ATP utilization also promotes NAD+ regeneration in the mitochondria, thereby increasing electron acceptor availability and promoting proliferative metabolism. The idea ATP hydrolysis, rather than ATP synthesis, could be limiting for cancer cell metabolism has historical support (Racker, 1972; Scholnick et al., 1973), even though many more recent studies have focused on how cancer cells use metabolism optimize ATP production. The finding that ATP can be a limitation for the oxidative capacity of mitochondria also supports the notion that the Warburg effect may reflect the increased demand of proliferating cells to regenerate electron acceptors and provides insight into why this metabolic state is associated with proliferation in many different biological systems.

Materials and Methods

Cell Culture Experiments: Cell lines were cultured in DMEM (Corning 10-013-CV) supplemented with 10% fetal bovine serum. For all experiments, cells were washed three times in phosphate buffered saline (PBS), and then cultured in of

DMEM without pyruvate (Corning 10-017-CV) with 10% dialyzed fetal bovine serum, supplemented with the indicated treatment condition. The reagents used for the cell culture experiments are as follows: AZD7545 (Selleck Chemicals, s7517), sodium pyruvate (Sigma, P2256), sodium L-lactate (Sigma, L7022), duroquinone (Sigma, D223204), L-aspartic acid (Sigma A6683), rotenone (Sigma R8875), FCCP (carbonyl cyanide 4-(trifluoromethoxy)phenylhydrazone) (Sigma, C2920), gramicidin from *Bacillus aneurinolyticus* (*Bacillus brevis*) (Sigma, G5002), metformin hydrochloride (Sigma PHR1084). All cells were cultured at 37°C with 5% CO2.

Dynamic stable-isotope labeling experiments: Cells were plated in six-well plates in at a seeding density of 150,000 cells per well. Cells were permitted to settle overnight. Prior to the initiation of the experiment, cells were washed three times with PBS, and then cultured in media containing 5mM glucose and the indicated treatment condition. After cells were cultured for 5 hours, 30μL of a 1M [U-$^{13}C_6$]glucose solution was rapidly administered to each well of the plate and the plate was rocked gently. Following the appropriate incubation (ranging from 2 to 12 minutes), wells were washed as quickly as possible with ice-cold blood bank saline and lysed on the dish with 300μL of ice-cold 80% HPLC grade methanol in HPLC grade water. Samples were scraped, collected into Eppendorf tubes, and vortexed for 10 minutes at 4°C. Samples were centrifuged at 21,000×g for 10 minutes at 4°C to precipitate the protein. 50μM of each sample was collected for immediate analysis by liquid chromatography mass-spectrometry (LCMS).

LCMS Metabolite Profiling: Metabolite profiling was conducted on a QExactive bench top orbitrap mass spectrometer equipped with an Ion Max source and a HESI II probe, which was coupled to a Dionex UltiMate 3000 HPLC system (Thermo Fisher Scientific, San Jose, CA). External mass calibration was performed using the standard calibration mixture every 7 days. For each sample, 4μL of each sample was injected onto a SeQuant® ZIC®-pHILIC 150 × 2.1 mm analytical column equipped with a 2.1 × 20 mm guard column (both 5 mm particle size; EMD Millipore). Buffer A was 20mM ammonium carbonate, 0.1% ammonium hydroxide; Buffer B was acetonitrile. The column oven and autosampler tray were held at 25°C and 4°C, respectively. The chromatographic gradient was run at a flow rate of 0.150 mL/min as follows: 0-20 min: linear gradient from 80-20% B; 20-20.5 min: linear gradient form 20-80% B; 20.5-28 min: hold at 80% B. The mass spectrometer was operated in full-scan, polarity-switching mode, with the spray voltage set to 3.0 kV, the heated capillary held at 275°C, and the HESI probe held at 350°C. The sheath gas flow was set to 40 units, the auxiliary gas flow was set to 15 units, and the sweep gas flow was set to 1 unit. MS data acquisition was performed in a range of m/z = 70–1000, with the resolution set at 70,000, the AGC target at 1×10^6, and the maximum injection time (Max IT) at 20 msec. For detection of nicotinamide diadenine nucleotide cofactors, targeted selected ion monitoring (tSIM) scans in positive mode were included. The isolation window was set at 3.0 m/z and tSIM scans were centered at m/z = 665.1243 for NAD(H). For detection of ^{13}C-labeled citrate, a negative mode tSIM scan centered on 194.1985 was included. The

isolation window was set at 8.0 m/z. For all tSIM scans, the resolution was set at 70,000, the AGC target was 1×10^5, and the max IT was 250 msec. Relative quantitation of polar metabolites was performed with XCalibur QuanBrowser 2.2 (Thermo Fisher Scientific) using a 5ppm mass tolerance and referencing an in-house library of chemical standards.

Oxygen Consumption Measurements: An Agilent Seahorse Bioscience Extracellular Flux Analyzer (XF24) was used to measure oxygen consumption rates (OCR). Cells were plated at 50,000 cells per well in Seahorse Bioscience 24-well plates in 100μL of DMEM without pyruvate (Corning 10-017-CV) supplemented with 10% dialyzed fetal bovine serum. An additional 500μL of media was added following 1 hour incubation. The following day, cells were washed three times with PBS and incubated in DMEM without pyruvate with the indicated treatment. Five hours later, OCR measurements were made every 6 minutes, and injections of pyruvate at 16 minutes, FCCP (Sigma, C2920) at 32 minutes, and rotenone (Sigma R8875, 2μM) and antimycin (Sigma A8674, 2μM) at 48 minutes. Basal OCR was calculated by subtracting residual OCR following the addition of rotenone and antimycin from the initial OCR measurements. Maximal OCR was calculated by subtracting residual OCR from the oxygen consumption measure made following the addition of FCCP.

Proliferation Rate Measurements: Proliferation rate was determined as previously described (Gui et al., 2016; Sullivan et al., 2015). Cells were plated in replicate six-well plates in 2mL at an initial seeding density of 20,000 cells per well for all cells except for MDA-MB-231, which were seeded at 40,000 cells per well. Cells were permitted to settle overnight and one six-well dish was counted to calculate the starting cell number at the initiation of the experiment. For all remaining dishes, cells were washed three times with PBS and 4mL of treatment media was added to each well. After 48 hours, cells were washed again three times with PBS and 4mL of the treatment media was replenished. Four days after the initial treatment, cells were counted to obtain the final cell counts for the experiment. All counts were done using a Cellometer Auto T4 Plus Cell Counter (Nexcelcom Bioscience). The proliferation rate was calculated as follows.

$$Proliferation\ Rate\ (doublings/day) = \log_2\left(\frac{\frac{Final\ Cell\ Count\ (day = 4)}{Initial\ Cell\ count\ (day = 0)}}{4\ (days)}\right)$$

Immunoblotting: Cells were treated with 1μM AZD7545 for 2 hours, washed with ice-cold PBS, and scraped into cold RIPA buffer containing cOmplete Mini protease inhibitor (Roche 11836170001). Protein concentration was calculated using the BCA Protein Assay (Pierce 23225) with BSA as a standard. Lysates were resolved by SDS-PAGE and proteins were transferred onto nitrocellulose membranes using the iBlot2 Dry Blotting System (Thermo Fisher, IB21001, IB23001). Protein was

detected with the primary antibodies anti-Pyruvate Dehydrogenase E1-alpha subunit (phospho S293) (Abcam, ab92696), anti-FLAG (Sigma, F1804) and anti-Vinculin (Sigma, V9131). The secondary antibodies used were IR680LT dye conjugated anti-rabbit IgG (Licor Biosciences 925-68021) and IRDye 800CW conjugated anti-mouse IgG (Licor Biosciences 925-32210).

Generation of *Lb*NOX cell lines: *Lb*NOX-FLAG cDNA was cloned from pUC57-*Lb*NOX using the primers 5'-GGGGACAAGTTTGTACAAAAAAGCAGGCATGAAGGTCACCGTGGTC-3' and 5'-GGGGACCACTTTGTACAAGAAAGCTGGGTTTACTTGTCATCGTCATCCTTGTAATC-3'. pUC57-*Lb*NOX was a gift from Vamsi Mootha (Addgene, 75285). The PCR product was subsequently cloned into pInducer20 using LR Clonase II Plus (ThermoFischer 12538120). pInducer20 was a gift from Stephen Elledge (Addgene, 44012). A549 and 143B cells were infected with lentivirus containing pInducer20-*Lb*NOX-FLAG or pInducer20-E.V. and 10μg/mL polybrene (Millipore TR-1003-G). The infected cells were selected in 1mg/mL G418 (VWR-G5005). For proliferation experiments done with these cell lines, all conditions were supplemented with 500ng/mL doxycycline.

Mitochondrial Membrane Potential: Mitochondrial membrane potential was assessed by utilizing the TMRE (tetramethylrhodamine, ethyl ester) assay kit (Abcam, ab113852). 143B cells were treated with 0.1% DMSO, 1μM AZD7545,

500nM FCCP, or AZD7545 and FCCP at the indicated doses for 5 hours. The cells were then treated with 200nM TMRE for 30 minutes, trypsinized, washed with PBS, and resuspended in 1% BSA in PBS. TMRE fluorescence was measured on a BD LSR II flow cytometer.

Mouse experiments: Mouse xenografts were generated from A549 cells. Two million cells were injected into the flanks of NU/NU mice (Charles river Laboratories, 088). A caliper was used to measure flank tumor volume in two dimensions and volume was calculated using the equation $V = (\pi/6)(L \times W^2)$. Length was defined to be the longer of the two dimensions measured. The tumors were permitted to reach a size of $50mm^3$, after which the animals were random assigned to an experimental group and the treatment regimen was initiated. Metformin (500mg/kg) and AZD7545 (45mg/kg) were both administered once daily by oral gavage, with a vehicle of water and 0.5% (w/w) methocel/0.1% polysorbate 80 respectively.

References

Allen, K.T., Chin-Sinex, H., DeLuca, T., Pomerening, J.R., Sherer, J., Watkins, J.B., 3rd, Foley, J., Jesseph, J.M., and Mendonca, M.S. (2015). Dichloroacetate alters Warburg metabolism, inhibits cell growth, and increases the X-ray sensitivity of human A549 and H1299 NSC lung cancer cells. Free Radic Biol Med 89, 263-273.

Altman, B.J., Stine, Z.E., and Dang, C.V. (2016). From Krebs to clinic: glutamine metabolism to cancer therapy. Nat Rev Cancer 16, 619-634.

Birsoy, K., Wang, T., Chen, W.W., Freinkman, E., Abu-Remaileh, M., and Sabatini, D.M. (2015). An Essential Role of the Mitochondrial Electron Transport Chain in Cell Proliferation Is to Enable Aspartate Synthesis. Cell 162, 540-551.

Bonnet, S., Archer, S.L., Allalunis-Turner, J., Haromy, A., Beaulieu, C., Thompson, R., Lee, C.T., Lopaschuk, G.D., Puttagunta, L., Bonnet, S., et al. (2007). A mitochondria-K+ channel axis is suppressed in cancer and its normalization promotes apoptosis and inhibits cancer growth. Cancer Cell 11, 37-51.

Boroughs, L.K., and DeBerardinis, R.J. (2015). Metabolic pathways promoting cancer cell survival and growth. Nat Cell Biol 17, 351-359.

Brown, G.C. (1992). Control of respiration and ATP synthesis in mammalian mitochondria and cells. Biochem J 284 (Pt 1), 1-13.

Cairns, R.A., Harris, I.S., and Mak, T.W. (2011). Regulation of cancer cell metabolism. Nat Rev Cancer 11, 85-95.

Cairns, R.A., Papandreou, I., Sutphin, P.D., and Denko, N.C. (2007). Metabolic targeting of hypoxia and HIF1 in solid tumors can enhance cytotoxic chemotherapy. Proc Natl Acad Sci U S A 104, 9445-9450.

Chen, L.B. (1988). Mitochondrial membrane potential in living cells. Annu Rev Cell Biol 4, 155-181.

Contractor, T., and Harris, C.R. (2012). p53 negatively regulates transcription of the pyruvate dehydrogenase kinase Pdk2. Cancer Res 72, 560-567.

Corbet, C., and Feron, O. (2017). Cancer cell metabolism and mitochondria: Nutrient plasticity for TCA cycle fueling. Biochim Biophys Acta 1868, 7-15.

DeBerardinis, R.J., and Cheng, T. (2010). Q's next: the diverse functions of glutamine in metabolism, cell biology and cancer. Oncogene 29, 313-324.

DeBerardinis, R.J., Mancuso, A., Daikhin, E., Nissim, I., Yudkoff, M., Wehrli, S., and Thompson, C.B. (2007). Beyond aerobic glycolysis: transformed cells can engage in glutamine metabolism that exceeds the requirement for protein and nucleotide synthesis. Proc Natl Acad Sci U S A 104, 19345-19350.

Fang, M., Shen, Z., Huang, S., Zhao, L., Chen, S., Mak, T.W., and Wang, X. (2010). The ER UDPase ENTPD5 promotes protein N-glycosylation, the Warburg effect, and proliferation in the PTEN pathway. Cell 143, 711-724.

Fantin, V.R., St-Pierre, J., and Leder, P. (2006). Attenuation of LDH-A expression uncovers a link between glycolysis, mitochondrial physiology, and tumor maintenance. Cancer Cell 9, 425-434.

Faubert, B., Li, K.Y., Cai, L., Hensley, C.T., Kim, J., Zacharias, L.G., Yang, C., Do, Q.N., Doucette, S., Burguete, D., et al. (2017). Lactate Metabolism in Human Lung Tumors. Cell 171, 358-371 e359.

Garon, E.B., Christofk, H.R., Hosmer, W., Britten, C.D., Bahng, A., Crabtree, M.J., Hong, C.S., Kamranpour, N., Pitts, S., Kabbinavar, F., et al. (2014). Dichloroacetate should be considered with platinum-based chemotherapy in hypoxic tumors rather than as a single agent in advanced non-small cell lung cancer. J Cancer Res Clin Oncol 140, 443-452.

Gui, D.Y., Sullivan, L.B., Luengo, A., Hosios, A.M., Bush, L.N., Gitego, N., Davidson, S.M., Freinkman, E., Thomas, C.J., and Vander Heiden, M.G. (2016). Environment Dictates Dependence on Mitochondrial Complex I for NAD+ and Aspartate Production and Determines Cancer Cell Sensitivity to Metformin. Cell Metab 24, 716-727.

Hay, N. (2016). Reprogramming glucose metabolism in cancer: can it be exploited for cancer therapy? Nat Rev Cancer 16, 635-649.

Heerdt, B.G., Houston, M.A., and Augenlicht, L.H. (2005). The intrinsic mitochondrial membrane potential of colonic carcinoma cells is linked to the probability of tumor progression. Cancer Res 65, 9861-9867.

Hosios, A.M., Hecht, V.C., Danai, L.V., Johnson, M.O., Rathmell, J.C., Steinhauser, M.L., Manalis, S.R., and Vander Heiden, M.G. (2016). Amino Acids Rather than Glucose Account for the Majority of Cell Mass in Proliferating Mammalian Cells. Dev Cell 36, 540-549.

Hosios, A.M., and Vander Heiden, M.G. (2018). The redox requirements of proliferating mammalian cells. J Biol Chem.

Hui, S., Ghergurovich, J.M., Morscher, R.J., Jang, C., Teng, X., Lu, W., Esparza, L.A., Reya, T., Le, Z., Yanxiang Guo, J., et al. (2017). Glucose feeds the TCA cycle via circulating lactate. Nature 551, 115-118.

Hung, Y.P., Albeck, J.G., Tantama, M., and Yellen, G. (2011). Imaging cytosolic NADH-NAD(+) redox state with a genetically encoded fluorescent biosensor. Cell Metab 14, 545-554.

Kato, M., Li, J., Chuang, J.L., and Chuang, D.T. (2007). Distinct structural mechanisms for inhibition of pyruvate dehydrogenase kinase isoforms by AZD7545, dichloroacetate, and radicicol. Structure 15, 992-1004.

Kennedy, K.M., Scarbrough, P.M., Ribeiro, A., Richardson, R., Yuan, H., Sonveaux, P., Landon, C.D., Chi, J.T., Pizzo, S., Schroeder, T., et al. (2013). Catabolism of exogenous lactate reveals it as a legitimate metabolic substrate in breast cancer. PLoS One 8, e75154.

Kim, J.W., Tchernyshyov, I., Semenza, G.L., and Dang, C.V. (2006). HIF-1-mediated expression of pyruvate dehydrogenase kinase: a metabolic switch required for cellular adaptation to hypoxia. Cell Metab 3, 177-185.

Koppenol, W.H., Bounds, P.L., and Dang, C.V. (2011). Otto Warburg's contributions to current concepts of cancer metabolism. Nat Rev Cancer 11, 325-337.

Korotchkina, L.G., and Patel, M.S. (2001). Site specificity of four pyruvate dehydrogenase kinase isoenzymes toward the three phosphorylation sites of human pyruvate dehydrogenase. J Biol Chem 276, 37223-37229.

Le, A., Cooper, C.R., Gouw, A.M., Dinavahi, R., Maitra, A., Deck, L.M., Royer, R.E., Vander Jagt, D.L., Semenza, G.L., and Dang, C.V. (2010). Inhibition of lactate dehydrogenase A induces oxidative stress and inhibits tumor progression. Proc Natl Acad Sci U S A 107, 2037-2042.

LeBleu, V.S., O'Connell, J.T., Gonzalez Herrera, K.N., Wikman, H., Pantel, K., Haigis, M.C., de Carvalho, F.M., Damascena, A., Domingos Chinen, L.T., Rocha, R.M., et al. (2014). PGC-1alpha mediates mitochondrial biogenesis and oxidative phosphorylation in cancer cells to promote metastasis. Nat Cell Biol 16, 992-1003, 1001-1015.

Levine, A.J., and Puzio-Kuter, A.M. (2010). The control of the metabolic switch in cancers by oncogenes and tumor suppressor genes. Science 330, 1340-1344.

Liberti, M.V., and Locasale, J.W. (2016). The Warburg Effect: How Does it Benefit Cancer Cells? Trends Biochem Sci 41, 211-218.

Lin, G., Hill, D.K., Andrejeva, G., Boult, J.K., Troy, H., Fong, A.C., Orton, M.R., Panek, R., Parkes, H.G., Jafar, M., et al. (2014). Dichloroacetate induces autophagy in colorectal cancer cells and tumours. Br J Cancer 111, 375-385.

Locasale, J.W., and Cantley, L.C. (2011). Metabolic flux and the regulation of mammalian cell growth. Cell Metab 14, 443-451.

Luengo, A., Gui, D.Y., and Vander Heiden, M.G. (2017). Targeting Metabolism for Cancer Therapy. Cell Chem Biol 24, 1161-1180.

Lunt, S.Y., Muralidhar, V., Hosios, A.M., Israelsen, W.J., Gui, D.Y., Newhouse, L., Ogrodzinski, M., Hecht, V., Xu, K., Acevedo, P.N., et al. (2015). Pyruvate kinase isoform expression alters nucleotide synthesis to impact cell proliferation. Mol Cell 57, 95-107.

Lunt, S.Y., and Vander Heiden, M.G. (2011). Aerobic glycolysis: meeting the metabolic requirements of cell proliferation. Annu Rev Cell Dev Biol 27, 441-464.

Madhok, B.M., Yeluri, S., Perry, S.L., Hughes, T.A., and Jayne, D.G. (2010). Dichloroacetate induces apoptosis and cell-cycle arrest in colorectal cancer cells. Br J Cancer 102, 1746-1752.

Merker, M.P., Audi, S.H., Bongard, R.D., Lindemer, B.J., and Krenz, G.S. (2006). Influence of pulmonary arterial endothelial cells on quinone redox status: effect of hyperoxia-induced NAD(P)H:quinone oxidoreductase 1. Am J Physiol Lung Cell Mol Physiol 290, L607-619.

Michelakis, E.D., Sutendra, G., Dromparis, P., Webster, L., Haromy, A., Niven, E., Maguire, C., Gammer, T.L., Mackey, J.R., Fulton, D., et al. (2010). Metabolic modulation of glioblastoma with dichloroacetate. Sci Transl Med 2, 31ra34.

Morrell, J.A., Orme, J., Butlin, R.J., Roche, T.E., Mayers, R.M., and Kilgour, E. (2003). AZD7545 is a selective inhibitor of pyruvate dehydrogenase kinase 2. Biochem Soc Trans 31, 1168-1170.

Nicholls, D.G., and Locke, R.M. (1984). Thermogenic mechanisms in brown fat. Physiol Rev 64, 1-64.

Nobes, C.D., Lakin-Thomas, P.L., and Brand, M.D. (1989). The contribution of ATP turnover by the Na+/K+-ATPase to the rate of respiration of hepatocytes. Effects of thyroid status and fatty acids. Biochim Biophys Acta 976, 241-245.

Papandreou, I., Cairns, R.A., Fontana, L., Lim, A.L., and Denko, N.C. (2006). HIF-1 mediates adaptation to hypoxia by actively downregulating mitochondrial oxygen consumption. Cell Metab 3, 187-197.

Pate, K.T., Stringari, C., Sprowl-Tanio, S., Wang, K., TeSlaa, T., Hoverter, N.P., McQuade, M.M., Garner, C., Digman, M.A., Teitell, M.A., et al. (2014). Wnt signaling directs a metabolic program of glycolysis and angiogenesis in colon cancer. EMBO J 33, 1454-1473.

Pfeiffer, T., Schuster, S., and Bonhoeffer, S. (2001). Cooperation and competition in the evolution of ATP-producing pathways. Science 292, 504-507.

Racker, E. (1972). Bioenergetics and the problem of tumor growth. Am Sci 60, 56-63.

Rumsey, W.L., Schlosser, C., Nuutinen, E.M., Robiolio, M., and Wilson, D.F. (1990). Cellular energetics and the oxygen dependence of respiration in cardiac myocytes isolated from adult rat. J Biol Chem 265, 15392-15402.

Schockel, L., Glasauer, A., Basit, F., Bitschar, K., Truong, H., Erdmann, G., Algire, C., Hagebarth, A., Willems, P.H., Kopitz, C., et al. (2015). Targeting mitochondrial complex I using BAY 87-2243 reduces melanoma tumor growth. Cancer Metab 3, 11.

Scholnick, P., Lang, D., and Racker, E. (1973). Regulatory mechanisms in carbohydrate metabolism. IX. Stimulation of aerobic glycolysis by energy-linked ion transport and inhibition by dextran sulfate. J Biol Chem 248, 5175.

Schwartz, J.P., Passonneau, J.V., Johnson, G.S., and Pastan, I. (1974). The effect of growth conditions on NAD+ and NADH concentrations and the NAD+:NADH ratio in normal and transformed fibroblasts. J Biol Chem 249, 4138-4143.

Shahrzad, S., Lacombe, K., Adamcic, U., Minhas, K., and Coomber, B.L. (2010). Sodium dichloroacetate (DCA) reduces apoptosis in colorectal tumor hypoxia. Cancer Lett 297, 75-83.

Shim, H., Chun, Y.S., Lewis, B.C., and Dang, C.V. (1998). A unique glucose-dependent apoptotic pathway induced by c-Myc. Proc Natl Acad Sci U S A 95, 1511-1516.

Stacpoole, P.W. (2017). Therapeutic Targeting of the Pyruvate Dehydrogenase Complex/Pyruvate Dehydrogenase Kinase (PDC/PDK) Axis in Cancer. J Natl Cancer Inst 109.

Sullivan, L.B., Gui, D.Y., Hosios, A.M., Bush, L.N., Freinkman, E., and Vander Heiden, M.G. (2015). Supporting Aspartate Biosynthesis Is an Essential Function of Respiration in Proliferating Cells. Cell 162, 552-563.

Sullivan, L.B., Luengo, A., Danai L.V., Bush L.N., Diehl F.F., Hosios A.M., Lau A.N., Elmiligy S., Malstrom S., Lewis C.A., Vander Heiden M.G. (2018). Evidence for Aspartate as an Endogenous Metabolic Limitation for Tumour Growth. Nat Cell Bio. Manuscript Accepted.

Sun, R.C., Fadia, M., Dahlstrom, J.E., Parish, C.R., Board, P.G., and Blackburn, A.C. (2010). Reversal of the glycolytic phenotype by dichloroacetate inhibits metastatic breast cancer cell growth in vitro and in vivo. Breast Cancer Res Treat 120, 253-260.

Tan, A.S., Baty, J.W., Dong, L.F., Bezawork-Geleta, A., Endaya, B., Goodwin, J., Bajzikova, M., Kovarova, J., Peterka, M., Yan, B., et al. (2015). Mitochondrial genome acquisition restores respiratory function and tumorigenic potential of cancer cells without mitochondrial DNA. Cell Metab 21, 81-94.

Titov, D.V., Cracan, V., Goodman, R.P., Peng, J., Grabarek, Z., and Mootha, V.K. (2016). Complementation of mitochondrial electron transport chain by manipulation of the NAD+/NADH ratio. Science 352, 231-235.

Vander Heiden, M.G., Cantley, L.C., and Thompson, C.B. (2009). Understanding the Warburg effect: the metabolic requirements of cell proliferation. Science 324, 1029-1033.

Vander Heiden, M.G., Chandel, N.S., Schumacker, P.T., and Thompson, C.B. (1999). Bcl-xL prevents cell death following growth factor withdrawal by facilitating mitochondrial ATP/ADP exchange. Mol Cell 3, 159-167.

Vander Heiden, M.G., and DeBerardinis, R.J. (2017). Understanding the Intersections between Metabolism and Cancer Biology. Cell 168, 657-669.

Viale, A., Pettazzoni, P., Lyssiotis, C.A., Ying, H., Sanchez, N., Marchesini, M., Carugo, A., Green, T., Seth, S., Giuliani, V., et al. (2014). Oncogene ablation-resistant pancreatic cancer cells depend on mitochondrial function. Nature 514, 628-632.

Warburg, O. (1956). On the origin of cancer cells. Science 123, 309-314.

Ward, P.S., and Thompson, C.B. (2012). Metabolic reprogramming: a cancer hallmark even warburg did not anticipate. Cancer Cell 21, 297-308.

Weinberg, F., Hamanaka, R., Wheaton, W.W., Weinberg, S., Joseph, J., Lopez, M., Kalyanaraman, B., Mutlu, G.M., Budinger, G.R., and Chandel, N.S. (2010). Mitochondrial metabolism and ROS generation are essential for Kras-mediated tumorigenicity. Proc Natl Acad Sci U S A 107, 8788-8793.

Wheaton, W.W., Weinberg, S.E., Hamanaka, R.B., Soberanes, S., Sullivan, L.B., Anso, E., Glasauer, A., Dufour, E., Mutlu, G.M., Budigner, G.S., et al. (2014). Metformin inhibits mitochondrial complex I of cancer cells to reduce tumorigenesis. Elife 3, e02242.

Williamson, D.H., Krebs, H.A., Stubbs, M., Page, M.A., Morris, H.P., and Weber, G. (1970). Metabolism of renal tumors in situ and during ischemia. Cancer Res 30, 2049-2054.

Wuntch, T., Chen, R.F., and Vesell, E.S. (1970). Lactate dehydrogenase isozymes: further kinetic studies at high enzyme concentration. Science 169, 480-481.

Xie, H., Hanai, J., Ren, J.G., Kats, L., Burgess, K., Bhargava, P., Signoretti, S., Billiard, J., Duffy, K.J., Grant, A., et al. (2014). Targeting lactate dehydrogenase--a inhibits tumorigenesis and tumor progression in mouse models of lung cancer and impacts tumor-initiating cells. Cell Metab 19, 795-809

Ying, W. (2008). NAD+/NADH and NADP+/NADPH in cellular functions and cell death: regulation and biological consequences. Antioxid Redox Signal 10, 179-206.

Zhao, Y., Wang, A., Zou, Y., Su, N., Loscalzo, J., and Yang, Y. (2016). In vivo monitoring of cellular energy metabolism using SoNar, a highly responsive sensor for NAD(+)/NADH redox state. Nat Protoc 11, 1345-1359.

Chapter 4: Targeting lipid biosynthesis to treat breast cancer brain metastases

Authors: Alba Luengo[1,2,8], Gino B. Ferraro[3,4,8], Christopher R. Chin[1], Divya Bezwada[3,4], Shawn M. Davidson[1,2,5], Elena Brachtel[6], Matthew G. Vander Heiden[1,2,6], Rakesh K. Jain[3,4]

Author Affiliations:
[1] Koch Institute for Integrative Cancer Research, Massachusetts Institute of Technology, Cambridge, MA 02139, USA
[2] Department of Biology, Massachusetts Institute of Technology, Cambridge, MA 02139, USA
[3] Edwin L. Steele Laboratory, Department of Radiation Oncology, Massachusetts General Hospital
[4] Harvard Medical School Boston, MA 02114, USA
[5] Broad Institute of MIT and Harvard University, Cambridge, MA 02142, USA
[6] Department of Pathology, Massachusetts General Hospital and Harvard Medical School, Boston, MA 02114, USA
[7] Dana-Farber Cancer Institute, Boston MA 02115, USA
[8] Co-first author

This chapter is unpublished as of May 2018

Abstract

Breast cancer brain metastases are refractory to cancer therapies, even when the same treatment can be used to successfully treat extracranial breast cancer lesions. While challenges associated with therapeutic delivery to the brain can contribute to this phenomenon, the direct influence by the brain tumor microenvironment can also promote resistance to some drugs. To study how tissue site can influence breast cancer metabolism, we assessed glucose fate in a murine model of *HER2*-amplified breast cancer where human cells are implanted to form tumors in the brain or in the mammary fat pad (MFP). We found that breast cancers in the brain exhibit increased glucose consumption and use glucose differently than those growing in the MFP. We also found that breast cancers growing in the brain increase lipid biosynthesis, and that unlike breast tumors in the MFP, the use of glucose carbon to synthesize fatty acids was not dependent phosphoinositide-3-kinase signaling for breast tumors growing at this site. To study changes in metabolism caused by the brain microenvironment, we developed ex vivo platforms that recapitulate the metabolic phenotypes observed in vivo. We also assessed whether targeting lipid synthesis pharmacologically could be a strategy to slow proliferation of breast cancer brain metastasis. Taken together, these data illustrate that the tumor microenvironment can influence glucose metabolism and sensitivity to therapy.

Introduction

Tumor cells rewire metabolism to incorporate nutrients into biomass, balance cellular energetics, and support rapid uncontrolled proliferation (DeBerardinis and Chandel, 2016; Pavlova and Thompson, 2016). Most studies have aimed to define features of the metabolic network that are shared across many tumor types, or are induced by a particular oncogenic lesion. Cancer-associated mutations can cause specific changes in how nutrients are used (Nagarajan et al., 2016), but the phenotype of aerobic glycolysis is considered a hallmark of cancer metabolism and is observed in most tumors, regardless of driver mutation or tissue of origin (Liberti and Locasale, 2016; Vander Heiden et al., 2009). In fact, increased glycolysis is so pervasive among cancers that the associated increase in glucose uptake is routinely exploited to visualize tumors in patients using positron emission tomography of a radiolabeled glucose analogue (^{18}F-FDG-PET) (Hay, 2016). While it is important to define the pathways differentially required for proliferating tumor and normal tissues, how metabolic alterations across different cancer types are influenced by tissue location remains understudied. Despite the fact that mammalian organs have varied nutrient levels and tissue metabolism to support their physiological function, relatively little is known about how tumor cells adapt their metabolic program to permit growth in different microenvironments. Tissue environment has been shown to affect cancer cell metabolism and dependence on specific enzymes (Davidson et al., 2016; Hensley et al., 2016; Sellers et al., 2015), but the majority of cancer metabolism studies rely on standard cell culture, which does not accurately

recapitulate the nutrient conditions found in tissues (Cantor et al., 2017; Muir et al., 2017; Tardito et al., 2015). Thus, in vivo cancer metabolism studies are critical to understand how nutrient availability supports cancer growth in different tumor microenvironments and can help inform our understanding of both cancer cell metabolism and metastases.

Breast cancer brain metastasis (BCBM) is a significant clinical problem with limited treatment options. Patients with breast cancer positive for the receptor tyrosine-protein kinase erbB-2 (HER2) are at high risk of developing BCBM due to the proclivity of HER2-positive tumor cells to colonize the brain parenchyma (Eichler et al., 2011; Kodack et al., 2015). Inhibitors of HER2, including the antibody trastuzumab, are effective for controlling systemic extracranial disease, but BCBMs respond poorly to this treatment and consequently are a major cause of morbidity and mortality for HER2-positive breast cancer patients (Bachelot et al., 2013; Olson et al., 2013). Though resistance to HER2-targeted therapies is most commonly attributed to lack of drug delivery across the blood brain barrier, both preclinical and clinical studies have confirmed that anti-HER2 therapies can accumulate in brain metastases (Askoxylakis et al., 2016; Tamura et al., 2013). Furthermore, BCBM are insensitive to brain-penetrant small-molecule inhibitors of HER2, such as lapatinib (Bachelot et al., 2013; Lin et al., 2008; Lin et al., 2009) as well as brain-penetrant drugs that target signaling downstream of HER2, such as phosphoinositide-3-kinase (PI3K)-targeted therapies (Kodack et al., 2017; Ni et al., 2016). The different clinical response of breast cancers growing in different sites

suggests that tumor microenvironment may play a role in therapy resistance in these patients.

How the environment differs between breast cancer tumors growing in the brain versus other sites is not well characterized. However, metabolism influenced by environment and nutrient conditions can affect response to therapy (Cantor et al., 2017; Davidson et al., 2016; Gui et al., 2016; Muir et al., 2017). Whether environment changes metabolic dependencies of breast cancers growing in the brain in a way that influences response to HER2-targeted therapies is unknown.

Gene expression analysis of brain-tropic breast cancer cells have revealed increased expression of enzymes involved in both glycolysis and oxidative phosphorylation relative to parental breast cancer cells (Chen et al., 2007), but whether this affects metabolic vulnerabilities of breast tumors has not yet been investigated. The blood-brain barrier limits availability of many nutrients, and the brain is unique in relying primarily on glucose metabolism. There is also evidence that tumors growing in the brain exhibit more prominent glucose oxidation (Maher et al., 2012; Marin-Valencia et al., 2012), while another study has argued that BCBM depend more on gluconeogenesis for survival (Chen et al., 2015). A comprehensive assessment of how breast cancers growing in the brain parenchyma adapt their metabolism to proliferate and survive is lacking, and could be informative to understand how environment affects response to existing breast cancer therapies.

In this study, we sought to determine the differential metabolic dependencies of primary and metastatic disease and determine the mechanisms by which breast cancer cells adapt to survive in the brain microenvironment. We utilized an orthotopic mouse model of *HER2*-amplified breast cancer that has been previously shown to recapitulate the clinical response of human disease (Kodack et al., 2017; Kodack et al., 2012). We assessed the in vivo metabolism of breast tumors growing in the mammary fat pad (MFP) and brain parenchyma and found that relative to extracranial disease, BCBM increase glucose consumption and the contribution of glucose carbon to the tricarboxylic acid (TCA) cycle and to newly synthesized lipids. Importantly, we found that PI3K inhibition decreased fatty acid synthesis and the expression of lipid synthesis enzymes in breast tumors growing in the MFP, while the use of glucose to synthesize lipids in brain metastases was found to be independent of PI3K signaling. These findings were not evident from the examination of *HER2*-amplified breast cancer using standard cell culture techniques, and thus we optimized organotypic slices and glial-conditioned media culture systems that recapitulate in vivo metabolic phenotypes to develop platforms to study the tissue-site driven dependencies of breast cancer. Collectively, we present evidence that the brain microenvironment affects lipid metabolism of breast cancer cells and that this metabolic rewiring may contribute to targeted therapy resistance.

Results

Analysis of glucose metabolism in primary and brain metastatic HER2-*amplified breast cancer*

Glucose is a major nutrient consumed by proliferating mammalian cells (Hosios et al., 2016; Jain et al., 2012). Examining the fate of glucose carbons in tumors can provide insight into how breast cancers use metabolism to grow in different tissues and may reveal nodes that are differentially important for tumor growth in the brain versus other sites. To study differences in glucose metabolism between BCBM and disease in the primary tissue, we generated xenografts in the MFP and in the brain parenchyma from the *HER2*-amplified human breast cell line BT474, which had been previously engineered to express *Gaussia* luciferase to allow monitoring of tumor growth by measurement of luciferase activity in blood (Askoxylakis et al., 2016; Kodack et al., 2017; Kodack et al., 2012). We assessed glucose uptake in tumors formed at each site using ^{18}F-FDG-PET and found that BCBM take-up greater quantities of glucose relative to size-matched, isogenic tumors growing in the MFP (**Figure 1A**). These data suggest that tumor site could influence glucose metabolism of breast cancer cells.

To examine the fate of glucose in *HER2*-positive breast tumors derived from the same BT474 cells growing in the breast and in the brain, we performed a euglycemic infusion of ^{13}C-isotope labeled glucose into conscious, unrestrained mice bearing BT474 xenograft tumors at either site. This approach replaces extracellular glucose available to tumors with labeled [U-$^{13}C_6$]glucose, which can provide insight

into metabolic fluxes in tissues (Davidson et al., 2016; Hensley et al., 2016; Maher et al., 2012; Marin-Valencia et al., 2012). Following an infusion performed over a period of twelve hours, the majority of the circulating glucose was ^{13}C-labeled (**Figure 1B**). At this time point, metabolites were extracted from tumors and analyzed by gas chromatography-mass spectrometry (GCMS) to determine the ^{13}C-labeling of metabolites in tumor tissue.

Carbon from glucose can enter the tricarboxylic acid (TCA) cycle via two main routes that can be prominent in cancers (Davidson et al., 2016; Hensley et al., 2016; Sellers et al., 2015). The pyruvate dehydrogenase complex (PDH) can oxidize pyruvate to acetyl-CoA, which then can enter the TCA cycle (**Figure 1C**). Alternatively, glucose-derived pyruvate can enter the TCA cycle through an anaplerotic reaction catalyzed by pyruvate carboxylase (PC). Relative flux through these pathways can be estimated from the ^{13}C-label distribution of TCA intermediates. Oxidation of [U-$^{13}C_6$]glucose via PDH results in TCA metabolites with two ^{13}C carbons (m+2), while entry of labeled glucose via PC results in TCA intermediates with three labeled carbons (m+3) (**Figure 1C**). When compared to breast tumors growing in the mammary fat pad, breast tumors growing in the brain display increased m+2 and m+3 labeling of TCA cycle intermediates (**Figure 1D**), consistent with increased glucose oxidation of breast tumors growing in the brain. Relative PC flux also appears to be elevated in BCBM, as the m+3 isotopomers of citrate, alpha-ketoglutarate, succinate, fumarate, malate and aspartate are all much higher in BCBM compared to MFP tumors (**Figure 1D**).

To compare the glucose metabolism of tumors growing in each site with the glucose metabolism of non-cancerous tissue, we analyzed the labeling pattern of TCA cycle intermediates of normal brain and of white adipose tissue (WAT) collected from mice that had been infused with [U-$^{13}C_6$]glucose. The contribution of glucose to generate both m+2 and m+3 TCA cycle metabolite labeling was much higher in normal brain cortex than in white adipose tissue (WAT) (**Figure 1E**). This is perhaps unsurprising, as pyruvate carboxylase has been reported to have high activity in astrocytes (Shank et al., 1985; Yu et al., 1983) and adipose cells are glycolytic cells that secrete much of the glucose they consume as lactate (DiGirolamo et al., 1992; Sabater et al., 2014). Nevertheless, these findings suggest that the degree to which glucose contributes to the TCA cycle in tumors generated from the same parental cell line can be similar to the metabolism of the non-cancerous tissue where the tumor resides, highlighting that tissue microenvironment can impact tumor metabolism.

Signaling through the PI3K-AKT pathway is downstream of HER2 signaling, and is important for the progression and growth of HER2-positive breast cancers (Alimandi et al., 1995; Lee-Hoeflich et al., 2008; Zhou et al., 2001a; Zhou et al., 2001b). The pan-Class I PI3K inhibitor buparlisib (previously referred to as BKM120) has been shown to be effective against *HER2*-amplified breast cancer cells (Maira et al., 2012) and can cause regression of tumors growing in the MFP (Kodack et al., 2017). However, even though this compound can effectively cross the blood brain barrier (Bendell et al., 2012; Koul et al., 2012), and displays similar target

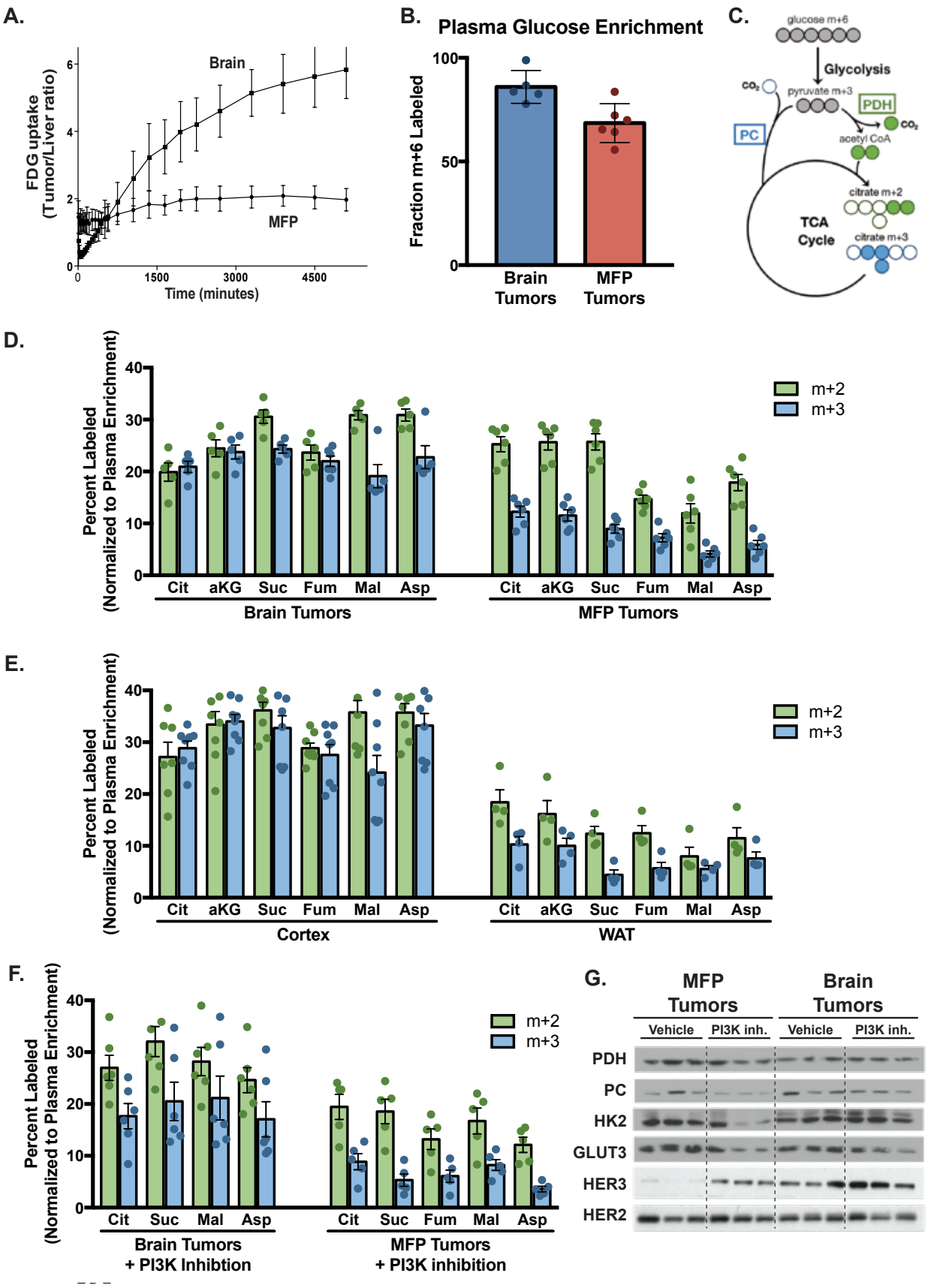
A.
FDG uptake (Tumor/Liver ratio)
Brain
MFP
Time (minutes)
B.
Plasma Glucose Enrichment
Fraction m+6 Labeled
Brain Tumors
MFP Tumors
C.
glucose m+6
Glycolysis
pyruvate m+3
PDH
PC
acetyl CoA
citrate m+2
TCA Cycle
citrate m+3
D.
Percent Labeled (Normalized to Plasma Enrichment)
m+2
m+3
Cit aKG Suc Fum Mal Asp
Brain Tumors
MFP Tumors
E.
Cortex
WAT
F.
Brain Tumors + PI3K Inhibtion
MFP Tumors + PI3K inhibition
G.
MFP Tumors
Brain Tumors
Vehicle
PI3K inh.
PDH
PC
HK2
GLUT3
HER3
HER2

Figure 1. Glucose is metabolized differently in BT474 *HER2*-amplified breast tumors depending on tissue site

(A) ^{18}F-fluorodeoxyglucose (FDG)-positron emission tomography was used to assess glucose uptake of tumors derived from *HER2*-amplified BT474 human breast cancer cells growing in the brain or the mammary fat pad (MFP) of female nu/nu mice. For each tumor, FDG uptake is shown at time points following FDG injection and was normalized to FDG uptake in the liver of the same animal.

(B) Enrichment of fully labeled glucose (m+6) in plasma was measured by GCMS following a twelve hour [U-$^{13}C_6$]glucose infusion into mice bearing *HER2*-amplified tumors in the mammary fat pad (MFP Tumors) or in the brain (Brain Tumors).

(C) Schematic depicting the dominant citrate isotopomers generated from fully labeled ^{13}C-glucose (m+6, indicated by grey circles). Fully-labeled pyruvate is generated from glucose by glycolysis (m+3) and can be oxidized by the pyruvate dehydrogenase (PDH) complex to generate acetyl-CoA with label on both carbons. This carbon can enter the tricarboxylic acid (TCA) cycle to produce citrate with two labeled carbons (m+2, indicated by green circles). Carbon from glucose-derived pyruvate can also enter the TCA cycle via pyruvate carboxylase (PC), resulting in citrate with three labeled carbons (m+3, indicated by blue circles).

(D and E) The percent labeling of TCA cycle intermediates from [U-$^{13}C_6$]glucose was assessed in (D) *HER2*-amplified breast tumors growing in the brain (Brain Tumors) and mammary fat pad (MFP Tumors), and in (E) normal brain (Cortex) and white adipose tissue (WAT). Data shown are labeling in tissue after a twelve hour [U-$^{13}C_6$]glucose infusion into female nude mice. The m+2 (green) and m+3 (blue) isotopomers of citrate (Cit), alpha-ketoglutarate (aKG), succinate (Suc), fumarate (Fum), malate (Mal), and aspartate (Asp) were measured by GCMS and normalized to $^{13}C_6$-glucose enrichment in plasma.

(F) The percent labeling of TCA cycle intermediates were measured following a twelve hour [U-$^{13}C_6$]glucose infusion in female nude mice harboring *HER2*-amplified breast tumors in the brain (Brain Tumors + PI3K inhibition) or mammary fat pad (MFP Tumors + PI3K inhibition) and that had been dosed with 30 mg/kg buparlisib daily for 3 days (PI3K inhibitor). Tissues were collected two hours following the third dose of buparlisib, and the m+2 (green) and m+3 (blue) isotopomers of citrate (Cit), succinate (Suc), malate (Mal), and aspartate (Asp) were normalized to plasma enrichment.

(G) Western blot analysis of pyruvate dehydrogenase (PDH), pyruvate carboxylase (PC), hexokinase 2 (HK2), glucose transporter 3 (GLUT3), receptor tyrosine-protein kinase erbB-3 (HER3), and receptor tyrosine-protein kinase erbB-2 (HER2) expression in three representative *HER2*-amplified lesions growing in the mammary fat pad (MFP Tumors) or brain (Brain Tumors) of mice that had been treated with vehicle or with 30 mg/kg buparlisib daily for 10 days (PI3K inh.). Tissues were harvested two hours following the final dose of buparlisib.

inhibition in tumors growing in the MFP and the brain, BT474-derived tumors growing in the brain are resistant to buparlisib treatment (Kodack et al., 2017). This suggests that that the brain microenvironment can alter dependence on the PI3K pathway in *HER2*-amplified breast tumors.

To assess whether PI3K inhibition had a differential effect on glucose metabolism in BT474 xenografts growing at different tumor sites, we assessed glucose fate in breast tumors after a 12-hour [U-$^{13}C_6$]glucose infusion in mice that had been treated with buparlisib. Though we did not observe dramatic changes, the m+2 and m+3 labeling of TCA cycle intermediates from glucose in both BCBM and MFP tumors decreased slightly upon PI3K inhibition, particularly the abundance of m+3 isotopomers in MFP tumors (**Figure 1D,F**).

Finally, we performed Western blot analysis to assess whether the expression of proteins involved in glucose metabolism in tumors growing in the MFP and in the brain was affected by buparlisib treatment. Interestingly, the relative expression of PC and PDH protein levels corresponded to the differences in relative glucose fate we observed in each site (**Figure 1D,F,G**). In addition, PDH expression in BT474 xenografts was found to be largely unaffected by tumor location or buparlisib treatment, whereas PC expression appears to be decreased by PI3K inhibition in the MFP, but not in the brain (**Figure 1G**). Collectively, these data suggest that isogenic tumors growing in different sites display differences in metabolic enzyme expression and glucose metabolism, and these differences appear to be conferred by

the tumor microenvironment. The differences are also differentially sensitive to PI3K inhibition depending on tumor site.

HER2-*amplified breast cancers display increased lipid metabolism in the brain parenchyma*

Dysregulation of fatty acid metabolism has been shown to play an important role for the proliferation and survival of breast cancer cells (Alli et al., 2005; Hilvo et al., 2011; Monaco, 2017). Thus, we next determined how lipid metabolism of *HER2*-ampliflied tumors was affected by tumor microenvironment. Fatty acid biosynthesis requires sequential ligation of two-carbon acetyl units. Since these two-carbon units are produced primarily from glucose (Kamphorst et al., 2014), [U-$^{13}C_6$]glucose tracing results in a binomial distribution of the even isotopomers of lipid species (**Figure 2A**) (Tumanov et al., 2015). Therefore, to assess the rate of lipid synthesis in vivo, we measured the distribution of labeled carbons in palmitate (an abundant fatty acid and important precursor for many lipids) in mouse tissues following a ^{13}C-labeled glucose infusion. Size-matched BT474 xenografts growing in the brain displayed greater incorporation of glucose-derived carbons into palmitate than tumors growing in the MFP, suggesting that *HER2*-amplified breast cancers exhibit increased lipid biosynthesis from glucose when growing in the brain (**Figure 2B**).

The different fatty acid synthesis activity in breast tumors growing in different locations appears to be mediated by distinct transcriptional regulation.

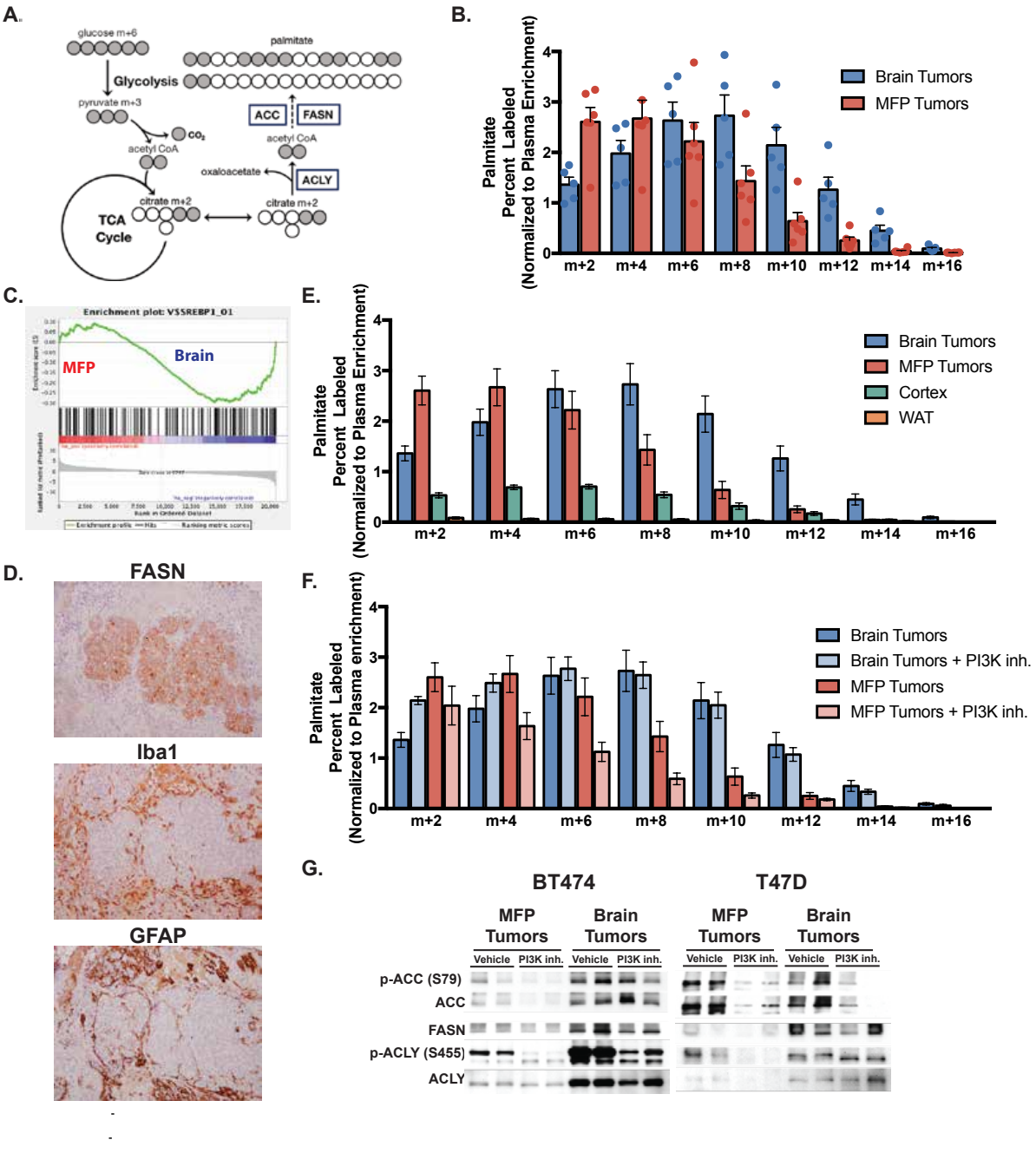
A.
glucose m+6
palmitate
Glycolysis
pyruvate m+3
ACC
FASN
CO_2
acetyl CoA
acetyl CoA
oxaloacetate
ACLY
citrate m+2
citrate m+2
TCA Cycle
B.
Palmitate Percent Labeled (Normalized to Plasma Enrichment)
Brain Tumors
MFP Tumors
m+2 m+4 m+6 m+8 m+10 m+12 m+14 m+16
C.
Enrichment plot: VSSREBP1_01
MFP
Brain
D.
FASN
Iba1
GFAP
E.
Palmitate Percent Labeled (Normalized to Plasma Enrichment)
Brain Tumors
MFP Tumors
Cortex
WAT
m+2 m+4 m+6 m+8 m+10 m+12 m+14 m+16
F.
Palmitate Percent Labeled (Normalized to Plasma enrichment)
Brain Tumors
Brain Tumors + PI3K inh.
MFP Tumors
MFP Tumors + PI3K inh.
m+2 m+4 m+6 m+8 m+10 m+12 m+14 m+16
G.
BT474
T47D
MFP Tumors
Brain Tumors
MFP Tumors
Brain Tumors
Vehicle
PI3K inh.
Vehicle
PI3K inh.
Vehicle
PI3K inh.
Vehicle
PI3K inh.
p-ACC (S79)
ACC
FASN
p-ACLY (S455)
ACLY

Figure 2. Lipid metabolism of tumors derived from BT474 *HER2*-amplified breast cancer cells is affected by the tissue microenvironment

(A) Schematic showing how carbons from fully labeled ^{13}C-glucose (m+6, indicated by grey circles) can contribute to labeled palmitate. Glucose labels mitochondrial citrate, which is transported into the cytoplasm and cleaved into acetyl-CoA and oxaloacetate by ATP citrate lyase (ACLY). A series of reactions involving acetyl-CoA carboxylase (ACC) and fatty acid synthase (FASN) sequentially condense the two carbon units of cytosolic acetyl-CoA, some of which may be labeled from glucose, to synthesize the sixteen-carbon fatty acid palmitate.

(B) The percent labeling of even isotopomers of palmitate after a twelve hour [U-$^{13}C_6$]glucose infusion was assessed in *HER2*-amplified breast tumors derived from BT474 cells growing in the brain (Brain Tumors) and mammary fat pad (MFP Tumors). The isotopomers were measured by GCMS and normalized to enrichment of labeled glucose in plasma.

(C) Gene-set enrichment analysis of mRNA transcripts profiled from *HER2*-amplified breast tumors growing in the mammary fat pad (MFP) or in the brain (Brain) shows that SREBP1 targets are enriched when BT474 breast cancer cells from tumors in the brain relative to when they form tumors in the MFP.

(D) Immunohistochemical analysis of fatty acid synthase (FASN), glial fibrillary acidic protein (GFAP) and ionized calcium binding adaptor molecule 1 (Iba1) expression in a HER2+ human breast cancer brain metastasis.

(E) The percent labeling of even isotopomers of palmitate in normal brain (Cortex) and in white adipose tissue (WAT) after a twelve hour [U-$^{13}C_6$]glucose infusion in mice. The isotopomers were measured by GCMS and normalized to enrichment of labeled glucose in plasma.

(F) Percent labeling of even isotopomers of palmitate in tumors derived from BT474 breast cancer cells in brain (Brain Tumors) or MFP (MFP Tumors). Palmitate labeling was measured following a twelve hour [U-$^{13}C_6$]glucose infusion in mice that had been dosed with vehicle or 30 mg/kg buparlisib daily for 3 days (PI3K inhibitor). Tissues were collected two hours following the third dose of buparlisib, and the isotopomers were normalized to enrichment of labeled glucose in plasma.

(G) Western blot analysis of phospho-acetyl-CoA-carboxylase at Ser79 (p-ACC (S79)), total ACC (ACC), fatty acid synthase (FASN), phospho-ATP citrate lyase at Ser455 (p-ACLY (S455)), and total ACLY (ACLY) in two representative *HER2*-amplified (derived from BT474 cells) or *PIK3CA*-mutant (derived from T47D cells) tumors growing in the mammary fat pad (MFP Tumors) or brain (Brain Tumors) of mice that had been treated with vehicle or with 30 mg/kg buparlisib daily for 3 days (PI3K inh). Tissues were harvested two hours following the third and final dose of buparlisib.

Values indicate mean ± SEM.

Gene set enrichment analysis comparing the transcriptomes of BT474 lesions growing in the MFP and in the brain suggests that targets of the transcription factor sterol regulatory element-binding protein isoform 1 (SREBP1) were selectively enriched in brain tumors (**Figure 2C**). SREBP1 is a master transcriptional regulator that activates fatty acid biosynthesis and has been shown to be important for growth of some cancers (Currie et al., 2013; Furuta et al., 2008). Thus, higher activity of SREBP1 could explain why lipid synthesis is observed to be higher in breast cancers growing in the brain.

To determine whether enzymes involved in lipid synthesis were also found in human breast cancer brain metastases, we performed immunohistochemistry assessing fatty acid synthase (FASN) expression on a patient-derived HER2-positive breast cancer brain metastasis (**Figure 2D**). FASN was specifically expressed in the metastatic breast tumor at levels that are much higher than the surrounding brain tissue. Staining for FASN was found to be mutually exclusive with two markers of brain stroma – ionized calcium binding adaptor molecule 1 (Iba1), which localizes to microglia (Ito et al., 1998) and glial fibrillary acidic protein (GFAP), which is enriched in astrocyte cells (Eng et al., 2000). This finding is consistent with literature suggesting that lipid synthesis is increased in cancer cells (Medes et al., 1953; Ookhtens et al., 1984).

To confirm that tumors synthesize more lipids than the relevant normal tissues in our tumor model, we assessed incorporation of glucose carbon into palmitate in the brain and WAT of mice that had been infused with [U-$^{13}C_6$]glucose.

We find that these non-cancerous tissues incorporate less glucose carbon into lipids than tumor lesions growing in either site (**Figure 2E**), confirming that elevated lipid synthesis can be a feature of cancer (Baenke et al., 2013; Medes et al., 1953). It was surprising that white adipose tissue had virtually no detectable lipid synthesis in these mice, since glucose has been show to contribute to adipocyte lipid stores (Hosios et al., 2016). However, it is possible that because in this case WAT was collected from tumor bearing mice, these animals had reduced lipogenesis due to adipose atrophy induced by cancer (Ebadi and Mazurak, 2014).

We next wondered whether lipid metabolism of *HER2*-amplified breast tumors is altered following PI3K inhibition by buparlisib. We analyzed the palmitate isotopomer distribution of BT474 xenografts following three doses of buparlisib and a twelve-hour infusion of ^{13}C-labeled glucose. Interestingly, we found that PI3K inhibition reduced lipid synthesis in breast cancers growing in the MFP, but not in those growing in the brain parenchyma (**Figure 2F**). This suggests that, in contrast to MFP breast tumors, lipid synthesis from glucose in breast tumors growing in the brain is independent of PI3K signaling.

We next analyzed the expression of proteins involved in lipid synthesis in breast cancer cell lines proliferating in the MFP and in the brain by Western blot. We performed this analysis on tumors generated from BT474 cells, as well as on tumors generated from the *PIK3CA*-mutant (H1047R) T47D cell line. We found that the expression of many lipid biosynthesis enzymes, including FASN, acetyl-CoA carboxylase (ACC), and acetyl-CoA lyase (ACLY) were elevated in tumors growing

in the brain relative to those growing in the MFP. We also found that expression of these enzymes was reduced by PI3K inhibition in breast cancers growing in the MFP, while expression of the same enzymes in brain tumors either remained unchanged or was only modestly affected by buparlisib treatment (**Figure 2G**).

Taken together, the data from our glucose tracing experiments, gene set enrichment analysis, and protein expression analysis suggests that lipid metabolism is dysregulated in breast tumors growing in different tissue sites, and that tumors growing in the brain have increased lipid synthesis from glucose that is independent of PI3K signaling. These findings argue that increased lipid biosynthesis may be a metabolic adaptation of breast cancers proliferating in the brain that tracks with therapy resistance to PI3K inhibition.

Organotypic slice cultures, but not standard tissue culture conditions, recapitulate in vivo metabolic phenotypes related to lipid synthesis from glucose

Our data argue that *HER2*-amplified BCBM exhibit increased glucose flux into lipids; however, an ability to dissect the mechanism of this effect in vivo is technically challenging. Standard tissue culture methods are more amenable to assess response to drug treatment and allow manipulation of nutrient conditions (Lane et al., 2016), but may not reflect differences caused by the tumor microenvironment (Mayers and Vander Heiden, 2015). To determine whether we could study the increased contribution of glucose carbons to lipids observed in

BCBM in vitro, we first assessed whether this phenotype requires constant exposure to the brain microenvironment. We dissociated BT474 xenografts that had been growing in the brain parenchyma and cultured cancer cells from these tumors in standard conditions used to passage BT474 cells in vitro. We then assessed the rate of lipid synthesis in these cells by measuring the incorporation of carbons from [U-$^{13}C_6$]glucose into palmitate, and found no change in the palmitate labeling compared to the parental cell lines (**Figure 3A**). This finding highlights the difficulty of studying site-dependent metabolic alterations that are driven by tissue environment and argues that alternative culture systems are needed to recapitulate in vivo breast cancer metabolism.

Previous studies have shown that organotypic slice cultures can retain cellular architecture and some characteristics of in vivo metabolism (Lane et al., 2016; Sellers et al., 2015; Warburg, 1923). To determine whether breast cancer slice cultures exhibit the same metabolic phenotypes observed in the orthotopic mouse model, we cut freshly resected BT474 xenograft tumors from the MFP and from the brain into 250-300μM slices, placed them in culture media containing [U-$^{13}C_6$]glucose, and traced the metabolic fate of labeled glucose. We analyzed the ^{13}C label distribution in palmitate and found that BCBM explants exhibit increased lipid synthesis relative to tissue slices derived from tumors growing in the MFP (**Figure 3B**). Similar findings were obtained in explants from tumors generated from the *HER2*-amplified and *PIK3CA*-mutant (E545K) MDA-MB-361 cell line (**Figure 3C**).

We next assessed whether synthesis of lipids from glucose in the organotypic slices could be influenced by PI3K inhibition, and whether the response observed in explants would reflect that of our orthotopic mouse model. We traced [U-$^{13}C_6$]glucose into BT474 organotypic slices and found that buparlisib treatment decreased the ^{13}C-label distribution of palmitate in explants from MFP tumors, while lipid synthesis from glucose in brain slices appeared to be unaffected by PI3K inhibition (**Figure 3D**). Interestingly, unlike BT474 tumor slices, slices from MDA-MB-361 xenografts growing in the brain also displayed decreased label from glucose into palmitate upon buparlisib treatment, although these explants maintained a higher rate of lipid synthesis than was observed in organotypic slices generated from MFP xenografts (**Figure 3C**). This data is potentially relevant, because MDA-MB-361 tumors proliferating in the brain are less resistant to PI3K inhibition than BT474 brain tumors (Kodack et al., 2017). The finding that MDA-MB-361 brain explants are more sensitive to buparlisib than BT474 brain explants serves as further evidence that organotypic slice cultures can recapitulate breast cancer phenotypes observed in vivo. Furthermore, data generated from these organotypic slice cultures suggest that increased lipid synthesis is a general feature of BCBM that can be reproduced in ex vivo explants, and argues that this could be a viable platform to both study metabolism, and test therapeutic agents targeting BCBM.

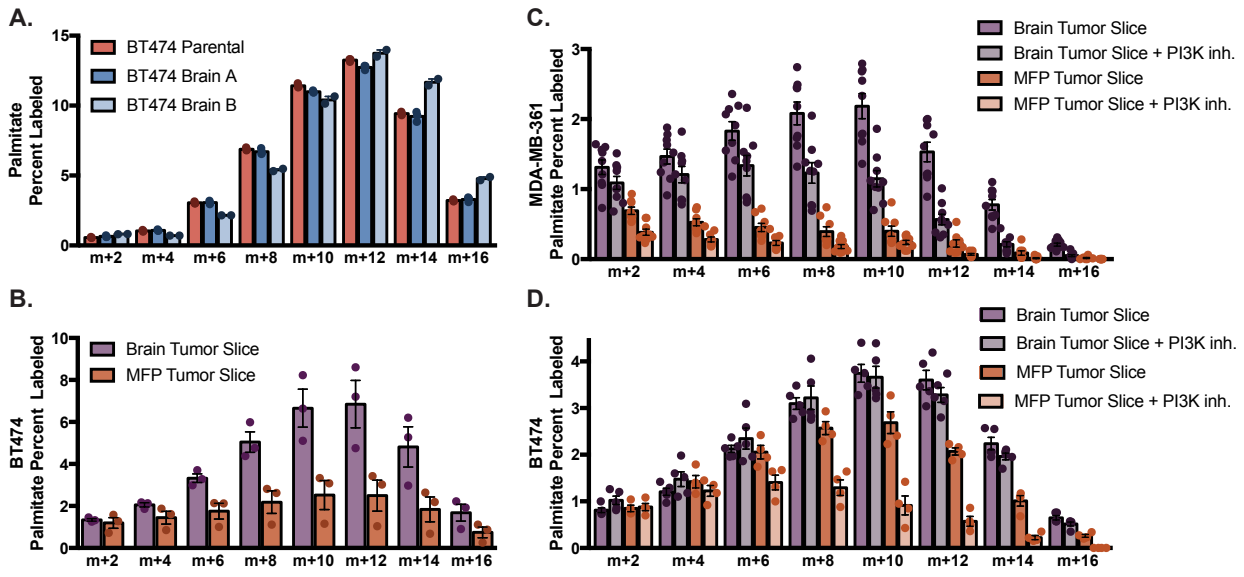

Figure 3. Ex vivo organotypic cultures recapitulate in vivo site-specific metabolic phenotypes of breast cancers more accurately than standard tissue culture conditions.

(A) The percent labeling of the even isotopomers of palmitate was assessed in parental BT474 cell lines and in two different lines of BT474 cells that had previously grown as brain tumors that were then re-seeded in vitro.

(B) The percent labeling of even isotopomers of palmitate were measured by GCMS after culturing ex vivo tissue slice cultures from tumors growing in the brain (Brain Tumor Slice) or mammary fat pad (MFP Tumor Slice) derived from*HER2*-amplified BT474 cells.in media supplemented with [U-$^{13}C_6$]glucose.

(C and D). The percent labeling of even isotopomers of palmitate were measured by GCMS after culturing organotypic slice cultures generated from (C) *HER2*-amplified and *PIK3CA*-mutant (MDA-MB-361) or (D) *HER2*-amplified (BT474) tumors growing in the brain (Brain Tumor Slice) and in the breast (MFP Tumor Slice) in media containing [U-$^{13}C_6$]glucose and either DMSO or 1μM buparlisib (PI3K inh.).

Values indicate mean ± SEM.

Medium conditioned by primary glial cultures confers a proliferative advantage to breast cancer cells and induces resistance to PI3K inhibition

The fact that organotypic slice cultures appear to recapitulate features of the brain microenvironment in vitro suggests that the presence of brain stroma may be sufficient to induce relevant metabolic alterations. To assess whether these metabolic changes were a result of a physical interaction between breast cancer cells and the surrounding tissue or a result of a soluble factor released by brain stroma, we assessed whether culturing breast cancer cells in media that had been preconditioned by primary glial cells could confer resistance to PI3K inhibition or alter the rate of lipid biosynthesis in breast cancer cells. When cultured in minimum essential media (MEM) that had been conditioned for 4 days by primary glial cell culture, the *HER2*-amplified cancer cell line BT474 displayed a proliferative advantage in conditioned media relative to culture in standard MEM or RPMI (**Figure 4A**). Additionally, medium conditioned by glial cells decreases sensitivity of BT474 cells to buparlisib, mimicking drug resistance observed in BCBM in the orthotropic mouse model. These findings are also consistent with existing literature showing that brain stroma can promote the proliferation and survival of cancer cells (Kim et al., 2011; Lin et al., 2010).

We next wanted to determine whether the rate of lipid biosynthesis in breast cancer cells could be altered by glial cells in culture. First, we supplemented standard MEM and MEM conditioned by glial cells with the same concentrations of unlabeled and ^{13}C-isotope labeled glucose, and assessed the incorporation of labeled

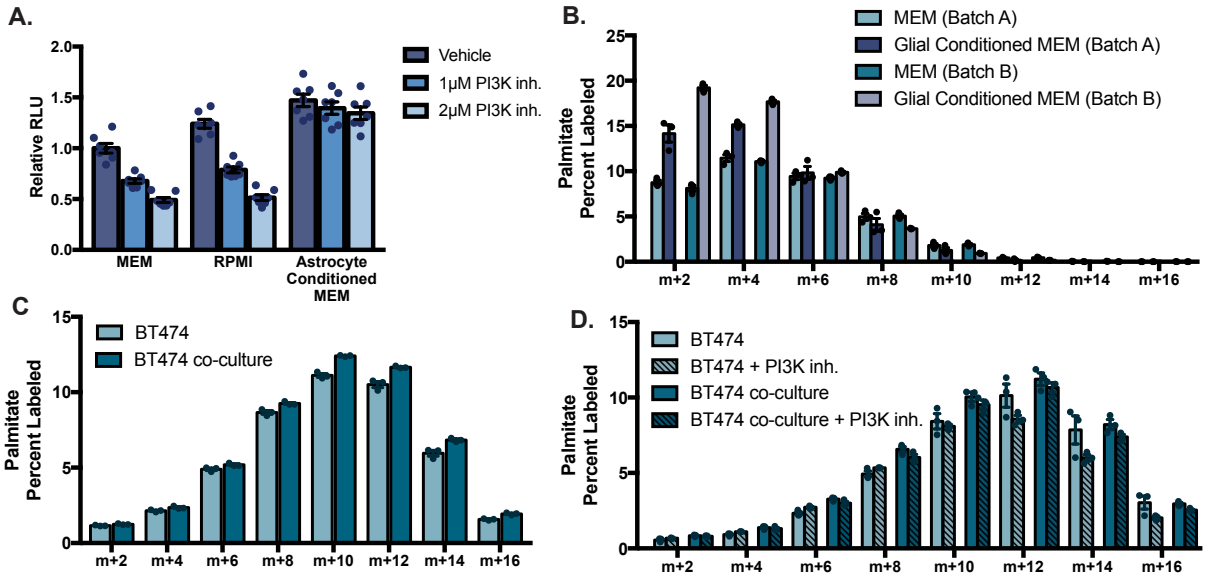

Figure 4. Conditioned media from primary glial cell cultures can promote lipid synthesis and confer resistance to PI3K inhibition

(A) Relative number of viable BT474 cells after treatment with the indicated doses of buparlisib (PI3K inh.) in media based on either minimal essential media (MEM), RPMI, or MEM that had been conditioned by primary glial cultures. Number of viable cells was assessed using Cell Titer-Glo Assay.

(B) The percent labeling of even isotopomers of palmitate were measured in BT474 cells that had been grown in MEM or glial conditioned MEM media that had been supplemented with [U-$^{13}C_6$]glucose. Two batches of conditioned media, which had been generated from two independent primary glial cultures, were assessed (Batch A and B respectively).

(C) The incorporation of glucose carbons into the even isotopomers of palmitate was measured in BT474 cells that had been cultured in [U-$^{13}C_6$]glucose in standard DMEM-based media, or in the same media that was shared with primary glial cells via a transwell culture system.

(D) The incorporation of glucose carbons into the even isotopomers of palmitate in BT474 cells that had been cultured alone in standard media, or co-cultured with primary glial cells in a transwell system. Cells were incubated with [U-$^{13}C_6$]glucose and 1μM buparlisib (PI3K inh.) as indicated.

Values indicate mean ± SEM.

carbon into palmitate in BT474 cells cultured in these different media. We found that incorporation of glucose carbons into lipids was increased in two independent batches of glial conditioned media (**Figure 4B**). We obtained similar results by co-culturing breast cancer cells with glia using a co-culture system in which the breast cancer and glial cells were cultured in separate compartments but shared the same culture media (**Figure 4C**). Interestingly, though buparlisib treatment decreased lipid synthesis in BT474 that were cultured alone, palmitate labeling in BT474 cells co-cultured with glial cells in a transwell system also appeared to be independent of PI3K signaling (**Figure 4D**). Taken together, these data suggest that a soluble factor secreted by glial cells, or depletion of a soluble factor by glial cells, is sufficient to alter the metabolism of breast cancer cells and increase lipid synthesis from glucose. This finding is consistent with constant exposure to the brain microenvironment being needed to induce both therapeutic resistance and the metabolic changes associated with BCBM.

Efforts to target lipid biosynthesis in BCBM using pharmacological agents

Because our data argue that BCBM exhibit increase glucose flux into lipids and that this correlated with resistance to PI3K inhibition, we wanted to test whether increased lipid biosynthesis is a metabolic dependency of BCBM. To this end, we sought to identify small molecules that could target this pathway. The ACLY inhibitor SB-204990, the ACC inhibitors TOFA and PF 05175157, and the FASN inhibitors C75 and GSK 2194069 have all been reported to block fatty acid

synthesis and can suppress tumor cell growth in some contexts (Flavin et al., 2010; Hatzivassiliou et al., 2005; Huang et al., 2015; Kuhajda, 2006; Li et al., 2013). However, when we assessed the degree to which these compounds inhibited the incorporation of glucose carbons into palmitate, the majority did not inhibit lipid synthesis at doses that were achievable for target inhibition in vivo (**Figure 5A-E**). Recently, 3V Biosciences has developed an oral, potent FASN inhibitor that is currently being assessed for clinical efficacy for the treatment of patients with advanced solid malignant tumors (Jones and Infante, 2015) (NCT02223247). We obtained TVB-3644, which is a tool compound related to the clinical drug candidate, and determined that TVB-3644 was very effective at inhibiting lipid production in vitro, as BT474 cells cultured in the presence of this inhibitor displayed low incorporation of glucose carbons into palmitate, even at doses as low as 50nM (**Figure 5F**).

To assess whether targeting lipid biosynthesis could represent a metabolic dependency of *HER2*-amplified breast cancer, we measured the proliferation of breast cancer cell lines that had been cultured in the presence or the absence of TVB-3644. We determined that this FASN inhibitor reduced proliferation of BT474 and MDA-MB-361 cell lines in standard culture almost as potently as the PI3K inhibitor buparlisib (**Figure 5G,H**). We next assessed the response to TVB-3644 in organotypic slices by measuring the incorporation of glucose carbons into palmitate, and determined that TVB-3644 can reduce the rate of lipid synthesis in both MFP and brain explants generated from BT474 and MDA-MB-361 tumor xenografts

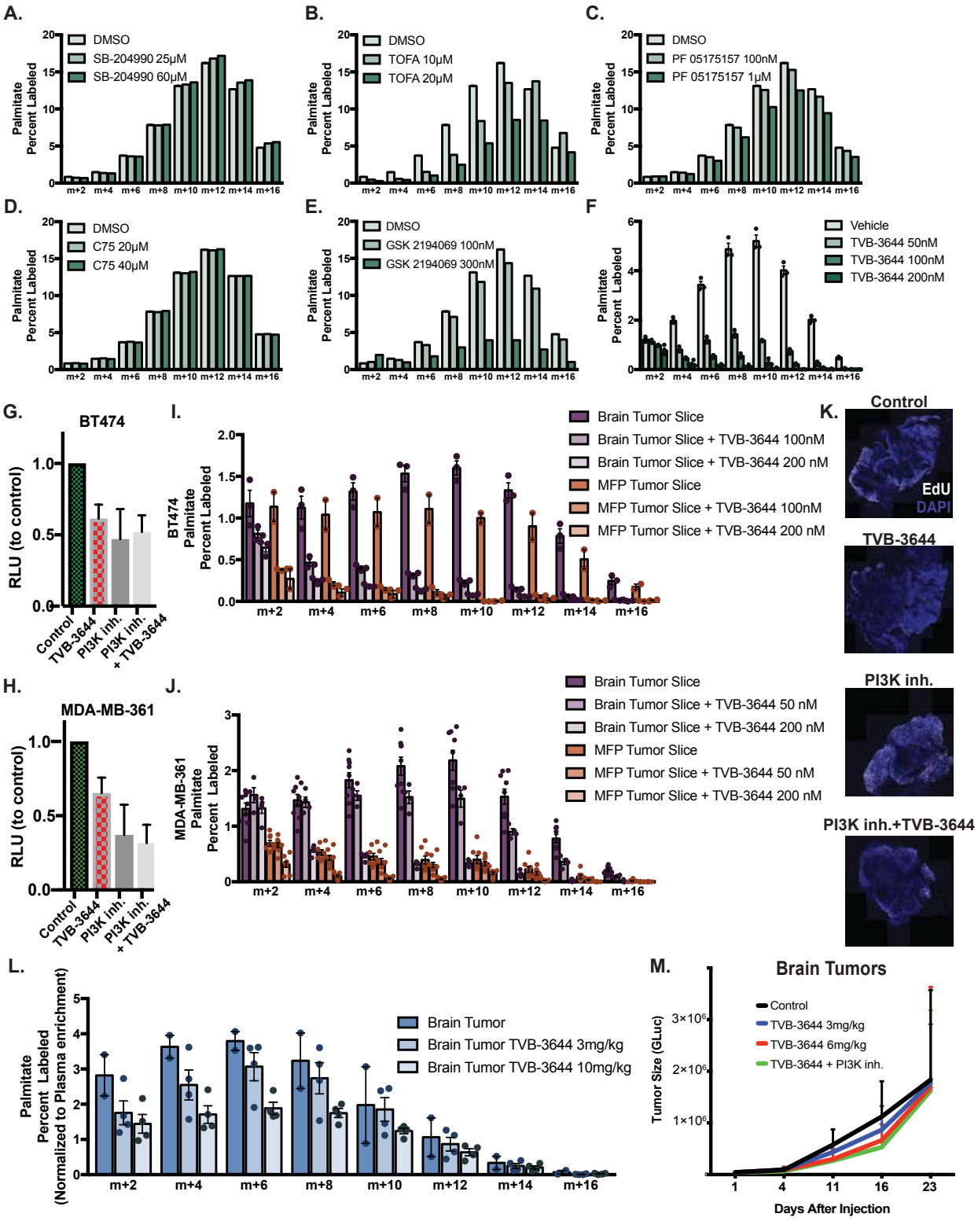
A.
DMSO
SB-204990 25μM
SB-204990 60μM
Palmitate Percent Labeled
B.
DMSO
TOFA 10μM
TOFA 20μM
C.
DMSO
PF 05175157 100nM
PF 05175157 1μM
D.
DMSO
C75 20μM
C75 40μM
E.
DMSO
GSK 2194069 100nM
GSK 2194069 300nM
F.
Vehicle
TVB-3644 50nM
TVB-3644 100nM
TVB-3644 200nM
m+2 m+4 m+6 m+8 m+10 m+12 m+14 m+16
G.
BT474
RLU (to control)
Control
TVB-3644
PI3K inh.
PI3K inh. + TVB-3644
H.
MDA-MB-361
I.
BT474 Palmitate Percent Labeled
Brain Tumor Slice
Brain Tumor Slice + TVB-3644 100nM
Brain Tumor Slice + TVB-3644 200 nM
MFP Tumor Slice
MFP Tumor Slice + TVB-3644 100nM
MFP Tumor Slice + TVB-3644 200 nM
J.
MDA-MB-361 Palmitate Percent Labeled
Brain Tumor Slice
Brain Tumor Slice + TVB-3644 50 nM
Brain Tumor Slice + TVB-3644 200 nM
MFP Tumor Slice
MFP Tumor Slice + TVB-3644 50 nM
MFP Tumor Slice + TVB-3644 200 nM
K.
Control
EdU
DAPI
TVB-3644
PI3K inh.
PI3K inh.+TVB-3644
L.
Palmitate Percent Labeled (Normalized to Plasma enrichment)
Brain Tumor
Brain Tumor TVB-3644 3mg/kg
Brain Tumor TVB-3644 10mg/kg
M.
Brain Tumors
Tumor Size (GLuc)
Control
TVB-3644 3mg/kg
TVB-3644 6mg/kg
TVB-3644 + PI3K inh.
Days After Injection

Figure 5. Targeting lipid synthesis in breast cancer cells utilizing existing pharmacologic agents.

(A-F) The percent labeling of even isotopomers of palmitate were measured by GCMS after culturing BT474 cells in media supplemented with [U-$^{13}C_6$]glucose and the indicated doses of the ACLY inhibitor (A) SB-204990, the ACC inhibitors (B) TOFA and (C) PF 05175157, and the fatty acid synthase inhibitors (D) C75, (E) GSK 2194069, and (F) TVB-3644.

(G and H) Relative number of viable (G) BT474 and (H) MDA-MB-361 cells after treatment with 200nM FASN inhibitor TVB-3644 and/or 750nM buparlisib (PI3K inh.) as determined by MTT assay as indicated.

(I and J) The percent labeling of even isotopomers of palmitate were measured by GCMS after culturing organotypic slice cultures generated from (I) *HER2*-amplified (BT474) or (J) *HER2*-amplified and *PIK3CA*-mutant (MDA-MB-361) breast tumors growing in the brain (Brain Tumor Slice) or in the breast (MFP Tumor Slice) in media containing [U-$^{13}C_6$]glucose and the indicated doses of the FASN inhibitor TVB-3644.

(K) To monitor proliferation, 5-ethynyl-2′-deoxyuridine (EdU) incorporation into ex vivo slice cultures generated from BT474 xenografts growing in the brain was assessed by imaging slices (250-300μm thick) using multispectral confocal microscopy. HER2+ breast cancer cells remain viable up to 5 days ex vivo as shown by the DAPI stain and EdU incorporation (active proliferation). Slices were incubated in media containing 200nM TVB-3644, 750nM buparlisib (PI3K inh.), or both as indicated.

(L) The percent labeling of even isotopomers of palmitate were measured following a twelve hour [U-$^{13}C_6$]glucose infusion in mice that had been dosed with the indicated doses of TVB-3644 and harbored *HER2*-amplified breast tumors in the brain (Brain Tumors). Tissues were collected two hours following the third dose of TVB-3644, and the isotopomers were normalized to enrichment of glucose in plasma.

(M) Growth kinetics of *HER2*-amplified BT474 breast tumors cell lines growing in the brain was assessed by the measurement of *Gaussia* luciferase (GLuc) activity in blood. Mice were treated with the indicated doses of the FASN inhibitor TVB-3644, buparlisib (PI3K inh.), or both drugs in combination.

Values indicate mean ± SEM.

(**Figure 5I,J**). Finally, we wanted to determine how FASN inhibition could influence tumor growth of BCBM. We assessed proliferation of *HER2*-amplified organotypic slices by measuring incorporation of 5-etnydyl-2'-deoxyuridine (EdU) by confocal microscopy. We find that brain explants established from BT474 brain tumors are refractory to PI3K inhibition, as buparlisib does not decrease the EdU incorporation of these slice cultures (**Figure 5K**). These results match the response to PI3K observed in vivo, as these same tumors are also refractory to buparlisib when grown in the brain parenchyma (Kodack et al., 2017). However, TVB-3644 was able to significantly reduce EdU labeling in BT474 brain explants, both as a single agent and combined with buparlisib (**Figure 5K**). The finding that FASN inhibition is able to reduce proliferation of *HER2*-amplified cells grown in standard tissue culture conditions as well as in brain organotypic slices suggest that lipid synthesis could be a targetable vulnerability of breast cancer, including in BCBM.

We also tested whether TVB-3644 could inhibit growth of BCBM in the BT474 orthotopic model. Unfortunately, TVB-3644 was found to be less effective in reducing lipid synthesis in BCBM in vivo, as tracing of [U-$^{13}C_6$]glucose fate into BT474 xenografts in the brain showed only a modest reduction of incorporation of label into palmitate at a dose of 3mg/kg (**Figure 5L**). Though there was stronger inhibition of lipid synthesis when mice were dosed with TVB-3644 at 10mg/kg (**Figure 5L**), this treatment was too toxic for extensive treatment of animals. As additional evidence that this compound is not brain penetrant, we did not observe a significant reduction of brain tumor proliferation upon treatment with TVB-3644

given at either 3mg/kg or 6mg/kg, or when combined with 30mg/kg buparlisib (**Figure 5M**). Thus, though our data suggests that lipid synthesis could be a metabolic dependency of breast cancers proliferating in the brain, a more brain penetrant compound is needed to test this hypothesis in vivo.

Discussion

HER2-positive breast cancer brain metastases are often refractory to the same therapies that successfully control extracranial disease, and how brain microenvironment affects the metabolism of breast tumors remains poorly understood. To assess the in vivo metabolism of breast cancer proliferating in different tissues, we assessed glucose metabolism in tumors derived from breast cancer cells with the aim of identifying metabolic dependencies unique to *HER2*-amplified tumors growing in the brain parenchyma. Though a prevailing view of cancer metabolism is that tumors universally diminish glucose oxidation in favor of lactate production (Vander Heiden et al., 2009; Warburg, 1956), we observe evidence of glucose oxidation in *HER2*-amplified breast tumors in both the MFP and brain tissue, albeit to a greater extent in the cancers proliferating in the brain. Despite the fact that most cells in culture require glutamine to supply carbons to the TCA cycle (Altman et al., 2016), oxidative glucose metabolism has been reported in a number of in vivo cancer metabolism studies (Davidson et al., 2016; Hensley et al., 2016; Maher et al., 2012; Sellers et al., 2015; Yuneva et al., 2012) and mitochondrial metabolism is a potential target for cancer therapy (Weinberg and

Chandel, 2015). Previous studies have shown that breast tumors display increased mitochondrial activity relative to surrounding stroma (Whitaker-Menezes et al., 2011), and that the expression of enzymes involved in the TCA cycle and glucose oxidation are elevated when breast cancers metastasize to the brain (Chen et al., 2007). Furthermore, HER2 signaling has been shown to promote glucose oxidation in breast cancer cells (Grassian et al., 2011). Our in vivo tracing analyses extend these findings, and suggest that glucose may be a more important substrate for oxidative metabolism of breast cancer in brain metastases.

The increased glucose metabolism in *HER2*-amplified tumors appears to serve a biosynthetic function, as we observe increased incorporation of glucose carbons into fatty acids in these cancers relative to normal tissues. This phenotype is enhanced by the brain microenvironment, as we found higher incorporation glucose carbons into lipids and increased expression of SREBP1 targets in breast tumors growing in this site. Lipid synthesis can contribute to malignancy and has been described as a potential cancer therapy target (Röhrig and Schulze, 2016). Breast tumors have been shown to display aberrant lipid metabolism (Hilvo et al., 2011) and FASN expression is elevated in breast cancer and associated with poor prognosis (Kuhajda et al., 1994; Kuhajda et al., 1989). FASN protein levels have been described to be elevated in HER2-positive breast cancer that metastasizes to the brain (Jung et al., 2015). Our findings support these published studies, suggesting that fatty acid biosynthesis is an adaptation of breast cancers growing in the brain microenvironment.

Lipids are more reduced than other nutrients, and thus synthesis of fatty acids requires large amounts of the electron carrier NADPH (Fan et al., 2014; Hosios and Vander Heiden, 2018). Breast cancer cells derived from brain lesions have been reported to increase expression of enzymes required for the oxidative branch of the pentose phosphate pathway (Chen et al., 2007), which is a major source of NADPH in cells. Though detoxification of reactive oxygen species has been proposed as a major consequence of enhanced oxidative pentose phosphate flux in BCBM, increased NADPH production may also help support the increased rate of lipid synthesis observed in breast tumors proliferating in the brain. From a carbon perspective, glucose is the primary source of lipids synthesized de novo (Kamphorst et al., 2013), and the increased glucose synthesis of BCBM could contribute to the increased fatty acid biosynthesis observed in these lesions.

Recently, it has been shown that increased lipid synthesis can promote resistance to antiangiogenic therapies in breast and in other tumor types (Sounni et al., 2014). This finding provides one potential mechanism by which the brain microenvironment promotes resistance to targeted breast cancer treatments. Culturing *HER2*-amplified cancer cells in presence of brain stroma, either in vivo or in tissue culture systems, was found to enhance the rate of lipid synthesis and reduce sensitivity to PI3K inhibition by buparlisib. Furthermore, we found that inhibiting lipid synthesis with the FASN inhibitor TVB-3644 could decrease proliferation and potentiate the anticancer effects of buparlisib in organotypic slice cultures generated from brain tumors, suggesting that breast cancer cells are

reliant on lipid synthesis for evasion of targeted therapies. Testing this hypothesis in vivo was limited by the lack of a sufficiently brain-penetrant molecule; however, the response observed in organotypic slice cultures suggests that this approach can allow the use of existing inhibitors and help prioritize medicinal chemistry efforts to enhance brain delivery.

The resistance to buparlisib and increased lipid synthesis we observe in BCBM appears to be essentially mediated by the brain microenvironment, as this phenotype was only observed in the brain parenchyma or when cancer cells were grown in culture systems optimized to mimic this tumor site. This finding is consistent with emerging literature that the brain represents a unique microenvironment that can decrease the sensitivity of tumors to many targeted therapies (Kodack et al., 2017; Kodack et al., 2012). Though the mechanism by which the brain environment confers resistance is not well understood, tumors are often surrounded by reactive astrocytes, which have been shown to promote survival of cancer cells and decrease sensitivity to chemotherapeutics (Kim et al., 2011; Lin et al., 2010). Furthermore, breast tumors can undergo genetic alterations (Valiente et al., 2014) or adopt features of brain metabolism to promote their proliferation and survival at this site. Breast cancers proliferating in the brain have been shown to upregulate enzymes required to metabolize γ-aminoburtyric acid (GABA) (Neman et al., 2014) and express a brain specific cadherin in order to form gap junctions between cancer cells and astrocytes (Chen et al., 2016). Our data also suggests that brain microenvironment can alter breast cancer cell metabolism, as

we see increased lipid synthesis in *HER2*-amplified cells grown in the presence of brain stroma. However, this change does not appear to be mediated by a genetic adaptation, as breast cancer cells seem to require constant exposure to the brain microenvironment in order to evade PI3K inhibition and increase the rate of lipid synthesis. Furthermore, these metabolic alterations appear to be mediated by changes in a soluble factor rather than direct interaction, as media conditioned by primary glial cultures are also able to confer these phenotypes.

It has been shown in other cancer models that tumors of the same genotype can display different in vivo metabolism depending on the tissues in which they are arise (Mayers et al., 2016; Yuneva et al., 2012). In our study, rather than permitting cancer of the same genotype to develop in different tissues, tumors from the same parental cell line were injected into two tumor sites. Despite the fact that these breast tumors are isogenic, we still observed large difference in metabolism and sensitivity to chemotherapies between cancers growing in the breast or in the brain. This finding has clinical significance, because many cancer therapies are often selected based on the genetic profile of tumors (Garraway, 2013). While the genetic mutations that drive malignancy of cancer cells are important, the results of the present study highlight that it is critical to also consider the metabolic environment in therapy studies. Standard cell culture does not recapitulate the nutrient conditions found in tissues, and may not be the optimal culture system for the validation of some drug targets, particularly in relation to metabolism (Cantor et al., 2017; Davidson et al., 2016; Gui et al., 2016; Muir et al., 2017; Tardito et al.,

2015). Alternative culture systems, such as the ones developed here using conditioned media and organotypic slice cultures, could be useful to assess vulnerabilities that are sensitive to tissue site. Additional in vivo metabolism studies, combined with the use of culture systems that mimic the environment of tissues, can serve to further reveal unique metabolic dependencies of the brain that might be able to be exploited for the development of new cancer targets or to improve the efficacy of existing drugs.

Materials and Methods

Mouse Breast Cancer Models: All animal studies were approved by the MIT and MGH Committees on Animal Care. Breast cancer xenografts were generated in female nude mice of 8-9 weeks of age as previously described (Kodack et al., 2012). Briefly, to generate MFP tumors 5×10^6 BT474 cells were resuspended in 50μL of a 1:1 ratio of PBS and Matrigel Matrix, High Concentration (BD Biosciences, 354248). For Brain tumors, 1×10^5 BT474 cells were diluted in 1μL of PBS and stereotactically injected into the left frontal lobe of the mouse brain. The day before implantation of tumor cells, a 0.36-mg or 0.72-mg 17β-estradiol pellet (Innovative Research of America, SE121) was implanted subcutaneously. Buparlisib (PI3K inhibitor) and TVB-3644 (FASN inhibitor) were administered once per day via oral gavage and were obtained from Novartis and 3V Biosciences, respectively.

Glucose Infusions in Mice: Catheters were surgically implanted into the jugular vein of tumor bearing animals three days before the infusion experiment. Prior to the initiation of the study, mice were fasted for 6 hours. [U-$^{13}C_6$]glucose (Cambridge Isotope Laboratories, CLM-1396-PK) was infused at a constant rate of 30mg/kg/min for twelve hours into conscious, free-moving animals, after which the animals were terminally anesthetized with 120mg/kg sodium pentobarbital. Blood was collected immediately by cardiac puncture, and tumors, brain and white adipose tissue were harvested quickly, within five minutes of sacrifice. Tissues were frozen using the BioSqueezer (BioSpec Products) and stored at -80°C for subsequent metabolite extraction and analysis.

Metabolite Extraction: Tissues were fragmented into small (~10-30mg) fragments, weighed, and homogenized cryogenically (Retsch Cryomill). For ex vivo tumor explants, the slice was picked up with forceps, rapidly submerged into ice-cold blood bank saline, and transferred to an Eppendorf tube. For cell culture samples, cells were washed rapidly with ice-cold blood bank saline, lysed directly in six-well dishes with HPLC-grade methanol, scraped, and transferred to an Eppendorf tube. Metabolites were extracted using ice-cold HPLC-grade methanol, water, and chloroform at a volume ratio of 600:400:300. Samples were vortexed for 10 minutes at 4°C and centrifuged for 10 minutes at 21,000×g and 4°C to separate the top, aqueous layer and the bottom, organic layer. Each layer was collected and

dried under nitrogen gas, and stored at -80°C for subsequent analysis by liquid or gas-chromatography mass-spectrometry (GCMS).

Derivatization of Polar Metabolites for analysis by Gas-Chromatography Mass Spectrometry (GCMS): Frozen and dried metabolites from the aqueous phase were dissolved in 20μL of Methoxamine (MOX) Reagent (2% solution of methoxyamine-hydrogen chloride in pyridine, Sigma TS-45950) and incubated at 37°C for 90 minutes. Subsequently, 25μL of N-tert-Butyldimethylsilyl-N-methyltrifluoroacetamide (MTBSTFA) with 1% tert-Butyldimethylchlorosilane (t-BDMCS) (Sigma 375934) was added and samples were held at 60°C for one hour. Samples were vortexed, transferred to GCMS vials and capped.

GCMS Fatty Acid Methyl Ester (FAME) Derivatization: Frozen and dried metabolites from the organic phase were saponified to free fatty acids and esterified to form fatty acid methyl esters. First, 500μL of 2%H_2SO_4 was added to each sample and incubated for two hours at 60°C. Next 100 μL of a saturated salt solution (sodium chloride dissolved in HPLC-grade water) and 500μL of HPLC-grade hexane was added and the sample was vortexed. The top hexane layer was collected and evaporated under nitrogen gas. Each sample was resuspended with 50μL of fresh HPLC-grade hexane, vortexed, and transferred to glass GCMS sample vial (Agilent 5181-8872).

Metabolite Profiling by GCMS: GCMS analysis was performed using an Agilent 7890 GC equipped with 30m DB-35MS capillary column connected to an Agilent 5975B MS operating under electron impact ionization at 70eV. For each sample, 1μL was injected at 270°C using helium gas as a carrier with a flow rate of 1mL/min. For the measurement of polar metabolites, the GC oven temperature was kept at 100°C for three minutes and increased to 30°C at a rate of 3.5°C/min. The MS source and quadrupole were kept at 230°C and 150°C, respectively, and the detector was run in scanning mode, recording ion abundance within 100-605 m/z. Mass Isotopomer distributions were determined by integrating the appropriate ion fragments and correcting for natural isotope abundance using in house algorithms adapted as previously reported (Lewis et al., 2014).

Cell culture experiments: BT474 cells were transduced with an expression cassette encoding Gaussia Luciferase and GFP separated by an internal ribosomal entry site using a lentiviral system as previously described (Chung et al., 2009). All cell lines in this study were purchased from ATCC and were authenticated (CellCheck). BT474 cells were cultured in RPMI 1640 culture media supplemented with 10% FBS and 2mM glutamine at 21% oxygen, 37°C, and 5% CO_2. The reagents used for cell culture experiments included buparlisib (BKM120), C75 (4-methylene-2-octyl-5-oxotetra- hydrofuran-3-carboxylic acid), TOFA (5-tetradecyloxy-2-furoic acid), GSK 2194069 (4-[4-(5-Benzofuranyl)phenyl]-5-[[(3S)-1-(cyclopropylcarbonyl)-3-pyrrolidinyl]methyl]-2,4-dihydro-3H-1,2,4-triazol-3-one), SB-204990 ((3R,5S)-rel-

5-[6-(2,4-Dichlorophenyl)hexyl]tetrahydro-3-hydroxy-2-oxo-3-furanacetic acid), PF 05175157 (1,4-Dihydro-1'-[2-methyl-1H-benzimidazol-6-yl)carbonyl]-1-(1-methylethyl)-spiro[5H-indazole-5,4'-piperidin]-7(6H)-one), and TVB-3644.

For tracing experiments done at standard tissue culture conditions, cells were plated in six well dishes at a seeding density of 150,000 cells per well. The following day, cells were washed three times with phosphate buffered saline (PBS) and incubated in DMEM without glucose, glutamine, or sodium pyruvate (Corning, 17-207-CV) that had been supplemented with 25mM [U-$^{13}C_6$]glucose, 4mM glutamine, 10% dialyzed fetal bovine serum and the indicated treatment condition. Metabolites were extracted after a 72hour incubation with the tracing medium.

Western Blot Analysis: Tumor samples were homogenized in RIPA buffer (Boston BioProducts) supplemented protease inhibitors (Roche, cOmplete ULTRA tablets, 05892970001) and phosphatase inhibitors (Roche, phosSTOP, PHOSS-RO) using a tissue homogenizer (Cole-Palmer, Lab-GEN). Lysates were centrifuged at 18,000×g for 30 minutes at 4°C. Protein concentration was quantified and samples were subsequently boiled in Laemmli buffer.

Gene Set Enrichment Analysis: RNA was extracted from BT474 tumors grown in the mammary fat pad and brain parenchyma. RNA was extracted and processed according to the manufacturer's instructions and subsequently hybridized to Affymetrix GeneChip Human Genome U133 Plus 2.0 Arrays.

Isolation of BT474 cells from BT474 xenografts growing in brain: Tumors were minced in RPMI media and subsequently incubated for one hour shaking at 37°C in BT474 culture media (RPMI 1640 + 10% FBS) supplemented with 1% penicillin/streptomycin (P/S) and 1 mg/mL collagenase/dispase enzyme mix (Roche, COLLDISP-RO). Tissues were then centrifuged at 1500rpm for 5 minutes, and supernatant was removed. The pellet was resuspended BT474 culture media supplemented with 1% P/S and pipetted well to disaggregate clumps. Media was changed the following day.

Organotypic slice cultures: Explants were generated from BT474 mouse xenografts using a microtome (Precisionary Instruments, Compresstome VF-300). To trace the tissue explants, each sample was carefully washed three times with PBS and media was replaced with tracing media (DMEM without glucose, glutamine, or sodium pyruvate [Corning, 17-207-CV] supplemented with 25mM [U-$^{13}C_6$]glucose, 4 mM glutamine and 10% dialyzed fetal bovine serum) and the indicated treatment condition. The slice cultures were incubated with tracing media for three days before metabolites were extracted from all samples.

Primary Glial Cultures: Primary glial cultures were generated as described (Schildge et al., 2013). Cortices were dissected from mouse pups of age P1 to P4 and cut into small pieces with sharp blades. The tissue was transferred to a 50mL tube

containing 22.5 mL of Hank's Buffered Saline Solution (HBSS) and 2.5 mL of 2.5% trypsin. The tube was incubated at 37°C for thirty minutes and then centrifuged for 5 minutes at 500×g. The supernatant was removed by decantation, and the pellet was washed twice with PBS and subsequently plated in a T75 tissue culture dish. Primary glial cells were cultured in DMEM (Corning 10-013-CV) supplemented with 10% fetal bovine serum and in dishes that had been coated with a 50μg/mL solution of poly-L-lysine.

To generate conditioned media from primary glial cultures, glial cells were passaged to a 15cm diameter dish at a confluence of approximately 40%. The cells were permitted to settle overnight, and then were washed three times with PBS before being incubated with 30mL of Minimal Essential Medium without glutamine (MEM, Corning 15-010-CV) supplemented with 10% dialyzed fetal bovine serum and 2mM glutamine. Four days later, conditioned media was collected and filtered through a vacuum filter with a pore size of 0.22μM (VWR, 28199-774). To assess the proliferation response to glia-conditioned media, BT474 cells were plated in 96 well dishes at 7,500 cells per well. After the cells were permitted to settle over night, they were washed three times PBS, and cultured in the indicated treatment condition for 48 hours. Cells were washed three times and number of viable cells was assessed utilizing the CellTiter-Glo Luminescent Cell Viability Assay (Promega G7572).

Co-Culture experiment: For the glial-BT474 co-culture experiments, BT474 cells were plated in six well dishes at a seeding density of 150,000 cells/well. The same day, astrocytes were plated at the same seeding density into membrane-based transwell inserts (Sigma, Z353086). The next day, both cell populations were washed three times with PBS and then placed into DMEM without glucose, glutamine, or sodium pyruvate (Corning, 17-207-CV) that had been supplemented with 25mM [U-$^{13}C_6$]glucose, 4mM glutamine, 10% dialyzed fetal bovine serum, and either DMSO or 1μM buparlisib. Each co-culture was incubated in 2mL of total media, with 1.5mL used beneath the transwell and 500μL used to cover the glial cells in the insert. After incubation with the tracing media for three days, metabolites were extracted from the BT474 cells.

References

Alimandi, M., Romano, A., Curia, M.C., Muraro, R., Fedi, P., Aaronson, S.A., Di Fiore, P.P., and Kraus, M.H. (1995). Cooperative signaling of ErbB3 and ErbB2 in neoplastic transformation and human mammary carcinomas. Oncogene 10, 1813-1821.

Alli, P.M., Pinn, M.L., Jaffee, E.M., McFadden, J.M., and Kuhajda, F.P. (2005). Fatty acid synthase inhibitors are chemopreventive for mammary cancer in neu-N transgenic mice. Oncogene 24, 39-46.

Altman, B.J., Stine, Z.E., and Dang, C.V. (2016). From Krebs to clinic: glutamine metabolism to cancer therapy. Nat Rev Cancer 16, 619-634.

Askoxylakis, V., Ferraro, G.B., Kodack, D.P., Badeaux, M., Shankaraiah, R.C., Seano, G., Kloepper, J., Vardam, T., Martin, J.D., Naxerova, K., et al. (2016). Preclinical Efficacy of Ado-trastuzumab Emtansine in the Brain Microenvironment. J Natl Cancer Inst 108.

Bachelot, T., Romieu, G., Campone, M., Dieras, V., Cropet, C., Dalenc, F., Jimenez, M., Le Rhun, E., Pierga, J.Y., Goncalves, A., et al. (2013). Lapatinib plus capecitabine in patients with previously untreated brain metastases from HER2-positive metastatic breast cancer (LANDSCAPE): a single-group phase 2 study. Lancet Oncol 14, 64-71.

Baenke, F., Peck, B., Miess, H., and Schulze, A. (2013). Hooked on fat: the role of lipid synthesis in cancer metabolism and tumour development. Dis Model Mech 6, 1353-1363.

Bendell, J.C., Rodon, J., Burris, H.A., de Jonge, M., Verweij, J., Birle, D., Demanse, D., De Buck, S.S., Ru, Q.C., Peters, M., et al. (2012). Phase I, dose-escalation study of BKM120, an oral pan-Class I PI3K inhibitor, in patients with advanced solid tumors. J Clin Oncol 30, 282-290.

Cantor, J.R., Abu-Remaileh, M., Kanarek, N., Freinkman, E., Gao, X., Louissaint, A., Jr., Lewis, C.A., and Sabatini, D.M. (2017). Physiologic Medium Rewires Cellular Metabolism and Reveals Uric Acid as an Endogenous Inhibitor of UMP Synthase. Cell 169, 258-272 e217.

Chen, E.I., Hewel, J., Krueger, J.S., Tiraby, C., Weber, M.R., Kralli, A., Becker, K., Yates, J.R., 3rd, and Felding-Habermann, B. (2007). Adaptation of energy metabolism in breast cancer brain metastases. Cancer Res 67, 1472-1486.

Chen, J., Lee, H.J., Wu, X., Huo, L., Kim, S.J., Xu, L., Wang, Y., He, J., Bollu, L.R., Gao, G., et al. (2015). Gain of glucose-independent growth upon metastasis of breast cancer cells to the brain. Cancer Res 75, 554-565.

Chen, Q., Boire, A., Jin, X., Valiente, M., Er, E.E., Lopez-Soto, A., Jacob, L., Patwa, R., Shah, H., Xu, K., et al. (2016). Carcinoma-astrocyte gap junctions promote brain metastasis by cGAMP transfer. Nature 533, 493-498.

Chung, E., Yamashita, H., Au, P., Tannous, B.A., Fukumura, D., and Jain, R.K. (2009). Secreted Gaussia luciferase as a biomarker for monitoring tumor progression and treatment response of systemic metastases. PLoS One 4, e8316.

Currie, E., Schulze, A., Zechner, R., Walther, T.C., and Farese, R.V., Jr. (2013). Cellular fatty acid metabolism and cancer. Cell Metab 18, 153-161.

Davidson, S.M., Papagiannakopoulos, T., Olenchock, B.A., Heyman, J.E., Keibler, M.A., Luengo, A., Bauer, M.R., Jha, A.K., O'Brien, J.P., Pierce, K.A., et al. (2016). Environment Impacts the Metabolic Dependencies of Ras-Driven Non-Small Cell Lung Cancer. Cell Metab 23, 517-528.

DeBerardinis, R.J., and Chandel, N.S. (2016). Fundamentals of cancer metabolism. Sci Adv 2, e1600200.

DiGirolamo, M., Newby, F.D., and Lovejoy, J. (1992). Lactate production in adipose tissue: a regulated function with extra-adipose implications. FASEB J 6, 2405-2412.

Ebadi, M., and Mazurak, V.C. (2014). Evidence and mechanisms of fat depletion in cancer. Nutrients 6, 5280-5297.

Eichler, A.F., Chung, E., Kodack, D.P., Loeffler, J.S., Fukumura, D., and Jain, R.K. (2011). The biology of brain metastases-translation to new therapies. Nat Rev Clin Oncol 8, 344-356.

Eng, L.F., Ghirnikar, R.S., and Lee, Y.L. (2000). Glial fibrillary acidic protein: GFAP-thirty-one years (1969-2000). Neurochem Res 25, 1439-1451.

Fan, J., Ye, J., Kamphorst, J.J., Shlomi, T., Thompson, C.B., and Rabinowitz, J.D. (2014). Quantitative flux analysis reveals folate-dependent NADPH production. Nature 510, 298-302.

Flavin, R., Peluso, S., Nguyen, P.L., and Loda, M. (2010). Fatty acid synthase as a potential therapeutic target in cancer. Future Oncol 6, 551-562.

Furuta, E., Pai, S.K., Zhan, R., Bandyopadhyay, S., Watabe, M., Mo, Y.Y., Hirota, S., Hosobe, S., Tsukada, T., Miura, K., et al. (2008). Fatty acid synthase gene is up-regulated by hypoxia via activation of Akt and sterol regulatory element binding protein-1. Cancer Res 68, 1003-1011.

Garraway, L.A. (2013). Genomics-driven oncology: framework for an emerging paradigm. J Clin Oncol 31, 1806-1814.

Grassian, A.R., Metallo, C.M., Coloff, J.L., Stephanopoulos, G., and Brugge, J.S. (2011). Erk regulation of pyruvate dehydrogenase flux through PDK4 modulates cell proliferation. Genes Dev 25, 1716-1733.

Gui, D.Y., Sullivan, L.B., Luengo, A., Hosios, A.M., Bush, L.N., Gitego, N., Davidson, S.M., Freinkman, E., Thomas, C.J., and Vander Heiden, M.G. (2016). Environment Dictates Dependence on Mitochondrial Complex I for NAD+ and Aspartate Production and Determines Cancer Cell Sensitivity to Metformin. Cell Metab 24, 716-727.

Hatzivassiliou, G., Zhao, F., Bauer, D.E., Andreadis, C., Shaw, A.N., Dhanak, D., Hingorani, S.R., Tuveson, D.A., and Thompson, C.B. (2005). ATP citrate lyase inhibition can suppress tumor cell growth. Cancer Cell 8, 311-321.

Hay, N. (2016). Reprogramming glucose metabolism in cancer: can it be exploited for cancer therapy? Nat Rev Cancer 16, 635-649.

Hensley, C.T., Faubert, B., Yuan, Q., Lev-Cohain, N., Jin, E., Kim, J., Jiang, L., Ko, B., Skelton, R., Loudat, L., et al. (2016). Metabolic Heterogeneity in Human Lung Tumors. Cell 164, 681-694.

Hilvo, M., Denkert, C., Lehtinen, L., Muller, B., Brockmoller, S., Seppanen-Laakso, T., Budczies, J., Bucher, E., Yetukuri, L., Castillo, S., et al. (2011). Novel theranostic opportunities offered by characterization of altered membrane lipid metabolism in breast cancer progression. Cancer Res 71, 3236-3245.

Hosios, A.M., Hecht, V.C., Danai, L.V., Johnson, M.O., Rathmell, J.C., Steinhauser, M.L., Manalis, S.R., and Vander Heiden, M.G. (2016). Amino Acids Rather than Glucose Account for the Majority of Cell Mass in Proliferating Mammalian Cells. Dev Cell 36, 540-549.

Hosios, A.M., and Vander Heiden, M.G. (2018). The redox requirements of proliferating mammalian cells. J Biol Chem.

Huang, T., Sun, J., Wang, Q., Gao, J., and Liu, Y. (2015). Synthesis, Biological Evaluation and Molecular Docking Studies of Piperidinylpiperidines and Spirochromanones Possessing Quinoline Moieties as Acetyl-CoA Carboxylase Inhibitors. Molecules 20, 16221-16234.

Ito, D., Imai, Y., Ohsawa, K., Nakajima, K., Fukuuchi, Y., and Kohsaka, S. (1998). Microglia-specific localisation of a novel calcium binding protein, Iba1. Brain Res Mol Brain Res 57, 1-9.

Jain, M., Nilsson, R., Sharma, S., Madhusudhan, N., Kitami, T., Souza, A.L., Kafri, R., Kirschner, M.W., Clish, C.B., and Mootha, V.K. (2012). Metabolite profiling identifies a key role for glycine in rapid cancer cell proliferation. Science 336, 1040-1044.

Jones, S.F., and Infante, J.R. (2015). Molecular Pathways: Fatty Acid Synthase. Clin Cancer Res 21, 5434-5438.

Jung, Y.Y., Kim, H.M., and Koo, J.S. (2015). Expression of Lipid Metabolism-Related Proteins in Metastatic Breast Cancer. PLoS One 10, e0137204.

Kamphorst, J.J., Chung, M.K., Fan, J., and Rabinowitz, J.D. (2014). Quantitative analysis of acetyl-CoA production in hypoxic cancer cells reveals substantial contribution from acetate. Cancer Metab 2, 23.

Kamphorst, J.J., Cross, J.R., Fan, J., de Stanchina, E., Mathew, R., White, E.P., Thompson, C.B., and Rabinowitz, J.D. (2013). Hypoxic and Ras-transformed cells support growth by scavenging unsaturated fatty acids from lysophospholipids. Proc Natl Acad Sci U S A 110, 8882-8887.

Kim, S.J., Kim, J.S., Park, E.S., Lee, J.S., Lin, Q., Langley, R.R., Maya, M., He, J., Kim, S.W., Weihua, Z., et al. (2011). Astrocytes upregulate survival genes in tumor cells and induce protection from chemotherapy. Neoplasia 13, 286-298.

Kodack, D.P., Askoxylakis, V., Ferraro, G.B., Fukumura, D., and Jain, R.K. (2015). Emerging strategies for treating brain metastases from breast cancer. Cancer Cell 27, 163-175.

Kodack, D.P., Askoxylakis, V., Ferraro, G.B., Sheng, Q., Badeaux, M., Goel, S., Qi, X., Shankaraiah, R., Cao, Z.A., Ramjiawan, R.R., et al. (2017). The brain microenvironment mediates resistance in luminal breast cancer to PI3K inhibition through HER3 activation. Sci Transl Med 9.

Kodack, D.P., Chung, E., Yamashita, H., Incio, J., Duyverman, A.M., Song, Y., Farrar, C.T., Huang, Y., Ager, E., Kamoun, W., et al. (2012). Combined targeting of HER2 and VEGFR2 for effective treatment of HER2-amplified breast cancer brain metastases. Proc Natl Acad Sci U S A 109, E3119-3127.

Koul, D., Fu, J., Shen, R., LaFortune, T.A., Wang, S., Tiao, N., Kim, Y.W., Liu, J.L., Ramnarian, D., Yuan, Y., et al. (2012). Antitumor activity of NVP-BKM120--a selective pan class I PI3 kinase inhibitor showed differential forms of cell death based on p53 status of glioma cells. Clin Cancer Res 18, 184-195.

Kuhajda, F.P. (2006). Fatty acid synthase and cancer: new application of an old pathway. Cancer Res 66, 5977-5980.

Kuhajda, F.P., Jenner, K., Wood, F.D., Hennigar, R.A., Jacobs, L.B., Dick, J.D., and Pasternack, G.R. (1994). Fatty acid synthesis: a potential selective target for antineoplastic therapy. Proc Natl Acad Sci U S A 91, 6379-6383.

Kuhajda, F.P., Piantadosi, S., and Pasternack, G.R. (1989). Haptoglobin-related protein (Hpr) epitopes in breast cancer as a predictor of recurrence of the disease. N Engl J Med 321, 636-641.

Lane, A.N., Higashi, R.M., and Fan, T.W. (2016). Preclinical models for interrogating drug action in human cancers using Stable Isotope Resolved Metabolomics (SIRM). Metabolomics 12.

Lee-Hoeflich, S.T., Crocker, L., Yao, E., Pham, T., Munroe, X., Hoeflich, K.P., Sliwkowski, M.X., and Stern, H.M. (2008). A central role for HER3 in HER2-amplified breast cancer: implications for targeted therapy. Cancer Res 68, 5878-5887.

Lewis, C.A., Parker, S.J., Fiske, B.P., McCloskey, D., Gui, D.Y., Green, C.R., Vokes, N.I., Feist, A.M., Vander Heiden, M.G., and Metallo, C.M. (2014). Tracing compartmentalized NADPH metabolism in the cytosol and mitochondria of mammalian cells. Mol Cell 55, 253-263.

Li, S., Qiu, L., Wu, B., Shen, H., Zhu, J., Zhou, L., Gu, L., and Di, W. (2013). TOFA suppresses ovarian cancer cell growth in vitro and in vivo. Mol Med Rep 8, 373-378.

Liberti, M.V., and Locasale, J.W. (2016). The Warburg Effect: How Does it Benefit Cancer Cells? Trends Biochem Sci 41, 211-218.

Lin, N.U., Carey, L.A., Liu, M.C., Younger, J., Come, S.E., Ewend, M., Harris, G.J., Bullitt, E., Van den Abbeele, A.D., Henson, J.W., et al. (2008). Phase II trial of lapatinib for brain metastases in patients with human epidermal growth factor receptor 2-positive breast cancer. J Clin Oncol 26, 1993-1999.

Lin, N.U., Dieras, V., Paul, D., Lossignol, D., Christodoulou, C., Stemmler, H.J., Roche, H., Liu, M.C., Greil, R., Ciruelos, E., et al. (2009). Multicenter phase II study of lapatinib in patients with brain metastases from HER2-positive breast cancer. Clin Cancer Res 15, 1452-1459.

Lin, Q., Balasubramanian, K., Fan, D., Kim, S.J., Guo, L., Wang, H., Bar-Eli, M., Aldape, K.D., and Fidler, I.J. (2010). Reactive astrocytes protect melanoma cells from chemotherapy by sequestering intracellular calcium through gap junction communication channels. Neoplasia 12, 748-754.

Maher, E.A., Marin-Valencia, I., Bachoo, R.M., Mashimo, T., Raisanen, J., Hatanpaa, K.J., Jindal, A., Jeffrey, F.M., Choi, C., Madden, C., et al. (2012). Metabolism of [U-13 C]glucose in human brain tumors in vivo. NMR Biomed 25, 1234-1244.

Maira, S.M., Pecchi, S., Huang, A., Burger, M., Knapp, M., Sterker, D., Schnell, C., Guthy, D., Nagel, T., Wiesmann, M., et al. (2012). Identification and characterization of NVP-BKM120, an orally available pan-class I PI3-kinase inhibitor. Mol Cancer Ther 11, 317-328.

Marin-Valencia, I., Yang, C., Mashimo, T., Cho, S., Baek, H., Yang, X.L., Rajagopalan, K.N., Maddie, M., Vemireddy, V., Zhao, Z., et al. (2012). Analysis of tumor metabolism reveals mitochondrial glucose oxidation in genetically diverse human glioblastomas in the mouse brain in vivo. Cell Metab 15, 827-837.

Mayers, J.R., Torrence, M.E., Danai, L.V., Papagiannakopoulos, T., Davidson, S.M., Bauer, M.R., Lau, A.N., Ji, B.W., Dixit, P.D., Hosios, A.M., et al. (2016). Tissue of origin dictates branched-chain amino acid metabolism in mutant Kras-driven cancers. Science 353, 1161-1165.

Mayers, J.R., and Vander Heiden, M.G. (2015). Famine versus feast: understanding the metabolism of tumors in vivo. Trends Biochem Sci 40, 130-140.

Medes, G., Thomas, A., and Weinhouse, S. (1953). Metabolism of neoplastic tissue. IV. A study of lipid synthesis in neoplastic tissue slices in vitro. Cancer Res 13, 27-29.

Monaco, M.E. (2017). Fatty acid metabolism in breast cancer subtypes. Oncotarget 8, 29487-29500.

Muir, A., Danai, L.V., Gui, D.Y., Waingarten, C.Y., Lewis, C.A., and Vander Heiden, M.G. (2017). Environmental cystine drives glutamine anaplerosis and sensitizes cancer cells to glutaminase inhibition. Elife 6.

Nagarajan, A., Malvi, P., and Wajapeyee, N. (2016). Oncogene-directed alterations in cancer cell metabolism. Trends Cancer 2, 365-377.

Neman, J., Termini, J., Wilczynski, S., Vaidehi, N., Choy, C., Kowolik, C.M., Li, H., Hambrecht, A.C., Roberts, E., and Jandial, R. (2014). Human breast cancer metastases to the brain display GABAergic properties in the neural niche. Proc Natl Acad Sci U S A 111, 984-989.

Ni, J., Ramkissoon, S.H., Xie, S., Goel, S., Stover, D.G., Guo, H., Luu, V., Marco, E., Ramkissoon, L.A., Kang, Y.J., et al. (2016). Combination inhibition of PI3K and mTORC1 yields durable remissions in mice bearing orthotopic patient-derived xenografts of HER2-positive breast cancer brain metastases. Nat Med 22, 723-726.

Olson, E.M., Abdel-Rasoul, M., Maly, J., Wu, C.S., Lin, N.U., and Shapiro, C.L. (2013). Incidence and risk of central nervous system metastases as site of first recurrence in patients with HER2-positive breast cancer treated with adjuvant trastuzumab. Ann Oncol 24, 1526-1533.

Ookhtens, M., Kannan, R., Lyon, I., and Baker, N. (1984). Liver and adipose tissue contributions to newly formed fatty acids in an ascites tumor. Am J Physiol 247, R146-153.

Pavlova, N.N., and Thompson, C.B. (2016). The Emerging Hallmarks of Cancer Metabolism. Cell Metab 23, 27-47.

Röhrig, F., and Schulze, A. (2016). The multifaceted roles of fatty acid synthesis in cancer. Nat Rev Cancer 16, 732-749.

Sabater, D., Arriaran, S., Romero Mdel, M., Agnelli, S., Remesar, X., Fernandez-Lopez, J.A., and Alemany, M. (2014). Cultured 3T3L1 adipocytes dispose of excess medium glucose as lactate under abundant oxygen availability. Sci Rep 4, 3663.

Schildge, S., Bohrer, C., Beck, K., and Schachtrup, C. (2013). Isolation and culture of mouse cortical astrocytes. J Vis Exp.

Sellers, K., Fox, M.P., Bousamra, M., 2nd, Slone, S.P., Higashi, R.M., Miller, D.M., Wang, Y., Yan, J., Yuneva, M.O., Deshpande, R., et al. (2015). Pyruvate carboxylase is critical for non-small-cell lung cancer proliferation. J Clin Invest 125, 687-698.

Shank, R.P., Bennett, G.S., Freytag, S.O., and Campbell, G.L. (1985). Pyruvate carboxylase: an astrocyte-specific enzyme implicated in the replenishment of amino acid neurotransmitter pools. Brain Res 329, 364-367.

Sounni, N.E., Cimino, J., Blacher, S., Primac, I., Truong, A., Mazzucchelli, G., Paye, A., Calligaris, D., Debois, D., De Tullio, P., et al. (2014). Blocking lipid synthesis overcomes tumor regrowth and metastasis after antiangiogenic therapy withdrawal. Cell Metab 20, 280-294.

Tamura, K., Kurihara, H., Yonemori, K., Tsuda, H., Suzuki, J., Kono, Y., Honda, N., Kodaira, M., Yamamoto, H., Yunokawa, M., et al. (2013). 64Cu-DOTA-trastuzumab PET imaging in patients with HER2-positive breast cancer. J Nucl Med 54, 1869-1875.

Tardito, S., Oudin, A., Ahmed, S.U., Fack, F., Keunen, O., Zheng, L., Miletic, H., Sakariassen, P.O., Weinstock, A., Wagner, A., et al. (2015). Glutamine synthetase activity fuels nucleotide biosynthesis and supports growth of glutamine-restricted glioblastoma. Nat Cell Biol 17, 1556-1568.

Tumanov, S., Bulusu, V., and Kamphorst, J.J. (2015). Analysis of Fatty Acid Metabolism Using Stable Isotope Tracers and Mass Spectrometry. Methods Enzymol 561, 197-217.

Valiente, M., Obenauf, A.C., Jin, X., Chen, Q., Zhang, X.H., Lee, D.J., Chaft, J.E., Kris, M.G., Huse, J.T., Brogi, E., et al. (2014). Serpins promote cancer cell survival and vascular co-option in brain metastasis. Cell 156, 1002-1016.

Vander Heiden, M.G., Cantley, L.C., and Thompson, C.B. (2009). Understanding the Warburg effect: the metabolic requirements of cell proliferation. Science 324, 1029-1033.

Warburg, O. (1923). Versuche an überlebendem Carcinomgewebe (Methoden). Biochemische Zeitschrift 142, 317–333.

Warburg, O. (1956). On the origin of cancer cells. Science 123, 309-314.

Weinberg, S.E., and Chandel, N.S. (2015). Targeting mitochondria metabolism for cancer therapy. Nat Chem Biol 11, 9-15.

Whitaker-Menezes, D., Martinez-Outschoorn, U.E., Flomenberg, N., Birbe, R.C., Witkiewicz, A.K., Howell, A., Pavlides, S., Tsirigos, A., Ertel, A., Pestell, R.G., et al. (2011). Hyperactivation of oxidative mitochondrial metabolism in epithelial cancer cells in situ: visualizing the therapeutic effects of metformin in tumor tissue. Cell Cycle 10, 4047-4064.

Yu, A.C., Drejer, J., Hertz, L., and Schousboe, A. (1983). Pyruvate carboxylase activity in primary cultures of astrocytes and neurons. J Neurochem 41, 1484-1487.

Yuneva, M.O., Fan, T.W., Allen, T.D., Higashi, R.M., Ferraris, D.V., Tsukamoto, T., Mates, J.M., Alonso, F.J., Wang, C., Seo, Y., et al. (2012). The metabolic profile of tumors depends on both the responsible genetic lesion and tissue type. Cell Metab 15, 157-170.

Zhou, B.P., Liao, Y., Xia, W., Spohn, B., Lee, M.H., and Hung, M.C. (2001a). Cytoplasmic localization of p21Cip1/WAF1 by Akt-induced phosphorylation in HER-2/neu-overexpressing cells. Nat Cell Biol 3, 245-252.

Zhou, B.P., Liao, Y., Xia, W., Zou, Y., Spohn, B., and Hung, M.C. (2001b). HER-2/neu induces p53 ubiquitination via Akt-mediated MDM2 phosphorylation. Nat Cell Biol 3, 973-982.

Chapter 5: Discussion and Future Directions

Summary

Tumor cells rewire their metabolic network to efficiently incorporate nutrients into biomass, balance cellular energetics, and support rapid, uncontrolled proliferation. The discovery that the metabolism of cancer cells differs from that of normal tissues was made almost a century ago by Otto Warburg in the late 1920s, who determined that tumors consume large quantities of glucose and excrete the majority of glucose-derived carbon as lactate. Since this initial finding, it has been determined that many cancer cells display the "Warburg effect," and the reprogrammed glucose metabolism of cancer cells is now considered a hallmark of the disease. Since this phenotype represents one of the largest metabolic differences distinguishing cancer cells from their tissues of origin, there has been attempts to target this pathway for the treatment of cancer. However, efforts to directly target the Warburg effect have seen limited clinical success, likely because the same glycolytic enzymes are expressed in both tumors and non-cancerous cells and high glucose uptake is important in some normal tissues such as the brain. Thus, in order to exploit metabolism for cancer therapy, it is important to first define pathways that are essential to support the progression of specific cancers.

In this dissertation, we explore several strategies to target the metabolism of cancer cells. We first utilized an unbiased approach to identify metabolites that accumulate in lung tumors relative to lung tissue, and determined that the

antioxidant glutathione is elevated in tumors. We found that in lung lesions, one function of high levels of glutathione is to react with and scavenge endogenously produced electrophiles, including methylglyoxal, a reactive error-product of glycolysis. We established that production of methylglyoxal is higher in lung cancers and that blocking detoxification of this metabolite can reduce cancer cell fitness and impair lung tumor growth. Though glycolytic enzymes are present in normal and malignant tissues, glycolytic flux and, by extension, reactive metabolite production are greatly enhanced in cancer contexts. Thus, while inhibitors of glycolysis can result in unwanted toxicity, targeting detoxification pathways of reactive metabolites could offer a more selective therapeutic strategy. That is, an indirect effect of the reprogrammed glucose metabolism of cancer cells is production of reactive metabolite byproducts, and this could represent a targetable vulnerability of highly glycolytic tumors.

Though the Warburg effect has been studied extensively since its initial discovery, the ontology of this process remains controversial. To investigate how high glycolytic flux promotes tumor proliferation, we next repressed the Warburg effect in cancer cells by inhibiting PDK, which results in increased entry of glucose-derived carbons into the tricarboxylic acid cycle. We found that stimulating glucose oxidation in cancer cells perturbs NAD+/NADH homeostasis, and that this imbalance is caused by limited oxidative capacity of mitochondrial respiration. We determined that the mitochondrial respiration of tumor cells is endogenously constrained by the membrane potential across the inner mitochondrial membrane

and by the ATP utilization of the cell. This finding suggests that tumors may rewire glucose metabolism to optimize for electron acceptor generation, and suggests that therapies that restrict availability of NAD+ could be another strategy to target the enhanced glycolytic flux of cancer cells.

Finally, we interrogated how cancer cells adapt their metabolic program to permit growth in different tumor microenvironments. We investigated the differential metabolic phenotypes and dependencies of *HER2*-amplified breast cancers growing in the primary site and as metastases in the brain. We found that breast cancers growing in the brain exhibit increased glucose consumption and lipid synthesis relative to those in the mammary fat pad. Furthermore, we provide evidence that inhibiting fatty acid synthesis could be a way to augment the efficacy of therapies that otherwise are ineffective in treating breast cancer in this tissue context.

Collectively, these studies investigate how the metabolic dependencies of cancer cells differ relative to normal cells, and explore whether any of these altered pathways could provide opportunities to improve therapies for cancer patients. Though it has proven challenging to directly target the glucose metabolism of tumors for clinical benefit, treatment strategies that target secondary consequences of glycolysis, such as methylglyoxal production, or metabolic drivers of the phenotype, such as electron acceptor insufficiency, may represent a more tractable avenue to target the Warburg effect for cancer treatment. Additionally, investigation of how metabolic rewiring supports tumor proliferation in different

tumor sites can help guide therapies for cancers with limited treatment options, as is the case for breast cancer brain metastases.

Discussion

Reactive byproducts of cancer metabolism

Altered flux through metabolic pathways results in different steady-state concentrations of metabolites in tumors relative to normal tissues, which can have important implications for cell signaling, bioenergetics, and proliferation (DeBerardinis and Chandel, 2016; Sullivan et al., 2016). Some metabolites accumulate inappropriately in cancer cells and their local microenvironment as byproducts or error products of metabolism. This class of metabolites are generated by promiscuous enzyme activity, or non-enzymatically due to the inherent reactivity of certain metabolic pathway intermediates (Sullivan et al., 2016). Many of these byproducts are themselves chemically unstable, producing reactive metabolites that can further react non-specifically with other nearby molecules.

Accumulation of reactive metabolites can have negative consequences for cellular fitness, as these molecules can react with and damage macromolecules in the cell. Thus, cells with enhanced production of reactive metabolites rely on pathways that robustly detoxify these species to prevent accumulation of damaged biomolecules.

In the work presented in this thesis, we determined that methylglyoxal production is elevated in tumors and that targeting detoxification of this metabolite

can impair cancer cell growth. However, other reactive error products of metabolism, including reactive oxygen species (ROS), formaldehyde, and byproducts of lipid peroxidation have also been found to be generated at higher levels in tumors. We and others have determined that tumor cells have increased levels of antioxidants to detoxify these reactive intermediates and allow cancer progression (Gorrini et al., 2013; Piskounova et al., 2015; Schafer et al., 2009). The increased antioxidant capacity of tumor cells appears to be downstream of oncogenic signaling pathways that promote flux through pathways that produce NADPH, which is required for the synthesis of glutathione (DeNicola et al., 2015; DeNicola et al., 2011; Harris et al., 2015; Ye et al., 2014).

Limiting the availability of antioxidants or targeting pathways that detoxify reactive metabolites could represent a promising approach to exploit a metabolic feature common to many cancer cells. Targeting detoxification pathways could selectively kill cells that produce higher levels of reactive metabolites, thereby treating tumors by potentiating, rather than repressing, a metabolic phenotype of cancer cells. Inhibition of glutathione synthesis induces accumulation of ROS, resulting in toxicity and reduced tumor progression (Garama et al., 2015; Harris et al., 2015; Raj et al., 2011; Trachootham et al., 2006). We have reported in Chapter 2 of this thesis that ablation of the methylglyoxal detoxification enzyme glyoxalase 1 can inhibit cancer cell proliferation, which is in agreement with published studies (Hosoda et al., 2015; Sakamoto et al., 2001; Thornalley et al., 1996). The toxicity of the lipid peroxidation error product 4-hydroxy-2-nonenal has been reported to be

enhanced by blocking its detoxification by depletion of intracellular glutathione (Spitz et al., 1991). Conversely, enhancing the ability of tumors to detoxify reactive metabolites by providing antioxidants has been reported to accelerate tumor growth (Le Gal et al., 2015; Omenn et al., 1996; Sayin et al., 2014), suggesting that reactive metabolites can endogenously restrain tumor cell proliferation.

Though therapies that induce excessive accumulation of reactive metabolites could impair tumor progression, a potential pitfall of this approach is that accumulation of reactive metabolites at low levels can also contribute to malignancy. ROS has been shown to activate oncogenic signaling pathways and contribute to genomic instability (Arnold et al., 2001; Irani et al., 1997; Suh et al., 1999; Weinberg et al., 2010). Endogenously produced formaldehyde can promote systemic DNA damage and malignant transformation (Burgos-Barragan et al., 2017). Repression of Glyoxalase 1 in breast cancer has been shown to increase tumor growth (Nokin et al., 2016), and it has been reported that methylglyoxal can enhance tumorigenesis at low doses while inhibiting tumor progression at higher concentrations (Nokin et al., 2017). A better understanding of the regimes in which reactive metabolites can promote malignancy or induce cancer cell toxicity, while sparing non-cancerous tissues, is essential the successful clinical translation of strategies that exploit elevated production of reactive metabolites in cancers.

Metabolic Drivers of the Warburg effect

Why cancer cells consume large quantities of glucose, only to secrete the majority of the carbons as lactate, remains poorly understood and has been debated since Warburg's initial discovery. Tumor cells require energy to support proliferation, and yet the Warburg effect is inefficient for ATP production. The conversion of glucose to lactate produces 2 ATP, whereas complete oxidation of each glucose molecule generates as many as 36 ATP (Vander Heiden et al., 2009). It has been proposed that though the yield of ATP generated by glycolysis low, the rapid rate of this pathway grants a selective advantage to cancer cells under conditions of nutrient limitation (Pfeiffer et al., 2001). However, it has been calculated that the relative amount of ATP required for growth may be less than what is required for cellular maintenance (Kilburn et al., 1969), and evidence suggests that ATP is not limiting for proliferation of cancer cells (Locasale and Cantley, 2011; Lunt and Vander Heiden, 2011). In fact, there are cases where ATP hydrolysis, rather than ATP itself, could may be limiting for proliferation (Fang et al., 2010; Racker, 1972; Scholnick et al., 1973). The study described in Chapter 3 of this thesis provides further evidence that ATP hydrolysis may be a constraint for cancer cell proliferation in some contexts.

A commonly invoked explanation for the Warburg effect is that the rapid rates of glycolysis observed in cancer cells facilitates shunting of carbon into anabolic pathways (Boroughs and DeBerardinis, 2015; Cairns et al., 2011; Hsu and Sabatini, 2008; Koppenol et al., 2011; Vander Heiden et al., 2009). However, the

vast majority of glucose consumed by tumors is excreted as lactate, and it has been shown that carbons derived from glucose are incorporated into the new biomass of proliferating cells only at low levels (Hosios et al., 2016). However, levels of glycolytic intermediates are not necessarily changed in tumor cells (Lunt et al., 2015) arguing against this hypothesis being the sole explanation for the Warburg effect in all cancers.

Another proposed benefit of the Warburg effect is generation of electron carriers. Proliferating cells require electrons in the form of NADPH, as this cofactor is needed to synthesize macromolecules and antioxidants (Cairns et al., 2011). It has been proposed that NADPH production could be limiting for cancer cell proliferation (Vander Heiden et al., 2009). However, in this dissertation, we determine that two processes that are highly demanding for NADPH, glutathione production (**Chapter 2**) and lipid synthesis (**Chapter 4**) are increased in cancers. Additionally, it has been shown that increasing proline synthesis, an NADPH consuming process, promotes tumor cell growth (Liu et al., 2015), further arguing against NADPH being a limitation for all tumors.

Recently, it has been argued that the regeneration of the oxidizing equivalent NAD+ could be limiting for tumor proliferation (Birsoy et al., 2015; Gui et al., 2016; Sullivan et al., 2015; Titov et al., 2016). NAD+ is required to remove electrons from nutrients cells consume and to oxidize precursors of nucleotides and amino acids (Hosios and Vander Heiden, 2018). Though proliferating cells have high NAD+/NADH ratios in order to support these pathways (Schwartz et al., 1974), it

has recently been shown that the NAD+/NADH ratio is lower in cancer cells than what was originally assumed (Hung et al., 2011; Hung and Yellen, 2014; Zhao et al., 2016b), serving as further evidence that NAD+ could be limiting for tumors.

The conversion of pyruvate to lactate can be influenced by the availability of NAD+, as the enzyme lactate dehydrogenase (LDH) is highly efficient and abundant in cancer cells (Lunt and Vander Heiden, 2011; Wuntch et al., 1970). Additionally, activity of pyruvate dehydrogenase (PDH) has been shown to be regulated by the NAD+/NADH ratio (Pettit et al., 1975), and increasing NAD+ regeneration in cancer cells can stimulate PDH (Titov et al., 2016). Since the relative activity of PDH and LDH dictates pyruvate fate in cells, we wondered whether NAD+ availability could influence the Warburg effect phenotype. Since PDH consumes NAD+ and LDH produces it (**Figure 1A**), we hypothesized that depleting NAD+ could suppress glucose oxidation in favor of lactate excretion, thereby repressing the Warburg effect.

To test this idea, we cultured A549 cells with a variety of agents that could alter the NAD+/NADH ratio and performed a dynamic stable-isotope labeling experiment with [U-$^{13}C_6$]glucose to measure the incorporation of glucose-derived carbons into citrate, which corresponds to PDH flux. We found that the complex I inhibitor rotenone decreases the both relative NAD+/NADH and PDH activity, and both these effects were suppressed by treatment with duroquinone, which enhances NAD+ regeneration (Gui et al., 2016; Merker et al., 2006) (**Figure 1B,C**). This confirms that depletion of NAD+ decreases glucose oxidation, as expected.

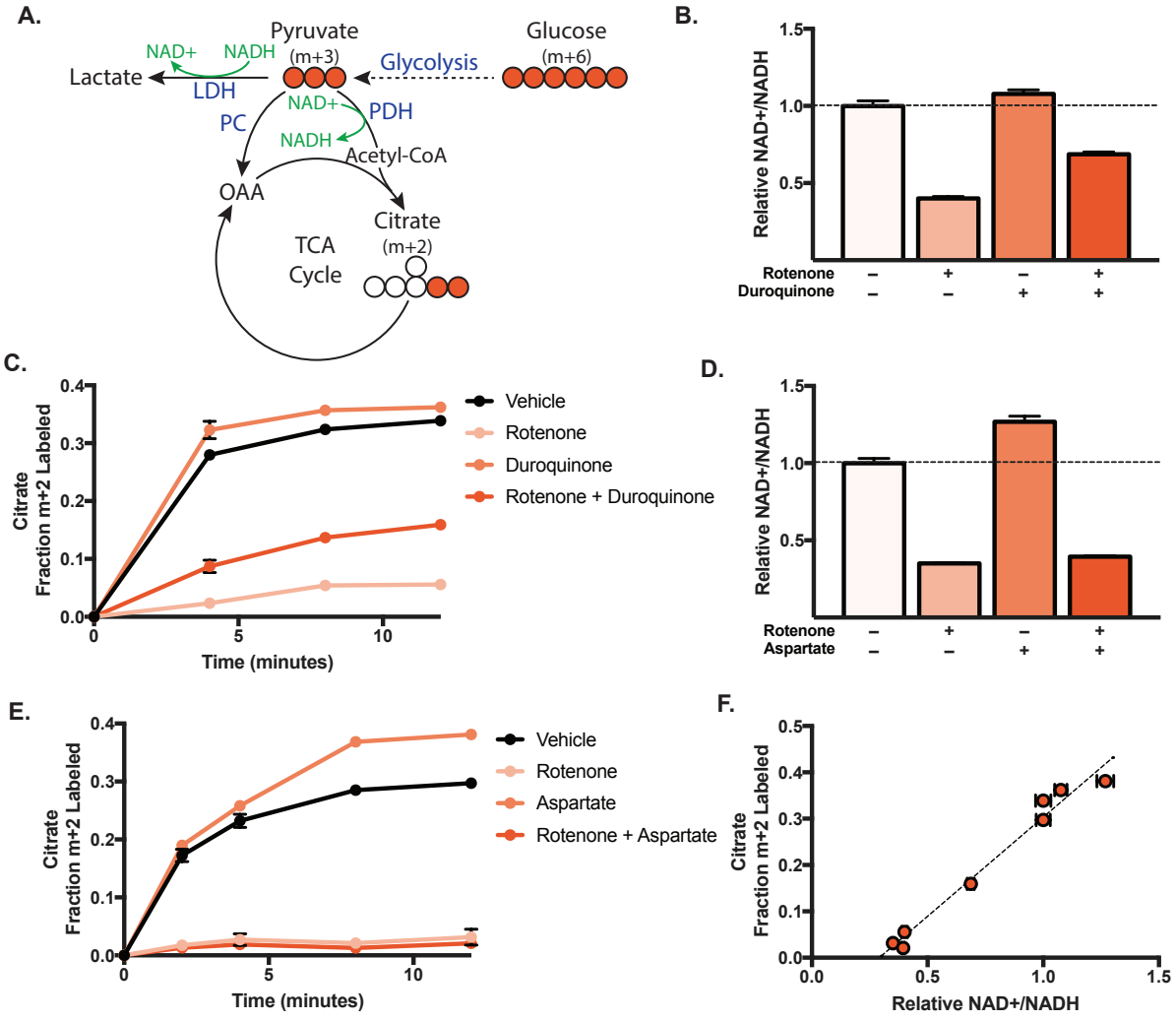
A.
Pyruvate
(m+3)
Glucose
(m+6)
Glycolysis
Lactate
NAD+
NADH
LDH
PC
NAD+
PDH
NADH
Acetyl-CoA
OAA
Citrate
(m+2)
TCA
Cycle
B.
Relative NAD+/NADH
1.5
1.0
0.5
Rotenone
Duroquinone
C.
Citrate
Fraction m+2 Labeled
0.4
0.3
0.2
0.1
0.0
0
5
10
Time (minutes)
Vehicle
Rotenone
Duroquinone
Rotenone + Duroquinone
D.
Relative NAD+/NADH
Rotenone
Aspartate
E.
Citrate
Fraction m+2 Labeled
Time (minutes)
Vehicle
Rotenone
Aspartate
Rotenone + Aspartate
F.
Citrate
Fraction m+2 Labeled
Relative NAD+/NADH

Figure 1. NAD+ availability dictates PDH flux

(A) Schematic illustrating the relationship between the fate of pyruvate and NAD+. The primary metabolic fates of pyruvate include: (1) conversion to lactate by lactate dehydrogenase (LDH), which generates NAD+ (2) entry into the TCA cycle via the enzyme pyruvate carboxylase (PC), which converts pyruvate to oxaloacetate (OAA), (3) entry into the TCA cycle via oxidation by pyruvate dehydrogenase (PDH) to acetyl-CoA, which consumes NAD+. PDH flux can be assessed by the measurement of citrate with two labeled carbons (m+2, indicated by red circles) from fully labeled [U-$^{13}C_6$]glucose (m+6, indicated by red circles).

(B) Relative change in the ratio of NAD+ to NADH in A549 cells as measured by LCMS. Cells were treated with rotenone (80nM), duroquinone (20mM), or untreated for 2 hours. Relative NAD+/NADH ratio was normalized to the untreated condition (n=12).

(C) Kinetic labeling of citrate from labeled glucose to assess PDH flux in the conditions described in panel (B). Cells were incubated for 2 hours in media containing 5mM unlabeled glucose with the treatments described in panel (B), after which 20mM [U-$^{13}C_6$]glucose was added to all conditions. Metabolites were rapidly extracted at the indicated time points and citrate labeling was determined by LCMS (n=3 per time point).

(D) Relative change in the ratio of NAD+ to NADH in A549 cells as measured by LCMS. Cells were treated with rotenone (80nM), aspartate (20mM), or untreated for 5 hours. Relative NAD+/NADH ratio is normalized to the untreated condition (n=12).

(E) Kinetic labeling of citrate from labeled glucose to assess PDH flux in the conditions described in panel (D). Cells were incubated for 5 hours in media containing 5mM unlabeled glucose with the doses described in panel (D), after which 20mM [U-$^{13}C_6$]glucose was added to all conditions. Metabolites were rapidly extracted at the indicated time points and citrate labeling was determined by LCMS (n=3 per time point).

(F) Plot of fraction of citrate that is m+2 labeled after a 12 minute incubation in 20mM [U-$^{13}C_6$]glucose (as measured in panels C and E) versus the NAD+/NADH ratio in these same cells (as measured in panels B and D). The dashed line indicates the best linear fit, which has an R^2 value of 0.98 (n=3).

Values shown denote the mean ± SEM.

To ensure that PDH activity is reflective of the intracellular NAD+/NADH ratio, rather than a read-out of proliferation, we next performed the same dynamic labeling experiment but substituted duroquinone with 20mM exogenous aspartate. Aspartate supplementation has been shown to rescue the proliferation defects caused by rotenone without restoring the NAD+/NADH ratio (Sullivan et al., 2016), decoupling these two parameters. We found that exogenous aspartate did not increase the relative NAD+/NADH ratio or glucose oxidation of cells that had been incubated with rotenone (**Figure 1D,E**). This indicates that in these cells, PDH flux depends on the availability of NAD+ rather than growth rate.

Interestingly, when we plotted the effects that these agents have on the relative change of the NAD+/NADH ratio against the fraction of m+2 citrate after a 12 minute pulse of [U-$^{13}C_6$]glucose, we found a linear correlation between NAD+/NADH and glucose oxidation (**Figure 1E**). This indicated to us that, as we hypothesized, NAD+ availability influences the rate of glucose oxidation and, by extension, the Warburg effect. This experiment, along with the findings presented in Chapter 3 of this dissertation, argues that the Warburg effect may be an adaptation to increased demand for oxidizing equivalents in proliferating cancer cells. In Appendix B of this thesis, we further address whether electron acceptor availability could be a constraint for tumor growth in vivo.

Models to study cancer metabolism

Much of what we know about the metabolic requirements of tumor proliferation was discovered by growing cancer cell lines in vitro using tissue culture systems. Though these techniques have permitted researchers to advance the understanding of cancer cell metabolism, it has proven difficult to translate therapeutic vulnerabilities identified in these systems to the clinic (Horvath et al., 2016; Niu and Wang, 2015). Better culture systems are required to ensure that cancer metabolism studies identify metabolic dependencies that hold relevance for human disease.

One potential explanation for the discrepancy between metabolic vulnerabilities of tumors in vivo and in culture systems is that the sensitivity of cancer cells to drugs is not necessarily a cell intrinsic property and instead can be affected by the tumor environment (Gui et al., 2016). Tissue culture media poorly recapitulates physiological concentrations of nutrients (Eagle, 1955), and thus the sensitivity of cancer cells to therapy can differ greatly between tissue culture and in vivo settings. For example, cancer cells grown in culture consume large amounts of glutamine to supply intermediates of the tricarboxylic acid cycle (TCA), and require glutaminase activity for survival (Gao et al., 2009; Gross et al., 2014; Le et al., 2012; Son et al., 2013; Wang et al., 2010; Yuneva et al., 2012). These findings prompted the development of pharmacological inhibitors of glutaminase, which are now being evaluated in clinical trials for the treatment of cancer (NCT02071862). However, it has been determined that many tumors growing in vivo utilize more glucose than

glutamine for anaplerosis (Davidson et al., 2016; Hensley et al., 2016; Maher et al., 2012; Marin-Valencia et al., 2012; Sellers et al., 2015), and that the same cells that exhibit sensitivity to glutaminase inhibition in tissue culture settings can be refractory to this treatment in vivo (Davidson et al., 2016). These findings highlight that standard media conditions can misrepresent vulnerabilities of cancer metabolism, complicating the translation of metabolic liabilities of cancer cells identified in culture into effective cancer therapies.

The development of culture systems that more accurately recapitulate the tumor microenvironment may provide improved models to study dependencies of cancer metabolism. Tissue culture media was formulated to optimize proliferation (Eagle, 1955) and it can be adapted to better reflect levels of nutrients found in vivo. Growing cancer cells in serum or in serum-like media was found to repress glutamine catabolism and sensitivity to glutaminase inhibitors (Muir et al., 2017; Tardito et al., 2015), suggesting that these culture conditions can more accurately replicate features of the metabolism of cancers grown in vivo. The use of more physiological culture media could help reveal liabilities of metabolism that have greater possibilities for successful in vivo translation (Cantor et al., 2017).

Another consideration for the development of more physiological culture systems is that tumors in vivo are highly heterogeneous and consist of both tumor cells and a variety of noncancerous stromal cells. Stromal cells have been shown to confer resistance to chemotherapies to tumors (Gilbert and Hemann, 2011). Furthermore, these tumor and stromal cells share a nutrient environment which

can alter the availability of resources and dependencies on metabolic pathways. It has been reported that tumor associated-stroma can supply tumor cells with amino acids, either by direct excretion of alanine (Sousa et al., 2016), cystine (Zhang et al., 2012) or by production of exosomes (Zhao et al., 2016a). Existent cell culture methods fail to recapitulate these interactions. As we have presented in Chapter 4 of this thesis, the use of conditioned media or of co-culture systems can be one way to mimic the tumor microenvironment within the constraints of standard tissue culture techniques.

The use of ex vivo organotypic slice cultures, introduced in Chapter 4 of this dissertation, is another method to model the interaction between cancer cells and stroma in tissue culture systems, with the additional benefit of maintaining the native tissue architecture of tumors. In this method, metabolism studies are performed on thin slices generated from freshly resected tumors, and cultured in defined media conditions. This approach was used by Warburg when he first identified the reprogrammed glucose metabolism of tumors (Warburg, 1923) and since this initial discovery, it has been confirmed that ex vivo organotypic slices can recapitulate features of in vivo tumor metabolism (Lane et al., 2016; Sellers et al., 2015) and display drug sensitivities that match those observed in the clinic (Askoxylakis et al., 2016; de Graaf et al., 2010; Parrish et al., 1995). Expanded use of this platform in future cancer metabolism studies can aid identification of metabolic dependencies that more accurately reflect those of tumors growing in vivo.

As tumor metabolism is influenced by a panoply of cell-extrinsic factors, it is likely impossible to model all these features using a single in vitro system. Measurement of metabolic fluxes in intact tumors is becoming standard in the field of cancer metabolism, and these studies may prove essential in determining metabolic liabilities that are amenable to therapeutic targeting. Several studies have assessed the fate of isotope-labeled nutrients in mice and human cancer, permitting direct examination of the activities of metabolic pathways in vivo. However, functional interpretation of the data obtained from these studies proves challenging due to the complexity of in vivo physiology. Tumors have been shown to be highly heterogeneous (Hensley et al., 2016) and it is challenging to distinguish the metabolic phenotypes of different cell types within the tumor microenvironment. Additionally, metabolite labeling in vivo depends on a variety of factors including enrichment of the labeled precursors, exchange flux, and the metabolism of tissues distal to the tumor. However, in vivo metabolism studies can still provide important information about the activity of various metabolic pathways, and the techniques for analyzing metabolism in vivo are rapidly expanding.

Standard cell culture systems have been essential for the discovery of genetic drivers of proliferation. However, these same approaches have proved less successful in modeling the drug response of compounds targeting core pathways of metabolism. It is now acknowledged that environmental factors are important regulators of cell metabolism and can alter the essentially of certain biochemical pathways. To maximize the translation of metabolic vulnerabilities identified in

pre-clinical studies, future studies of metabolism will need to rely on experimental culture models that that more accurately mimic the nutrient environment seen by tumor cells in vivo. Though it can be highly informative to measure metabolic fluxes in intact tumors, complete reliance on these techniques for the identification of metabolic targets is impractical due to the limits on experimental manipulation and throughput. Identification of which features of the tumor microenvironment are most important for altering metabolic dependencies is needed to develop culture medias that recapitulate metabolic network of tumors in vivo, and the use of these model systems will be critical to identify metabolic dependencies that can be exploited for the treatment of cancer.

Conclusion

The metabolism of cancer cells is considerably different than that of normal, differentiated cells, as tumors must balance their requirement for energy production, macromolecule biosynthesis, and redox homeostasis. Though metabolic pathways that are altered in cancer often appear to be attractive therapeutic targets, inhibition of metabolic enzymes often result in significant toxic effects, as the metabolism of cancer cells can share many features with proliferating non-cancerous cell types, including immune and stem cells. Though this represents a significant challenge for translating metabolic dependencies of cancer cells to clinical therapies, the fact that antimetabolites, which target nucleotide metabolism, have been an integral part of standard chemotherapeutic regimens for

decades suggests that a therapeutic window exists to target the malignant metabolism of cancer cells.

The work presented in this dissertation investigates metabolic vulnerabilities of cancer cells, with the aim of identifying opportunities for clinical translation. Glycolytic enzymes are expressed in both cancer cells and normal tissues, and thus inhibitors of glucose metabolism may not offer sufficient selectivity for effective cancer treatment. However, production of reactive metabolite byproducts is a secondary, indirect effect of the reprogrammed metabolism of glucose in cancer cells and could provide an opportunity to clinically target tumors that are glucose avid. Increased activity of other metabolic pathways may also create analogous liabilities. Furthermore, we have determined that the Warburg effect is an adaptation to the limited oxidative capacity of cancer cells, suggesting that electron acceptor availability is a constraint for tumor cell growth and that further perturbing the redox potential of cancer cells could be a potential treatment strategy. Finally, we interrogated metabolic fluxes of tumors in vivo and determined that breast cancers that have metastasized to the brain increase their rate of fatty acid biosynthesis, suggesting that targeting the lipid metabolism of these tumors could be a way to develop therapies towards a cancer with inadequate treatment options.

Future investigation of the metabolic dependencies of tumor growth face several challenges. Many existent cancer metabolism studies were performed in cancer cell lines cultured in standard tissue culture conditions, rather than in intact tumors. Though these studies have been informative for determining the

requirements of proliferation, there is growing evidence that the metabolic dependencies of tumors can be greatly influenced by features of the tumor microenvironment, including the availability of nutrients and interaction with surrounding non-malignant stromal cells, tumor-initiation cells, and non-proliferating cancer cells. These variables may make translating metabolic vulnerabilities identified in tissue culture conditions to viable therapeutic strategies difficult. Extending our understanding of these challenging questions in metabolism will be critical to design therapies targeting the metabolic vulnerabilities of tumors for the treatment of cancer patients.

Materials and Methods

Cell Culture Experiments: A549 cells were cultured in DMEM (Corning 10-013-CV) supplemented with 10% fetal bovine serum. For all experiments, cells were washed three times in phosphate buffered saline (PBS), and then cultured in DMEM without pyruvate (Corning 10-017-CV) with 10% dialyzed fetal bovine serum, supplemented with the indicated treatment condition. The reagents used for the cell culture experiments are as follows: duroquinone (Sigma, D223204), L-aspartic acid (Sigma A6683), rotenone (Sigma R8875). Cells were cultured at 37°C with 5% CO_2.

Dynamic stable-isotope labeling experiments: Cells were plated in six-well plates in at a seeding density of 150,000 cells per well. Cells were permitted to

settle overnight. Prior to the initiation of the experiment, cells were washed three times with PBS, and then cultured in media containing 5mM glucose and the indicated treatment condition. After cells were cultured for 5 hours, 30μL of a 1M [U-$^{13}C_6$]glucose solution was rapidly administered to each well of the plate and the plate was rocked gently. Following the appropriate incubation (ranging from 2 to 12 minutes), cells were washed as quickly as possible with ice-cold blood bank saline and lysed on the dish with 300μL of ice-cold 80% HPLC-grade methanol in HPLC-grade water. Samples were scraped, collected into Eppendorf tubes, and vortexed for 10 minutes at 4°C, centrifuged at 21,000×g for 10 minutes at 4°C to precipitate the protein. 50μM of each sample was collected for immediate analysis by liquid chromatography mass-spectrometry (LCMS).

LCMS Metabolite Profiling: Metabolite profiling was conducted on a QExactive bench top orbitrap mass spectrometer equipped with an Ion Max source and a HESI II probe, which was coupled to a Dionex UltiMate 3000 HPLC system (Thermo Fisher Scientific, San Jose, CA). External mass calibration was performed using the standard calibration mixture every 7 days. For each sample, 4μL of each sample was injected onto a SeQuant® ZIC®-pHILIC 150 × 2.1 mm analytical column equipped with a 2.1 × 20 mm guard column (both 5 mm particle size; EMD Millipore). Buffer A was 20mM ammonium carbonate, 0.1% ammonium hydroxide; Buffer B was acetonitrile. The column oven and autosampler tray were held at 25°C and 4°C, respectively. The chromatographic gradient was run at a flow rate of 0.150

mL/min as follows: 0-20 min: linear gradient from 80-20% B; 20-20.5 min: linear gradient form 20-80% B; 20.5-28 min: hold at 80% B. The mass spectrometer was operated in full-scan, polarity-switching mode, with the spray voltage set to 3.0 kV, the heated capillary held at 275°C, and the HESI probe held at 350°C. The sheath gas flow was set to 40 units, the auxiliary gas flow was set to 15 units, and the sweep gas flow was set to 1 unit. MS data acquisition was performed in a range of m/z = 70–1000, with the resolution set at 70,000, the AGC target at 1×10^6, and the maximum injection time (Max IT) at 20 msec. For detection of nicotinamide diadenine nucleotide cofactors, targeted selected ion monitoring (tSIM) scans in positive mode were included. The isolation window was set at 3.0 m/z and tSIM scans were centered at m/z = 665.1243 for NAD(H). For detection of ^{13}C-labeled citrate, a negative mode tSIM scan centered on 194.1985 was included. The isolation window was set at 8.0 m/z. For all tSIM scans, the resolution was set at 70,000, the AGC target was 1×10^5, and the max IT was 250 msec. Relative quantitation of polar metabolites was performed with XCalibur QuanBrowser 2.2 (Thermo Fisher Scientific) using a 5ppm mass tolerance and referencing an in-house library of chemical standards.

References

Arnold, R.S., Shi, J., Murad, E., Whalen, A.M., Sun, C.Q., Polavarapu, R., Parthasarathy, S., Petros, J.A., and Lambeth, J.D. (2001). Hydrogen peroxide mediates the cell growth and transformation caused by the mitogenic oxidase Nox1. Proc Natl Acad Sci U S A 98, 5550-5555.

Askoxylakis, V., Ferraro, G.B., Kodack, D.P., Badeaux, M., Shankaraiah, R.C., Seano, G., Kloepper, J., Vardam, T., Martin, J.D., Naxerova, K., et al. (2016). Preclinical Efficacy of Ado-trastuzumab Emtansine in the Brain Microenvironment. J Natl Cancer Inst 108.

Birsoy, K., Wang, T., Chen, W.W., Freinkman, E., Abu-Remaileh, M., and Sabatini, D.M. (2015). An Essential Role of the Mitochondrial Electron Transport Chain in Cell Proliferation Is to Enable Aspartate Synthesis. Cell 162, 540-551.

Boroughs, L.K., and DeBerardinis, R.J. (2015). Metabolic pathways promoting cancer cell survival and growth. Nat Cell Biol 17, 351-359.

Burgos-Barragan, G., Wit, N., Meiser, J., Dingler, F.A., Pietzke, M., Mulderrig, L., Pontel, L.B., Rosado, I.V., Brewer, T.F., Cordell, R.L., et al. (2017). Mammals divert endogenous genotoxic formaldehyde into one-carbon metabolism. Nature 548, 549-554.

Cairns, R.A., Harris, I.S., and Mak, T.W. (2011). Regulation of cancer cell metabolism. Nat Rev Cancer 11, 85-95.

Cantor, J.R., Abu-Remaileh, M., Kanarek, N., Freinkman, E., Gao, X., Louissaint, A., Jr., Lewis, C.A., and Sabatini, D.M. (2017). Physiologic Medium Rewires Cellular Metabolism and Reveals Uric Acid as an Endogenous Inhibitor of UMP Synthase. Cell 169, 258-272 e217.

Davidson, S.M., Papagiannakopoulos, T., Olenchock, B.A., Heyman, J.E., Keibler, M.A., Luengo, A., Bauer, M.R., Jha, A.K., O'Brien, J.P., Pierce, K.A., et al. (2016). Environment Impacts the Metabolic Dependencies of Ras-Driven Non-Small Cell Lung Cancer. Cell Metab 23, 517-528.

de Graaf, I.A., Olinga, P., de Jager, M.H., Merema, M.T., de Kanter, R., van de Kerkhof, E.G., and Groothuis, G.M. (2010). Preparation and incubation of precision-cut liver and intestinal slices for application in drug metabolism and toxicity studies. Nat Protoc 5, 1540-1551.

DeBerardinis, R.J., and Chandel, N.S. (2016). Fundamentals of cancer metabolism. Sci Adv 2, e1600200.

DeNicola, G.M., Chen, P.H., Mullarky, E., Sudderth, J.A., Hu, Z., Wu, D., Tang, H., Xie, Y., Asara, J.M., Huffman, K.E., et al. (2015). NRF2 regulates serine biosynthesis in non-small cell lung cancer. Nat Genet 47, 1475-1481.

DeNicola, G.M., Karreth, F.A., Humpton, T.J., Gopinathan, A., Wei, C., Frese, K., Mangal, D., Yu, K.H., Yeo, C.J., Calhoun, E.S., et al. (2011). Oncogene-induced Nrf2 transcription promotes ROS detoxification and tumorigenesis. Nature 475, 106-109.

Eagle, H. (1955). The specific amino acid requirements of a human carcinoma cell (Stain HeLa) in tissue culture. J Exp Med 102, 37-48.

Fang, M., Shen, Z., Huang, S., Zhao, L., Chen, S., Mak, T.W., and Wang, X. (2010). The ER UDPase ENTPD5 promotes protein N-glycosylation, the Warburg effect, and proliferation in the PTEN pathway. Cell 143, 711-724.

Gao, P., Tchernyshyov, I., Chang, T.C., Lee, Y.S., Kita, K., Ochi, T., Zeller, K.I., De Marzo, A.M., Van Eyk, J.E., Mendell, J.T., et al. (2009). c-Myc suppression of miR-23a/b enhances mitochondrial glutaminase expression and glutamine metabolism. Nature 458, 762-765.

Garama, D.J., Harris, T.J., White, C.L., Rossello, F.J., Abdul-Hay, M., Gough, D.J., and Levy, D.E. (2015). A Synthetic Lethal Interaction between Glutathione Synthesis and Mitochondrial Reactive Oxygen Species Provides a Tumor-Specific Vulnerability Dependent on STAT3. Mol Cell Biol 35, 3646-3656.

Gilbert, L.A., and Hemann, M.T. (2011). Chemotherapeutic resistance: surviving stressful situations. Cancer Res 71, 5062-5066.

Gorrini, C., Harris, I.S., and Mak, T.W. (2013). Modulation of oxidative stress as an anticancer strategy. Nat Rev Drug Discov 12, 931-947.

Gross, M.I., Demo, S.D., Dennison, J.B., Chen, L., Chernov-Rogan, T., Goyal, B., Janes, J.R., Laidig, G.J., Lewis, E.R., Li, J., et al. (2014). Antitumor activity of the glutaminase inhibitor CB-839 in triple-negative breast cancer. Mol Cancer Ther 13, 890-901.

Gui, D.Y., Sullivan, L.B., Luengo, A., Hosios, A.M., Bush, L.N., Gitego, N., Davidson, S.M., Freinkman, E., Thomas, C.J., and Vander Heiden, M.G. (2016). Environment Dictates Dependence on Mitochondrial Complex I for NAD+ and Aspartate Production and Determines Cancer Cell Sensitivity to Metformin. Cell Metab 24, 716-727.

Harris, I.S., Treloar, A.E., Inoue, S., Sasaki, M., Gorrini, C., Lee, K.C., Yung, K.Y., Brenner, D., Knobbe-Thomsen, C.B., Cox, M.A., et al. (2015). Glutathione and thioredoxin antioxidant pathways synergize to drive cancer initiation and progression. Cancer Cell 27, 211-222.

Hensley, C.T., Faubert, B., Yuan, Q., Lev-Cohain, N., Jin, E., Kim, J., Jiang, L., Ko, B., Skelton, R., Loudat, L., et al. (2016). Metabolic Heterogeneity in Human Lung Tumors. Cell 164, 681-694.

Horvath, P., Aulner, N., Bickle, M., Davies, A.M., Nery, E.D., Ebner, D., Montoya, M.C., Ostling, P., Pietiainen, V., Price, L.S., et al. (2016). Screening out irrelevant cell-based models of disease. Nat Rev Drug Discov 15, 751-769.

Hosios, A.M., Hecht, V.C., Danai, L.V., Johnson, M.O., Rathmell, J.C., Steinhauser, M.L., Manalis, S.R., and Vander Heiden, M.G. (2016). Amino Acids Rather than Glucose Account for the Majority of Cell Mass in Proliferating Mammalian Cells. Dev Cell 36, 540-549.

Hosios, A.M., and Vander Heiden, M.G. (2018). The redox requirements of proliferating mammalian cells. J Biol Chem.

Hosoda, F., Arai, Y., Okada, N., Shimizu, H., Miyamoto, M., Kitagawa, N., Katai, H., Taniguchi, H., Yanagihara, K., Imoto, I., et al. (2015). Integrated genomic and functional analyses reveal glyoxalase I as a novel metabolic oncogene in human gastric cancer. Oncogene 34, 1196-1206.

Hsu, P.P., and Sabatini, D.M. (2008). Cancer cell metabolism: Warburg and beyond. Cell 134, 703-707.

Hung, Y.P., Albeck, J.G., Tantama, M., and Yellen, G. (2011). Imaging cytosolic NADH-NAD(+) redox state with a genetically encoded fluorescent biosensor. Cell Metab 14, 545-554.

Hung, Y.P., and Yellen, G. (2014). Live-cell imaging of cytosolic NADH-NAD+ redox state using a genetically encoded fluorescent biosensor. Methods Mol Biol 1071, 83-95.

Irani, K., Xia, Y., Zweier, J.L., Sollott, S.J., Der, C.J., Fearon, E.R., Sundaresan, M., Finkel, T., and Goldschmidt-Clermont, P.J. (1997). Mitogenic signaling mediated by oxidants in Ras-transformed fibroblasts. Science 275, 1649-1652.

Kilburn, D.G., Lilly, M.D., and Webb, F.C. (1969). The energetics of mammalian cell growth. J Cell Sci 4, 645-654.

Koppenol, W.H., Bounds, P.L., and Dang, C.V. (2011). Otto Warburg's contributions to current concepts of cancer metabolism. Nat Rev Cancer 11, 325-337.

Lane, A.N., Higashi, R.M., and Fan, T.W. (2016). Preclinical models for interrogating drug action in human cancers using Stable Isotope Resolved Metabolomics (SIRM). Metabolomics 12.

Le, A., Lane, A.N., Hamaker, M., Bose, S., Gouw, A., Barbi, J., Tsukamoto, T., Rojas, C.J., Slusher, B.S., Zhang, H., et al. (2012). Glucose-independent glutamine metabolism via TCA cycling for proliferation and survival in B cells. Cell Metab 15, 110-121.

Le Gal, K., Ibrahim, M.X., Wiel, C., Sayin, V.I., Akula, M.K., Karlsson, C., Dalin, M.G., Akyurek, L.M., Lindahl, P., Nilsson, J., et al. (2015). Antioxidants can increase melanoma metastasis in mice. Sci Transl Med 7, 308re308.

Liu, W., Hancock, C.N., Fischer, J.W., Harman, M., and Phang, J.M. (2015). Proline biosynthesis augments tumor cell growth and aerobic glycolysis: involvement of pyridine nucleotides. Sci Rep 5, 17206.

Locasale, J.W., and Cantley, L.C. (2011). Metabolic flux and the regulation of mammalian cell growth. Cell Metab 14, 443-451.

Lunt, S.Y., Muralidhar, V., Hosios, A.M., Israelsen, W.J., Gui, D.Y., Newhouse, L., Ogrodzinski, M., Hecht, V., Xu, K., Acevedo, P.N., et al. (2015). Pyruvate kinase isoform expression alters nucleotide synthesis to impact cell proliferation. Mol Cell 57, 95-107.

Lunt, S.Y., and Vander Heiden, M.G. (2011). Aerobic glycolysis: meeting the metabolic requirements of cell proliferation. Annu Rev Cell Dev Biol 27, 441-464.

Maher, E.A., Marin-Valencia, I., Bachoo, R.M., Mashimo, T., Raisanen, J., Hatanpaa, K.J., Jindal, A., Jeffrey, F.M., Choi, C., Madden, C., et al. (2012). Metabolism of [U-13 C]glucose in human brain tumors in vivo. NMR Biomed 25, 1234-1244.

Marin-Valencia, I., Yang, C., Mashimo, T., Cho, S., Baek, H., Yang, X.L., Rajagopalan, K.N., Maddie, M., Vemireddy, V., Zhao, Z., et al. (2012). Analysis of tumor metabolism reveals mitochondrial glucose oxidation in genetically diverse human glioblastomas in the mouse brain in vivo. Cell Metab 15, 827-837.

Merker, M.P., Audi, S.H., Bongard, R.D., Lindemer, B.J., and Krenz, G.S. (2006). Influence of pulmonary arterial endothelial cells on quinone redox status: effect of hyperoxia-induced NAD(P)H:quinone oxidoreductase 1. Am J Physiol Lung Cell Mol Physiol 290, L607-619.

Muir, A., Danai, L.V., Gui, D.Y., Waingarten, C.Y., Lewis, C.A., and Vander Heiden, M.G. (2017). Environmental cystine drives glutamine anaplerosis and sensitizes cancer cells to glutaminase inhibition. Elife 6.

Niu, N., and Wang, L. (2015). In vitro human cell line models to predict clinical response to anticancer drugs. Pharmacogenomics 16, 273-285.

Nokin, M.J., Durieux, F., Bellier, J., Peulen, O., Uchida, K., Spiegel, D.A., Cochrane, J.R., Hutton, C.A., Castronovo, V., and Bellahcene, A. (2017). Hormetic potential of methylglyoxal, a side-product of glycolysis, in switching tumours from growth to death. Sci Rep 7, 11722.

Nokin, M.J., Durieux, F., Peixoto, P., Chiavarina, B., Peulen, O., Blomme, A., Turtoi, A., Costanza, B., Smargiasso, N., Baiwir, D., et al. (2016). Methylglyoxal, a glycolysis side-product, induces Hsp90 glycation and YAP-mediated tumor growth and metastasis. Elife 5.

Omenn, G.S., Goodman, G.E., Thornquist, M.D., Balmes, J., Cullen, M.R., Glass, A., Keogh, J.P., Meyskens, F.L., Valanis, B., Williams, J.H., et al. (1996). Effects of a combination of beta carotene and vitamin A on lung cancer and cardiovascular disease. N Engl J Med 334, 1150-1155.

Parrish, A.R., Gandolfi, A.J., and Brendel, K. (1995). Precision-cut tissue slices: applications in pharmacology and toxicology. Life Sci 57, 1887-1901.

Pettit, F.H., Pelley, J.W., and Reed, L.J. (1975). Regulation of pyruvate dehydrogenase kinase and phosphatase by acetyl-CoA/CoA and NADH/NAD ratios. Biochem Biophys Res Commun 65, 575-582.

Pfeiffer, T., Schuster, S., and Bonhoeffer, S. (2001). Cooperation and competition in the evolution of ATP-producing pathways. Science 292, 504-507.

Piskounova, E., Agathocleous, M., Murphy, M.M., Hu, Z., Huddlestun, S.E., Zhao, Z., Leitch, A.M., Johnson, T.M., DeBerardinis, R.J., and Morrison, S.J. (2015). Oxidative stress inhibits distant metastasis by human melanoma cells. Nature 527, 186-191.

Racker, E. (1972). Bioenergetics and the problem of tumor growth. Am Sci 60, 56-63.

Raj, L., Ide, T., Gurkar, A.U., Foley, M., Schenone, M., Li, X., Tolliday, N.J., Golub, T.R., Carr, S.A., Shamji, A.F., et al. (2011). Selective killing of cancer cells by a small molecule targeting the stress response to ROS. Nature 475, 231-234.

Sakamoto, H., Mashima, T., Sato, S., Hashimoto, Y., Yamori, T., and Tsuruo, T. (2001). Selective activation of apoptosis program by S-p-bromobenzylglutathione cyclopentyl diester in glyoxalase I-overexpressing human lung cancer cells. Clin Cancer Res 7, 2513-2518.

Sayin, V.I., Ibrahim, M.X., Larsson, E., Nilsson, J.A., Lindahl, P., and Bergo, M.O. (2014). Antioxidants accelerate lung cancer progression in mice. Sci Transl Med 6, 221ra215.

Schafer, Z.T., Grassian, A.R., Song, L., Jiang, Z., Gerhart-Hines, Z., Irie, H.Y., Gao, S., Puigserver, P., and Brugge, J.S. (2009). Antioxidant and oncogene rescue of metabolic defects caused by loss of matrix attachment. Nature 461, 109-113.

Scholnick, P., Lang, D., and Racker, E. (1973). Regulatory mechanisms in carbohydrate metabolism. IX. Stimulation of aerobic glycolysis by energy-linked ion transport and inhibition by dextran sulfate. J Biol Chem 248, 5175.

Schwartz, J.P., Passonneau, J.V., Johnson, G.S., and Pastan, I. (1974). The effect of growth conditions on NAD+ and NADH concentrations and the NAD+:NADH ratio in normal and transformed fibroblasts. J Biol Chem 249, 4138-4143.

Sellers, K., Fox, M.P., Bousamra, M., 2nd, Slone, S.P., Higashi, R.M., Miller, D.M., Wang, Y., Yan, J., Yuneva, M.O., Deshpande, R., et al. (2015). Pyruvate carboxylase is critical for non-small-cell lung cancer proliferation. J Clin Invest 125, 687-698.

Son, J., Lyssiotis, C.A., Ying, H., Wang, X., Hua, S., Ligorio, M., Perera, R.M., Ferrone, C.R., Mullarky, E., Shyh-Chang, N., et al. (2013). Glutamine supports pancreatic cancer growth through a KRAS-regulated metabolic pathway. Nature 496, 101-105.

Sousa, C.M., Biancur, D.E., Wang, X., Halbrook, C.J., Sherman, M.H., Zhang, L., Kremer, D., Hwang, R.F., Witkiewicz, A.K., Ying, H., et al. (2016). Pancreatic stellate cells support tumour metabolism through autophagic alanine secretion. Nature 536, 479-483.

Spitz, D.R., Sullivan, S.J., Malcolm, R.R., and Roberts, R.J. (1991). Glutathione dependent metabolism and detoxification of 4-hydroxy-2-nonenal. Free Radic Biol Med 11, 415-423.

Suh, Y.A., Arnold, R.S., Lassegue, B., Shi, J., Xu, X., Sorescu, D., Chung, A.B., Griendling, K.K., and Lambeth, J.D. (1999). Cell transformation by the superoxide-generating oxidase Mox1. Nature 401, 79-82.

Sullivan, L.B., Gui, D.Y., Hosios, A.M., Bush, L.N., Freinkman, E., and Vander Heiden, M.G. (2015). Supporting Aspartate Biosynthesis Is an Essential Function of Respiration in Proliferating Cells. Cell 162, 552-563.

Sullivan, L.B., Gui, D.Y., and Vander Heiden, M.G. (2016). Altered metabolite levels in cancer: implications for tumour biology and cancer therapy. Nat Rev Cancer 16, 680-693.

Tardito, S., Oudin, A., Ahmed, S.U., Fack, F., Keunen, O., Zheng, L., Miletic, H., Sakariassen, P.O., Weinstock, A., Wagner, A., et al. (2015). Glutamine synthetase activity fuels nucleotide biosynthesis and supports growth of glutamine-restricted glioblastoma. Nat Cell Biol 17, 1556-1568.

Thornalley, P.J., Edwards, L.G., Kang, Y., Wyatt, C., Davies, N., Ladan, M.J., and Double, J. (1996). Antitumour activity of S-p-bromobenzylglutathione cyclopentyl diester in vitro and in vivo. Inhibition of glyoxalase I and induction of apoptosis. Biochem Pharmacol 51, 1365-1372.

Titov, D.V., Cracan, V., Goodman, R.P., Peng, J., Grabarek, Z., and Mootha, V.K. (2016). Complementation of mitochondrial electron transport chain by manipulation of the NAD+/NADH ratio. Science 352, 231-235.

Trachootham, D., Zhou, Y., Zhang, H., Demizu, Y., Chen, Z., Pelicano, H., Chiao, P.J., Achanta, G., Arlinghaus, R.B., Liu, J., et al. (2006). Selective killing of oncogenically transformed cells through a ROS-mediated mechanism by beta-phenylethyl isothiocyanate. Cancer Cell 10, 241-252.

Vander Heiden, M.G., Cantley, L.C., and Thompson, C.B. (2009). Understanding the Warburg effect: the metabolic requirements of cell proliferation. Science 324, 1029-1033.

Wang, J.B., Erickson, J.W., Fuji, R., Ramachandran, S., Gao, P., Dinavahi, R., Wilson, K.F., Ambrosio, A.L., Dias, S.M., Dang, C.V., et al. (2010). Targeting mitochondrial glutaminase activity inhibits oncogenic transformation. Cancer Cell 18, 207-219.

Warburg, O. (1923). Versuche an überlebendem Carcinomgewebe (Methoden). Biochemische Zeitschrift 142, 317–333.

Weinberg, F., Hamanaka, R., Wheaton, W.W., Weinberg, S., Joseph, J., Lopez, M., Kalyanaraman, B., Mutlu, G.M., Budinger, G.R., and Chandel, N.S. (2010). Mitochondrial metabolism and ROS generation are essential for Kras-mediated tumorigenicity. Proc Natl Acad Sci U S A 107, 8788-8793.

Wuntch, T., Chen, R.F., and Vesell, E.S. (1970). Lactate dehydrogenase isozymes: further kinetic studies at high enzyme concentration. Science 169, 480-481.

Ye, J., Fan, J., Venneti, S., Wan, Y.W., Pawel, B.R., Zhang, J., Finley, L.W., Lu, C., Lindsten, T., Cross, J.R., et al. (2014). Serine catabolism regulates mitochondrial redox control during hypoxia. Cancer Discov 4, 1406-1417.

Yuneva, M.O., Fan, T.W., Allen, T.D., Higashi, R.M., Ferraris, D.V., Tsukamoto, T., Mates, J.M., Alonso, F.J., Wang, C., Seo, Y., et al. (2012). The metabolic profile of tumors depends on both the responsible genetic lesion and tissue type. Cell Metab 15, 157-170.

Zhang, W., Trachootham, D., Liu, J., Chen, G., Pelicano, H., Garcia-Prieto, C., Lu, W., Burger, J.A., Croce, C.M., Plunkett, W., et al. (2012). Stromal control of cystine metabolism promotes cancer cell survival in chronic lymphocytic leukaemia. Nat Cell Biol 14, 276-286.

Zhao, H., Yang, L., Baddour, J., Achreja, A., Bernard, V., Moss, T., Marini, J.C., Tudawe, T., Seviour, E.G., San Lucas, F.A., et al. (2016a). Tumor microenvironment derived exosomes pleiotropically modulate cancer cell metabolism. Elife 5, e10250.

Zhao, Y., Wang, A., Zou, Y., Su, N., Loscalzo, J., and Yang, Y. (2016b). In vivo monitoring of cellular energy metabolism using SoNar, a highly responsive sensor for NAD(+)/NADH redox state. Nat Protoc 11, 1345-1359.

Appendix A: Understanding the complex-I-ty of metformin action: limiting mitochondrial respiration to improve cancer therapy

A version of this chapter has been previously published:
Luengo, A., Sullivan, L.B., and Heiden, M.G. (2014). Understanding the complex-I-ty of metformin action: limiting mitochondrial respiration to improve cancer therapy. BMC Biol 12, 82.

Abstract

Metformin has been a first-line treatment for type II diabetes mellitus for decades and is the most widely prescribed antidiabetic drug. Retrospective studies have found that metformin treatment is associated with both reduced cancer diagnoses and cancer-related deaths. Despite the prevalence of metformin use in the clinic, its molecular mechanism of action remains controversial. In this appendix, we discuss evidence that supports the role of metformin as a cancer therapeutic.

Introduction

The biguanide metformin is an antihyperglycemic agent used to treat type II diabetes. Metformin decreases blood glucose levels by suppressing liver gluconeogenesis and stimulating glucose uptake in skeletal muscle and adipose tissues. Metformin is prescribed to over 120 million people, providing a wealth of epidemiological data. Retrospective studies have found that metformin treatment is

associated with diminished tumorigenesis, with a recent meta-analysis of these studies reporting a 31% reduction in cancer incidence and a 34% reduction in cancer-specific mortality across many tumor types (Gandini et al., 2014). While these findings are provocative, it remains controversial whether the effects of metformin on improving cancer outcomes are a result of altered whole body metabolism or if metformin can act in a cell autonomous manner. Indeed, the anticancer action of metformin can be divided into two categories: 'indirect effects' resulting from systemic changes in metabolism, such as reduced concentrations of blood glucose and insulin, and 'direct effects' on tumor cells (**Figure 1**). Importantly, both could act synergistically or have differential importance depending on the cancer context. The molecular mechanisms by which metformin can impact tumor biology are an area of active research and clinical trials are ongoing to define the role of metformin in cancer treatment.

Metformin action on cells and tissues

Although the molecular underpinnings of metformin action remain an area of active investigation, the best described mechanism is inhibition of complex I, the first component of the mitochondrial electron transport chain (**Figure 2**). Complex I inhibition by metformin interrupts mitochondrial respiration and decreases proton-driven synthesis of ATP, causing cellular energetic stress and elevation of the AMP:ATP ratio. These changes result in allosteric activation of 5'-AMP-activated protein kinase (AMPK), a primary metabolic sensor. Hepatic AMPK activation can

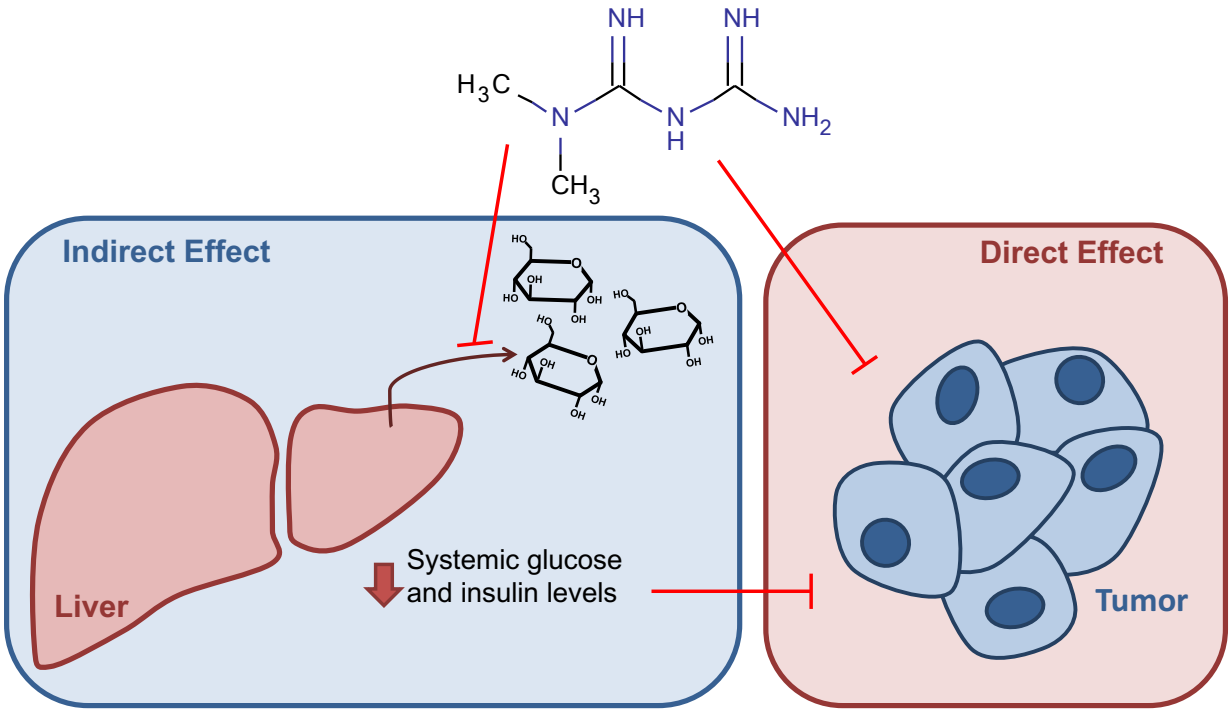

Figure 1. Indirect and direct effects of metformin on tumors.

Metformin can suppress tumor progression by modulating metabolic whole-body physiology or by acting directly on cancer cells. Metformin diminishes hepatic glucose output leading to lower systemic glucose and insulin levels, which could impair malignant growth indirectly without requiring accumulation of metformin in the tumor. Alternatively, metformin can act on cancer cells directly, inhibiting cancer progression by suppressing mTOR signaling, mitochondrial glucose oxidation, and/or reducing stability of HIF under hypoxic conditions.

inhibit gluconeogenesis and activate glycolysis (Mihaylova and Shaw, 2011). AMPK activation in the muscle can also increase glucose consumption, and is another potential site of metformin action (Hardie and Alessi, 2013). Both of these consequences of metformin can lower blood glucose and contribute to therapeutic benefit in in type II diabetes.

Though AMPK was once considered the primary executor of metformin antidiabetic action, genetic loss-of-function studies in mice have indicated that hepatic expression of AMPK and its upstream activating kinase LKB1 may not be absolutely required for suppression of gluconeogenesis by metformin (Foretz et al., 2010). An AMPK-independent mechanism has been proposed, by which metformin antagonizes glucagon-dependent cyclic AMP (cAMP) signaling (Miller et al., 2013). Glucagon activates adenylyl cyclase to produce cAMP and stimulate cAMP-dependent protein kinase (PKA) signaling. PKA activation decreases fructose-2,6,-bisphosphate levels, thereby favoring gluconeogenesis in the liver and increasing blood glucose levels. Metformin opposes glucagon action because inhibition of the mitochondrial electron transport chain elevates cytosolic AMP:ATP ratios, which in turn abrogates cAMP production (Miller et al., 2013). Therefore, inhibition of PKA signaling by metformin may be another mechanism for inhibition of hepatic gluconeogenesis and reduced hyperglycemia in patients treated with the drug.

In addition to targeting complex I, metformin has recently been shown to inhibit mitochondrial glycerol-phosphate dehydrogenase (mGPD) (**Figure 2**) (Madiraju et al., 2014). mGPD transports cytosolic reducing equivalents from

NADH into the mitochondria via the glycerol-phosphate shuttle. Interestingly, inhibition of mGPD and complex I both compromise the ability of mitochondria to oxidize cytosolic NADH and decrease the entry of these reducing equivalents into the electron transport chain. Therefore, both complex I and mGPD inhibition are expected to have similar downstream consequences on cellular bioenergetics.

Regardless of how metformin disrupts mitochondrial respiration, the resulting energy stress, changes in cofactor balance, and reliance on alternative metabolic pathways to obtain ATP could have several effects that contribute to the therapeutic benefits of this drug. AMPK activation, PKA inhibition, and redox stress may act separately or in concert to repress hepatic gluconeogenesis and stimulate insulin sensitivity. There are many ways in which metformin might act across tissues to alter metabolic physiology, and these complexities make it challenging to understand how metformin improves outcomes in cancer patients.

Role of metformin in cancer therapy

The association between metformin and decreased cancer risk may be a result of the antidiabetic effects of the drug. Increased glucose consumption is a hallmark of many cancer cells, and increased blood glucose and insulin levels seen in type II diabetes are associated with worse cancer prognosis (Pollak, 2012). Metformin improves glycemic control and lowers insulin levels, which can influence other hormones and cytokines, including insulin-like growth factor 1 (IGF-1), a known mitogen that has been shown to promote carcinogenesis. Most of the patients

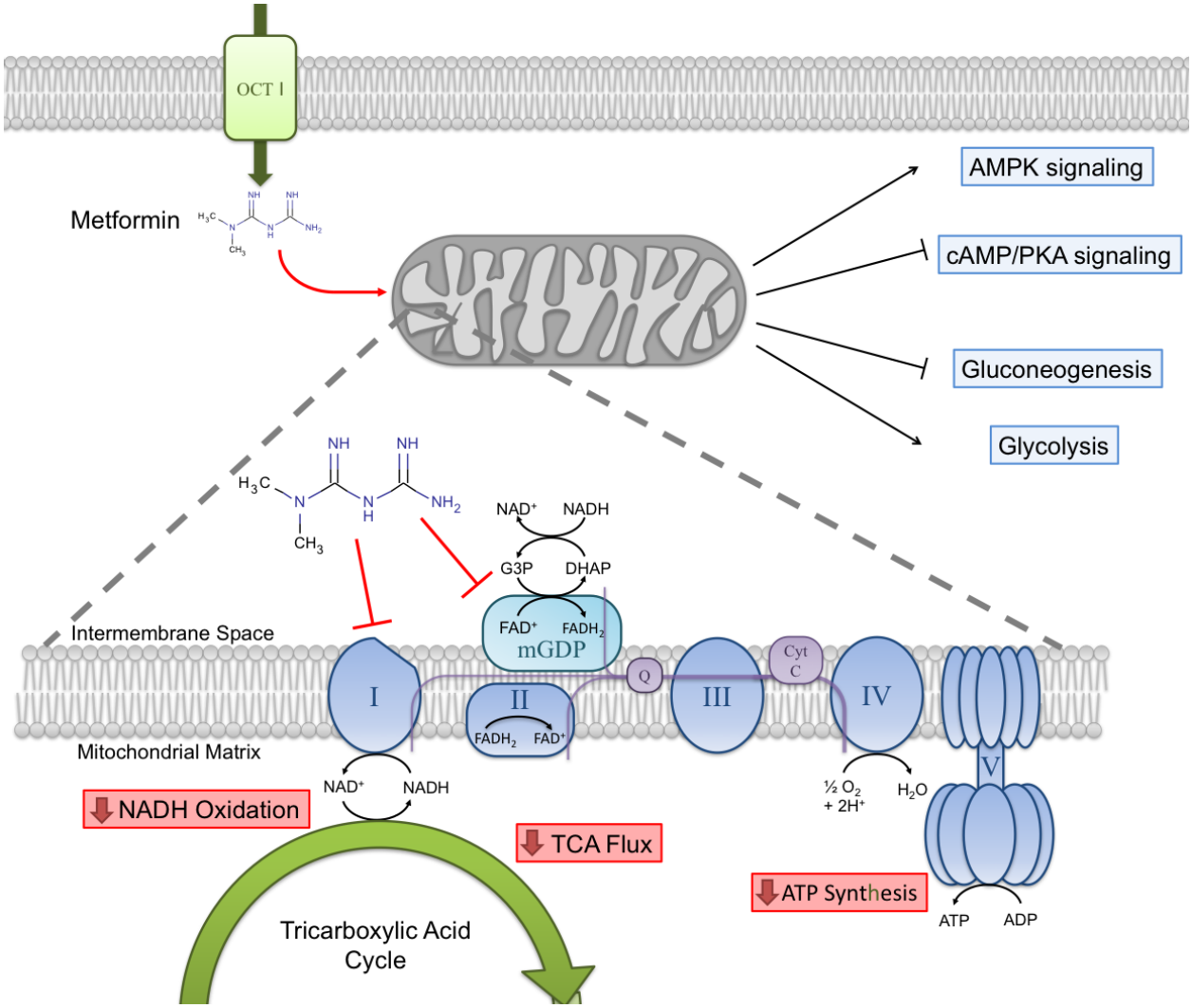

Figure 2. Cellular consequences of metformin action at the mitochondria. Metformin enters the cell by organic cation transporter 1 (OCT1) and subsequently accumulates in the mitochondria. There, metformin inhibits complex I of the electron transport chain and mGDP, resulting in decreased NADH oxidation. Decreased electron chain activity suppresses tricarboxylic acid (TCA) cycle flux and decreases mitochondrial ATP synthesis. These actions result in increased AMPK signaling, decreased cAMP/PKA signaling, decreased gluconeogenesis and increased glycolysis.

in existing retrospective metformin studies were diabetic, so ongoing efforts to define the benefit of metformin in non-diabetic cancer patients will provide important insight into the role indirect metformin effects play in improved cancer outcomes.

Metformin affects systemic metabolism, but can also influence cell autonomous energetics. Metformin treatment leads to energy stress and AMPK activation in cancer cells, which can impair proliferation by suppressing anabolic processes and growth signaling through mammalian target of rapamycin (mTOR). Increased mTOR activation has been implicated in a wide variety of different cancers, and AMPK-mediated attenuation of anabolic metabolism and/or mTOR signaling by metformin may contribute to the antitumor effects of metformin in some situations. However, LKB1-deficient tumors, which are compromised in their ability to activate AMPK, are particularly sensitive to biguanides (Shackelford et al., 2013). This suggests that induction of energy stress may account for some of the ability of metformin to limit cancer progression.

It has long been known that malignant cells avidly consume glucose and preferentially metabolize glucose to lactate. However, studies of tumor metabolism in vivo have suggested that some tumor cells also oxidize glucose in the mitochondria (Davidson et al., 2016; Hensley et al., 2016; Maher et al., 2012; Marin-Valencia et al., 2012; Sellers et al., 2015). Since metformin prevents mitochondrial glucose metabolism, metformin might be particularly effective in tumors that rely on glucose oxidation via the tricarboxylic acid cycle.

Decreased vascularization of tumors affects the availability of both glucose and oxygen and may influence how glucose is used by cancer cells in vivo. Stabilization of hypoxia-inducible factors (HIFs) is a critical part of the metabolic adaptation to low-oxygen and activation of HIFs is reported in many cancers (Semenza, 2013). Metformin has recently been shown to reduce hypoxia-induced HIF1α stabilization and diminish expression of HIF target genes in tumors (Wheaton et al., 2014), suggesting that metformin may serve a therapeutic role in cancers that are dependent on HIF signaling for survival in hypoxic environments. A better understanding of the signaling and metabolic effects of metformin on cancer cells will help define other tumor contexts likely to be sensitive to metformin.

Despite increasing evidence that metformin can have profound effects on cancer cells, it is not well understood if the drug accumulates to sufficient levels to cause these direct effects in patient tumors. The liver is a clear site of drug action, as it is exposed to high levels of oral metformin and expresses the metformin transporter OCT1, facilitating uptake and allowing for drug accumulation in this tissue. At metformin doses prescribed to diabetic patients, the circulating levels in plasma and peripheral tissues are orders of magnitude below the concentrations used in vitro to elicit a biological effect in cancer cells. How the concentrations used in vitro translate to the effects on tumor tissues remains controversial, but some studies have shown that metformin induces cancer autonomous metabolic changes in vivo. Metformin has been shown to activate AMPK in intestinal tumors, even in the absence of changes in organismal blood glucose or insulin levels (Tomimoto et

al., 2008). In another study, tumors engineered to express a surrogate for complex I that is refractory to metformin are resistant to the drug in vivo (Wheaton et al., 2014). These data argue that the direct effect of metformin on mitochondrial electron transport can be relevant for tumor growth in a cell autonomous manner. A better understanding of the pharmacokinetic properties and the molecular mechanisms of metformin will better define how best to use this antidiabetic drug in cancer therapy.

References

Davidson, S.M., Papagiannakopoulos, T., Olenchock, B.A., Heyman, J.E., Keibler, M.A., Luengo, A., Bauer, M.R., Jha, A.K., O'Brien, J.P., Pierce, K.A., et al. (2016). Environment Impacts the Metabolic Dependencies of Ras-Driven Non-Small Cell Lung Cancer. Cell Metab 23, 517-528.

Foretz, M., Hebrard, S., Leclerc, J., Zarrinpashneh, E., Soty, M., Mithieux, G., Sakamoto, K., Andreelli, F., and Viollet, B. (2010). Metformin inhibits hepatic gluconeogenesis in mice independently of the LKB1/AMPK pathway via a decrease in hepatic energy state. J Clin Invest 120, 2355-2369.

Gandini, S., Puntoni, M., Heckman-Stoddard, B.M., Dunn, B.K., Ford, L., DeCensi, A., and Szabo, E. (2014). Metformin and cancer risk and mortality: a systematic review and meta-analysis taking into account biases and confounders. Cancer Prev Res (Phila) 7, 867-885.

Hardie, D.G., and Alessi, D.R. (2013). LKB1 and AMPK and the cancer-metabolism link - ten years after. BMC Biol 11, 36.

Hensley, C.T., Faubert, B., Yuan, Q., Lev-Cohain, N., Jin, E., Kim, J., Jiang, L., Ko, B., Skelton, R., Loudat, L., et al. (2016). Metabolic Heterogeneity in Human Lung Tumors. Cell 164, 681-694.

Madiraju, A.K., Erion, D.M., Rahimi, Y., Zhang, X.M., Braddock, D.T., Albright, R.A., Prigaro, B.J., Wood, J.L., Bhanot, S., MacDonald, M.J., et al. (2014). Metformin suppresses gluconeogenesis by inhibiting mitochondrial glycerophosphate dehydrogenase. Nature 510, 542-546.

Maher, E.A., Marin-Valencia, I., Bachoo, R.M., Mashimo, T., Raisanen, J., Hatanpaa, K.J., Jindal, A., Jeffrey, F.M., Choi, C., Madden, C., et al. (2012). Metabolism of [U-13 C]glucose in human brain tumors in vivo. NMR Biomed 25, 1234-1244.

Marin-Valencia, I., Yang, C., Mashimo, T., Cho, S., Baek, H., Yang, X.L., Rajagopalan, K.N., Maddie, M., Vemireddy, V., Zhao, Z., et al. (2012). Analysis of tumor metabolism reveals mitochondrial glucose oxidation in genetically diverse human glioblastomas in the mouse brain in vivo. Cell Metab 15, 827-837.

Mihaylova, M.M., and Shaw, R.J. (2011). The AMPK signalling pathway coordinates cell growth, autophagy and metabolism. Nat Cell Biol 13, 1016-1023.

Miller, R.A., Chu, Q., Xie, J., Foretz, M., Viollet, B., and Birnbaum, M.J. (2013). Biguanides suppress hepatic glucagon signalling by decreasing production of cyclic AMP. Nature 494, 256-260.

Pollak, M.N. (2012). Investigating metformin for cancer prevention and treatment: the end of the beginning. Cancer Discov 2, 778-790.

Sellers, K., Fox, M.P., Bousamra, M., 2nd, Slone, S.P., Higashi, R.M., Miller, D.M., Wang, Y., Yan, J., Yuneva, M.O., Deshpande, R., et al. (2015). Pyruvate carboxylase is critical for non-small-cell lung cancer proliferation. J Clin Invest 125, 687-698.

Semenza, G.L. (2013). HIF-1 mediates metabolic responses to intratumoral hypoxia and oncogenic mutations. J Clin Invest 123, 3664-3671.

Shackelford, D.B., Abt, E., Gerken, L., Vasquez, D.S., Seki, A., Leblanc, M., Wei, L., Fishbein, M.C., Czernin, J., Mischel, P.S., et al. (2013). LKB1 inactivation dictates therapeutic response of non-small cell lung cancer to the metabolism drug phenformin. Cancer Cell 23, 143-158.

Tomimoto, A., Endo, H., Sugiyama, M., Fujisawa, T., Hosono, K., Takahashi, H., Nakajima, N., Nagashima, Y., Wada, K., Nakagama, H., et al. (2008). Metformin suppresses intestinal polyp growth in ApcMin/+ mice. Cancer Sci 99, 2136-2141.

Wheaton, W.W., Weinberg, S.E., Hamanaka, R.B., Soberanes, S., Sullivan, L.B., Anso, E., Glasauer, A., Dufour, E., Mutlu, G.M., Budigner, G.S., et al. (2014). Metformin inhibits mitochondrial complex I of cancer cells to reduce tumorigenesis. Elife 3, e02242.

Appendix B: Evidence for electron acceptor limitation in vivo

Authorship statement:
Some passages and figures have been adapted or quoted verbatim from the following published articles:
Gui, D.Y., Sullivan, L.B., Luengo, A., Hosios, A.M., Bush, L.N., Gitego, N., Davidson, S.M., Freinkman, E., Thomas, C.J., and Vander Heiden, M.G. (2016). Environment Dictates Dependence on Mitochondrial Complex I for NAD+ and Aspartate Production and Determines Cancer Cell Sensitivity to Metformin. Cell Metab 24, 716-727.
Sullivan, L.B., Luengo, A., Danai L.V., Bush L.N., Diehl F.F., Hosios A.M., Lau A.N., Elmiligy S., Malstrom S., Lewis C.A., Vander Heiden M.G. (2018). Evidence for Aspartate as an Endogenous Metabolic Limitation for Tumour Growth. Nat Cell Bio. Manuscript Accepted

Defining the endogenous metabolic limitations of tumor growth can help guide new strategies for cancer therapy. Cancer cells proliferate more slowly in vivo than in standard tissue culture systems, suggesting that tumor proliferation could be restricted by a metabolic limitation. In Chapter 3 of this dissertation, we provide evidence that electron acceptors could be limiting for cancer cell growth in some contexts, thus increasing dependence on pathways that regenerate NAD+. The dramatic differences in oxygen and nutrient availability between cancer cells growing in vitro versus those proliferating as tumors make it likely that electron acceptors are further limited in vivo, suggesting that the findings presented in this thesis could hold relevance for in vivo tumor growth. A better understanding of NAD+/NADH homeostasis in cancers growing in vivo is critical for identifying

contexts in which therapies that limit electron acceptor availability could be used to benefit cancer patients.

Recent data suggests that a primary function of respiration is to provide electron acceptors and regenerate oxidized cofactors required for proliferation (Birsoy et al., 2015; Sullivan et al., 2015; Titov et al., 2016). The biguanide metformin can impair respiration by inhibition of the glycerol-phosphate shuttle (Madiraju et al., 2014) and direct inhibition of mitochondrial complex I (NADH dehydrogenase), resulting in decreased mitochondrial respiration (Bridges et al., 2014; El-Mir et al., 2000; Luengo et al., 2014; Owen et al., 2000; Wheaton et al., 2014). Supporting the role of complex I as an important target of metformin in cancer, expression of a metformin-resistant yeast analog of complex I (NDI1) renders cells insensitive to metformin in culture and resistant to the anti-tumor growth effects of metformin in xenograft models (Birsoy et al., 2015; Wheaton et al., 2014). These data support the hypothesis that metformin targets complex I and could serve as an intervention to decrease mitochondrial electron transport, and thus electron acceptor availability, in tumors.

To explore whether electron acceptor availability could be limiting in vivo, we first wanted to assess the effects of metformin on tumor growth. For these studies, we injected A549 cells into the flanks of nude mice. When xenograft tumors reached a size of 50mm^3, the mice were randomized into three groups and treated once a day with vehicle, 500mg/kg metformin, or 1,500 mg/kg metformin by oral gavage. We found that metformin treatment inhibited tumor growth in a dose-dependent

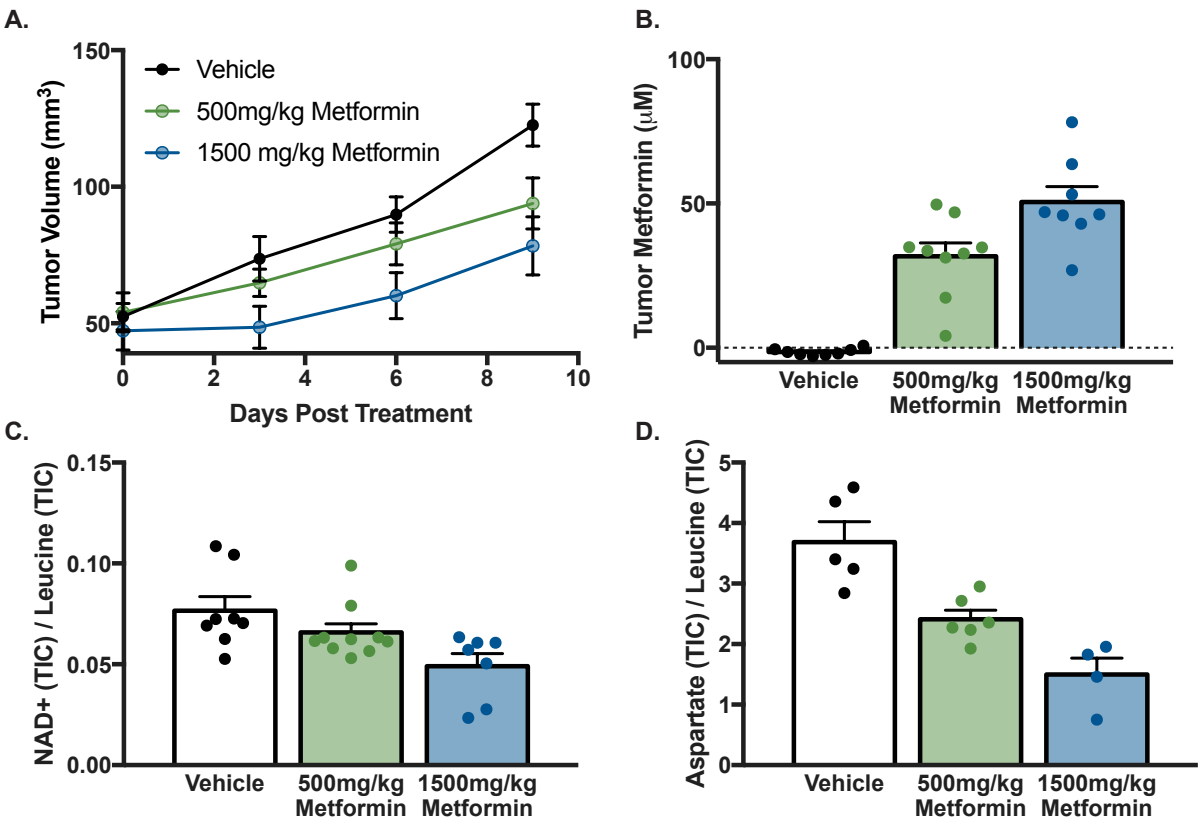

Figure 1. Metformin slows tumor growth and decreases intratumoral NAD+ and aspatate levels

(A) Assessment of tumor volume over time of xenograft tumors generated from A549 cells. Mice were treated with either vehicle (sterile water) or the indicated dose of metformin by daily oral gavage. Treatment was initiated in mice with size-matched tumors upon reaching a volume of 50mm^3.

(B) Concentrations of metformin in tumors of mice that had been treated for 10 days with the indicated dose of metformin. Tissues were collected 2 hours following the final treatment.

(C and D) Relative intratumoral (C) NAD+ and (E) aspartate were measured after 10 days of vehicle or metformin treatment at the indicated dose. Relative NAD+ and aspartate levels are shown as total ion counts (TIC) normalized to leucine TIC.

Values shown denote the mean ± SEM

manner (**Figure 1A**). Measurement of metformin concentration in tumors confirmed that escalating doses of the drug resulted in an increase in the intratumoral concentration of metformin (**Figure 1B**), and the levels achieved by these treatments were therapeutically relevant and expected to be tolerable in humans (Dell'Aglio et al., 2009). Though levels of NADH were undetectable, we found that NAD+ levels decreased in tumors treated with increasing doses of metformin (**Figure 1C**). Importantly, the tumor proliferation defect correlated with intratumoral NAD+ levels, suporting the argument that electron acceptor availability could constrain tumor growth.

Previous work has shown that maintaining NAD+/NADH balance supports de novo aspartate biosynthesis required for the proliferation of cancer cells (Birsoy et al., 2015; Sullivan et al., 2015). To assess whether aspartate was affected by metformin treatment in vivo, we measured levels of this amino acid in A549 tumors that had been treated with metformin and discovered a dose-dependent decrease in intratumoral aspartate levels (**Figure 1D**). This finding raises the possibility that aspartate synthesis could constrain cancer cell proliferation, and thus we next wanted to determine whether aspartate availability could limit tumor growth.

Transport of aspartate into most mammalian cells is inefficient, with millimolar concentrations of aspartate required to restore proliferation of cells in which electron transport is impaired (Birsoy et al., 2015; Sullivan et al., 2015). Aspartate levels in circulation are very low (Mayers and Vander Heiden, 2015) and most mammalian cells do not have a known asparaginase activity, the enzymatic

activity that converts asparagine to aspartate (**Figure 2A**). Thus, aspartate could represent a metabolic limitation for tumor proliferation in vivo.

We hypothesized that if cancer cells were able to convert asparagine to aspartate, circulating asparagine, which is permeable to cells, might be able to contribute to intracellular aspartate pools (**Figure 2B**). Guinea pigs have long been known to be unique among mammals in possessing asparaginase activity in their blood (Broome, 1963). The protein responsible for this activity, guinea pig asparaginase 1 (gpASNase1), has only recently been identified (Schalk et al., 2014). We expressed an epitope tagged gpASNase1 in cells (**Figure 2C**) and assessed whether heterologous gpASNase1 expression could support aspartate production in tumor cells, and thus promote tumor growth. We implanted control cells and gpASNase1-expressing 143B cells into the flanks of nude mice and found that tumors expressing gpASNase1 proliferated at a higher rate than tumors derived from control cells (**Figure 2D**), suggesting that obtaining aspartate could be a limitation for the growth of some tumors.

Metformin was found to decrease intratumoral NAD+ levels and intratumoral asparate (**Figure 1C,D**); however, it is unclear which of these limitations contributed more significantly to suppression of tumor proliferation. To test whether metformin could suppress tumor growth by depleting intracellular aspartate, we assessed whether heterologous gpASNase expression could confer resistance to metformin treatment in vivo. We implanted 143B cells with or without

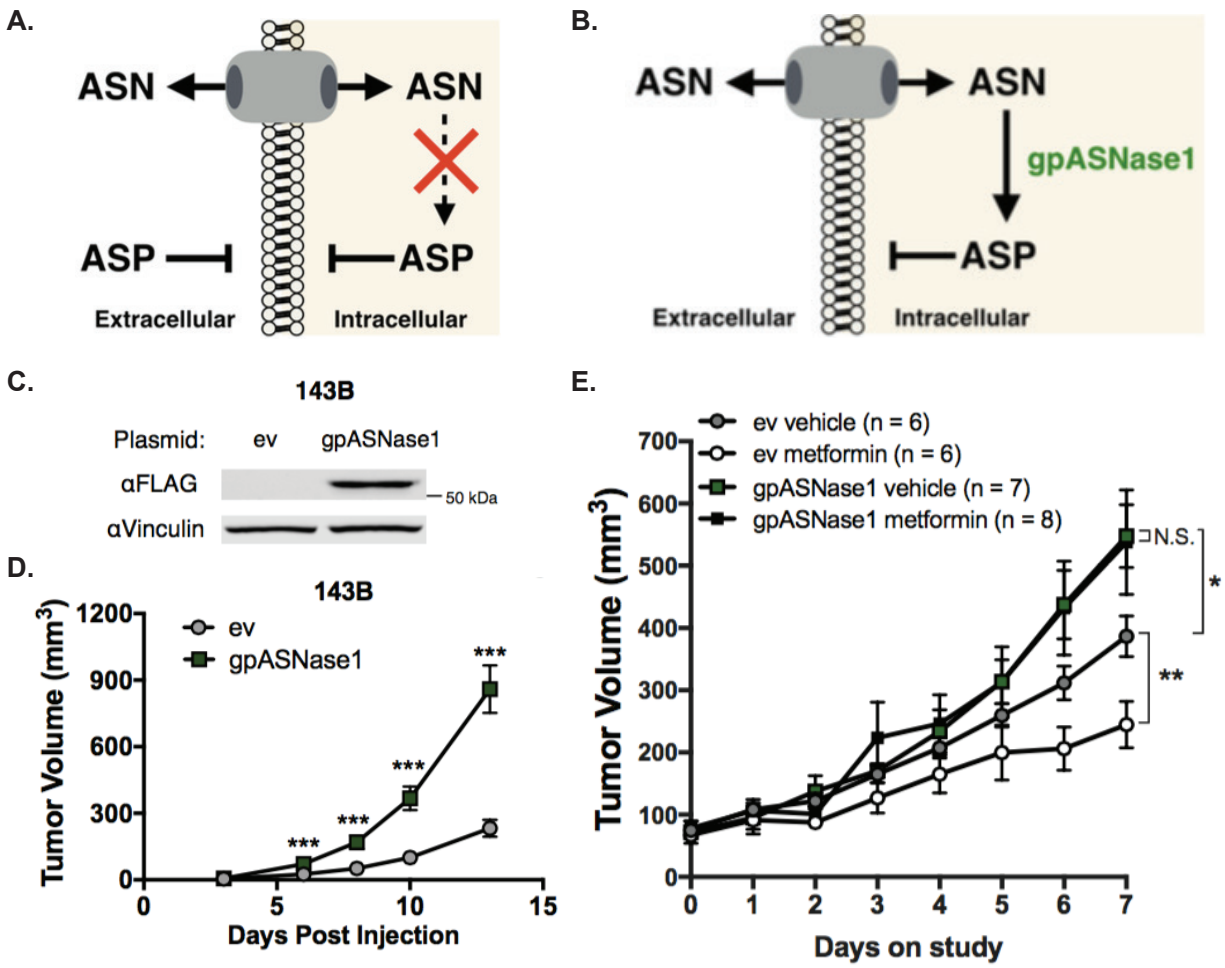

Figure 2. Heterologous expression of guinea pig asparaginase 1 promotes tumor proliferation and confers resistance to metformin treatment in vivo

(A) Schematic summarizing the permeability of asparagine (ASN) and aspartate (ASP) and in the inabilitly of cells to convert ASN to ASP.

(B) Schematic depicting how intracellular expression of gpASNase1 allows environmental asparagine to support intracelluar aspartate levels.

(C) Western blot analysis of 143B cells expressing empty vector (ev) of FLAG-tagged gpASNase1 as indicated. gpASNase1 expression is detected with an anti-FLAG antibody, and vinculin expression is assessed as a loading control. Predicted molecular weight of gpASNase1 is 60kDa.

(D) Assessment of tumor volume over time of xenograft tumors generated from 143B cells expressing empty vector (ev) or gpASNase1 as indicated.

(E) Volumes of tumors derived from 143B cells expressing ev or gpASNase1 were measured over time in mice that were treated with either vehicle (water) or 1g/kg metformin once daily by oral gavage. Treatment was initiated in mice with size-matched tumors after reaching 45mm^3.

Values shown denote the mean ± SEM; NS is $p>0.05$; *$p<0.05$; **$p<0.01$; ***$p<0.001$

gpASNase1 expression into nude mice and treated the mice with either 1000 mg/kg metformin or vehicle by daily oral gavage after xenograft tumors reached a size of 45mm^3. Though metformin suppressed growth of control tumors, metformin had no effect on the growth of gpASNase-expressing tumors (**Figure 2E**). Collectively, these data support the hypothesis that metformin can suppress tumor growth by exacerbating an endogenous aspartate limitation. Furthermore, targeting the pathways of aspartate production may have particular efficacy to inhibit growth of some tumors.

Materials and Methods

Mouse studies: All experiments performed in this appendix were approved by the MIT Committee on Animal care (IACUC). Two million A549 or one million 143B cells were suspended in 100 μL of PBS and cells were injected into flanks of nu/nu mice (088) (Charles River Laboratories). When tumours became palpable, tumor volume was measured by caliper in two dimensions, and volumes were estimated using the equation $V = (\pi/6)(L \times W^2)$. Length was defined to be the longer of the two dimensions measured. The tumors were permitted to grow to 50 mm^3, after which the animals were randomly assigned to a treatment or vehicle group. Vehicle (sterile water), 500 mg/kg, or 1500 mg/kg of metformin was dosed via oral gavage daily for 10 days. Only tumour sites that formed tumours by the end point of the growth assay were measured and factored into the tumour volume calculation. The tumors and plasma samples were collected two hours after the final dosage on day

10, and metformin and metabolite concentrations were quantified by liquid chromatography-mass spectrometry (LCMS). Mice were sacrificed at endpoints consistent with our mouse protocol or prior if recommended by the veterinary staff.

Western Blot Analysis: Cells expressing either empty vector or c-terminal FLAG tagged gpASNase1 were washed with cold PBS and lysed with cold RIPA buffer containing cOmplete Mini protease inhibitors (Roche). Protein concentration was determined by BCA Protein Assay (Pierce) using BSA as a standard. Samples were resolved by SDS-PAGE using standard techniques, and protein was detected with the following antibodies: primary antibodies: FLAG (Cell Signaling, 2368), Vinculin (Abcam, ab18058); secondary antibodies: IR680LT dye conjugated anti-rabbit IgG (Licor Biosciences, 925-68021), IR800 dye conjugated anti-mouse IgG (Licor Biosciences, 925-32210). Blot were imaged by an Odyssey infrared scanner (Licor Biosciences) and analyzed using Image Studio Lite.

Polar Metabolite Quantification by Liquid Chromatography-Mass Spectrometry: Briefly, metabolites were first extracted using ice-cold 80% methanol and chloroform. Relative metabolites abundances were measured using a Dionex UltiMate 3000 ultra-high performance liquid chromatography system connected to a Q Exactive benchtop Orbitrap mass spectrometer equipped with an Ion Max source and a HESI II probe (Thermo Fisher Scientific). To quantify metabolite abundance, the chromatogram XCalibur QuanBroswer 2.2 (Thermo

Fisher Scientific) was used in conjunction with the in-house retention time library of chemical standards.

Generation of gpASNase1 expressing cell lines: The protein sequence of gpASNase1 was reverse translated into a nucleotide sequence which was synthesized and inserted into a pUC57 plasmid (Biomatik). Primers were designed to amplify the gpASNase1 sequence, encode a C-terminal FLAG tag, and use restriction cloning to insert gpASNase1 into the plasmid pLHCX. Retrovirus was generated in HEK293T cells by transfection using standard techniques. Cells were infected with virus containing either empty vector pLHCX or gpASNase1 pLHCX and were selected with 200μg/mL hygromycin B (Invitrogen). Cell were maintained in hygromycin B containing media until all uninfected control cells had died.

References

Birsoy, K., Wang, T., Chen, W.W., Freinkman, E., Abu-Remaileh, M., and Sabatini, D.M. (2015). An Essential Role of the Mitochondrial Electron Transport Chain in Cell Proliferation Is to Enable Aspartate Synthesis. Cell 162, 540-551.

Bridges, H.R., Jones, A.J., Pollak, M.N., and Hirst, J. (2014). Effects of metformin and other biguanides on oxidative phosphorylation in mitochondria. Biochem J 462, 475-487.

Broome, J.D. (1963). Evidence that the L-asparaginase of guinea pig serum is responsible for its antilymphoma effects. I. Properties of the L-asparaginase of guinea pig serum in relation to those of the antilymphoma substance. J Exp Med 118, 99-120.

Dell'Aglio, D.M., Perino, L.J., Kazzi, Z., Abramson, J., Schwartz, M.D., and Morgan, B.W. (2009). Acute metformin overdose: examining serum pH, lactate level, and metformin concentrations in survivors versus nonsurvivors: a systematic review of the literature. Ann Emerg Med 54, 818-823.

El-Mir, M.Y., Nogueira, V., Fontaine, E., Averet, N., Rigoulet, M., and Leverve, X. (2000). Dimethylbiguanide inhibits cell respiration via an indirect effect targeted on the respiratory chain complex I. J Biol Chem 275, 223-228.

Gui, D.Y., Sullivan, L.B., Luengo, A., Hosios, A.M., Bush, L.N., Gitego, N., Davidson, S.M., Freinkman, E., Thomas, C.J., and Vander Heiden, M.G. (2016). Environment Dictates Dependence on Mitochondrial Complex I for NAD+ and Aspartate Production and Determines Cancer Cell Sensitivity to Metformin. Cell Metab 24, 716-727.

Luengo, A., Sullivan, L.B., and Heiden, M.G. (2014). Understanding the complex-I-ty of metformin action: limiting mitochondrial respiration to improve cancer therapy. BMC Biol 12, 82.

Madiraju, A.K., Erion, D.M., Rahimi, Y., Zhang, X.M., Braddock, D.T., Albright, R.A., Prigaro, B.J., Wood, J.L., Bhanot, S., MacDonald, M.J., et al. (2014). Metformin suppresses gluconeogenesis by inhibiting mitochondrial glycerophosphate dehydrogenase. Nature 510, 542-546.

Mayers, J.R., and Vander Heiden, M.G. (2015). Famine versus feast: understanding the metabolism of tumors in vivo. Trends Biochem Sci 40, 130-140.

Owen, M.R., Doran, E., and Halestrap, A.P. (2000). Evidence that metformin exerts its anti-diabetic effects through inhibition of complex 1 of the mitochondrial respiratory chain. Biochem J 348 Pt 3, 607-614.

Schalk, A.M., Nguyen, H.A., Rigouin, C., and Lavie, A. (2014). Identification and structural analysis of an L-asparaginase enzyme from guinea pig with putative tumor cell killing properties. J Biol Chem 289, 33175-33186.

Sullivan, L.B., Luengo, A., Danai L.V., Bush L.N., Diehl F.F., Hosios A.M., Lau A.N., Elmiligy S., Malstrom S., Lewis C.A., Vander Heiden M.G. (2018). Evidence for Aspartate as an Endogenous Metabolic Limitation for Tumour Growth. Nat Cell Bio. Manuscript Accepted

Sullivan, L.B., Gui, D.Y., Hosios, A.M., Bush, L.N., Freinkman, E., and Vander Heiden, M.G. (2015). Supporting Aspartate Biosynthesis Is an Essential Function of Respiration in Proliferating Cells. Cell 162, 552-563.

Titov, D.V., Cracan, V., Goodman, R.P., Peng, J., Grabarek, Z., and Mootha, V.K. (2016). Complementation of mitochondrial electron transport chain by manipulation of the NAD+/NADH ratio. Science 352, 231-235.

Wheaton, W.W., Weinberg, S.E., Hamanaka, R.B., Soberanes, S., Sullivan, L.B., Anso, E., Glasauer, A., Dufour, E., Mutlu, G.M., Budigner, G.S., et al. (2014). Metformin inhibits mitochondrial complex I of cancer cells to reduce tumorigenesis. Elife 3, e02242.